Technische Universität München
Max-Planck-Institut für Quantenoptik

# Coherent Effects in Mesoscopic Quantum Systems

Eric Matthias Kessler

Vollständiger Abdruck der von der Fakultät für Physik
der Technischen Universität München
zur Erlangung des akademischen Grades eines

Doktors der Naturwissenschaften (Dr. rer. nat.)

genehmigten Dissertation.

| | |
|---|---|
| Vorsitzende: | Univ.-Prof. Dr. N. Brambilla |
| Prüfer der Dissertation: | 1. Hon.-Prof. J. I. Cirac, Ph.D. |
| | 2. Univ.-Prof. J. J. Finley, Ph.D. |

Die Dissertation wurde am 11.09.2012
bei der Technischen Universität München eingereicht
und durch die Fakultät für Physik am 02.10.2012 angenommen.

# Abstract

The role of dissipation in the emergence of coherent quantum phenomena is ambiguous. On the one hand, the dissipative coupling to an environment is the biggest adversary of coherence, corrupting the quantum properties (e. g., entanglement) of a physical state. On the other hand, recent theoretical and experimental results revealed that under certain circumstances, dissipation itself can be the driving force behind the occurrence of coherent behavior. This Thesis theoretically investigates this interplay in mesoscopic solid-state quantum systems, such as quantum dots (QDs) and Nitrogen-Vacancy (NV) centers, from different perspectives.

In the first part of this Thesis, we put forward a novel strategy to protect coherence from the malicious influences of the environment. We show that a quantum interference effect in the optical absorption of single photon emitters can be used to prepare the surrounding nuclear spin in states with narrow field distribution, and thereby reducing the dephasing of electronic spin degrees of freedom. In the second part, we demonstrate how certain types of dissipation lead to highly coherent phenomena in the above systems. First, we investigate superradiant photon emission from the nuclear spin system of a QD or NV center under optical pumping conditions. We theoretically show that under realistic experimental conditions, an initially polarized nuclear system shows pronounced signatures of cooperative behavior in the optical de-excitation. Thereafter, we demonstrate that an analogous effect can be observed in the electron transport through an electrically defined QD. Intriguingly, this setting gives rise to superradiant signatures in electric currents rather than in the optical emission profile. Under realistic conditions, the tunnel current through the QD shows a pronounced characteristic intensity burst. Further, we develop from first principles a mathematical framework for the description of electron transport in the presence of hyperfine coupling. Building up on the insight that coherence can emerge in the transient evolution of a single-photon emitter, we next investigate the steady-

state behavior of a driven central spin model under optical pumping conditions. We develop a series of theoretical methods that enable the complete analytical description of the phase diagram. This comprises various quantum effects, such as first- and second-order phase transitions and regions of bistability, squeezing, and altered spin pumping dynamics. Finally, in the last part of this Thesis, we develop an analytical tool for the formalized adiabatic elimination of fast evolving degrees of freedom in open systems. It is formulated in the language of a generalized Schrieffer-Wolff transformation, and closes a gap in the theoretical toolbox for the description of open systems.

# Zusammenfassung

Die Rolle von Dissipation im Zusammenhang mit dem Auftreten von kohärenten Quantenphänomenen ist zweideutig. Auf der einen Seite ist die dissipative Kopplung an eine Umgebung der größte Gegenspieler von Kohärenz, da sie zum Verlust von Quanteneigenschaften (z. B. Verschränkung) physikalischer Zustände führt. Auf der anderen Seite haben aktuelle theoretische und experimentelle Arbeiten aufgezeigt, dass unter bestimmten Umständen ebendiese Dissipation die treibende Kraft hinter dem Erscheinen kohärenten Verhaltens sein kann. Die vorliegende Dissertation untersucht dieses Wechselspiel von verschiedenen Perspektiven in mesoskopischen Festkörper-Quantensystemen, wie zum Beispiel Quantenpunkten (QDs) und Stickstoff-Fehlstellen-Zentren (NV-Zentren).

Im ersten Teil der Dissertation schlagen wir eine neuartige Methode zur Erhaltung von Kohärenz unter dem schädlichen Einfluss einer Spinumgebung vor. Wir zeigen auf, dass ein Quanteninterferenzeffekt in der optischen Absorption von Ein-Photonen Emittenten dazu genutzt werden kann, das umgebende nukleare Spinsystem in Zuständen zu präparieren, welche reduzierte magnetische Fluktuationen aufweisen, um so die Kohärenzzeit der elektronischen Spin-Freiheitsgrade zu verlängern. In dem zweiten Teil legen wir dar, wie bestimmte Arten von Dissipation in obigen Systemen zu hoch kohärentem Verhalten führt: Zunächst untersuchen wir superradiante Photonenemissionen aus der nuklearen Spinumgebung eines QD oder NV-Zentrums unter optischem Pumpen. Wir demonstrieren theoretisch, dass ein anfänglich polarisiertes nukleares System unter realistischen experimentellen Bedingungen deutliche Signaturen von kooperativem Verhalten während der optischen Abregung zeigt. Des Weiteren zeigen wir, dass ein analoger Effekt im elektronischen Transport durch elektrisch definierte QDs beobachtet werden kann. Bemerkenswerterweise treten hierbei die superradianten Signaturen nicht in einem optischen Emissionsprofil sondern in elektrischen Tunnelströmen auf. Diese weisen in

Analogie zum optischen Fall eine deutliche charakteristische Intensitätsspitze auf. In diesem Zusammenhang entwickeln wir einen mathematischen Rahmen zur Behandlung von elektronischen Transport in der Anwesenheit von Hyperfeinkopplungen. Aufbauend auf der Erkenntnis, dass Kohärenz in der transienten Evolution von Ein-Photonen Emittenten erwachsen kann, untersuchen wir dann das stationäre Verhalten eines getriebenen Zentralspin Modells unter optischem Pumpen. Wir entwickeln diverse theoretische Methoden, die eine vollständige Beschreibung des Phasendiagramms ermöglichen, welches verschiedenste Quanteneffekte aufweist, wie z. B. Phasenübergänge erster und zweiter Ordnung, sowie Regionen von Bistabilität, Squeezing und geänderter Spin-Pumpdynamik. Schließlich, im letzten Teil der Dissertation, entwickeln wir ein analytisches Werkzeug zur formalisierten adiabatischen Elimination von schnell rotierenden Freiheitsgraden in offenen Systemen. Es stellt eine Verallgemeinerung der sogenannten Schrieffer-Wolff Methode dar und schließt eine Lücke in dem theoretischen Werkzeugkasten zur Beschreibung offener Systeme.

# Contents

# Publications

1. **Superradiance-like Electron Transport through a Quantum Dot**

   *M. J. A. Schuetz, E. M. Kessler, J. I. Cirac, and G. Giedke*

   Physical Review B **86**, 085322 (2012)

   Acronym: "SET"

2. **Generalized Schrieffer-Wolff Formalism for Dissipative Systems**

   *E. M. Kessler*

   Physical Review A **86**, 012126 (2012)

   Acronym: "GSW"

3. **Dissipative Phase Transition in a Central Spin System**

   *E. M. Kessler, G. Giedke, A. Imamoglu, S. F. Yelin, M. D. Lukin, and J. I. Cirac*

   Physical Review A **86**, 012116 (2012)

   Acronym: "DPT"

4. **Nuclear Spin Cooling using Overhauser-Field Selective Coherent Population Trapping**

   *M. Issler, E. M. Kessler, G. Giedke, S. F. Yelin, J. I. Cirac, M. D. Lukin, and A. Imamoglu*

   Physical Review Letters **105**, 267202 (2010)

   Acronym: "OSCPT"

5. **Superradiance from Nuclear Spin Environment of Single-Photon Emitters**

   *E. M. Kessler, S. F. Yelin, M. D. Lukin, J. I. Cirac, and G. Giedke*

   Physical Review Letters **104**, 143601(2010)

   Acronym: "OSR"

# Chapter 0

# Introduction

> We are currently in the midst of a second quantum revolution. While the first revolution gave us laws for understanding physical reality at very small scales, the second revolution will take these rules and develop new technologies.[1]
>
> *G. J. Milburn*

Since its theoretical beginnings in the early twentieth century, quantum physics has come a long way. With the advent of more and more sophisticated theoretical and experimental techniques over the last decades, formerly purely theoretical concepts of quantum mechanics became accessible in the laboratory. This astonishing technological advancement promoted quantum physics from a purely fundamental discipline, to a field that nowadays faces the beginning of its technological and economical exploitation. One of the first examples of a quantum mechanical technology is the laser, which was developed in the 1950's [2, 3]. This milestone marks the first exploitation of man-made quantum coherence in history, creating a new technology which in the following decades would find its way into manifold application areas and change the face of science and technology sustainably. Other novel technologies based on quantum phenomena are at different early stages of their development cycle, and bear the potential to revolutionize such disparate fields as telecommunication [4, 5], cryptography [6, 7, 8], computation [9, 10] and metrology [11, 12, 13], just to name a few. As in the example of the laser, a break-through in any of those technologies holds promise to have beneficial effects far beyond their respective field, coinciding with a great socio-economic impact.

Against this background, most diverse areas of research, from semiconductor physics to cold atoms, are driven by a shared goal: to understand and harness *quantum coherence*, which is the underlying property defining the power of these novel quantum devices and technologies.

In the following we outline the research topics of this Thesis in relation to the state of the art in the respective fields. In Section 0.1 we shed light on the ambiguous relation between quantum coherence and dissipation. At the concrete examples of quantum information processing and dissipative phase transitions, which are highly relevant for our work, we discuss how dissipation can be both the obstacle to overcome, and the driving force behind the emergence of coherence. This Thesis investigates aspects of these fields in nanoscopic solid-state quantum systems, namely quantum dots (QDs) and Nitrogen-Vacancy (NV) centers. Section 0.2 carefully introduces these physical systems and gives an overview of the state of the art. Thereafter, in

Section 0.3, we present an overview of the research results of this work.

## 0.1 Quantum coherence and dissipation: obstacle or virtue?

In classical physics, coherence is the property of a wave that enables the occurrence of interference effects. In analogy, quantum coherence is defined as the potential of the probability amplitudes of a quantum state to interfere [14]. As such, it is a necessary prerequisite for quantum phenomena to appear. Since the early days of quantum mechanics, it has been known that coherent behavior does not exclusively occur under isolated conditions, but also – under certain circumstances – in the dissipative coupling to a bath. The most prominent example is the emergence of coherent radiation in lasing, rooted in the quantum phenomena of *stimulated emission* [15]. In analogy, the phenomenon of *superradiance*, first predicted by Dicke in the 1950's [16], demonstrates that coherence may also arise in *spontaneous emission*. In the generic situation described by Dicke, an ensemble of atoms couples collectively to a mode of the electromagnetic field: For sufficiently small spatial dimensions of the atomic cloud the individual atoms are indiscernible at the relevant transition wavelength, causing a coherent and permutationally symmetric de-excitation of an initially population-inverted ensemble. The most prominent feature of this coherent quantum effect is a characteristic intensity burst which scales linearly with the number of particles [17]. As we outline in detail below, Chapters 3 and 4 of this Thesis are devoted to put forward and analyze an analogous coherent effect in the de-excitation of nuclear spin environment of nanoscopic quantum systems such as QDs or NV centers.

Despite these early examples of quantum coherence under open-system conditions, for a long time the consensus in the community became that more pronounced quantum phenomena are rooted in a better isolation from the environment, in order to protect initially prepared coherence [18, 19, 20]. Dissipation was almost exclusively considered as the mechanism, which corrupts useful quantum properties of a state, such as entanglement, and consequently the main focus was to develop increasingly sophisticated mechanisms to isolate quantum systems from any environmental influences.

Yet, this conviction began to falter with the advent of novel techniques, such as the engineering of dissipation [21], and the better understanding of coherent open-system quantum phenomena. Nowadays, a paradigm shift can be observed in quantum physics. More and more examples are discovered where dissipation is not the obstacle to overcome, but the driving force behind the emergence of coherent quantum phenomena. These novel approaches aim at utilizing dissipative processes, both natural and engineered, to create and harness quantum coherence. For instance, theoretical and experimental works put forward their use for quantum state preparation [22, 23, 24, 25, 26, 27, 28, 29, 30, 31], quantum computation [32], quantum memories and error correction [33, 34], as well as for open-system quantum simulators [35, 36]. Since they operate in the steady state of the dynamics, all these *dissipative gadgets* offer the intriguing advantage of an increased robustness in the presence of noise. For example, in the case of quantum state engineering, the system is actively pumped into a (for instance highly entangled) steady state, with a rate that is typically much higher than the decoherence rate induced by the inevitable environmental exchange. This gives rise to the possibility of a robust and long-lasting creation of entanglement or other useful quantum properties [22, 32].

The present Thesis aims to contribute to both of the above research lines. On the one hand, we propose a novel scheme to enhance the coherence times of solid state qubits for *quantum*

*information processing* (Chapter 1). On the other hand, we demonstrate in the second block of this Thesis (Chapter 2 - 4) how dissipation in nanoscopic solid-state systems can lead to *coherent many-body phenomena* in the context of superradiance and dissipative phase transitions. In the following we provide a brief overview of this two research areas, tailored to the objectives of this Thesis.

### 0.1.1 Quantum information processing: Protection from environment

> “Quantum computation is a distinctively new way of harnessing nature. [37]” *D. Deutsch*

The field of quantum information science recently celebrated its thirtieth anniversary. In 1981, Richard Feynman for the first time formulated the idea, that a device operating on the laws of quantum mechanics could potentially outperform classical devices. In his talk at the First Conference on the Physics of Computation, held at the Massachusetts Institute of Technology in May, he pointed out the apparent impossibility to efficiently simulate a generic quantum system on a classical device. The reason lies in the exponential growth of the dimension of the Hilbert space with the particle number: Already the description of a quantum system composed of only about 50 spins is practically impossible, and the description of 300 would requires the simulation of more classical dimensions than there are particles in the universe. Yet, in the same talk Feynman presented an ingenious solution to this problem [38]. If the device which simulates the quantum system operates according at laws of quantum mechanics itself, an efficient simulation should be possible[1]. The idea of a *quantum simulator* was born. Three years later this idea was generalized in a seminal work by David Deutsch [39], where he first introduced the idea of a *universal quantum computer*, as a generalization of the classical Turing machine.

At the time that these new ideas were developed, they were mostly considered as purely theoretical constructs designed to address conceptual questions in computer science, but without real world applications in sight. It took another nine years until the field gathered momentum. In 1994, Shor presented the first quantum algorithm, which demonstrated that quantum computers can outperform all known classical algorithms in specific tasks. Using this algorithm, a quantum computer can factorize large numbers efficiently (i.e., in polynomial time), whereas any known classical algorithm requires exponential time. Less than one year after the milestone of the first quantum algorithm was achieved, the first proposal for an actual physical realization of a quantum computer was released [40]. This widely celebrated model envisaged the use of trapped ions as the elementary building block (qubits) of a quantum computer and demonstrated how the necessary two-qubit operations can be realized in this system. The experimental proof of principle of this concept, followed only a few month later [41]. These two seminal works elevated the concept of quantum computation from the realm of abstract theoretical computer science to a physical device with real world applications and the potential of an experimental realization in the medium-term. It was the starting signal for a breathtaking development in the field. Numerous theoretical and experimental groups all over the world attended to the fundamental questions of quantum computation and the physical realization of building blocks of

[1] Efficient in this context means that the employed resources (e.g., the operation time or the size of the computation device) do not grow faster than polynomially with the number of particles to be simulated (size of the input).

quantum computers, and turned the field of quantum information in the vibrant and significant area of research it is nowadays (see [42] for a recent review).

Apart from the original model of circuit quantum computation, in which (in analogy to classical computers) calculations are performed sequentially according to an algorithm, a number of alternative schemes have been developed over the years. The most relevant models are measurement-based [43], adiabatic [44], and topological quantum computation [45], all of which were shown to be universal but featuring different advantages and disadvantages. Besides the ambitious goal to construct a full-fledged universal quantum computer, many groups devoted their work to develop less general quantum devices designed to address more specific tasks resulting, for instance, in the concept of quantum annealing [46, 10], but also in the advancement of the field of quantum simulation[2] [47].

Just like the various models for quantum computation, countless physical systems have been put forward for the implementation of the elementary building blocks, the qubits. Up to this date, it is by no means decided, which system is the most promising one and most likely in the future there will be a coexistence of several physical systems for different tasks in quantum information processing. While the first proposal in form of the trapped ion quantum computer [40] originated from the field of atomic physics, also many solid-state systems have been proposed in the past, such as phosphor donors in silicon [48], superconducting circuits [49], and – in the focus of this Thesis – the promising systems of self-assembled or electrically defined QDs [50, 51], and NV centers in diamond [52]. The state of the art for the latter two will be discussed in detail in this Introduction in Section 0.2.1 and 0.2.2, respectively. All of the proposed solid-state systems share the advantage that they hold promise for an "on-chip" realization of quantum computation devices, bearing the potential to facilitate the up-scaling of proof-of-principle setups towards working devices. Hereby, the community profits from the experience of half a century of industrial semiconductor manufacturing.

The strongest adversary in quantum information science, and the solid-state section in particular, is *decoherence*, which arises from the inevitable coupling of quantum systems to their environment. The induced dissipation tends to corrupt and wash out the quantum properties that give rise to the power of quantum computation and simulation. A key idea in this context was presented simultaneously by Shor and Steane in 1996 [53, 54, 55]: Fault-tolerant quantum error correction. They showed that if the decoherence rate per qubit and qubit-operation is below a certain threshold, it is possible to correct for the erroneous evolution in a fault tolerant way (i.e., taking into account, that the corrective operations themselves introduce additional noise in the system). This, in principle, demonstrated that quantum computation in the presence of noise is feasible. Over the years, improved error correction schemes (such as the surface code [56, 57, 58, 59]) have been developed, shifting the threshold to more realistic values [57], but still it is a great challenge in the community to protect the quantum coherence of qubit systems against the malicious influence of the environment. This Thesis contributes to this mission by proposing a novel scheme to prepare the nuclear spin environment of QDs and NV centers in a state, which minimizes decoherence of the quantum information carried by the electronic spin in these systems (Chapter 1).

The second research line of this work is dedicated not to the protection of coherence from dissipation, but, in contrast, to the emergence of coherence from dissipation itself. In the following Section, we explain at the example of dissipative phase transitions, how coherent behavior

[2] Note that, a universal quantum computer is also a universal quantum simulator.

can emerge from the dissipative evolution in open systems, and we we introduce the topical background needed in the remainder of this Thesis.

### 0.1.2 Coherent many-body phenomena: Harnessing the environment

> “It would indeed be remarkable if nature fortified herself against further advances in knowledge behind the analytical difficulties of the many-body problem. [60]” *M. Born*

A system composed out of many simple constituents, whose interactions and dynamics are governed by simple rules can engender highly complex phenomena. All complex pattern in nature, like molecules, materials and ultimately life itself arise from elementary particles and the simple rules of quantum mechanics. This fundamental principle of nature is called *emergence* (e.g., see [61]), and has vast implications for science in general and physics in particular. Although we have a deep understanding of the microscopic laws and particles, the understanding of the macroscopic behavior of an ensemble in a bottom-up approach is a tremendously difficult task, as Max Born underlines the above quote from 1960. The discipline dedicated to this quest is *many-body theory*, and it has developed a series of powerful (mostly perturbative) tools to tackle the difficulties arising in the description of large ensembles and their complex behavior. These theoretical methods – such as various mean field strategies, Green's function and Monte Carlo approaches and density functional theory, just to name a few [62] – were successfully used to develop a deep understanding of many interesting quantum many-body phenomena. They enabled the development of a comprehensive theory of critical phenomena in the solid state [63], and perhaps most prominently, allowed the derivation of a theory explaining the intriguing phenomenon of superconductivity [64].

Superconductivity is an example for an *equilibrium phase transition*, which are at the heart of the most intriguing coherent phenomena in many-body physics. A particular kind of phase transition occurs at zero temperature: In this case, the quantum system is described by its ground state wave function, which depends on a set of external parameters (e.g., magnetic fields, defect density, anisotropy). Any structural change of the ground state wave function at some critical point in the parameter space defines a so-called quantum phase transition (QPT) [65, 66]. In contrast to the finite temperature case, at these quantum critical points the transition between two phases is driven by quantum fluctuations instead of thermal ones. The well-established theory of QPTs allows for a rigorous classification of different types of transitions and has enabled a series of intriguing theoretical results about the nature of criticality in quantum systems. Perhaps most striking is the concept of universality [67]. It was shown that the functional dependence of central system properties close to a critical point do not depend on the specific microscopic details of the system's Hamiltonian, but rather on macroscopic properties like dimensionality and symmetry. Accordingly, all QPTs appearing in nature can be grouped into just a few so-called universality-classes, which represent a powerful tool for investigating complex many-body systems. QPTs have been a subject of intensive research in the past forty years, and their implications for contemporary physics are far too ample to be listed here exhaustively. For instance, they are at the core of some of the most intriguing low-temperature quantum phenomena of the past decades, such as the superfluid to Mott-insulator transition in systems of bosonic atoms at nanokelvin temperatures [68], and the Bose-Einstein

condensation [69], the experimental realization of which [70, 71] was awarded with the Nobel price in physics in 2001. QPTs are further believed to give rise to novel exotic states of matter with desired properties, such as topologically ordered states [72] and quantum spin liquids [73], and are essential to understand the phenomena of superconductivity [64], -fluidity [74, 75], and -solidity [76]. However, phase transitions do not exclusively occur in thermal equilibrium. Also in non-equilibrium situations, where the system's coupling to the environment does not lead to thermalization, highly coherent many-body phenomena and quantum phase transitions can occur [77, 78, 79, 80, 29, 81]. With the advent of new theoretical and experimental techniques – such as the concept of engineered dissipation described above – these dissipative (quantum[3]) phase transitions (DPTs) increasingly moved into the focus of the community. They hold promise of a real time, non-destructive examination of critical quantum phenomena, due to the typically strong exchange with the environment [83]. Further, it has been shown that some phases in these systems display distinct and potentially useful properties, such as, for instance, long-range order, multipartite entanglement, squeezing and supercriticality [22, 29, 80, 84, 79]. The deeper understanding of DPTs paves the way to a (dissipative) preparation of intriguing, highly correlated many-body quantum states, which are robust under other (malicious) influences of the environment.

The theory of DPTs in many respects parallels the considerations in the context of QPTs. Here, the system is described by the (generally mixed) steady state, and non-analytic changes in the steady-state properties indicate a phase transition. The occurrence of dissipative critical phenomena and the classification of different transitions have recently been connected to the low-excitation spectrum of the Liouville operator describing the system dynamics [79, 25]. However, the theory of DPTs is far less developed than its equilibrium counterpart and only a few model systems for DPTs are known. Important questions concerning the rigorous classification of transitions and the existence of a concept of universality are yet unanswered.

This Thesis makes a contribution to this research field under several aspects. First, we show in Chapters 2 and 3, that under realistic conditions a highly coherent, superradiant-like evolution can take place in the nuclear spin ensemble of semiconductor nanostructures. The insight that here coherent many-body effects naturally occur under open-system conditions stimulates the investigation of the steady-state behavior under resonant driving conditions in these systems. Chapter 4 is dedicated to the investigation of a class of first- and second-order DPT's and a variety of associated coherent effects like steady-state squeezing, bistabilities and supercriticality. Finally, in Chapter 5, we present in detail a formalized perturbative tool which we developed for the adiabatic elimination of fast degrees of freedom in open systems. Formulated in the language of a generalized Schrieffer-Wolff transformation, it has proven to be a powerful tool in the description of open many-body systems and it fills a gap in the theoretical toolbox for open systems.

Before we describe the research objectives of this Thesis in greater detail in Section 0.3, in the following Section we present the theoretical background of the physical systems in the focus of this Thesis; their importance and prospects in the field of quantum physics, as well as the experimental state of the art.

[3] In the following we will only discuss dissipative phase transitions in quantum systems. Classical dissipative phase transitions are not subject of this work [82].

## 0.2 Nanoscopic solid-state quantum systems

> When we get to the very, very small world we have a lot of new things that would happen that represent completely new opportunities for design. Atoms on a small scale behave like nothing on a large scale, for they satisfy the laws of quantum mechanics. So, as we go down and fiddle around with the atoms down there, we are working with different laws, and we can expect to do different things. [85]
>
> *Richard Feynman*

In his visionary presentation "There's plenty of room at the bottom" at the America Physical Society meeting 1959 [85], Richard Feynman anticipated the great technological opportunities that quantum mechanics can offer at the atomic scale. While the idea of nanoscopic devices operating at the laws of quantum mechanics were a vision at the time, the technological development of the past few decades have brought these ideas to reality. Nowadays, single atoms or ions are routinely controlled in the laboratory and the direct observation of intriguing quantum effects have become part of the scientific daily life. Technological advances in semiconductor- and nano-technology enabled the creation of "artificial atoms", solid-state devices which behave like single particles (i.e., according to quantum mechanics). They offer the great advantage to realize on-chip quantum devices, avoiding the experimental difficulties of trapping and addressing single atoms or ions, and holding promise of an automatized large-scale manufacturing, while profiting from the experience of the existing powerful semiconductor industry. In this Section, we will review the development which two of these systems, namely QDs and NV centers, have experienced in the past 20 years and discuss their future prospects.

### 0.2.1 Quantum Dots

Quantum dots are nanoscopic semiconductor heterostructures, which confine electrons or holes in three spatial dimensions. Due to this confinement of the order of the particle's wavelength their energy spectrum is quantized,[4] which gave rise to their informal name "artificial atoms" [86]. There are numerous possibilities known to achieve such a confinement [87]. In this Section, we will present the two arguably most promising and important ones, self-assembled (SA), and lateral or electrically-defined (ED) QDs, which are also in the focus of the present Thesis. SAQDs are created by a random semiconductor growth process. When a material is grown on the surface of a second material with deviating lattice constant (e.g., by molecular beam epitaxy [88]), it may occur that after a critical thickness, the material spontaneously rearranges by forming randomly distributed islands, minimizing the surface energy. The most common example of this phenomenon is the growth of InGaAs on a GaAs substrate. These islands typically are lens-shaped with heights of $\sim 5$ nm in the growth direction and a diameter of about 20 nm. They can subsequently be covered by an additional layer of GaAs and form the QDs, which confine the carriers due to an energy mismatch in the valence and conduction band of the two materials. Most importantly, this particular band structure across the QD gives rise to a confinement of both electrons and holes (positively charged quasiparticles, describing missing

[4] Throughout this Thesis, we will only consider the motional ground state of the carriers. Higher excitation have a very large energy, due to the narrow confinement.

electrons in the otherwise filled valence band). This allows for the optical creation of localized electron-hole pairs, by promoting electrons from the valence to the conduction band under incident laser light [89]. This mechanism allows for accurate and fast optical control of the electron degrees of freedom, demonstrated in many experiments (e.g., [51] and references therein).

The second category under consideration, EDQDs, starts from similar layered semiconductor heterostructures, where the self-relaxation mechanism via droplet formation has not occurred. The resulting so-called quantum well (for instance a thin GaAs layer on a AlGaAs substrate with very good lattice matching), realizes a narrow confining potential for electrons and holes in the growth direction. Optical excitation, current injection or doping leads to the formation of a two-dimensional electron or hole gas (2DEG, 2DHG), respectively. Lithographically-defined metal contacts (Schottky contacts) on top of the quantum well allow to establish confinement also in the third, i.e., lateral direction, creating quasi two-dimensional QDs with typical diameters of about 100 nm. Due to the opposite electrical charges of electrons and holes, an electrostatic trapping potential for electrons acts repulsively on holes, and vice versa. Therefore, in contrast to SAQDs, there is no stable optical excitation, since the created electron hole pairs in the material are being pulled apart by the electrostatic potential. Consequently, these systems lack the optical controllability of the electron degrees of freedom, and typically rely on electrically controlled qubit rotations, which are typically several orders of magnitude slower than their optical counterparts (An up-to-date comparison of typical operation times, decoherence rates, etc. in QD systems can be found in [90]).

A second important difference arises from the fact that the electrical confinement is typically much weaker than the confinement arising from band structure mismatches. Therefore, SAQDs are typically operational at temperatures around 4K, the boiling temperature of $^4$He, while EDQDs require temperatures well below 1K. Despite these apparent disadvantages of EDQDs, with regard to quantum computation they offer the great advantage that large arrays can in principle be manufactured with high accuracy, holding promise of a scalable approach to quantum computation. SAQDs in contrast are created by a random self-organization process (discussed above), which complicates the realization of a scalable computation architecture. This beneficial property was first pointed out in the Loss & DiVincenzo quantum computer proposal from 1998 [50]. They suggested to use the electron spin states of singly charged EDQDs to encode quantum information. Two-qubit interactions were envisaged to be realized by gate voltage control, changing the position of the individual spins and giving rise to a time-dependent, controllable Heisenberg exchange interaction between neighboring spins. Nowadays, all important building blocks of the proposal have been demonstrated in proof-of-principle experiments, such as initialization of the qubit, single-shot electrical read-out of spin states (realized by spin-to-charge conversion) [91], the coherent control of single spins [92] and two-qubit gates between two electron spins in a double dot system [93].

Only one year after the DiVincenzo proposal, the first quantum computation proposal for SAQDs appeared [94]. It relies on the coupling of the optically active QD transition to an high-finesse cavity mode (successfully realized in 2005 [95, 96]), which mediates a long-range interaction between remote quantum dots. Harnessing the optical addressability with almost hard selection rules [97, 98], the proposal is all optical, and single-qubit gates can be performed on a picosecond timescale using ultra-short laser pulses [99, 100]. Electrons [101] (and holes [102]) can be initialized with $\geq 99\%$ fidelity. However, although the coupling of single SAQDs to optical high-finesse cavities has been demonstrated [95, 96], and the mutual coupling of two

remote SAQDs via a photonic crystal cavity has been shown in 2010 [103], the realization of a two-qubit gate between remote dots as envisaged in the original proposal, has not been achieved up to this date.

The biggest obstacle to overcome towards a quantum computation architecture is the decoherence of the electron spin degrees of freedom due to the hyperfine interaction with the nuclear ensemble of the host material. The effect of the nuclear spins (about $10^4 - 10^6$ spins for typical GaAs QDs [98]) on the electron can be understood as an effective fluctuating magnetic quantum field, the so called Overhauser field (OF). For large external magnetic fields hyperfine-induced electron spin-flip processes are suppressed and the main effect of the OF is a broadening of the electron spin levels, which is the dominant decoherence mechanism in QD systems. It gives rise to the decoherence time $T_2$, which defines the time scale on which phase information of an individual electron spin state is washed out.

A common strategy to reduce the fluctuations in the nuclear OF is to polarize the nuclear spins using the isotropic hyperfine interaction with the electron spin and the optical, electrical, or magnetic control over the electron degrees of freedom (dynamical nuclear polarization, DNP). The different approaches and experimental results are far too numerous to list here exhaustively (for an recent extensive review, see [51]), but polarizations $50\% < p < 80\%$ can be achieved in state of the art experiments [104, 105]. However, since an improvement of decoherence time by a factor of ten, requires polarizations over $99\%$, DNP presently cannot significantly reduce decoherence of the electron spin.

A second attractive approach besides polarizing, is to narrow the nuclear spin distribution using indirect measurement [106, 107, 108], or intrinsic feedback mechanisms in DNP schemes [109, 110]. Along these lines, we propose in this Thesis a novel approach for the narrowing of the nuclear spin distribution in Chapter 1. It relies on a quantum interference effect in the optical absorption of the electronic system, which is sensitive to the nuclear OF and allows the preparation of sharp nuclear distributions, which significantly enhance the electronic decoherence time.

Aside the applied interest in DNP for the reduction of spin decoherence, this procedure is also interesting from a conceptual point of view. The intriguing interplay and feedback between the electron spin and the surrounding non-Markovian nuclear spin bath (realizing a so called central spin model [111, 98, 112]) gives rise to numerous intriguing open-system effects, like bistabilities, memory and dragging [113, 114, 115, 109, 116]. In Chapter 4, we study an open central spin model, and paint a complete picture of its rich steady state phase diagram. Amongst the many quantum effects we describe, we find phase transitions, bistabilities and hysteresis, under similar conditions like in [116]. Our work contributes to a deeper understanding of these non-linear effects in DNP, and predicts several coherent effects in these systems, like the emergence of regions of squeezing, supercriticality and altered spin pumping dynamics.

This brief overview shows that despite all difficulties, QDs are highly promising systems for the realization of quantum information tasks. At the time of the first proposal of spin based quantum computation, the experimental situation was not encouraging. But the theoretical and experimental developments in the field, have nowadays brought the realization of solid-state quantum information devices into reach (for an extensive review of the prospects of QD based quantum computation, see [90]). Besides these aspects, the many-body system comprising the coupled electron and nuclear spins, was show to display a variety of conceptually interesting quantum effects. The technological advancement of the field has by far not reached an end yet

and with the better control of the electronic and nuclear degrees of freedom exciting developments can be expected for the upcoming years.

### 0.2.2 Nitrogen-Vacancy centers

Diamond has a track record of extremes. It is one of the hardest materials in nature, its thermal conductivity is unmatched in the solid-state and its 5.5 eV band gap is amongst the largest appearing in nature. This large band gap and the purity of natural diamond crystals result in the extraordinary transparency over a large range of the optical spectrum. Over 100 optically active centers – irregularities or defects in the carbon lattice – are known in diamond, amongst them the so called Nitrogen-Vacancy (NV) center [117] which has attracted wide attention in the past years, due to its extraordinary quantum properties. Its optical transition (1.945 eV) being situated well within the diamond band gap, it features excellent optical properties and nearly perfect photostability [118].

The center consists of a nitrogen impurity next to a vacancy in the diamond carbon lattice [Fig. 1 a)]. The dangling electron bonds of the unpaired carbon and nitrogen atoms together with an additional electron (giving rise to a negative total charge of the center) form a stable multi-electron state located at the center. This electronic state behaves like a spin $S = 1$ particle with a narrow optical transition (The NV center is informally also referred to as "nature's own trapped ion"; for a review, see [119]). Its level scheme is displayed in Fig. 1 a): The optical

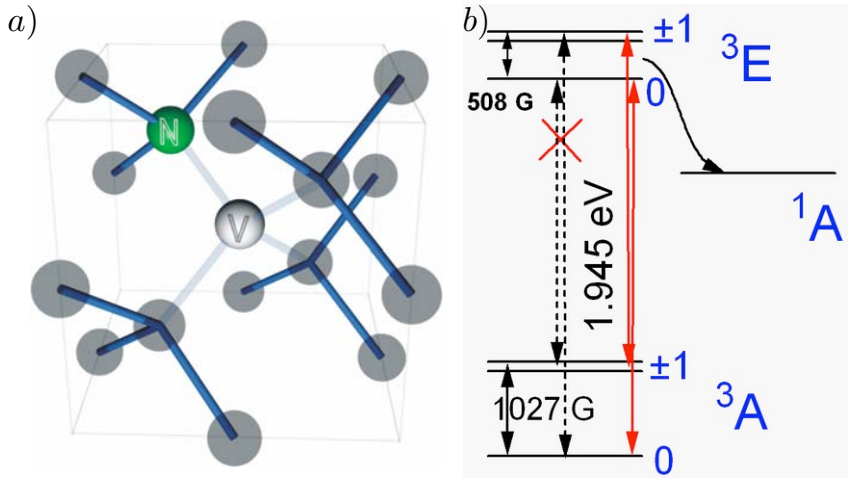


Figure 1: a) Schematic representation of an NV center in carbon matrix of diamond. Figure with courtesy taken from [119]. b) NV center level scheme with the relevant transitions. For strain-free NV centers at zero electric field, optical cycling transitions (red) are the only ones allowed by selection rules. Electrostatic fields mix excited state levels and allows for optical spin-flip (Raman) transitions (dashed).

ground state ($^3A$) is split into a paramagnetic spin triplet ($S = 1$) with a zero field splitting of about $D = 2.87$ GHz, due to the crystal anisotropy. While the level arrangement in the ground state is very robust, the exact energies of the excited state manifold ($^3E$) varies from center to center, due to local differences in the crystal field caused by strain [120, 121]. The latter also

defines the optical selection rules between the ground and excited states. For strain-free or quasi strain-free NV centers, the selection rules give rise to cycling transitions which conserve the spin quantum number [as is displayed in Fig. 1 b)]. However, strain electrostatic fields can introduce transition elements between different spin states (Raman transitions), such that external electric fields can be used to control the optical properties of a single center [120]. The excited state has a radiative lifetime of about $\tau = 13$ ns, which gives rise to the photoluminescence of the center under radiation with green laser light. A second, non-radiative decay channel via an additional singlet state ($^1A$), leads to incoherent transitions from the $m_S = \pm 1$ states to the $m_S = 0$ state. This simple mechanism allows for high-fidelity spin-state initialization via off-resonant laser pumping [122]. Besides, highly efficient read-out and coherent single spin manipulations using optical, and microwave fields have been demonstrated [123, 119, 122, 124, 125, 126].

The most remarkable features of NV centers are its striking coherence and optical properties even at room temperature. Coherence times of up to $T_2 > 600\mu s$ in high-purity diamond have been reported recently [127] without the use of additional decoupling schemes [128] which can further enhance these times (in comparison, typical coherence times in SAQDs are two orders of magnitude smaller and achieved at cryogenic temperatures). This holds promise of a room temperature realization of quantum devices, not only for quantum information processing [129, 130, 52], but also for high-precision in-vivo magnetometry [131, 132, 133].

Also for NV centers, the surrounding spin environment is, on the one hand, the main source of decoherence but, on the other hand, also adding richness to the system. In particular the nuclear $^{13}$C environment (with a natural abundance of about $1\%$) has been subject to intense research [134]. The coherent control of proximal nuclear spins via the NV center, and the state mapping from nuclear to electronic spins have been demonstrated already in 2006 [135]. Building on this achievement, the idea was developed to use proximal nuclear spins as quantum registers and exploit the extraordinary coherence times of nuclear spins in diamond [129]. This research line culminated in the recent demonstration of a diamond-based quantum memory system, which reached memory times of over 1s at room temperature [136].

Throughout this Thesis, NV centers and their small nuclear spin environment (typically only a few $^{13}$C spin are found in the vicinity of the center) will be used as clean and simple model systems to derive and test our ideas, for instance, in the case of superradiance (Chapter 2), or nuclear state preparation (Chapter 1). In the latter case the feasibility of our approach has recently been demonstrated in a proof-of-principle experiment using NV centers [137]. On the other hand, recent experimental advances, such as the manufacturing of diamond nano-crystals with a functionalized surface of nitroxide spin labels which contain single NV centers [138], realize large central spin systems like the one we study in Chapters 2 and 4.

## 0.3 Outline of this Thesis

Against the background described in the previous Sections, this Thesis pursues two seemingly contradictory goals. On the one hand, we develop novel schemes to protect coherence from dephasing through the environment. On the other hand, we investigate how coherent behavior can arise in open systems from particular dissipative interactions with the environment. These two research blocks are schematically depicted in Fig. 2 and will be explained in detail in the following.

In the first block of the Thesis (Chapter 1 [OSCPT]), we put forward a novel scheme to pro-

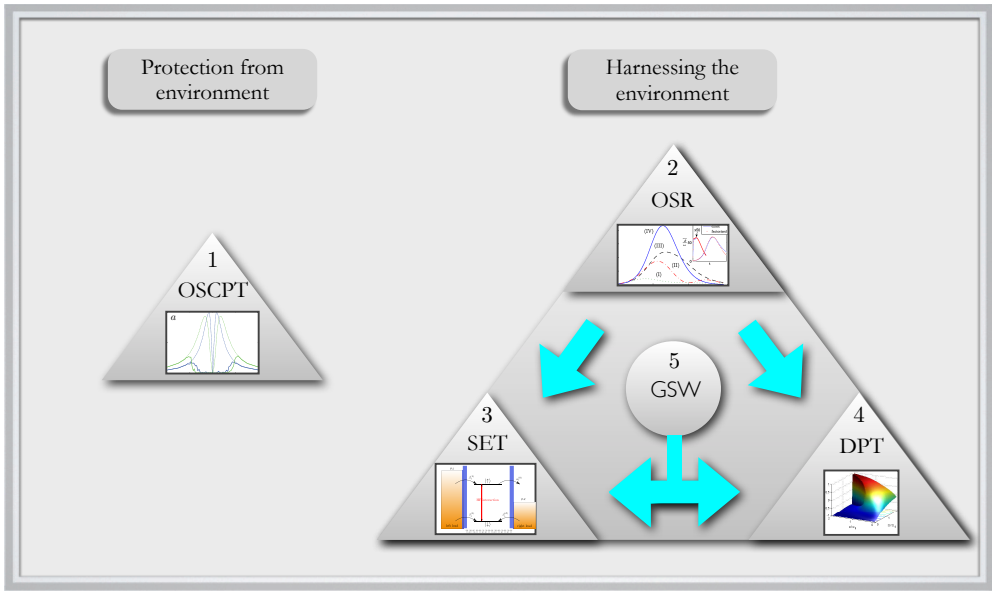


Figure 2: The research goals of this Thesis can be grouped into two blocks. The first research goal (Chapter 1 [OSCPT]) proposes a novel scheme to prepare the nuclear spin environment of QDs or NV centers in an inert state which minimizes its decohering influence on the electron spin. The second block aims at harnessing the dissipative coupling to the environment for the creation of coherence in the transient and steady-state behavior of nanoscopic solid-state systems. The individual projects and their mutual dependencies are displayed. In the first part (Chapter 2 [OSR]) we establish the pivot of this research block, the demonstration that superradiance, i.e. spontaneous emergence of coherence, can occur in the optical de-excitation of the nuclear ensemble of SAQDs and NV centers. Generalizing this insight, we show that a similar effect can also be observed in EDQDs in a transport setting (Chapter 3 [SET]). The signatures of coherence in the electronic current through the dot gives rise to the new paradigm of electronic superradiance. The superradiant evolution in central spin systems, motivates the investigation of coherent steady-state behavior. In Chapter 4 [DPT], we investigate dissipative phase transitions which arise from the superradiant dynamics in the long-time limit. We show analytically that the phase diagram comprises effects like first- and second-order phase transitions and regions of squeezing, bistability, and altered spin pumping dynamics. Finally, in Chapter 5 [GSW], we develop a powerful analytical tool for the adiabatic elimination of fast degrees of freedom, which enabled the derivation of the analytic results in the DPT and SET projects.

tect the spin coherence of the electron spin of SAQDs or NV centers from the dephasing influences of the surrounding nuclear spin environment. To this end, we propose an optical pumping mechanism related to a well known laser cooling technique, velocity selective coherent population trapping [139]. Coherent optical excitation of the electron leads to a random nuclear diffusion mechanism. Only for a specific, tunable value of the nuclear OF, a two-photon resonance condition is fulfilled which renders the system transparent (electrically induced transparency) causing the diffusion to come to rest. We show that this Overhauser-field-selective coherent population trapping mechanism (OSCPT) allows for a reduction of the OF fluctuations down to

the single-spin-flip level and a corresponding enhancement of the electronic coherence times by several orders of magnitude. Recently, the feasibility of this approach has been demonstrated in a proof-of-principle experiment in NV centers [137].

In the second block of this work, we turn to the question of how coherence in nuclear spin systems can arise from the dissipative coupling to the environment (cf. right hand side of Fig. 2). In Chapter 2 [OSR], we show that spontaneous emergence of coherence appears in the collective optical de-excitation of the nuclear ensemble in a superradiant-like evolution. Starting from an initially uncorrelated, highly polarized state, the nuclear system experiences a strong correlation build up, due to the collective nature of the coupling to the central electron spin. We show that under realistic experimental conditions, this results in a sudden intensity burst in the light scattered from the QD system, which exceeds the maximal emission intensity of a corresponding classical system by several orders of magnitude. The establishment of this connection between the fields quantum optics with atoms, where the effect of SR has been first described, and solid-state physics acts as a pivot for this research block.

Subsequently, in Chapter 3 [SET], we demonstrate that this mechanism can be generalized to EDQDs in a transport setting. Mapping quantum optical concepts to the realm of quantum electronics, we show that analogous superradiant signatures can be detected in the electronic tunneling current, giving rise to the new paradigm of electronic superradiance. To this end, we develop from first principles a master equation formalism for the description of the combined dynamics of electrons and nuclear spins in a transport setting.

Building on the insight that the nuclear spin pumping dynamics in QDs and NV centers are governed by collective interactions which give rise to coherent effects like superradiance, we investigate in Chapter 4 [DPT] the steady-state behavior of a similar central spin model under additional resonant driving. The rich steady-state phase diagram comprises a variety of intriguing quantum effects, including first- and second-order phase transitions, and regions of squeezing, bistability, supercriticality and altered spin-pumping dynamics. We develop a series of theoretical tools which enable a complete analytic description of the phase diagram. This analytic solution allows for deep insights into the nature of critical phenomena in open systems, and the establishment of general theoretical concepts in the theory of DPTs.

Finally, in Chapter 5 [GSW], we develop a theoretical tool for the adiabatic elimination of fast degrees of freedom in Markovian open systems. It generalized the celebrated method of the Schrieffer-Wolff transformation in Hamiltonian systems [140] to the non-hermitian case of Liouvillian operators and fills a gap in the theoretical description of open systems. Just like its Hamiltonian counterpart, it naturally allows for a systematic expansion in the adiabatic elimination and the derivation of higher-order corrections. This formalism proved its usefulness in the derivation of several analytical results in the course of the projects SET and DPT. Moreover, we exemplarily employ the formalism in two model systems, designed to illustrate its application and potential to facilitate the otherwise tedious derivation of higher-order corrections in the adiabatic elimination process.

# Chapter 1

# Nuclear Spin Cooling using Overhauser-Field Selective Coherent Population Trapping

**Hyperfine interactions with a nuclear spin environment fundamentally limit the coherence properties of confined electron spins in solid-state systems. In this Chapter, we show that a quantum interference effect in the optical absorption from two electronic spin states of a solid-state emitter can be used to prepare the surrounding environment of nuclear spins in well-defined states, thereby suppressing electronic spin dephasing. The evolution of the coupled electron-nuclei system into a coherent population trapping state by optical-excitation-induced nuclear spin diffusion can be described in terms of Lévy flights, in close analogy with sub-recoil laser cooling of atoms. The large difference in electronic and nuclear time scales simultaneously allows for a measurement of the magnetic field produced by nuclear spins, making it possible to turn off the lasers that cause the anomalous spin diffusion process when the strength of the resonance fluorescence reveals that the nuclear spins are in the desired narrow state with well defined z-component of the Overhauser field. This Chapter is based on Publication 4 [OSCPT].**

## 1.1 Introduction

The phenomenon of coherent population trapping (CPT) in three-level emitters [141] is at the heart of a number of key advances in quantum optics, such as sub-recoil cooling of atoms [139] and slow-light propagation [142, 143, 144]. In these experiments, optical excitation from two low energy (spin) states to a common optically excited state vanishes due to a quantum interference effect, leading to the formation of a *dark resonance* whenever the two driving laser fields satisfy the two-photon resonance condition. The fundamental limit on how well quantum interference eliminates optical absorption is provided by the decoherence rate of the two low-energy spin states. Typically, this decoherence rate is assumed to be induced by a reservoir which could be treated using the usual Born-Markov approximation, implying that the reservoir has a short correlation time and its density operator is not influenced by the interactions with the system.

Unlike their atomic counterparts, solid-state spins are in general subject to non-Markovian

dephasing [145, 146, 147] due to their coupling to reservoirs with long correlation times. In particular, hyperfine coupling to nuclear spins constitutes the most important source of decoherence for spin qubits. It has been proposed that polarizing or cooling nuclear spins could alleviate this decoherence process [145], which prompted theoretical [108, 107] as well as experimental efforts aimed at narrowing down the Overhauser field (OF) distribution [148, 110, 109]. These schemes could be considered as a form of *reservoir engineering*; remarkably, recent experiments showed that the substantial manipulation of the nuclear spins (reservoir) can be achieved by using the electron spin (system) itself [149, 150, 151, 110, 109, 152].

In this Chapter, we show that CPT in the spin states of a solid-state emitter could be used to prepare a nuclear-spin environment with ultranarrow OF distribution. This is achieved via anomalous diffusion processes associated with optical excitation [139]. As a con- sequence of the anomalous diffusion, the coupled electron-nuclei system dynamically switches back and forth between a trapped regime where nuclear-spin diffusion slows down drastically due to the formation of an electronic dark state, and a non-trapped regime where optical excitation leads to fast diffusion. When the coupled system is in the dark state, the nuclear-spin distribution has a standard deviation that is close to the single-spin limit. An additional feature of the scheme is the possibility of using the resonance fluorescence signal to verify the preparation of a narrow nuclear-spin distribution [153]. Turning off the laser fields after determining the coupled system to be in the dark state ensures that the OF distribution remains in the single-spin regime within time scales determined by the (intrinsic) nuclear-spin lifetime. The electron spin $T_2^*$ time is then prolonged by a factor $\sim \sqrt{N}$, where N is the number of nuclear spins. Remarkably, nuclear spins in the prepared state do not evolve due to electron-mediated indirect interactions, eliminating a principal contribution to electron spin $T_2$ time [146, 145].

## 1.2 Executive summary

This Chapter is organized as follows. We first start in Section 1.3 by introducing the physical model and describing the principal mechanism of Overhauser-field-selective coherent population trapping (OSCPT). We demonstrate that the optically-induced nuclear diffusion mechanism comes to rest only if the system is in an eigenstate of the *generalized Overhauser field*. This field contains besides the standard OF in $z$ direction a perturbative correction from the perpendicular nuclear fields, and is the true nuclear field seen by the electron up to second order. In the following Section 1.4, we explicitly derive a quantum master equation for the nuclear spin diffusion. From this equation we extract diffusion rates both in the semiclassical and quantum limit, which display a remarkable agreement. Further, we demonstrate that the proposed mechanism can in principle achieve a reduction of the OF fluctuations down to the single-spin-flip level in the absence of spurious nuclear processes which lead to optical-excitation-independent spin diffusion. The subsequent Section 1.5, confirms these results in semiclassical simulations, and discusses how the mechanism accounts for the appearance of a large transparency window in CPT experiments: The nuclear field actively finds a configuration to restore two-photon resonance, which turns the electronic system transparent. The nuclear diffusion process accounting for this effect is undirected and shows characteristics of stochastic Lévy processes. Consequently, in Section 1.6, we analyze the nuclear dynamics using a Lévy-flights analysis. We discuss the different time scales that arise due to this random diffusion process, and introduce the concept of a *trapping* and *recycling region* in the space of nuclear OFs. We find that,

even taking into account other optical-excitation-independent nuclear diffusion processes, the nuclear distribution can be narrowed significantly, and we discuss the possibility to use feedback mechanisms in order to prepare the value of the nuclear field near-deterministically. We close with a discussion of the experimental feasibility, which recently has been demonstrated in a proof-of-principle experiment [137].

While we refrained from the exact derivation of the key equations in the main text, this theoretical background is provided in the supplementary material 1.A. In Appendix 1.A.1, we provide a detailed derivation of the central Master Eqn. (1.2). We carefully exert the perturbative approach using a Schrieffer-Wolff transformation, and discuss the validity of neglecting higher-order corrections. In Appendix 1.A.2, we discuss extensively the effect of a potential inhomogeneous Zeeman term with regard to the presented scheme, and we show that under minor restrictions the conclusions remain unchanged. Thereafter, in Appendix 1.A.3 we discuss the key concept of the generalized Overhauser field in greater detail. Employing Monte Carlo techniques, we demonstrate that this operator fulfills all the properties for the OSCPT scheme to work. Finally, in the last Appendix 1.A.4, we provide the detailed theoretical background for the semiclassical simulations of Section 1.5.

## 1.3 Nuclear-spin selective coherent population trapping

We consider a solid-state emitter (such as a QD or NV center) where the two ground electronic spin states, denoted by $|\uparrow\rangle$ and $|\downarrow\rangle$, are coupled by two laser fields to a common optically excited state $|t\rangle$ (Fig. 1.1 a). The laser field with frequency $\omega_p$ ($\omega_c$) that couples the $|\uparrow\rangle \leftrightarrow |t\rangle$ ($|\downarrow\rangle \leftrightarrow |t\rangle$) transition with Rabi frequency $\Omega_p$ ($\Omega_c$) is referred to as the probe (coupling) field. The state $|t\rangle$ decays in turn via spontaneous emission back to the two ground spin states with an (for simplicity) equal rate $\Gamma_{t\uparrow} = \Gamma_{t\downarrow} \equiv \Gamma/2$. Denoting the Zeeman energy of the electron spin due to the external field $B_z$ with $\omega_z$ and the energy of the optically excited state with $\omega_t$, we express the bare optical detunings relevant for the CPT system as $\Delta\omega_p = -\omega_p + (\omega_t + \omega_z/2)$ and $\Delta\omega_c = -\omega_c + (\omega_t - \omega_z/2)$. In the absence of any spin interactions or decoherence, laser fields satisfying the two-photon resonance condition ($\delta = \Delta\omega_p - \Delta\omega_c = 0$) pump the electron spin into the dark state $|D\rangle = \frac{\Omega_c}{\sqrt{\Omega_p^2+\Omega_c^2}}\,|\uparrow\rangle - \frac{\Omega_p}{\sqrt{\Omega_p^2+\Omega_c^2}}\,|\downarrow\rangle$, which is decoupled from optical excitation. If $\Delta\omega_c = 0$ and $\Omega_p, \Omega_c \ll \Gamma$, the absorption lineshape of the emitter appears as a Lorentzian with a quantum interference induced transparency dip in the center, with a width $\delta\nu_{\text{trans}} \sim (\Omega_p^2 + \Omega_c^2)/\Gamma \ll \Gamma$.

In practice, the electronic spin states of most solid-state emitters are mutually coupled via hyperfine interaction with a nuclear spin ensemble consisting of $N$ nuclei

$$H_{\text{hyp}} = g \sum_{i=1}^{N} g_i \left( \sigma_z^i S_z + \frac{1}{2}(\sigma_+^i S_- + \sigma_-^i S_+) \right) . \tag{1.1}$$

Here, $g_i$ defines the normalized hyperfine coupling constant between the emitter electron and the $i^{th}$ nucleus ($\sum g_i^2 = 1$). In this convention $g = A_H/\sum g_i$ quantifies the collective hyperfine coupling strength, with $A_H$ denoting the hyperfine interaction constant of the material. $S_\alpha$ and $\sigma_\alpha^i$ ($\alpha = +, -, x$) are the electronic and the $i$th nuclear spin operators, respectively.[1]

[1]For simplicity, in the remainder of this Chapter we assume nuclear spins $I = 1/2$. However, the scheme works in the same way for larger individual spins.

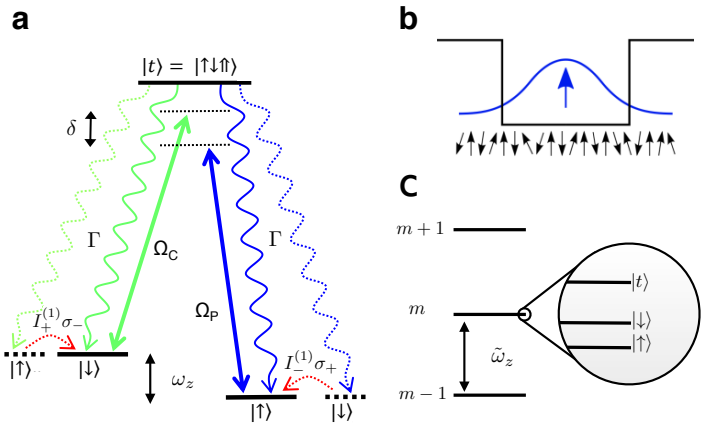


Figure 1.1: (a) Scheme of the electronic levels in the CPT setting. The dashed lines illustrate the hyperfine assisted decay processes, which are responsible for the nuclear spin diffusion in an optically active system. (b) The confined electron spin of the charged quantum dot interacts with a large nuclear spin bath ($N \sim 10^4 - 10^5$) via hyperfine contact interaction. (c) In a rotating frame that renders the Hamiltonian time-independent the spectrum of the diagonal part of the Hamiltonian splits into submanifolds, labelled by the nuclear quantum number $m$ (spin projection in $z$-direction), which consist of the three different electronic states (and further degenerate states due to nuclear total spin and permutation quantum numbers). The weak coupling between the different manifolds motivates a perturbative treatment which is described in detail in Appendix 1.A.1.

Our analysis of CPT in the presence of hyperfine interactions with a nuclear spin reservoir starts with the master equation, obtained by eliminating the radiation field reservoir using the standard Born-Markov approximation. In the limit of a large external field ($\omega_z \gg g$), the direct electron-nuclei flip-flop processes $I_+S_- + I_-S_+$ (collective spin operators are defined as $I_\alpha = \sum_i g_i \sigma_\alpha^i$) are strongly suppressed due to the large mismatch in the electronic and nuclear Zeeman splitting. In contrast, optical excitation does allow for energy conservation in an optically assisted electron-nuclear spin-flip process. We take these second-order processes into account by applying a Schrieffer Wolff transformation to eliminate the direct hyperfine flip-flop interaction in a systematic expansion in the small parameter $\epsilon = g/(2\omega_z)$. This procedure is explained in detail in Appendix 1.A.1. There we also consider in detail the effects of higher-order corrections and potential inhomogeneous nuclear Zeeman terms which are neglected during the following discussion. After these steps, the central master equation describing the OSCPT effect reads

$$\begin{aligned}\dot{\rho} &= \underbrace{\frac{\Gamma}{2}(\mathbb{1}_S \otimes \rho_{tt} - \{|t\rangle\langle t|, \rho\}_+) - i[H_{\text{laser}} + \tilde{H}_{\text{spin}}, \rho]}_{\mathcal{L}_0(\rho)} + \epsilon^2 \underbrace{\frac{\Gamma}{4}\mathbb{1}_S \otimes D(\rho_{tt})}_{\epsilon^2 \quad \mathcal{L}_1(\rho_{tt}),} \\ &= \end{aligned} \tag{1.2}$$

where $\rho_{tt} = \langle t|\rho|t\rangle$ acts on the Hilbert space of nuclear spins and $\mathbb{1}_S = |\uparrow\rangle\langle\uparrow| + |\downarrow\rangle\langle\downarrow|$. The first term proportional to $\Gamma$ describes the incoherent optical decay of the excited level $|t\rangle$, while

$H_{\text{laser}}$ describes the effect of the coherent laser driving. The second order term in $\epsilon$ containing

$$D(\rho) = I_+\rho I_- + I_-\rho I_+ - \frac{1}{2}\{I_+I_- + I_-I_+, \rho\}_+ \tag{1.3}$$

describes an optically-induced random nuclear diffusion process caused by the optically-assisted hyperfine flip-flop processes. We assume that in the absence of optical excitation, the electron spin is well isolated from all reservoirs other than the nuclear spins [101], and spin-flip co-tunneling or phonon emission rates are negligible within the time scales of interest. Further, in Eqn. (1.2) we neglect terms $\propto \epsilon^2$ that only affect the electron evolution. The latter, as well as higher-order corrections are discussed in Appendix 1.A.1.[2]

After the Schrieffer–Wolff transformation, the Hamiltonian relevant for electron spin dynamics (to highest order in $\epsilon$) is $\tilde{H}_{\text{spin}} = gS_z(I_z + \epsilon/2\{I_+, I_-\}_+ - \delta/g)$. The electron experiences an effective magnetic field, which is composed of the two-photon detuning $\delta$, as well as a contribution originating from the nuclei, which we refer to as the *generalized Overhauser field* (GOF): $\tilde{I}_z = I_z + \epsilon/2\{I_+, I_-\}_+$. The GOF is the true nuclear magnetic field experienced by the electron to first order in $\epsilon$, and as such it is the relevant quantity which determines the electron spin coherence time. For a given laser detuning $\delta$ each eigenvector of the GOF $\tilde{I}_z |\lambda\rangle = \lambda |\lambda\rangle$ corresponds to a steady state $\rho_\lambda = \rho^e(\lambda) \otimes |\lambda\rangle \langle\lambda|$ of the unperturbed evolution $\mathcal{L}_0(\rho_\lambda) = 0$. Here, $\rho^e(\lambda)$ is given as the solution of the optical Bloch equations (OBE) found after projection of the unperturbed master equation on the respective nuclear state $|\lambda\rangle$; in the OBE $\delta_{\text{eff}} = g\lambda - \delta$ gives the effective two-photon detuning that determines the CPT condition. The lifetime of such quasi-steady states $\rho_\lambda$ under the full dynamics of Eqn. (1.2) is determined by hyperfine assisted scattering events, which are described by the term $\mathcal{L}_1$. Each nuclear spin flip event of this kind changes $\langle\tilde{I}_z\rangle$ by a value of order $g_i$.

For nuclear states with $\delta_{\text{eff}} = 0$ the system is in two-photon resonance and the electronic system is transparent such that $\rho^e_{tt} = 0$: as a consequence, the nuclear spin diffusion vanishes and the system is trapped in a dark state. Since the GOF in an electronic–nuclear dark state is locked to a fixed value, its variance will be strongly reduced (nuclear state narrowing), suppressing the hyperfine-induced electron spin decoherence. Strikingly, by narrowing the GOF, even electron-mediated nuclear spin diffusion – which arises from the $\epsilon$ term in the GOF – is suppressed, thus eliminating the second-order contribution to hyperfine-induced electron spin decoherence as well. For all nuclear states satisfying $\delta_{\text{eff}} \approx 0$, the excited electronic state population scales as $\rho^e_{tt} \propto \delta^2_{\text{eff}}$, ensuring that the spin diffusion rate will remain vanishingly small: we refer to this subspace as the *trapping region*.

In contrast, nuclear states with $\delta_{\text{eff}} \not\approx 0$ render the electron optically active and the GOF experiences random diffusion (*recycling region*). To illustrate the dynamics allowing the nuclei to move from the recycling to the trapping region, we consider an electron that is optically excited to state $|t\rangle$: as it decays, it could induce a nuclear spin flip event in either direction with probability $\sim \epsilon^2$ [described by the term $\mathcal{L}_1$ in Eqn. (1.2)]. Through successive spin-flip events, the nuclear reservoir probes different spin configurations with distinct generalized Overhauser shifts. When the diffusion allows the nuclei to reach a configuration that yields $\delta_{\text{eff}} \approx 0$, the electron becomes trapped in the dark state; further optical excitation is then inhibited and nuclear spin flips are strongly suppressed.

[2] Contribution to the master equation arising from the Schrieffer–Wolff transformation applied to the laser coupling terms do not lead to terms of order $\epsilon$, provided that the laser polarizations match that of the corresponding optical transitions.

Owing to the quasi-continuous nature of the GOF spectrum (cf. Appendix 1.A.3), the dark-state condition $\delta_{\text{eff}} = 0$ can be satisfied for a wide range of initial detunings $\Delta\omega_p$. This leads to a drastic change in the CPT signature in absorption spectroscopy: instead of exhibiting a narrow transparency dip at (bare) two-photon-resonance ($\delta = 0$), the coupled electron-nuclei system displays a broad transparency window (cf. Section 1.5 and Fig. 1.3).

## 1.4 Nuclear spin dynamics

To capture the full quantum dynamics, we derive a master equation which depends only on nuclear degrees of freedom, allowing for both an analytical steady-state solution and the comparison between the quantum and the semiclassical limit. First, we eliminate the state $|t\rangle$ in the weak excitation limit $\Omega_p, \Omega_c \ll \Gamma$, to derive a master equation involving the nuclear and electronic spins only. For simplicity, we assume the external two-photon detuning $\delta = 0$ as well as $\Omega_c = \Omega_p = \Omega$, which ensures that the relevant dark and bright electron spin states in the rotating frame are states polarized in $\hat{x}$-direction $|D(B)\rangle = (|\uparrow\rangle - (+)\,|\downarrow\rangle)/\sqrt{2}$. A generalization to a finite detuning $\delta$ and arbitrary Rabi frequencies is straightforward, but offers no further insight. The adiabatic elimination of $|t\rangle$ from Eqn. (1.2) yields the reduced master equation

$$\begin{aligned}\dot{\rho} =&\Gamma_{\text{eff}}(S_-^x \rho S_+^x - \frac{1}{2}\{S_+^x S_-^x, \rho\}_+) \\ &+ \frac{\Gamma_{\text{eff}}}{2}[S_x,[S_x,\rho]] - ig\tilde{I}_z[S_z,\rho] \\ &+ \epsilon^2 \mathbb{1}_S \otimes D_1(\Gamma_{\text{eff}}\rho_{BB}),\end{aligned} \tag{1.4}$$

where $S_\pm^x$ are the electron spin flip operators in $\hat{x}$-basis ($S_-^x\,|B\rangle = |D\rangle$, $S_+^x\,|D\rangle = |B\rangle$) and $\Gamma_{\text{eff}} = \frac{\Omega^2}{(\Gamma/2)^2+(g\tilde{I}_z/2)^2}\frac{\Gamma}{2}$ is an operator valued effective (electron) spin decay rate. The last line of Eqn. (1.4) describes the nuclear spin diffusion determined by the nuclear operator proportional to the bright state population $\rho_{BB} = \langle B|\rho|B\rangle$[3].

In order to eliminate the electronic degrees of freedom from Eqn. (1.4), we use the fact that on the time scales of the electron evolution, the nuclear field can be considered as quasi-static and hence the electron settles quickly (on nuclear time scales) to its interim steady state. We find that on this coarse-grained time scale $\rho_{BB} = \frac{1}{2}[1 - (\frac{\Gamma_{\text{eff}}}{|\Delta_{\text{eff}}|})^2]\text{Tr}_S(\rho)$, with $\text{Tr}_S$ denoting the trace over electron spin and $|\Delta_{\text{eff}}|^2 = \Gamma_{\text{eff}}^2 + (g\tilde{I}_z)^2$. Using this relation, the electron spin can be eliminated from Eqn. (1.4), yielding a nuclear rate equation

$$\dot{\rho^n} = \text{Tr}_S(\dot{\rho}) = D(\Gamma_{\text{nuc}}\rho^n), \tag{1.5}$$

where we defined the state-dependent nuclear diffusion rate $\Gamma_{\text{nuc}} = \epsilon^2[1 - (\frac{\Gamma_{\text{eff}}}{|\Delta_{\text{eff}}|})^2]\Gamma_{\text{eff}}$. In concordance with the above considerations $\Gamma_{\text{nuc}}$ vanishes for all states in the kernel of $\tilde{I}_z$, i.e., states of zero GOF that fulfill the two-photon resonance condition are steady states of the dynamics. For large detunings ($\tilde{I}_z \sim 1$) the optically induced change of $\tilde{I}_z$ is of order

[3] For Eqn. (1.4) to generate a physical (completely positive) dynamics, $\tilde{I}_z$ must commute with $\rho$ at all times. This is ensured by Eqn. (1.4) (in the homogeneous case or in the semiclassical limit) provided it holds initially (e.g., for initially fully mixed nuclear spins).

$\frac{d}{dt}\mathrm{Tr}(\rho\tilde{I}_z) \sim \Gamma_{\mathrm{nuc}} N^{-1/2} \sim \epsilon^2 \frac{\Omega^2}{\Gamma}$ which provides the diffusion process driving the system into the dark state.

Equation (1.5) can be used to directly compare the quantum mechanical and semiclassical diffusion rates in the homogeneous limit ($g_i = 1/\sqrt{N}, \forall i$). For any eigenstate $|m\rangle$ of $\tilde{I}_z$ with $\tilde{I}_z |m\rangle = m/\sqrt{N} |m\rangle$ ($\Gamma_{\mathrm{nuc}} |m\rangle = \Gamma^m_{\mathrm{nuc}} |m\rangle$) the nuclear spin flip rate in negative (positive) direction is given by $D^- = \langle I_+ I_- \Gamma_{\mathrm{nuc}} \rangle_m$ ($D^+ = \langle I_- I_+ \Gamma_{\mathrm{nuc}} \rangle_m$). For simplicity, we will evaluate these expectation values for $I_z$ eigenstates and neglect the $\epsilon$ correction of the GOF. In the semiclassical limit under the assumption $\langle \sigma^i_+ \sigma^j_- \rangle = 0$ ($i \neq j$) the rates are simply given as $D^{\mp}_{sc} = (\frac{1}{2} \pm \frac{m}{N}) \Gamma^m_{\mathrm{nuc}}$. For the quantum description the characterization via the spin projection quantum number $m$ is not sufficient; the rates also depend on the symmetry of the nuclear state, quantified by the total spin $J \in \{0, ..., N/2\}$. For a Dicke state $|J, m\rangle$ the rates are given as $D^{\mp}_{qm} = \langle I_{\pm} I_{\mp} \Gamma_{\mathrm{nuc}} \rangle_{J,m} = \frac{1}{N} [J(J+1) - m(m \mp 1)] \Gamma^m_{\mathrm{nuc}}$. Surprisingly, the two opposite regimes of semiclassical and quantum mechanical description show both qualitative (evolution can be fully characterized by rate equations) and quantitative (for the relevant states the calculated rates are comparable) agreement [cf. Fig. 1.2 a]; this result is particularly interesting since we would expect the semiclassical description to fail in the homogeneous limit.

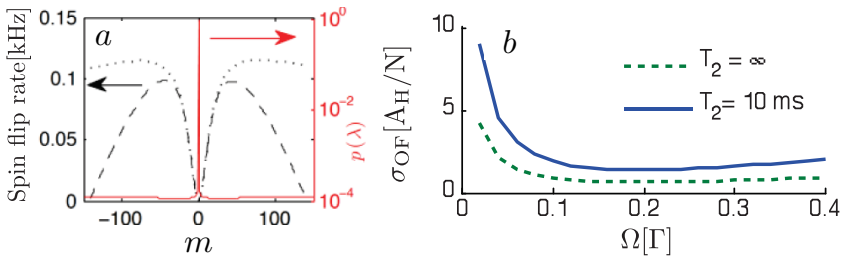


Figure 1.2: Nuclear spin diffusion rates depending on the nuclear spin projection $m$ assuming homogeneous coupling. Parameters are $N = 4 \times 10^4$, $\Gamma = 1$ GHz, $A_H = \omega_z = 100$ $\mu$eV, and $\Omega = \Omega_p = \Omega_c = 0.1$ GHz. The rates calculated using the quantum mechanical (for the subspace $J = \sqrt{N/2}$, dashed line) and the semiclassical (dotted line) descriptions show both qualitative and quantitative agreement. The solid (red) curve shows nuclear spin distribution for $\Omega = 0.02\ \Gamma$ and $T_2^{-1} = 100\ s^{-1}$. (b) The dependence of the steady-state OF standard deviation $\sigma_{\mathrm{OF}}$ as a function of $\Omega$ in the limit of homogeneous coupling; the solid (dashed) line is obtained by taking $T_2^{-1} = 100\ s^{-1}$ ($T_2^{-1} = 0\ s^{-1}$).

In order to calculate the achievable OF standard deviation $\sigma_{\mathrm{OF}}$ we numerically compute the exact steady-state solution of the full master equation before the Schrieffer Wolff approxiamtion [cf. Appendix 1.A.1 Eqn. (1.8)] for homogeneously coupled nuclei. To this end, we explicitly consider all orders of the hyperfine interaction including processes that result in a (small) finite decay rate out of the dark state[4]. Fig. 1.2 b shows $\sigma_{\mathrm{OF}}$ as a function of $\Omega$, where we find that $\sigma_{\mathrm{OF}}$ decreases with decreasing $\Omega$ until it reaches a minimum of $\sigma_{\mathrm{OF}} \simeq 2A_H/N$ ($\sigma_{\mathrm{OF}} \simeq 0.7 A_H/N$) for $\Omega \simeq 0.2\Gamma$ and an electron spin decoherence rate of $T_2^{-1} = 100 s^{-1}$ ($T_2^{-1} = 0$). The fluctuations in the nuclear OF are of the order of the change induced by a single spin flip ($A_H/N$). This result can be understood by recalling that the width of the transparency dip

[4] An example of such a process is off-resonant hyperfine-assisted laser scattering $\propto \epsilon^2 (\Gamma/\omega_z)^2$.

in CPT scales as $\Omega^2/\Gamma$, implying that the range of OF values yielding transparency can be narrowed simply by reducing $\Omega$. For $\Omega < 0.2\Gamma$, we find that $\sigma_{\mathrm{OF}}$ increases rapidly; for such small values of $\Omega$, the coupled electron-nuclei system spends substantial amount of time outside the narrow transparency region, leading to the observed increase in steady-state value of $\sigma_{\mathrm{OF}}$.

This remarkable level of OF narrowing could only be observed if optical-excitation-independent nuclear spin diffusion processes are sufficiently small. Below in Section 1.6, we discuss processes of this kind and the associated limitations of the scheme in detail. We show that under realistic conditions a narrowing to the single-spin level $\sigma_{\mathrm{OF}} \approx A_H/N$ can be achieved by using a feedback mechanism.

The operator valued correction $\tilde{I}_z$ to the two-photon detuning $\delta$ and the optically induced diffusive dynamics of $\tilde{I}_z$ described by Eqn. (1.3) are at the heart of the nuclear-spin cooling scheme we analyze in this work. The predictions we outlined hold in general for any nuclear operator $\tilde{I}_z$ with a sufficiently large density of states around $\delta_{\mathrm{eff}} = 0$. In Appendix 1.A.3, we show that this requirement is in particular fulfilled for the GOF $\tilde{I}_z = I_z + \epsilon/2\{I_+, I_-\}_+$, and that its properties are very similar to those of $I_z$ for the parameters we consider. Therefore, for the sake of simplicity, we will proceed by neglecting the $\epsilon$ correction and consider the standard OF instead of the GOF. As a further simplification we will constrain our analysis to nuclear spin-$1/2$ systems. While our results apply to a broad class of solid-state emitters, ranging from various types of quantum dots to NV centers, we will focus primarily on a single electron charged quantum dot (QD) where the optically excited state is a trion state consisting of an electron singlet and a valence-band hole [Fig. 1.1] [153, 154, 155]. For most QD systems, the assumptions we stated earlier are realized in Voigt geometry where $B_z$ is applied perpendicular to the growth direction.

## 1.5 Semiclassical analysis

In this Section, we consider the semiclassical limit to numerically confirm the principal striking features of the coupled electron-nuclei system – altered CPT signatures and the drastic nuclear state narrowing – for inhomogeneous electron-nuclear coupling. To obtain a semiclassical description of the coupled electron-nuclei dynamics, we start by assuming that the electron ($\rho^e$) and the nuclear ($\rho^n$) spins remain factorized throughout the system evolution ($\rho = \rho^e \otimes \rho^n$). Since the electron dynamics takes place on a timescale that is faster by a factor $\epsilon^{-2} \gg 1$ than the nuclear dynamics, it is justified to solve the steady state OBE to determine the trion population $\rho^e_{tt}$ for a given nuclear spin configuration (and the associated effective magnetic field).

To describe the nuclear spin dynamics semiclassically, we assume that the nuclear density operator $\rho^n$ is diagonal in the basis of individual nuclear spin eigenstates. This assumption is justified for QDs in which either strongly inhomogeneous hyperfine coupling or inhomogeneous quadrupolar fields lead to large variations in the splitting of the nuclear spin states; when this is the case, the nuclear superposition states will effectively dephase, justifying the assumption of a diagonal density operator. In this limit, the Master Eqn. (1.2) reduces to rate equations which can be numerically solved using Monte Carlo techniques. The theoretical background of this approach is explained in detail in Appendix 1.A.4.

Figure 1.3 shows the result of the Monte Carlo simulations of the coupled electron-nuclei evolution. To obtain the probe field absorption lineshape, as well as the OF variance, we assume that for each probe field detuning, we start out from a completely mixed $\rho^n$, take $\Delta\omega_c = 0$

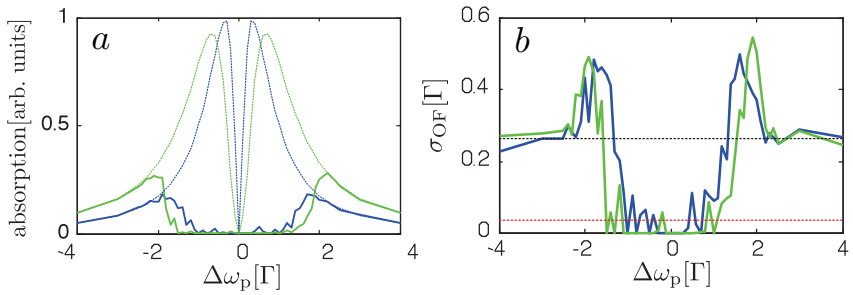


Figure 1.3: (a) The CPT absorption lineshape in the presence of hyperfine interactions for Rabi frequencies $\Omega_p = \Omega_c = 0.2\Gamma$ (blue) and $\Omega_p = \Omega_c = 0.4\Gamma$ (green): in stark contrast to the standard coherent population trapping profile (dashed lines), the dark resonance is drastically broadened (solid lines). The broadening of the dark resonance is a consequence of the fact that optical-excitation-induced nuclear spin diffusion allows the coupled electron-nuclei system to find a OF configuration that satisfies the dark-state condition for a broad range of initial laser detunings. (b) The standard deviation of the OF $\sigma_{\rm OF}$ for $\Omega_p = \Omega_c = 0.2\Gamma$ (blue) and $\Omega_p = \Omega_c = 0.4\Gamma$ (green) is reduced to the level below that of a single nuclear spin flip (red dashed line). The dashed black line shows the standard deviation in the absence of laser drive.

and evolve the coupled system to its steady state for a range of probe laser detunings. We find that the transparency window that has a width of $\sim 0.12\Gamma$ ($\sim 0.48\Gamma$) for $\Omega_c = \Omega_p = 0.2\Gamma$ ($\Omega_c = \Omega_p = 0.4\Gamma$) in the absence of hyperfine coupling (Fig. 1.3 a, red dashed curve) is drastically broadened and assumes a width $\delta\nu_{\rm trans} > \Gamma$ (Fig. 1.3 a, solid curves). This *dragging of the dark resonance* effect is in contrast to Faraday geometry experiments where nuclear spin polarization ensures that the applied laser field remains locked to a detuning that ensures maximal absorption [109]. Concurrently, the OF distribution is narrowed dramatically from its value in the absence of optical excitation (Fig. 1.3 b, black dashed line) such that its standard deviation $\sigma_{\rm OF}$ is smaller than the change induced by flipping one nuclear spin of the most weakly coupled class (Fig. 1.3 b, solid curves). These simulations show all the striking features that are a consequence of the optically induced nuclear spin diffusion [Eqn. (1.3)] which leads to a uni-directional evolution into the electronic-nuclear dark state $\rho_D = |D\rangle\langle D| \otimes \rho_D^n$, where $\rho_D^n$ is a nuclear spin density operator that yields $\delta_{\rm eff} = 0$.

We remark that the narrowing of the OF distribution could be measured by using the same two-laser set-up and scanning the probe laser on time scales short compared to those required to polarize the nuclear spins, thanks to the large separation between the electronic and nuclear dynamical timescales. In the following Section, we will address the question how quickly the nuclear system reaches the narrowed state, and how stable the distribution is under the presence additional nuclear diffusion processes. Furthermore, we will discuss a potential feedback mechanism to further reduce the OF narrowing, which is made possible due to the large separation of time scales in the system.

## 1.6 Evolution of the nuclear spins as Lévy flights

There is close analogy between the problem of CPT in the presence of inhomogeneous hyperfine interactions with a slow nuclear spin ensemble and that of a one-dimensional velocity selective CPT [139, 156]; the role of atomic momentum in the latter case is assumed by the nuclear OF $I_z$ in the present problem[5]. Just like the atomic momentum along the direction of interest can change by any value up to the full recoil momentum upon light scattering, the OF can change by any value, thanks to an inhomogeneous distribution of hyperfine interaction constants $0 \leq g_i \leq g_i^{max}$. The two models differ in two important aspects: first, there is a maximum value of the OF $\langle gI_z \rangle \leq A_H$ given by full polarization of the nuclei, and second, only a small fraction $\epsilon^2 \ll 1$ of light scattering events give rise to a change in the nuclear spin configuration. The latter makes it possible to monitor the sharp decrease in QD resonance fluorescence to verify that the coupled system is in the trapping region on time scales short compared to average nuclear spin flip time.

Continuous-time random walks are used in a wide range of fields to describe stochastic processes that are characterized by two probability distributions: one for the spatial jump length and another for the waiting time between two consecutive jumps. If one allows the jump length distribution to assume a Lévy-type distribution that is marked by so-called "fat tails", extremely long spatial jumps will occur. This is due to the fact that, asymptotically, Lévy distributions decay as power laws rather than exponentially, which gives rise to larger probabilities for extreme events that dominate the evolution of the system. These "fat tails" are also responsible for diverging variance and possibly infinite mean. Compared to the Brownian motion, the described random walk will show superdiffusive behavior. On the other hand, if the waiting time distribution obeys Lévy distribution, the system can become trapped for long times between jumps, which leads to subdiffusion [157]. Lévy distributions have been used to describe a very wide variety of phenomena ranging from human travel [158] to anomalous transport of photons [159, 160], and in particular, to subrecoil laser cooling [156]. The problem of subrecoil laser cooling shares many features with the anomalous diffusion process that appears in the cooling of nuclear spins in OSCPT, and we apply this method to determine the timescale over which we expect the nuclear spins to reach a configuration with a narrowed OF distribution.

The jump length distribution of the continuous-time random walk that describes this physical process is not of Lévy type, but is given by the distribution of the hyperfine coupling strength of the nuclei. The hyperfine interaction depends on the electronic envelope wave function, which is assumed to be Gaussian in the QD. A typical jump will thus induce a change in the OF by $A_H/N$. However, the waiting time distribution $P(t)$ between consecutive nuclear spin flips shows signatures of Lévy statistics. For fixed laser detunings $\Delta\omega_p$ and $\Delta\omega_c$ the absorption depends on the value that the nuclear OF assumes. In particular, for $\delta_{\text{eff}} = g\lambda - \delta = 0$ with $\delta$ fixed, absorption vanishes due to the formation of a dark state. We define the region around this dark state in the CPT dip to be the *trapping region*, while the remaining part is called the *recycling region*. For all practical purposes, the waiting time distribution in the recycling region does not exhibit Lévy statistics (see below). On the other hand, in the trapping region one finds an infinite average trapping time if no optical-excitation-independent nuclear diffusion processes are present. The fact that $P(t)$ in the trapping region is a Lévy distribution is responsible for

[5]Note that as mentioned above and shown in the Appendix 1.A.3, the discussion below is true also for the GOF. We consider the more familiar standard OF only for the sake of simplicity and to illustrate the arguments.

the overall subdiffusive behavior of the random walk of the nuclear spins.

The temporal evolution of the system shows switching between two regimes: diffusion in the recycling region and locking in the trapping region. To describe these dynamics, we introduce the recycling time $\hat{t}$ and the associated probability distribution function $\hat{P}(\hat{t})$. The recycling time is the time an initially trapped OF would diffuse in the recycling region before returning to the the trap. In other words, it is a measure for the time scales of switching between the diffusive and trapping regimes.

First, we will neglect optical-excitation-independent nuclear spin diffusion and focus on the case where $\Delta\omega_p = \Delta\omega_c = 0$ and $\Omega_p = \Omega_c$. To simplify the estimation of the recycling and trapping (waiting) time, we consider a limiting case where the width for the CPT transparency dip fulfills $\Omega^2/\Gamma \ll A_H/N$; i.e., a typical single nuclear spin flip will take the system out of the transparency window. We remark that the condition $\Omega^2/\Gamma \ll A_H/N$ is not necessarily optimal for nuclear spin cooling since it requires very small $\Omega$, which in turn leads to a small nuclear spin flip rate in the recycling region (see below) and longer than optimal return times. On the other hand, in this limit a single nuclear spin flip takes the system out of the trapping region, simplifying the analysis.

We assume that the width of the recycling region is determined by $A_H/\sqrt{N} \approx \Gamma/4$; since the density of states of the OF quickly drops for large polarizations, the OF cannot explore extreme polarizations. This observation is supported by numerical simulations, justifying the assumption of hard walls at $A_H/\sqrt{N} \approx \Gamma/4$. For the assumed parameter range, the light scattering rate is nearly constant outside the transparency dip and up to the hard walls that define the recycling region. We therefore take the light scattering rate to be constant in the recycling region and equal to $\Omega^2/\Gamma$ in this simplified model. As mentioned above, the nuclear spin flips are suppressed by a factor $\epsilon^2$ as compared to the light-scattering rate, which leads to the nuclear spin-flip rate $\tau_0^{-1} \approx \epsilon^2\Omega^2/\Gamma$ in the recycling region. In the limit of many nuclear spin flips, the number of steps in the recycling region required to return to the trapping region is thus given by the total range of OF values the system explores divided by the size of the trap: $\langle M\rangle = \frac{A_H/\sqrt{N}}{\Omega^2/\Gamma}$. This expression is valid provided $\langle M\rangle \gg N$, where $N = (\frac{A_H/\sqrt{N}}{A_H/N})^2$ is the number of spin flips that allows the system to diffuse to the hard walls, starting from an arbitrary polarization within the recycling region [161]. Since the time for a single spin flip is taken to be independent of the Overhauser field, the average (recycling) time to return to the trapping region is given by

$$\langle\hat{t}\rangle = \langle M\rangle\tau_0 = \frac{A_H/\sqrt{N}}{\Omega^2/\Gamma}\frac{\Gamma}{\Omega^2}\frac{1}{\epsilon^2}. \tag{1.6}$$

Since we assumed $\langle M\rangle \gg N$, this estimate is valid only in the limit $\Omega^2/\Gamma \ll A_H/N^{3/2}$.

Given the measurement-feedback strategy for minimizing $\sigma_{\mathrm{OF}}$ mentioned before, we are, strictly speaking, interested in the time for an OF that is initially in the recycling region to reach the trapping region. In contrast, $\langle\hat{t}\rangle$ gives the average return time from the recycling to the trapping region, starting from an OF that is initially in the trap. Since the analysis for the recycling time we presented is valid in the limit of many nuclear spin flips in the recycling region before the system reaches the trap, it follows that the OF explores the whole recycling region uniformly. In this case, the starting point of the OF becomes irrelevant in the sense that if the OF initially was in the trap, events where the OF returned to the trap after only a few spin flips in the recycling region are excluded from the analysis. As a consequence, the recycling

(first return) time and the time for an OF that initially was in the recycling region to reach the trap, are comparable.

In the experimentally interesting limit $\Omega^2/\Gamma \geq A_H/N$, the number of steps needed to reach the trapping region is no longer given by Eqn. (1.6). Since the step size is now comparable to the width of the trap, reaching the middle of the recycling region (where the trapping region is) starting from an arbitrary point within the hard walls is sufficient for trapping. The number of steps is then given by the whole interval divided by the step size squared: $\langle \tilde{M} \rangle = (\frac{A_H/\sqrt{N}}{A_H/N})^2 \simeq N$. Consequently, the time required to find the trap is given by $\langle \hat{t} \rangle = \langle \tilde{M} \rangle \tau_0 = N \frac{\Gamma}{\Omega^2} \frac{1}{\epsilon^2} = \frac{N^2}{A_H \epsilon^2} \approx \frac{N^3}{A_H}$, where the last expression follows for $\omega_z \approx A_H$.

The unfavorable scaling of $\langle \hat{t} \rangle$ with the number of nuclear spins, $N$, necessitates considering the effect of optical-excitation-independent nuclear spin diffusion or decay processes. Such processes would lead to a non-vanishing rate of nuclear spin flips that take the system out of the dark state. In the long term limit, this would establish a steady state between diffusion in the recycling region and finite-time trapping in the transparency region. Clearly, the presence of optical-excitation-independent nuclear spin diffusion processes limits the reduction in the standard deviation of the OF. We denote the single nuclear spin diffusion rate of any such mechanism by $\gamma_n$. If we assume that $N\gamma_n < \epsilon^2 \Omega^2/\Gamma$, we can write the steady-state standard deviation of the OF as

$$\sigma_{\mathrm{OF}} \simeq \tilde{\delta} \frac{\langle t \rangle}{\langle t \rangle + \langle \hat{t} \rangle} + \frac{A_H}{\sqrt{N}} \frac{\langle \hat{t} \rangle}{\langle t \rangle + \langle \hat{t} \rangle}, \tag{1.7}$$

where the average time spent in the trapping region is $\langle t \rangle = (N\gamma_n)^{-1}$ (assuming that a single spin-flip takes the system out of the trap) and $\tilde{\delta}$ is the effective width of the trap; the latter is determined as the detuning for which the intrinsic scattering rate in the trap ($N\gamma_n$) equals the expected optically induced nuclear spin flip rate in the CPT dip given by $\epsilon^2 \frac{\Gamma}{\Omega^2} \langle \tilde{I}_z \rangle^2$; i.e. $\tilde{\delta}$ satisfies $\epsilon^2 \frac{\Gamma}{\Omega^2} \tilde{\delta}^2 = N\gamma_n$, yielding $\tilde{\delta} = \epsilon^{-1} \Omega \sqrt{N\gamma_n/\Gamma}$. The dependence $\propto \langle I_z \rangle^2$ comes from the coupling between the states $|B\rangle$ and $|D\rangle$ by $\tilde{H}_{\mathrm{spin}}$ with the matrix element $\langle B|\tilde{H}_{\mathrm{spin}}|D\rangle \propto \langle I_z \rangle$. The rate of this coupling is proportional to $|\langle B|\tilde{H}_{\mathrm{spin}}|D\rangle|^2 \propto \langle I_z \rangle^2$ (for $\delta = 0$[6]), which leads to $P(t) \propto t^{-3/2}$. This asymptotic decay of $P(t)$ is responsible for the infinite average trapping times [156] in the absence of optical-excitation independent nuclear spin diffusion.

The smallest steady-state (measurement-free) $\sigma_{\mathrm{OF}}$ is obtained when the contribution from the trapping region (first term) and from the recycling region (second term) to $\sigma_{\mathrm{OF}}$ are comparable. However, substantial OF narrowing in this case is only possible provided $\langle \hat{t} \rangle \ll \langle t \rangle$. This condition is unlikely to be satisfied for self-assembled QDs if one aims at $\sigma_{\mathrm{OF}} = A_H/N$, since $\langle \hat{t} \rangle \sim 10\mathrm{s}$ for $N = 10^4$ and $\gamma_n = 10^{-3}\mathrm{s}^{-1}$. On the other hand, a more modest narrowing yielding $\sigma_{\mathrm{OF}} = 10A_H/N$ (achieved by choosing $\Omega^2/\Gamma = 10A_H/N$) would give $\langle \hat{t} \rangle \sim 1\mathrm{s} \ll \langle t \rangle \simeq 100(N\gamma_n)^{-1}$.

A strategy to reduce the $\sigma_{\mathrm{OF}}$ below its steady-state value is to monitor the light scattering rate $W_{\mathrm{scat}}$ of the coupled system. Since $W_{\mathrm{scat}} \propto \delta_{\mathrm{eff}}^2$ in the neighborhood of the trapping region, a drastic reduction in $W_{\mathrm{scat}}$ verifies that the nuclear spins are in the desired state; turning the laser fields then off will ensure that $\sigma_{\mathrm{OF}}$ will be given by the width $\tilde{\delta} \sim A_H/N$ of the trapping region. This feedback is possible due to the fact that the time scale for flipping a nuclear spin is longer by a factor $\epsilon^2$ than that for a photon scattering event. To achieve this OF narrowing

[6] The generalization to finite $\delta$ is straightforward, and requires the replacement $I_z \to I_z - \delta/g$

in the single spin limit $\sigma_{\mathrm{OF}} \sim \tilde{\delta} \sim A_H/N$, it is necessary to ensure $\gamma_n < A_H/N^3$ and $1/T_2 < A_H/N^2$.

## 1.7 Experimental realization

While our proposal has been worked out for the example of self-assembled QDs, our findings are relevant for a wider range of solid-state emitters. Of particular interest are nitrogen-vacancy (NV) centers in diamond, where a recent proof-of-principle experiment demonstrated the general feasibility of our proposal [137]. The small number of nuclear spins coupled to the optically excited spin in the case of NV-centers makes it possible to reduce the time needed for the system to find the dark state drastically. A principal difference with respect to the large $N$ limit we analyzed is the fact that only a small set of optical detunings will allow the NV system to find a dark state. The OF can only assume certain discrete values while in the case of large N the OF is quasi continuous.

Let's next discuss the prospects of an experimental realization in QDs. We have seen that the strength $\gamma_n$ of optical excitation independent nuclear spin diffusion processes determines the degree of attainable OF narrowing. In this context, we remark that experimental observations reported by the Bayer group [162], obtained by driving an ensemble of single-electron charged QDs using periodic ultra-short optical pulses in the Voigt geometry, demonstrated that optically prepared nuclear spin states could survive for $\sim 10$ minutes[7]. Such long nuclear spin lifetimes in principle fulfill the above conditions, and allow for reaching $\sigma_{\mathrm{OF}} \sim A_H/N$ using the proposed CPT scheme. We also note that the basic signatures of CPT have been observed in both single electron [154] and hole [155] charged QDs.

Even though we have concentrated on nuclear spin diffusion associated with the ground-state hyperfine coupling, the conclusions of our work remain unchanged if the solid-state emitter has hyperfine coupling leading to nuclear spin diffusion in the optically excited state. This would be the case for example in QDs with vanishing heavy-light hole mixing leading to near-resonant hole-mediated nuclear spin-flips in the excited state due to the dominant $S_z^h I_z$ term in the hole-hyperfine interaction Hamiltonian. Finally, extensions to other solid state systems such as superconducting qubits may be possible [163].

## 1.A Supplementary material 1

The following supplementary material is divided into four sections. Each section provides background information to specific topics of the main text. The sections are not built upon each other and can be read independently. Appendix 1.A.1 provides a detailed derivation of the Master Eqn. (1.2) of the main text as well as a discussion of higher-order processes. In Appendix 1.A.2 we discuss in detail the effects of a potential inhomogeneous Zeeman term to the scheme. Appendix 1.A.3 contains a detailed analysis of the properties of the GOF. Finally, the details of the semiclassical Monte Carlo simulations of the OSCPT cooling scheme can be found in Appendix 1.A.4.

[7] Nuclear spin preparation in these experiments could be considered in the frame of a *time-dependent dark-state* where the electron spin is in a superposition state with a time-dependent phase arising from the effective Zeeman splitting. This phase evolves in a way to ensure that at the arrival time of the laser pulse, the electron is in a dark superposition of the spin states; this condition is enforced by nuclear spin polarization that is different for each QD.

### 1.A.1 Derivation of the Master Eqn.(1.2)

In the first three subsections of this Appendix, we present the intermediate steps for the derivation of Eqn. (1.2) of the main text. A detailed justification for neglecting higher-order terms appearing after the Schrieffer-Wolff transformation is given thereafter.

#### Preliminaries

In order to derive nuclear diffusion rates in the CPT setting, we consider the master equation describing the coupled electron and nuclear system, obtained after eliminating the radiation field reservoir using a Born-Markov approximation:

$$\begin{aligned}\dot{\rho} =&\frac{\Gamma}{2}(|\uparrow\rangle\langle t|\rho|t\rangle\langle\uparrow| - \frac{1}{2}\{|t\rangle\langle t|,\rho\}_+)\\ &+\frac{\Gamma}{2}(|\downarrow\rangle\langle t|\rho|t\rangle\langle\downarrow| - \frac{1}{2}\{|t\rangle\langle t|,\rho\}_+) - i[\mathcal{H},\rho]\\ =&\frac{\Gamma}{2}(\mathbb{1}_S\otimes\rho_{tt} - \{|t\rangle\langle t|,\rho\}_+) - i[\mathcal{H},\rho],\end{aligned} \tag{1.8}$$

where $\rho_{tt} = \langle t|\rho|t\rangle$ acts on the Hilbert space of nuclear spins, $\mathbb{1}_S = |\uparrow\rangle\langle\uparrow| + |\downarrow\rangle\langle\downarrow|$ and we defined $\{A,B\}_+ = AB + BA$. The Hamiltonian of the system consists of a diagonal part $\mathcal{H}_0$ and the laser and hyperfine Hamiltonians,

$$\mathcal{H} = \mathcal{H}_0 + \mathcal{H}_{\text{laser}} + \mathcal{H}_{\text{hyp}}, \tag{1.9}$$

$$\mathcal{H}_0 = \omega_t|t\rangle\langle t| - \omega_z S_z, \tag{1.10}$$

$$\mathcal{H}_{\text{laser}} = \Omega_c e^{i\omega_c t}|\downarrow\rangle\langle t| + \Omega_p e^{i\omega_p t}|\uparrow\rangle\langle t| + h.c., \tag{1.11}$$

$$\mathcal{H}_{\text{hyp}} = g\left(I_z^{(1)}S_z + \frac{1}{2}(I_+^{(1)}S_- + I_-^{(1)}S_+)\right). \tag{1.12}$$

Here, $\omega_t$ and $\omega_z$ denote the trion state and electron Zeeman energies, whereas $\omega_{c/p}$ and $\Omega_{c/p}$ are the coupling and probe laser's frequencies and Rabi energies, respectively. The nuclear quasi-spin operators are defined as $I_\alpha^{(n)} = \sum_{i=1}^N g_i^n \sigma_\alpha^i$ ($\alpha = +,-,z$); we note that in the main text, we used the simplified notation $I_\alpha \equiv I_\alpha^{(1)}$ since there we did not introduce collective operators with $n \neq 1$. For the analysis below, we (initially) neglect the nuclear Zeeman energy. The hyperfine coupling coefficients $g_i$ are normalized such that $\sum g_i^2 = 1$ (in this convention the hyperfine interaction constant of the material is given by $A_H = g\sum g_i$) and the electron operators $S_\alpha$ are the usual spin $1/2$ operators. We assume that in the absence of optical excitation, the electron spin is well isolated from all reservoirs other than the nuclear spins [101], and spin-flip co-tunneling or phonon emission rates are negligible within the time scales of interest.

The basis transformation

$$H' = e^{i\xi t}(\mathcal{H} - \xi)e^{-i\xi t}, \tag{1.13}$$

with

$$\xi = \left[\omega_t - \frac{1}{2}(\Delta\omega_c + \Delta\omega_p)\right]|t\rangle\langle t| - [\omega_z + (\Delta\omega_c - \Delta\omega_p)]\,(I_z^{(0)} + S_z), \tag{1.14}$$

renders the Hamiltonian time independent,

$$H' = \tilde{\omega}_z I_z^{(0)} + \frac{1}{2}(\Delta\omega_c + \Delta\omega_p)\,|t\rangle\langle t| - \delta S_z + H_{\text{laser}} + H_{\text{hyp}}, \tag{1.15}$$

where $H_{\text{laser}} = \Omega_c\,|\downarrow\rangle\langle t| + \Omega_p\,|\uparrow\rangle\langle t| + h.c.$ and $H_{\text{hyp}} \equiv \mathcal{H}_{\text{hyp}}$. The laser detunings are given as $\Delta\omega_p = -\omega_p + (\omega_t + \omega_z/2)$ and $\Delta\omega_c = -\omega_c + (\omega_t - \omega_z/2)$. The effective nuclear energy in the rotating frame is $\tilde{\omega}_z = \omega_z + \Delta\omega_c - \Delta\omega_p \approx \omega_z$ and the two-photon detuning is denoted by $\delta = \Delta\omega_p - \Delta\omega_c$. The dissipative part of Eqn. (1.8) - containing secular terms exclusively - remains unchanged under the transformation.

In the limit of a large external field ($\tilde{\omega}_z \gg g$), the direct electron-nuclei flip-flop processes $I_+^{(1)}S_- + I_-^{(1)}S_+$ are strongly suppressed due to the large mismatch in the electronic and nuclear Zeeman splitting. In the following, we derive the second-order effects of the energetically suppressed hyperfine flip-flop interaction using a systematic approach in the language of a Schrieffer-Wolff transformation [164, 165]. We will find that the higher-order corrections to the flip-flop interaction account for an optically assisted nuclear diffusion process [Fig. 1.1 a] and motivate the introduction of the novel concept of the GOF.

### Quasidegenerate perturbation theory

The clear separation of energy scales in the Hamiltonian of Eqn. (1.15) [$\tilde{\omega}_z \gg g,\ \delta,\ \Omega_{c/p},\ \Delta\omega_{c/p}$; see Fig. 1.1 c] allows us to partition the full Hamiltonian into a zero-order part $H_0' = \tilde{\omega}_z I_z^{(0)}$ and a small perturbation $V = H' - H_0'$. The eigenvectors of $H_0'$ are grouped into well separated manifolds, labeled by the nuclear spin projection quantum number $m$ [see Fig. 1.1 c]. According to this spectrum any operator $O$ can be partitioned into a block diagonal $O_D$ operator - containing terms that conserve $m$ - and a block off-diagonal $O_N$ operator - containing terms that drive transitions between different manifolds ($m$ non-conserving terms). For the Hamiltonian this separation yields

$$H_D' = H_0' + V_D, \tag{1.16}$$
$$H_N' = V_N, \tag{1.17}$$

where

$$V_D = +\frac{1}{2}(\Delta\omega_c + \Delta\omega_p)\,|t\rangle\langle t| - \delta S_z + (\Omega_c\,|\downarrow\rangle\langle t| + \Omega_p\,|\uparrow\rangle\langle t| + h.c.), + g I_z^{(1)} S_z \tag{1.18}$$
$$V_N = \frac{g}{2}\left(I_+^{(1)}S_- + I_-^{(1)}S_+\right). \tag{1.19}$$

Note that the above choice of $H_0'$ is not unique. Other choices that for instance render $V_N$ purely block-off-diagonal are equivalent, but complicate the fine-structure within the manifolds.

In the following we are going to construct a similarity transformation, generated by an anti-hermitian operator $G = -G^\dagger$

$$H = e^{-G} H' e^{G} \tag{1.20}$$

that renders the transformed Hamiltonian block diagonal and thus decouples the different manifolds from each other. Since the above condition does not define $G$ uniquely [165], we further demand $G_D = 0$ (canonical choice). Expanding the operators in orders of the perturbation

$$H = \sum_{n=0}^{\infty} H^{[n]}, \qquad G = \sum_{n=0}^{\infty} G^{[n]}, \tag{1.21}$$

one can derive conditional equations for $G$ order by order. Exploiting the fact that $V_N^2$ is block diagonal ($S_-^2 = S_+^2 = 0$) one finds the simple recursive equations:

$$\begin{aligned} G^{[0]} &= 0, \\ [H_0', G^{[1]}] &= -V_N, \\ [H_0', G^{[2]}] &= -[V_D, G^{[1]}], \\ [H_0', G^{[3]}] &= -[V_D, G^{[2]}] - \frac{1}{3}[[V_N, G^{[1]}], G^{[1]}], \\ &\vdots \end{aligned} \tag{1.22}$$

The expansion of the transformed Hamiltonian yields

$$\begin{aligned} H^{[0]} &= H_0', \\ H^{[1]} &= V_D, \\ H^{[2]} &= \frac{1}{2}[V_N, G^{[1]}], \\ H^{[3]} &= \frac{1}{2}[V_N, G^{[2]}], \\ &\vdots \end{aligned} \tag{1.23}$$

Note that $H^{[n]}$ only depends on lower orders of the transformation matrix. Higher-order expressions and a detailed derivation are given in [164].

### Second order corrections

We are going to expand our system's Master Eqn. (1.8) to second order in the perturbation, in order to identify the dominant hyperfine processes in the electron-nuclear CPT setting. From Eqn. (1.22) we readily derive the form of $G^{[1]}$,

$$G^{[1]} = \epsilon(S_+ I_-^{(1)} - S_- I_+^{(1)}), \tag{1.24}$$

where we defined the expansion parameter $\epsilon = \frac{g}{2\tilde{\omega}_z}$. $G^{[1]}$ generates the second order corrections to the Hamiltonian [Eqn. (1.23)]:

$$H^{[2]} = -\frac{1}{2}\epsilon g(S_z\{I_+^{(1)}, I_-^{(1)}\}_+ - I_z^{(2)}). \tag{1.25}$$

The transformed Hamiltonian up to second order then reads,

$$\begin{aligned} H &= H_0' + V_D + H^{[2]} \\ &= \tilde{\omega}_z I_z^{(0)} + \frac{1}{2}(\Delta\omega_c + \Delta\omega_p)\,|t\rangle\langle t| + (\Omega_c\,|\downarrow\rangle\langle t| + \Omega_p\,|\uparrow\rangle\langle t| + h.c.) \\ &+ gS_z(I_z^{(1)} - \frac{1}{2}\epsilon\{I_+^{(1)}, I_-^{(1)}\}_+ - \delta/g) + \epsilon g\frac{1}{2}I_z^{(2)} \\ &= \tilde{\omega}_z I_z^{(0)} + \frac{1}{2}(\Delta\omega_c + \Delta\omega_p)\,|t\rangle\langle t| + H_{\text{laser}} + gS_z(\tilde{I}_z^{(1)} - \delta/g) + \epsilon g\frac{1}{2}I_z^{(2)}, \end{aligned} \tag{1.26}$$

where we have introduced the notion of the *generalized Overhauser field (GOF)* $g\tilde{I}_z^{(1)} = g(I_z^{(1)} - \frac{1}{2}\epsilon\{I_+^{(1)}, I_-^{(1)}\}_+)$, which contains all electron-nuclear interactions up to second order and can be interpreted in our context as an effective two-photon detuning, which adds to the external laser detuning $\delta$.

In a similar procedure the system Liouvillian $\mathcal{K}'(\rho) = \frac{\Gamma}{2}(\mathbb{1}_S \otimes \rho_{tt} - \{|t\rangle\langle t|, \rho\}_+)$ is transformed under $G$ and expanded in orders of the perturbation

$$\mathcal{K}(\rho) = \sum_{n=0}^{\infty} \mathcal{K}^{[n]}(\rho). \tag{1.27}$$

Realizing that the transformation leaves the excited electron state invariant $e^{-G^{[1]}}\,|t\rangle = |t\rangle$ (and thus the second term of the Liouvillian $\propto \{|t\rangle\langle t|, \rho\}_+$) we only have to transform the jump term $\mathbb{1}_S \otimes \rho_{tt}$. The *Baker-Hausdorff formula* yields,

$$e^{-G^{[1]}}(\mathbb{1}_S \otimes \rho_{tt})e^{G^{[1]}} \approx \mathbb{1}_S \otimes \rho_{tt} + [\mathbb{1}_S \otimes \rho_{tt}, G^{[1]}] + \frac{1}{2}[[\mathbb{1}_S \otimes \rho_{tt}, G^{[1]}], G^{[1]}], \tag{1.28}$$

which is particularly simple to calculate since $\mathbb{1}_S S_\alpha = S_\alpha$. Grouped into orders of $\epsilon$ one finds

$$\begin{aligned} \mathcal{K}^{[0]}(\rho) =& \frac{\Gamma}{2}(\mathbb{1}_S \otimes \rho_{tt} - \{|t\rangle\langle t|, \rho\}_+), \\ \mathcal{K}^{[1]}(\rho) =& -\epsilon\frac{\Gamma}{2}\left(S_-[\rho_{tt}, I_+^{(1)}] + S_+[I_-^{(1)}, \rho_{tt}]\right), \\ \mathcal{K}^{[2]}(\rho) =& \epsilon^2\frac{\Gamma}{4}\mathbb{1}_S \otimes D_1(\rho_{tt}) + \epsilon^2\frac{\Gamma}{2}S_z \otimes D_2(\rho_{tt}). \end{aligned} \tag{1.29}$$

Note that the above procedure is equivalent to a straightforward transformation of the electronic jump operators $|\downarrow\rangle\langle t|$ and $|\uparrow\rangle\langle t|$ of the Liouvillian. The superoperators

$$\begin{aligned} D_1(\rho) =& I_+^{(1)}\rho I_-^{(1)} + I_-^{(1)}\rho I_+^{(1)} - \frac{1}{2}\{I_+^{(1)}I_-^{(1)} + I_-^{(1)}I_+^{(1)}, \rho\}_+, \\ D_2(\rho) =& I_-^{(1)}\rho I_+^{(1)} - I_+^{(1)}\rho I_-^{(1)} + \{I_z^{(2)}, \rho\}_+, \end{aligned} \tag{1.30}$$

describe optically induced random nuclear spin diffusion processes caused by optically assisted electron-nuclear spin flip events. Since this nuclear diffusion depends on the electron population in the excited state $\propto \rho_{tt}$ it will vanish for electronic dark states, which are defined via the condition $\rho_{tt} = 0$. Note that second order terms in the transformed Liouvillian arising from $G^{[2]}$ are non-secular and consistently neglected. $\mathcal{K}^{[1]}$ and the second summand in $\mathcal{K}^{[2]}$ do not

affect the nuclear evolution governed by $\dot{\rho}_I = \mathrm{Tr}_S(\dot{\rho})$, since $\mathrm{Tr}_S(S_z) = \mathrm{Tr}_S(S_\pm) = 0$ ($\mathrm{Tr}_S$ denotes the trace over all electronic degrees of freedom). For the electron evolution, which occurs on time scales $\propto \Gamma$ these terms merely represent a small $\epsilon^2$-correction ($\mathcal{K}^{[1]}$ acquires an additional factor $\propto \epsilon$ since it is non-secular) and are consequently neglected in the following. If we further assume resonance ($\Delta\omega_c = \Delta\omega_p = 0$) and neglect the last term of Eqn. (1.26) - which accounts for a small state independent nuclear diffusion and will be discussed in Section 1.A.1 - we arrive at the master Eqn. (1.2) of the main text (note that in the notation of the main text $I_\alpha \equiv I_\alpha^{(1)}$),

$$\begin{aligned}\dot{\rho} =& \frac{\Gamma}{2}(\mathbb{1}_S \otimes \rho_{tt} - \{|t\rangle\langle t|, \rho\}_+) + \epsilon^2 \frac{\Gamma}{4} \mathbb{1}_S \otimes D_1(\rho_{tt}) \\ & - i[H_{\mathrm{laser}} + \tilde{H}_{\mathrm{spin}}, \rho],\end{aligned} \tag{1.31}$$

where we further applied the trivial transformation into a frame rotating with $\tilde{\omega}_z I_z^{(0)}$. $\tilde{H}_{\mathrm{spin}} = gS_z(\tilde{I}_z^{(1)} - \delta/g)$ contains all electron nuclear interactions to leading order and can be interpreted as an effective two-photon detuning. If the nuclear system is in an eigenstate $|\lambda\rangle$ of the GOF operator $\tilde{I}_z^{(1)}$ with eigenvalue $\lambda = \delta/g$ the two photon detuning vanishes and the product state $|\lambda\rangle \otimes |D\rangle$ (with $|D\rangle = \frac{1}{\sqrt{\Omega_c^2+\Omega_p^2}}(\Omega_c|\uparrow\rangle - \Omega_p|\downarrow\rangle)$ being the electronic dark state) is a steady state of the dynamics. If, in contrast, the nuclear system is in a state where $\lambda \neq \delta/g$ (i.e. the two-photon resonance condition is violated) the electronic system is bright ($\rho_{tt} \neq 0$) inducing nuclear diffusion given by the term $\propto D_1(\rho_{tt})$.

### Higher-order corrections

We have seen in the foregoing section that nuclear states in the kernel of $\tilde{I}_z^{(1)} - \delta/g$ decouple completely from the electron degrees of freedom and the evolution of these states comes to rest and the system is trapped. However, higher-order corrections - which we have neglected so far - can contribute to a finite, state-independent nuclear diffusion rate out of the trapping region. In the following, we identify and discuss these corrections.

First, we consider the effect of the second order term $\epsilon g \frac{1}{2} I_z^{(2)}$, which we neglected in Eqn. (1.26) and which does not commute with the GOF $g\tilde{I}_z^{(1)}$. Consequently, GOF eigenstates evolve under its action. To estimate the corresponding nuclear diffusion rate we consider the equation of motion of the corresponding Heisenberg operator

$$\begin{aligned}\frac{d}{dt}\tilde{I}_z^{(1)} =& -i[\tilde{I}_z^{(1)}, \epsilon g \frac{1}{2} I_z^{(2)}] \\ =& -i\frac{1}{4}\epsilon^2 g(I_+^{(3)}I_-^{(1)} - I_+^{(1)}I_-^{(3)} + I_-^{(1)}I_+^{(3)} - I_-^{(3)}I_+^{(1)}) \\ =& -i\frac{1}{2}\epsilon^2 g(I_+^{(3)}I_-^{(1)} - I_+^{(1)}I_-^{(3)}).\end{aligned} \tag{1.32}$$

Note that, since the perturbation commutes with the zero order (i.e. standard OF) part of the GOF ($[I_z^{(1)}, I_z^{(2)}] = 0$) the effect is of higher order $\propto \epsilon^2$. Furthermore, the spin operators are normalized such that typical matrix elements of $I_+^{(n)}I_-^{(m)}$ are of order $\sim N^{1-(n+m)/2}$. In fact, the number of larger matrix elements (at most by a factor $N$) is exponentially small. Thus it can only reduce the trapping region (which is defined as the set of eigenvectors with

sufficiently small eigenvalues of $\tilde{I}_z^{(1)} - \delta/g$, and which is shown to be sizable in Appendix 1.A.3) insignificantly. Therefore we can roughly estimate the rate of change in the subspace of relevant states $\psi$

$$\left| \frac{d}{dt} \langle \tilde{I}_z^{(1)} \rangle_\psi \right| \sim \frac{\epsilon^2}{N} g. \tag{1.33}$$

which is smaller than the optically induced nuclear diffusion rate by a factor $(\frac{A_H/N}{\Omega^2/\Gamma})^{-1}$. Note however, that Eqn. (1.33) is a pessimistic estimate, since it does not take into account the Hamiltonian character of the perturbation $\epsilon I_z^{(2)}$: every nuclear dark state (small-eigenvalue eigenstate of $\tilde{I}_z^{(1)}$) that is also an eigenstate of $I_z^{(2)}$ maintains its dark state character. Since $I_z^{(2)}$ and $I_z^{(1)}$ (of which $\tilde{I}_z^{(1)}$ is a perturbation) commute, this subspace may be substantial. In particular, in the limiting case of homogeneous coupling, Eqn. (1.32) vanishes exactly. While Eqn. (1.33) is slow enough not to interfere with the measurement-based scheme, its influence on the steady-state scheme is subject of ongoing work.

Next we consider higher order corrections in the perturbation theory by expanding the Hamiltonian to third order. The generator of the third order correction $G^{[2]}$ can be calculated using Eqn. (1.22):

$$\begin{aligned} G^{[2]} =& \epsilon\epsilon_\delta (S_+ I_-^{(1)} - S_- I_+^{(1)}) \\ &+ \epsilon\epsilon_c (I_-^{(1)} |\uparrow\rangle \langle t| - h.c.) + \epsilon\epsilon_p (I_+^{(1)} |\downarrow\rangle \langle t| - h.c.) \\ &+ \epsilon^2 \left[ S_- I_+^{(2)} - S_+ I_-^{(2)} - 2(S_+ I_z^{(1)} I_-^{(1)} - S_- I_+^{(1)} I_z^{(1)}) \right], \end{aligned} \tag{1.34}$$

with the expansion parameters $\epsilon_\delta = \frac{\delta}{\tilde{\omega}_z}$, $\epsilon_{p/c} = \frac{\Omega_{p/c}}{\tilde{\omega}_z} \ll 1$. The third order Hamiltonian [Eqn. (1.23)] is then given by

$$\begin{aligned} H^{[3]} =& -\epsilon^2 \delta (S_z \{I_+^{(1)}, I_-^{(1)}\}_+ - I_z^{(2)}) \\ &+ \frac{1}{4}\epsilon^2 \{I_+^{(1)}, I_-^{(1)}\}_+ H_{\text{laser}} \\ &+ \frac{1}{2}\epsilon^2 I_z^{(2)} (\Omega_c |\downarrow\rangle \langle t| - \Omega_p |\uparrow\rangle \langle t| + h.c.) \\ &+ \epsilon^2 g S_z (I_+^{(1)} I_z^{(1)} I_-^{(1)} + h.c.) \\ &+ \frac{1}{8}\epsilon^2 g (\{I_+^{(2)}, I_-^{(1)}\}_+ + \{I_+^{(1)}, I_-^{(2)}\}_+ - I_z^{(1)} I_z^{(2)}), \end{aligned} \tag{1.35}$$

The first term is of the exact form as $H^{[2]}$ and can easily be incorporated in the above considerations of Section 1.A.1 as a small ($\epsilon$) correction. The second and third term describe two different types of laser assisted nuclear diffusion. The first type supports the scheme, since $H_{\text{laser}}$ only couples to the electronic bright state $|B\rangle$. Thus this diffusion comes to rest whenever the electron is in the dark state $|D\rangle$. The second type of laser-assisted nuclear diffusion couples to the dark state and thus, in principle, represents a possible escape mechanism from trapping states. However, since - as discussed above - the diffusion operator $I_z^{(2)}$ commutes with the zero order part of the GOF the contribution of the third term is yet of one order $\epsilon$ smaller than the process of Eqn. (1.33) and thus safely negligible. The fourth and fifth term of Eqn. (1.35) originate in third order contributions of the hyperfine interaction. While the fourth term can be

incorporated in the definition of the GOF, the fifth term represents a state independent nuclear diffusion, effectively of the same order as the one of Eqn. (1.33).

All these processes are taken into account exactly in the homogeneous simulations [based on Eqn. (1.8)] and account for the small but finite standard deviation in the steady state.

### 1.A.2 Inhomogeneous nuclear Zeeman terms

We have so far neglected the Zeeman energy of the nuclei, which is typically three orders of magnitude smaller than $\omega_z$. A *homogeneous* nuclear Zeeman term $\propto I_z^{(0)}$ has no effect on the analysis carried out in the subsections 1-5 since it commutes with the GOF $g\tilde{I}_z^{(1)}$. However, if different nuclear species with different gyromagnetic ratios are involved, this is no longer the case since the correction $\propto I_+^{(1)} I_-^{(1)}$ in $\tilde{I}_z^{(1)}$ includes the exchange of nuclear spin excitations between different nuclear species. Different Larmor frequencies associated with different species/isotopes will in general lead to a modulation of the GOF. Here, we will show that in the limit of large differences in Larmor frequencies, the dominant contribution to GOF stems from intra-species flip-flop terms; the fast time dependence of the inter-species flip-flop terms in this limit ensures that their contribution averages out.

For the relevant nuclei the energy differences (between different species) are often so large (up to 10 MHz per Tesla) that they cannot be neglected on the time scales of nuclear spin diffusion (see Table 1.1).

| Isotope | $^{69}$Ga | $^{71}$Ga | $^{75}$As | $^{113}$In | $^{115}$In |
|---|---|---|---|---|---|
| Natural Abundance (%) | 60.1 | 39.9 | 100 | 4.3 | 95.7 |
| gyromagnetic ratio ($10^7 \mathrm{rad} s^{-1} T^{-1}$) | 6.44 | 8.18 | 4.60 | 5.90 | 5.88 |

Table 1.1: Natural abundances and gyromagnetic ratios of typical isotopes. Source: WebElements [http://www.webelements.com/]

We consider here the case that $\mathcal{H}$ also contains an inhomogeneous nuclear Zeeman term

$$H_{nz} = \sum_j \omega_{nz,j} I_z^j. \tag{1.36}$$

We assume a number of different nuclear species labeled by $s$ and define nuclear operators referring to species $s$ by $I_\alpha^{(n,s)} \equiv \sum_{j\in s} g_j^n I_\alpha^j$ (where the sum runs only over the indices $j$ of nuclei belonging to species $s$). Then the correction term in the GOF splits into an intra-species part which commutes with $H_{nz}$ and a second (inter-species) part describing the exchange of spin excitations between different species:

$$\{I_+^{(1)}, I_-^{(1)}\}_+ = \sum_s \{I_+^{(1,s)}, I_-^{(1,s)}\}_+ + 2\sum_{s>s'} \left( I_+^{(1,s)} I_-^{(1,s')} + I_-^{(1,s)} I_+^{(1,s')} \right). \tag{1.37}$$

We show in the following that for sufficiently large magnetic fields the latter terms are off-resonant and thus suppressed to leading order. Only the intra-species terms $\sum_s \{I_+^{(1,s)}, I_-^{(1,s)}\}_+$ survive in the GOF. To higher orders, the inter-species terms provide small additional state-independent GOF-diffusion terms similar to the one generated by $I_z^{(2)}$ [see Eqn. (1.32)].

Generalizing the considerations of Section 1.A.1 we consider $H_{nz}$ to be part of $V_D$ and modify the generator of the Schrieffer-Wolff transformation such that the terms connecting different species in Eqn. (1.37) are canceled. This is achieved by adding

$$T = S_z \sum_{s>s'} \frac{\epsilon g}{2(\omega_{nz,s} - \omega_{nz,s'})} \left( I_+^{(1,s)} I_-^{(1,s')} - I_-^{(1,s)} I_+^{(1,s')} \right) \equiv S_z X \tag{1.38}$$

to $G$. This modification has the following effects: $H = e^{-G-T}(H' + H_{nz})e^{G+T} = H' + H_{nz} - [G, H'] - [T, H'] - [G, H_{nz}] - [T, H_{nz}] + \frac{1}{2}[G+T, [G+T, H' + H_{nz}]] + \ldots$, which leads to several new first and second order terms like $[G^{[1]}, H_{nz}]$, $[T, H_0 + V_N + V_D]$, $[T + G^{[1]}, [T + G^{[1]}, H_{nz}]]$ etc. Most of these terms are off-resonant either by $\omega_z$ or $\omega_{nz,s} - \omega_{nz,s'}$ and the secular terms lead to $I_z^{(0,s)}$-conserving second order corrections, which either modify the GOF or induce a small state-independent GOF-diffusion (similar to $I_z^{(2)}$ in Eqn. (1.32)). Since they are similar to and smaller (by $\epsilon\omega_{nz,s}/g$ or $\epsilon g/(\omega_{nz,s} - \omega_{nz,s'})$, respectively) than terms already considered, we do not discuss them in detail.

To determine the conditions under which it is allowed to neglect all non-secular terms, denote by $\Delta_{nz} = \min\{|\omega_{nz,s} - \omega_{nz,s'}| : s \neq s'\}$ the nuclear Zeeman inhomogeneity[8] and introduce $\epsilon_{nz} = g\epsilon/\Delta_{nz}$. Exemplarily we consider the laser term arising from $[T, V_D]$, which represents one of the major perturbations. It reads

$$\frac{\Omega_p}{2} |\uparrow\rangle \langle t| X - \frac{\Omega_c}{2} |\downarrow\rangle \langle t| X + \text{h.c.} \propto |D\rangle \langle t| + \text{h.c.} \tag{1.39}$$

It describes laser-assisted nuclear spin dynamics that changes the GOF and is only detuned by $\Delta_{nz}$. Thus we need

$$\frac{\Omega\epsilon g}{\Delta_{nz}} \ll \Delta_{nz} \Leftrightarrow \Delta_{nz}^2 \gg \frac{\Omega g^2}{2\tilde{\omega}_z}. \tag{1.40}$$

With typically $\Delta_{nz} \sim 10^{-3}\tilde{\omega}_z$ we need $10^{-6} \gg \frac{\Omega}{\tilde{\omega}_z}\frac{g^2}{\tilde{\omega}_z^2}$. In terms of $\epsilon_{nz}$ we need $\Omega\epsilon_{nz} \ll \Delta_{nz}$. For typical values (all energies in $\mu$eV) of $g \sim 1$ and $\Delta_{nz} \sim 10^{-3}\tilde{\omega}_z$ we could take $\tilde{\omega}_z \sim 100$, which yields $\epsilon_{nz} \sim 10^{-1}$ and thus would require $\Omega \sim 0.1$. Thus if $\Delta_{nz}$ is sufficiently large ($g\epsilon, \Omega\epsilon_{nz} \ll \Delta_{nz}$) these contributions are small and the non-secular terms can be neglected. This can always be ensured by sufficiently strong magnetic field. Using the same arguments one can show that under condition Eqn. 1.40 also the other terms arising from $T$ can safely be neglected.

Similarly, we have to transform the jump operators in the Liouvillian. Here we consider only the first-order correction to $\mathcal{K}^{[1]}$ arising from $|\downarrow\rangle \langle t| \to |\downarrow\rangle \langle t| - [G^{[1]} + T, |\downarrow\rangle \langle t|] \pm \ldots$. The new terms such as $[T, |\downarrow\rangle \langle t|] = -\frac{1}{2} X |\downarrow\rangle \langle t|$ describe an additional slow nuclear spin dynamics that occurs only in the optically excited state, thus enhancing nuclear diffusion outside the trapping region and improving the scheme.

In realistic systems, there may be other processes affecting the nuclear spins which have to be taken into account for a full description – in particular the dipolar interaction between nuclear spins and on-site quadrupolar terms; these terms would lead to a non-zero $T_2^*$ time of the nuclear spin ensemble. In addition, there may be $T_2$ processes affecting the nuclei, arising

[8] Only species with sizably different g factors are distinguished. The two In isotopes, e.g., are treated as one species for typical magnetic fields.

from fluctuating local magnetic fields. While these processes will be discussed in detail in future work, we provide here some simple estimates of how these processes relate quantitatively to other corrections considered in previous sections.

We consider pure dephasing of nuclear spins with rate $T_2^{-1}$

$$\dot{\rho} = \frac{1}{T_2}\sum_j (I_z^j \rho I_z^j - \rho)$$

affecting all nuclei. Computing the contribution to $\frac{d}{dt}\tilde{I}_z^{(1)}$ arising from this process we find in the subspace of relevant states $\psi$

$$|\frac{d}{dt}\langle \tilde{I}_z^{(1)}\rangle_\psi| \sim \epsilon \frac{1}{T_2}, \tag{1.41}$$

as the effective $T_2$-induced diffusion rate of $\tilde{I}_z^{(1)}$. This contribution is of the same order as the leading higher-order correction discussed in the preceding section if $1/T_2 \sim \epsilon N^{-3/2} A_H \sim 10^3 \mathrm{s}^{-1}$. For the measurement based nuclear spin cooling to yield $\sigma_{\mathrm{OF}} \leq A_H/N$, the condition $1/T_2 < A_H/N^2 \sim 10^3 \mathrm{s}^{-1}$ needs to be satisfied (see the discussion in Section 1.6).

### 1.A.3 Generalized Overhauser field (GOF)

In this Appendix, we show that the spectrum and the density of states of the GOF does not differ significantly from that of the standard OF. This property is important for justifying the assumptions leading to the semiclassical Monte Carlo simulations (see Fig. 1.3 of the main text), where we used the standard OF to reproduce the diffusive dynamics of the GOF.

For the main part of the nuclear Hilbert space – namely the domain where the operator $\tilde{I}_z^{(1)} - \delta/g$ is large (recycling region) – the $\epsilon$-correction in the GOF represents a negligible perturbation to the hyperfine interaction. However, in the domain of small eigenvalues of $\tilde{I}_z^{(1)} - \delta/g$ (we define this trapping region within a small interval $L(\delta,\eta) = (\delta-\eta, \delta+\eta)/g$ centered around $\delta/g$) this perturbative picture is not trivially justified.

Using Monte Carlo simulations we first show that the density of eigenstates of the homogeneous ($g_i = 1/\sqrt{N}, \forall i$) and inhomogeneous operator $I_z^{(1)}$, respectively, is identical (up to small corrections) for our system parameters ($N = 10^4$, Gaussian distribution of coupling strengths), see Fig. 1.4 a. Therefore, the number of eigenstates for the inhomogeneous operator $I_z^{(1)}$ with small eigenvalues is exponentially large in the number of spins (in the homogeneous case every eigenvalue $m/\sqrt{N}$ has degeneracy $B_m = \binom{N}{N/2+m}$). This implies that neglecting the $\epsilon$-correction, trapping regions close to the center of the spectrum $|\delta/g| \lesssim 1$ constitute a substantial part of the Hilbert space and can be reached in reasonable times by the nuclear random diffusion. For trapping regions $|\delta/g| \gtrsim 1$, i.e. very large laser detunings, the size of the trapping region drops exponentially [Fig. 1.4 a] and cannot be explored by the nuclear diffusion (see Fig. 1.3 a of the main text).

Next we are going to show that the GOF fulfills the same property by deriving a relation between the spectrum of the operators $\tilde{I}_z^{(1)}$ and $I_z^{(1)}$. In the homogeneous case the $\epsilon$-correction commutes with the unperturbed part $[I_z^{(1)}, \{I_+^{(1)}, I_-^{(1)}\}_+] = 0$, and a common eigenbasis is given by the well known Dicke states $|J,m\rangle$, where $J$ denotes the total spin and $m$

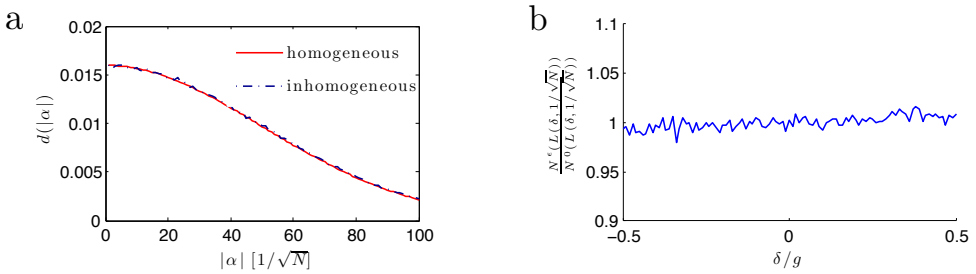


Figure 1.4: (a) Comparison of the density of eigenstates $d(|\alpha|)$ ($\tilde{I}_z\,|\alpha\rangle = \alpha\,|\alpha\rangle$) of the homogeneous and inhomogeneous nuclear operator $I_z^{(1)}$. The density of states is averaged over segments of size $1/\sqrt{N}$. While in the homogeneous case the density of states can be calculated exactly, in the inhomogeneous case it is evaluated using Monte Carlo simulations. (b) The number of eigenvalues in small intervals of size $1/\sqrt{N}$ of the GOF approximately equals the number of states for the standard OF. In the simulations we assumed $N = 10^4$ and coupling coefficients $a_i$ arising from a Gaussian electron wave function.

the spin projection in $\hat{z}$-direction. The vast majority states within the kernel of $I_z^{(1)}$ lie in $J$ subspaces around $J = \sqrt{N}/2$ (the degeneracy of each subspace $J$ is given by $D_J = \binom{N}{N/2-I} - \binom{N}{N/2-I-1}$). Thus, up to a negligible fraction, most states will be shifted in energy by a small amount of order $\epsilon$. The same can be shown for states with finite eigenvalue of $I_z^{(1)}$ in the range $\sim (-1, 1)$. The positive operator of the correction $\frac{1}{2}\epsilon\{I_+^{(1)}, I_-^{(1)}\}_+$ shifts the whole spectrum in the region of interest by a small amount $\propto \epsilon$ and thus preserves the required property of large density of states in any trapping region $L(\delta, \epsilon)$ close to the center of the spectrum.

In the inhomogeneous case this simple argument fails, since one cannot easily construct an eigenbasis of the GOF. We are going to estimate the density of states in the following. For the inhomogeneous GOF operator $\tilde{I}_z^{(1)}$ the number of states within the trapping region $L(\delta, \eta)$ is given by $N^\epsilon(L(\delta,\eta)) = \int_{L(\delta,\eta)} dE\ \mathrm{Tr}(\delta(E - I_z^{(1)} + \frac{1}{2}\epsilon\{I_+^{(1)}, I_-^{(1)}\}_+))$. Approximating the $\delta$-functions by Lorentzians of width $\gamma \ll \eta$: $\delta(E-\tilde{I}_z^{(1)}) \approx \frac{\gamma}{(E-\tilde{I}_z^{(1)})^2+\gamma^2}$, and using the expansion $\frac{1}{A-\epsilon B} = \frac{1}{A}\sum_{n=0}^{\infty}(\epsilon B\frac{1}{A})^n$ with the definitions

$$A = \gamma^2 + (E - I_z^{(1)})^2, \tag{1.42}$$

$$B = -\frac{1}{2}\{(E - I_z^{(1)}), \{I_+^{(1)}, I_-^{(1)}\}_+\}_+ - \frac{1}{4}\epsilon(\{I_+^{(1)}, I_-^{(1)}\}_+)^2 =: Q + \epsilon P, \tag{1.43}$$

we find

$$N^\epsilon(L(\delta,\eta)) = \sum_{n=0}^{\infty} U^{(n)} = N^0(L(\delta,\eta)) + \sum_{n=1}^{\infty} U^{(n)}, \tag{1.44}$$

$$U^{(n)} = \gamma\epsilon^n \int_{L(\delta,\eta)} dE\ \mathrm{Tr}\left(\frac{1}{A}\left[B\frac{1}{A}\right]^n\right). \tag{1.45}$$

A pessimistic approximation shows that the sum $\sum_{n=1}^{\infty} U^{(n)}$ can be upper bounded by $\sim N^0(L(\delta,\eta))$ for large trapping regions $\eta \gg \epsilon$, i.e. the number of eigenstates changes at most by a factor of order 1.

Using the above definitions the quotient of the number of states in the perturbed and unperturbed case can be written to first order in $\epsilon$ as

$$\frac{N^\epsilon(L(\delta,\eta))}{N^0(L(\delta,\eta))} = \frac{\int_{L(\delta,\eta)} dE\ \mathrm{Tr}(\frac{1}{A}(1+\epsilon Q\frac{1}{A}))}{\int_{L(\delta,\eta)} dE\ \mathrm{Tr}(\frac{1}{A})} = \frac{\sum_{\vec{n}} \int_{L(\delta,\eta)} dE\ g(\vec{n},E) f(\vec{n},E)}{\sum_{\vec{n}} \int_{L(\delta,\eta)} dE\ g(\vec{n},E)}, \tag{1.46}$$

where we defined

$$g(\vec{n},E) = \langle\vec{n}| \frac{1}{A} |\vec{n}\rangle\,, \tag{1.47}$$

$$f(\vec{n},E) = 1 + \epsilon \langle\vec{n}| Q\frac{1}{A} |\vec{n}\rangle\,, \tag{1.48}$$

for a nuclear product state $|\vec{n}\rangle$. Expressions like the one of Eqn.(1.46) can be efficiently evaluated using Monte Carlo simulation with *importance sampling* [166]. This method uses a more efficient sampling according to the probability distribution $g(\vec{n},E)$ (i.e. strongly weighted regions are favored in the sampling) instead of the sampling of random configurations $(\vec{n},E)$ within the entire state space. In particular it can be shown that

$$\frac{\sum_{\vec{n}} \int_{L(\delta,\eta)} dE\ g(\vec{n},E) f(\vec{n},E)}{\sum_{\vec{n}} \int_{L(\delta,\eta)} dE\ g(\vec{n},E)} = \lim_{t\to\infty} \frac{1}{t} \sum_{i=1}^{t} f(\vec{x}_i), \tag{1.49}$$

where the vectors $\vec{x}_i$ stand for particular configurations of the random variables $(\vec{n},E)$ which are distributed according to $g(\vec{x}_i)$.

The algorithm realizing the above scheme contains the following steps: (0.) We start from a random sample $\vec{x} := (\vec{n},E)$ ($E \in L(\delta,\eta)$) and then (1.) create a new sample $\vec{x}'$ by randomly changing one coordinate $x_i$ (the ratio of spin flips and change of $E$ is defined a priori). (2.) If $g(\vec{x}')/g(\vec{x}) > s$ - where $s$ is an (in each step) randomly created number $\in (0,1)$ - we add $f(\vec{x}')$ to a variable $F$, if not we discard the new state, return to $\vec{x}$ and add $f(\vec{x})$ to $F$. Successive repetition of steps (1.) and (2.) lets the quantity $F/t$ ($t$ denotes the number of steps) converge to the desired quotient in Eqn. (1.46). The method ensures that regions of higher importance are explored more frequently than others (according to $g(\vec{n},E)$), increasing the performance of the algorithm. The simulations for $N = 10^4$ inhomogeneously coupled spins suggest that even for $\eta \sim \epsilon$ the number of states in both the perturbed and unperturbed case differ by less than a few percent [see Fig. 1.4 b].

Furthermore, since $[\tilde{I}_z^{(1)}, I_-^{(1)}] = [I_z^{(1)}, I_-^{(1)}] + \mathcal{O}(\epsilon)$ the diffusion rate of the GOF equals the one in the unperturbed case up to an $\epsilon$ correction. This justifies the conclusion that the diffusive dynamics of the GOF is well reproduced by that of the standard OF.

### 1.A.4 Rate equation description of nuclear spin dynamics

In this Section, we present the details of the model used to obtain the semiclassical Monte Carlo simulation of the quantum dot absorption rate and the Overhauser field standard deviation presented in Fig. 1.3 of the main text.

The semiclassical limit can be derived from the Master Eqn. (1.4) by replacing the collective spin decay by independent decay of individual spins. This is accomplished by making the following substitutions in the master equation:

$$I_+^{(1)}\rho^n I_-^{(1)} = \sum_{ij} g_i g_j \sigma_+^i \rho^n \sigma_-^j \quad \rightarrow \quad \sum_i g_i^2 \sigma_+^i \rho^n \sigma_-^i, \tag{1.50}$$

$$I_-^{(1)}\rho^n I_+^{(1)} = \sum_{ij} g_i g_j \sigma_-^i \rho^n \sigma_+^j \quad \rightarrow \quad \sum_i g_i^2 \sigma_-^i \rho^n \sigma_+^i, \tag{1.51}$$

$$\begin{aligned} &\{I_+^{(1)} I_-^{(1)} + I_-^{(1)} I_+^{(1)}, \rho\}_+ \\ &\quad = \{\sum_{ij} g_i g_j (\sigma_+^i \sigma_-^j + \sigma_-^i \sigma_+^j), \rho\}_+ \quad \rightarrow \quad \{\sum_i g_i^2 (\sigma_+^i \sigma_-^i + \sigma_-^i \sigma_+^i), \rho\}_+. \end{aligned} \tag{1.52}$$

The replacement of the collective spin operators by single spin operators is justified in the limit where coherences between nuclear spin product states vanish on time scales short compared to their lifetime; this condition would be satisfied in systems with large inhomogeneities - either in the nuclear spin splitting or in hyperfine coupling. Since the spectrum, the density of states and the nuclear spin dynamics resulting from $\tilde{I}_z$ and $I_z$ are equivalent, we replace the GOF $\tilde{I}_z$ by the OF $I_z$ in the simulations (see Appendix 1.A.3). We now coarse grain the nuclear motion with respect to the electron dynamics and from the resulting master equation we obtain rate equations that describe the nuclear spin evolution.

In order to mimic the inhomogeneous character of the hyperfine coupling we introduce a shell model of the QD with $M$ different classes of nuclear spins; the nuclei in class ($\nu$) have identical $a_\nu$ and their net spin polarization is $m_\nu = \frac{1}{2}(N_\nu^+ - N_\nu^-) = \langle \sum_{i\epsilon\nu} \sigma_z^i \rangle$, where $N_\nu^+$ ($N_\nu^-$) denote the total number of up (down) spins in class ($\nu$). The derived rate equation for the joint probabilities $\mathcal{P}(\{m_\mu\})$ associated with the nuclear spin configuration $\{m_\mu\}$ is given by

$$\begin{aligned} \frac{\partial \mathcal{P}(\{m_\mu\})}{\partial t} &= \sum_\nu^M \mathcal{P}(\{\bar{m}_\mu\}) N_\nu^-(\{\bar{m}_\mu\}) \Gamma_+^\nu(\{\bar{m}_\mu\}) \\ &+ \sum_\nu^M \mathcal{P}(\{\tilde{m}_\mu\}) N_\nu^+(\{\tilde{m}_\mu\}) \Gamma_-^\nu(\{\tilde{m}_\mu\}) \\ &- \sum_\nu^M \mathcal{P}(\{m_\mu\}) [N_\nu^- \Gamma_+^\nu(\{m_\mu\}) + N_\nu^+ \Gamma_-^\nu(\{m_\mu\})], \end{aligned} \tag{1.53}$$

where $\Gamma_\pm^\nu(\{m_\mu\}) = (\frac{g a_\nu}{4\omega_z})^2 \frac{\Gamma}{2} \rho_{tt}(\{m_\mu\})$ are the rates at which nuclear spins of the $\nu$th class are flipped if the nuclear spin polarizations in each class are given by $\{m_\mu\}$. $\{\bar{m}_\mu\}$ ($\{\tilde{m}_\mu\}$) denotes the nuclear spin configuration that differs from the configuration $\{m_\mu\}$ only in the $\nu$th class, with polarization $m_\nu - 1$ ($m_\nu + 1$). The factors $N_\nu^-$ ($N_\nu^+$) account for the number of nuclear spins in the configuration $\{\bar{m}_\mu\}$ ($\{\tilde{m}_\mu\}$) that could be flipped to reach $\{m_\mu\}$.

We simulate the evolution of the nuclear spins with a Monte Carlo method. We assume in our numerical simulations that the QD contains 100 nuclear spins, grouped into five concentric shells ($M = 5$) with different hyperfine coupling constants that are determined by the 3D Gaussian electronic envelope function. The coupling constants $a_i$ for these shells are chosen to be 0.0934$\Gamma$, 0.0828$\Gamma$, 0.0678$\Gamma$, 0.0513$\Gamma$, 0.0358$\Gamma$ and the corresponding total numbers of nuclear

spins in each shell are chosen to be 2, 8, 16, 28, 46. The coupling constants are chosen to ensure that the standard deviation of the Overhauser field seen by the QD electron for nuclei in a completely mixed state satisfies $\sigma_{\mathrm{OF}}(\rho) = \frac{\Gamma}{4}$. We do not keep track of the exact configuration within each class ($\nu$) of nuclear spins and assume that any configuration of spins leading to the same $m_\mu$ is equally likely and that the nuclear spin distribution in each shell is independent of the other shells.

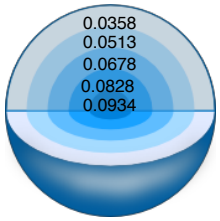


Figure 1.5: The confined electron wave-function leads to inhomogeneous hyperfine coupling with the nuclei. In the simulations, we assume that the dot can be described as consisting of 5 different classes of nuclei. All nuclei within a class have identical hyperfine coupling, with strength determined by the electron wave function.

As discussed in the main text, we keep $\Delta\omega_c = 0$ and then scan the probe laser across the resonance. For each probe laser detuning $\Delta\omega_p$ we assume that the initial nuclear state $\rho^n$ is completely mixed and then we evolve the system until $t_{fin} = 10^{12}\ \Gamma^{-1}$. Fig. 1.3 of the main text show the formation of an electronic-nuclear dark state and the concurrent reduction in Overhauser field standard deviation $\sigma_{\mathrm{OF}}$ for a range of probe laser detunings $\Delta\omega_p$ . The two-photon resonance condition $\delta_{\mathrm{eff}} = g\lambda - \delta = 0$ can be satisfied for a large range of initial detunings because the set of Overhauser fields resulting from all possible nuclear spin configurations of the toy model QD described above is quasi-continuous. However, the density of states in the toy model is not a smooth function of the Overhauser field, which explains the observed variations in the absorption strength and $\sigma_{\mathrm{OF}}$ within the *extended transparency region*: the Overhauser field required to fulfill $\delta_{\mathrm{eff}} = 0$ for some detunings $\Delta\omega_p$ is composed of a nuclear spin configuration that requires a large polarization in one of the nuclear spin classes. It will take many nuclear spin flips to reach such a state, since the initial state is taken to be Gaussian in all classes.

# Chapter 2

# Optical Superradiance from Nuclear Spin Environment of Single-Photon Emitters

**In this Chapter, we demonstrate that the nuclear spins of mesoscopic solid-state systems can display highly coherent effects under a dissipative evolution. We predict a superradiant optical emission that can be observed from the polarized nuclear spin ensemble surrounding a single photon emitter such as a single quantum dot (QD) or Nitrogen-Vacancy (NV) center. The superradiant light is emitted under optical pumping conditions and would be observable with realistic experimental parameters. This phenomenon of nuclear superradiance establishes an intriguing analogy between quantum optics and solid-state physics. It demonstrates the emergence of coherence from dissipation in these systems, and will serve as a pivot for the following Chapters. This Chapter is based on publication 5 [OSR].**

## 2.1 Introduction

In quantum optics, the concept of superradiance (SR) is a paradigmatic example for a coherent quantum effect arising from a dissipative coupling to the environment (for a review see [17]). When an large ensemble of (initially excited) optical emitters is confined in a volume with spatial dimensions much smaller than the wavelength of the emitted light, the characteristics of the de-excitation process deviate drastically from the classical expectations. The initially independent dipoles experience a spontaneous build-up and reinforcement of correlations, which results in a coherent light emission from the cloud. Its most prominent feature is a sudden burst of radiation intensity (scaling with the number of emitters) which causes the system to radiate and thus de-excite much faster than an otherwise identical system of classical emitters. This emergence of coherence in *spontaneous emission* is closely related to the phenomenon of lasing [2, 3]. While in the case of a laser, *stimulated emission* [15] leads to a coherent occupation of a particular light mode, in SR the emitters themselves evolve into a coherent state, giving rise to a quantum mechanically enhanced light emission.

The effect of SR was first described by Dicke in 1954 [16], and since then been studied ex-

tensively [167, 168, 169, 170, 171]. Its origin lies in the indiscernability of the individual emitters with regard to the emitted light. Due to the narrow spatial confinement smaller than the optical wavelength, emitted photons carry no information about the position of individual atoms. This results in the correlation build-up and the cooperative de-excitation of the ensemble; the atomic cloud behaves like a single quantum-mechanical entity with macroscopic dipole moment ("giant spin") [172]. Yet, in its original form optical SR is difficult to observe due to dephasing dipole-dipole Van der Waals interactions, which arise from the virtual exchange of high-energy photons (which can resolve the individual atom positions due to their short wavelength) and suppress the coherence build-up in atomic ensembles [17].

In this Chapter, we establish an intriguing analogy between mesoscopic solid-state physics and quantum optics: Identifying individual nuclear spin states with the internal levels of single atoms, we show that superradiant emission can occur from the ensemble of nuclear spins surrounding a quantum emitter such as a self-assembled QD or an NV center under optical spin pumping conditions. The indiscernability of individual emitters is guaranteed by the indirect nature of the coupling between the nuclear spins and the optical field: In the optical dynamical nuclear polarization (DNP) scheme we consider, this interaction is mediated by the electron spin of the emitter, masking the position information of individual spins due to the collective hyperfine coupling. The indirect character of the nuclear-optical coupling further causes the dephasing Van der Waals interactions to vanish in this setting.

## 2.2 Executive summary

This Chapter is organized as follows. We first explain the basic ideas of the proposal and the main characteristics of nuclear SR using the example of an NV center in diamond in Section 2.3. NV centers offer the advantage that one can study the effect in a small and relatively clean model system. After we have introduced the main ideas, we demonstrate the principal feasibility of the approach by simulating exactly a small spin environment of a NV center, taking into account all spurious effects resulting from inhomogeneities and anisotropies in the hyperfine coupling. We come to the conclusion that already for only about 10 nuclear spins, the emission is cooperatively enhanced by 100%, and we show the onset of a linear scaling of the effect with increasing particle number. Motivated by this scaling behavior, we adapt the model to QDs in Section 2.4, which holds promise of strong effects, due to the large number of involved nuclei. Since the large particle number prevent the exact simulation of the system, we develop a new factorization scheme, tailored for the requirements of a central spin problem, which allows the treatment of hundreds of nuclear spins. Using this approximative scheme we show that despite the inhomogeneity of the nuclear spin coupling and related dephasing processes, a SR-like correlation build-up takes place in the nuclear spin ensemble. We predict a significant intensity burst of several orders of magnitude in the optical emission profile. We show that the surprising conservation of coherence in the presence of strong dephasing processes, is due to an evolution of the system in so-called many-body-protected manifolds. Finally, in Section 2.5, we briefly discuss the implications of this proposal with respect to the following Chapters of this Thesis.

## 2.3 Proof-of-principle: SR in Nitrogen-Vacancy centers

Superradiance is known as a macroscopic collective quantum phenomenon which generalizes spontaneous emission from a single emitter to a many-body system of $N$ atoms [173]. Starting from a fully polarized initial state the system evolves within a subspace fully symmetric under permutation and experiences a strong correlation build-up due to a collective coupling to the environment. As a consequence, the emission intensity is not of the usual exponentially-decaying form, but conversely features a sudden peak occuring on a very rapid timescale $\sim 1/N$ with a maximum $\sim N^2$.

We show, that the same type of cooperative emission can occur from an ensemble of nuclear spins surrounding of a single photon quantum emitter. Here, the superradiant effect is based on the collective hyperfine (HF) interaction of the electronic spin of the defect (QD or NV) with $N$ initially polarized proximal nuclear spins. It is dominated by the isotropic Fermi-contact term [98, 134] and reads in an external magnetic field ($\hbar = 1$):

$$H = \frac{g}{2}(A^+S^- + A^-S^+) + gA^zS^z + \omega_S S^z. \tag{2.1}$$

Here $S^\mu$ and $A^\mu = \sum_{i=1}^N g_i \sigma_i^\mu$ ($\mu = +, -, z$) denote electron and collective nuclear spin operators, respectively. The coupling coefficients are normalized such that $\sum_i g_i^2 = 1$ and individual nuclear spin operators $\sigma_i^\mu$ are assumed to be spin-1/2 for simplicity; $g$ gives the overall HF coupling strength and $\omega_S$ denotes the electron Zeeman splitting. We neglect the typically very small nuclear Zeeman and nuclear dipole-dipole terms.

Let us first consider NV centers, for which the effect can be studied in a clean and relatively small spin environment. Due to their extraordinary quantum properties, such as ultra-long decoherence times even at room temperature, NV centers have attracted wide interest (for a recent review, see [119]) resulting, e.g., in the demonstration of entanglement and quantum gates between the electron and proximal nuclear spins [129]. Both the NV center's electronic ground ($^3A$) and optically excited states ($^3E$) are spin triplet ($S = 1$). In the absence of a magnetic field, the ground state sublevels $|m_S = \pm 1\rangle$ are split from $|m_S = 0\rangle$ due to the anisotropic crystal field. In the following, we assume that a static magnetic field $B$ is applied along the NV axis to bring $|m_S = 0\rangle$ and $|m_S = 1\rangle$ close to degeneracy[1]. In this case $|m_S = -1\rangle$ is off-resonance and can be disregarded. We focus on low-strain NV centers with well-defined selection rules, and assume that it is optically excited by selectively driving the weakly allowed transition from $|m_S = 1\rangle$ to a state $|E_x\rangle$ in the $^3E$ manifold which decays primarily into $|m_S = 0\rangle$ [120], see Fig. 2.1 (a).

The nuclear spin environment of the NV center consists of proximal $^{13}$C (spin $I = 1/2$) nuclei in the otherwise spinless $^{12}$C matrix, which are HF-coupled to the electronic spin of the defect center. The interaction is dominated by the Fermi-contact term such that the coupling is isotropic (to first order) and described by Eqn. (2.1) ($\omega_S$ here contains both zero field splitting and Zeeman energy). Nevertheless, in the simulations conducted below we included the small anisotropic dipole-dipole terms.

We describe now the coupling of the nuclear spin to the optical field as depicted in Fig. 2.1 (b). It is best understood as a two-step process: First, strongly driving a dipole-forbidden optical transition of the $|m_S = 1\rangle$ spin state (the allowed transition is far off-resonant) pumps the electron into $|m_S = 0\rangle$. Such Raman spin-flip transitions have been demonstrated recently [120].

[1] A field of $\sim$ 100mT is sufficient to compensate the zero-field splitting of 2.88GHz.

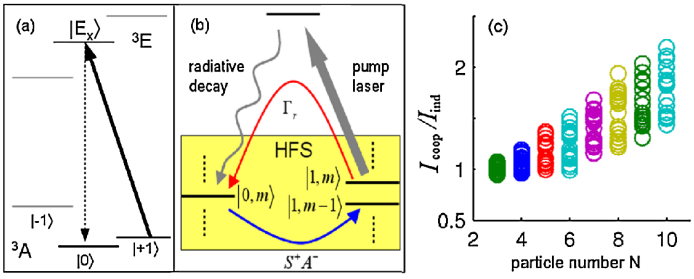


Figure 2.1: (a) Simplified level scheme of NV center with relevant $\Lambda$ system (cf. text and [120]); (b) Sketch of relevant processes: electronic ground states are coupled by optical pumping and HF flipflops; the states are labeled by the $z$-components of the electron and nuclear spin. (c) $I_{\mathrm{coop}}/I_{\mathrm{ind}}$ for randomly chosen nuclear environments of an NV center The first nuclear shell is taken to be spinless, as due to their very strong coupling they would evolve largely independent from the ensemble.

Since the short-lived excited state is populated negligibly throughout the process, we can adiabatically eliminate it from the dynamics using standard perturbation techniques and obtain a master equation for the electron spin decaying with effective rate $\Gamma_r$:

$$\dot{\rho} = \Gamma_r(S^-\rho S^+ - \frac{1}{2}S^+S^-\rho - \frac{1}{2}\rho S^+S^-) - i[H,\rho], \tag{2.2}$$

each decay process being accompanied by the emission of a Raman photon. Second, the return to state $|m_S = 1\rangle$, necessary for the next emission, occurs through $H$ via a HF mediated electron spin flip (and nuclear spin flop). Thus, each Raman photon indicates a nuclear spin flop and the emission intensity $I(t)$ is proportional to the change in nuclear polarization. Starting from a fully polarized state, SR is due to the increase in the operative HF matrix element $\langle A^+A^-\rangle$. The scale of the coupling is set by the hyperfine coupling constant $A_H := g\sum_i g_i$. For a small *relative coupling strength* $\epsilon = A_H/(2\Delta)$, where $\Delta := |\Gamma_r/2 + i\omega_S|$, the electron is predominantly in its $|m_S = 0\rangle$ spin state and we can project Eqn. (2.2) to the respective subspace. The reduced master equation for the nuclear density operator $\mu = \mathrm{Tr}_S(\rho)$ reads

$$\begin{aligned}\dot{\mu} =& c_r(A^-\mu A^+ - \frac{1}{2}A^+A^-\mu - \frac{1}{2}\mu A^+A^-) \\ &- ic_i[A^+A^-,\mu] - igm_S[A^z,\mu],\end{aligned} \tag{2.3}$$

where $c_r = g^2/(2\Delta)^2\Gamma_r$ and $c_i = g^2/(2\Delta)^2\omega_S$.

As the electron is optically pumped into $|m_S = 0\rangle$, the last term - representing the electron's Knight field - in Eqn. (2.3) vanishes. Assuming resonance ($\omega_S = 0$) the equation closely resembles the SR master equation which has been discussed extensively in the context of atomic physics [17] and thus SR effects might be expected. Conceptually, the emergence of SR sigantures can be understood immediately in the ideal case of homogeneous coupling ($g_i = 1/\sqrt{N}, \forall i$) in which the collective state of all nuclear spins can be described in terms of Dicke states $|J,m\rangle$[2]: The enhancement of the HF interaction is directly associated with the transition through nuclear states $|J,m\rangle$ with $m \ll J$. In this idealized setting, the spin operator $\mathbf{I}$

[2]Dicke states are the angular-momentum-like spin eigenstates (see, e.g., [16]).

of the nuclear spin ensemble obeys the SU(2) Lie algebra, from which one can deduce the ladder operator relation $I^- |J,m\rangle = \sqrt{J(J+1) - m\,(m-1)}\,|J,m-1\rangle$. This means that, starting from an initially fully polarized state $|J = N/2, m = N/2\rangle$, the nuclear system cascades down the Dicke-ladder with an effective rate

$$\tilde{\Gamma}_{m\to m-1} = \frac{c_r}{N}\,(N/2+m)\,(N/2-m+1)\,, \tag{2.4}$$

since, according to the first term in Eqn. (2.3), the populations of the Dicke states $\mu_{m,m} := \langle N,m|\,\mu\,|N,m\rangle$ evolve as

$$\begin{aligned}\dot{\mu}_{m,m} \;\; &= \;\; -\tilde{\Gamma}_{m\to m-1}\mu_{m,m} \\ &\quad\;\; +\tilde{\Gamma}_{m+1\to m}\mu_{m+1,m+1}.\end{aligned} \tag{2.5}$$

While the effective rate is $\tilde{\Gamma}_{N/2\to N/2-1} = c_r$ at the very top of the the ladder it increases up to $\tilde{\Gamma}_{|m|\ll N/2} \approx c_r N/4$ at the center of the Dicke ladder. This implies the characteristic intensity peaking as compared to the limit of independent classical emitters, the emission rate of which would be $\tilde{\Gamma}_{\rm cl} = \frac{c_r}{N}N_\uparrow = \frac{c_r}{N}\,(N/2+m)$. Note, that on this level, the quantum mechanical effect of SR is entirely described by a recursive set of diffusion equations. Based on these rate equations, we make a rough estimate for the average process duration $\langle t_D\rangle$ in the following. By linearizing Eqn.(2.4) for the beginning of the superradiant evolution [17] as $\tilde{\Gamma}_{m\to m-1} \approx c_r(s+1)$, where $s = N/2 - m$ gives the number of nuclear flips that have occurred, one finds that the first flip takes place in an average time $c_r^{-1}$, the second one in a time $(2c_r)^{-1}$ and so on. The summation of all these elementary time intervals gives an upper bound estimate for the process duration untill the SR peaking as

$$\langle t_D\rangle \lesssim \frac{2}{c_r}\left[1 + \frac{1}{2} + \cdots + \frac{1}{N/2}\right] \approx \frac{2\ln(N/2)}{c_r}. \tag{2.6}$$

Remarkably, the total duration of the superradiant process is only by a factor of $\ln(N/2)$ longer than the time it takes for the first spin flip to occur, which is in stark contrast to the behavior a corresponding classical ensemble. A more detailed study of the time scales of the nuclear superradiant process is presented in Chapter 3 [SET] where we consider nuclear superradiance effects in the electronic transport through an electrically-defined QD.

As compared to the ideal setting, in realistic solid-state systems there is a crucial difference: the *inhomogeneous nature* ($g_i \neq \text{const}$) of the operators $A^\mu$: they do not preserve the collective spin, affecting the relative phase between nuclei. This potentially prevents the phased emission necessary for SR [17, 168, 174]. However, as we shall see next, SR is still clearly present in small realistic systems with inhomogeneous and moderately anisotropic hyperfine interactions, such as NV centers. In Section 2.4 we will identify the mechanism, which prevents dephasing and protects the coherent evolution of the nuclear system, and we will extend our predictions to self-assembled QD systems with about $10^4 - 10^5$ nuclear spins. In the following, we take the ratio of the maximum intensity to the initial intensity (i.e., the maximum for independent spins) $I_{\rm coop}/I_{\rm ind}$ as our figure of merit: if this *relative intensity peak height* is $> 1$ it indicates cooperative effects.

To see that this effect can be observed at NV centers, we simulate Eqn. (2.2) numerically[3]. The number $N$ of effectively coupled nuclei can range from a few to a few hundred, since the

[3] Eqn. (2.2) allows for the full incorporation of anisotropies.

concentration of $^{13}$C can be widely tuned [175]. The HF constants $g_i$ between the defect and the nearest $\sim 40$ nuclei were derived in [134] in an ab-initio calculation. Nuclei outside this shell ($\sim 7$Å) have a coupling strength $gg_i$ weaker than $2\pi \cdot 0.5$MHz and are not considered here. The excited state lifetime of the NV center has been measured as $\tau \approx 13$ns [176, 177]. Thus, we adopt an effective rate $\Gamma_r = 2\pi \cdot 10$MHz for the decay from $|m_S = 1\rangle$ to $|m_S = 0\rangle$ enabled by driving the respective Raman transition. The intensity enhancements predicted by exact simulations for small, randomly chosen and initially polarized spin environments are shown in Fig. 2.1(c). For each number from three to ten nuclear spins, we simulate the exact system evolution for 20 randomly chosen spin spin configurations (i.e., random positioning of the nuclear spins within the 40 nearest cores according to [134]), to find the relative intensity peak height $I_{\mathrm{coop}}/I_{\mathrm{ind}}$. Already for a few particles, clear signatures of cooperativity ($I_{\mathrm{coop}}/I_{\mathrm{ind}} > 1$) are present. In samples of higher $^{13}$C concentration $N$ can be larger and stronger effects are expected.

One characteristic feature of SR is the linear $N$-dependence of the associated effects, the onset of which is already visible in Fig. 2.1 (c). Since the number of nuclei to which the electron couples is much larger in a QD than in a NV center, QDs are particularly attractive candidates for the investigation of SR. In the following, we study the dynamics of the QD system in different regimes, and we show that strong signatures of SR can be expected in realistic settings.

## 2.4 Quantitative analysis and theoretical concepts: Quantum dots

Let us consider a self-assembled QD in which a single conduction-band electron is coupled by isotropic Fermi contact interaction to a large number of nuclear spins. Optical pumping of the electron is realized by a Raman process, driving a forbidden transition to a trion state [101], and including the HF coupling we again obtain dynamics as sketched in Fig. 2.1(b). For the optical pumping rate values $\Gamma_r = 2\pi \cdot (0.1 - 1)$GHz are applicable [178, 179]. A comparison with the HF coupling constants reported for different materials[4] shows that for InGaAs and CdSe QDs at resonance Eqn. (2.3) is not valid since the relative coupling strength $\epsilon \geq 1$. We therefore consider the dynamics of the system under conditions of a finite electron inversion [using Eqn. (2.2)]. In this regime, the electron can be seen as a driven and damped two-level system: the nuclei 'pump' excitations into the electron, which are damped by the Raman-mediated decay; cooperative behavior manifests in enhanced HF interaction. This enhancement directly translates into increased electron inversion $\langle S^+ S^- \rangle$ to which the emitted photon rate is proportional and thus SR from a single QD can be expected. Let us rephrase this, since SR from a *single* emitter is somewhat counter-intuitive: Of course, on an optical time scale, anti-bunched single photons will be emitted at a rate below the optical decay rate. It is, in fact, typically much slower since the emitter is pumped into the optically inactive state $|m_S = 0\rangle$. SR on time scales $\sim 1/\Gamma_r$ consists thus of lifting this "spin-blockade" by HF coupling which becomes increasingly more efficient as nuclear cooperative effects kick in. As in the homogeneous case [17] this enhancement is associated with the transition through nuclear Dicke states $|J, m\rangle$, $|m| \ll J$. Although $J$ is not preserved by inhomogeneous $A^{\pm}$, we can use the Dicke states to illustrate the dynamics. For instance, due to the large homogeneous component in $A^-$, its matrix elements show a strong increase $\propto J$ for states $|J, m\rangle$, $|m| \ll J$.

[4] The HF coupling constants and typical numbers of nuclei ($A/\mu$eV,N) for important QD materials are [180, 98]: GaAs:(100,$10^4 - 10^6$), CdSe:(10,$10^3$), SiP:(0.1,$10^2$)

For large relative coupling strengths $\epsilon \gg 1$ the electron saturates and superradiant emission is capped by the decay rate $\Gamma_r/2$, prohibiting the observation of an intensity burst. In order to avoid this bottleneck regime we choose a detuning $\omega_S = A_H/2$ such that $0 < \epsilon = A_H/\sqrt{\Gamma_r^2 + A_H^2} \leq 1$. In this parameter range the early stage of the evolution - in which the correlation build-up necessary for SR takes place [17] - is well described by Eqn. (2.3). The nuclear phasing is counteracted by the dephasing (inhomogeneous) part of the Knight term ($\propto g\sqrt{\mathrm{Var}(g_i)}/2$ [167]), which can cause transitions $J \to J-1$. However, the system evolves in a *many-body protected manifold* (MPM) [181]: The term $\sim [A^+A^-, \rho]$ energetically separates different total nuclear spin-$J$ manifolds. A rough estimate of the ratio between detuning and dephasing shows a dependence $\propto \epsilon^2$, with proportionality factor $> 1$ (diverging in the homogeneous limit). Thus for values $\epsilon \approx 1$ the correlation build-up should be largely MPM-protected. We now confirm these considerations and show by numerical simulation of Eqn. (2.2) that a SR peaking of several orders of magnitude can be observed in the Raman radiation from an optically pumped QD, cf. Fig. 2.2. An exact numerical simulation of the dynamics is not feasible

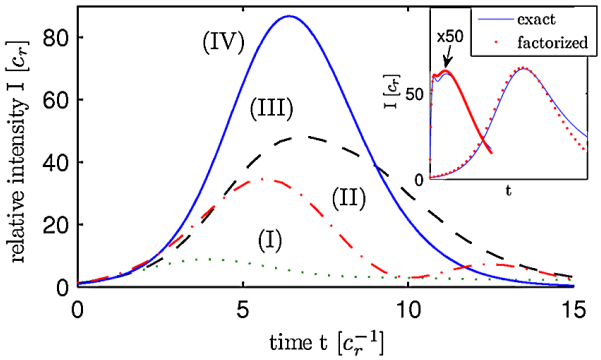


Figure 2.2: Relative intensity under dynamical Overhauser field compensation: $N = 441$, $\omega_S = A/2$ and $\epsilon = 0.3$(I), 0.7(II), 0.99(III). (IV) shows the ideal Dicke SR profile [16] as a reference. Inset: comparison of exact evolution and factorization for $N = 9$ inhomogeneously coupled spins (left peak, scaled by factor 50) and $N = 441$ homogeneous spins ($\epsilon = 0.7$). Fully independent emitters lead to an exponential curve slowly decaying from 1 to zero which is not depicted.

due to the large number of coupled nuclei and since the dynamics for inhomogeneous coupling cannot be restricted to a low-dimensional subspace. To obtain the photon emission intensity $I(t) \propto \frac{d}{dt}\sum_i \langle \sigma_i^+ \sigma_i^- \rangle$ we therefore use an approximative scheme. Via Eqn. (2.2) these expectation values are related to fourth-order correlation terms involving both the electron and nuclear spins. We use a factorization assumption to reduce the higher-order expressions in terms of the covariance matrix $\gamma_{ij}^+ = \left\langle \sigma_i^+ \sigma_j^- \right\rangle$. Following [182] we apply the bosonic Wick's theorem, incorporating the fermionic character of same-site nuclear spin operators ($\left[\sigma_i^+, \sigma_i^-\right]_+ = 1$) and replace, e.g., $\langle \sigma_i^+ \sigma_j^z S^- \rangle \to (\gamma_{jj}^+ - \frac{1}{2})\langle \sigma_i^+ S^- \rangle - \gamma_{ij}^+ \langle \sigma_j^+ S^- \rangle$. However, the electron spin plays a special role amongst the other spins, mediating the collective nuclear interaction, and factorizing it completely leads to poor results. Therefore, we also solve Eqn. (2.2) for the main

higher-order term involving the electron, the "mediated covariance matrix" $\gamma_{ij}^{-} = \left\langle \sigma_i^{+} S^z \sigma_j^{-} \right\rangle$. All other higher-order expectation values therein are factorized under consideration of special symmetries for operators acting on the same site.

In the regimes accessible to an exact treatment, i.e., the homogeneous case and for few inhomogeneously coupled particles, the factorization results agree well with the exact evolution (see inset in Fig. 2.2). This shows that it quantitatively captures the effect of nuclear spin coherences while allowing a numerical treatment of hundreds of spins. Finally, in addition to the constant detuning $\omega_S = A_H/2$ for the displayed simulations we compensated the Overhauser field dynamically[5]. Furthermore, we assume a two-dimensional Gaussian spatial electron wave function, which define the individual hyperfine coupling constants $g_i$. The results obtained

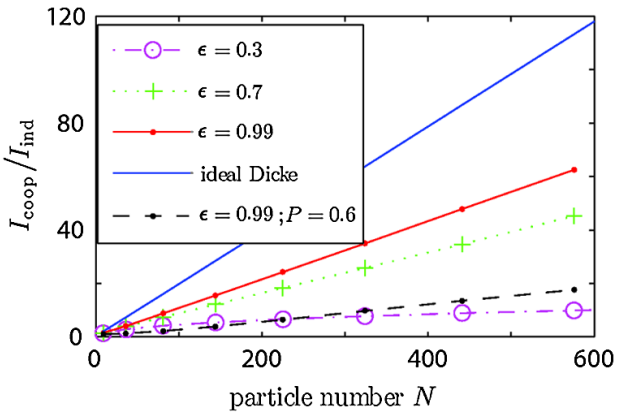


Figure 2.3: $I_{\mathrm{coop}}/I_{\mathrm{ind}}$ for different values of $\epsilon$ - the Overhauser field is dynamically compensated and $\omega_S = A/2$ in all cases - compared to the ideal Dicke case. Dashed line corresponds to a partially polarized dot with 60 % polarization (cf. text).

with these methods are displayed in Fig. 2.2 which show the real time evolution of the emitted photon intensity for different values of the relative coupling strength $\epsilon$ as compared to the ideal Dicke case. Figure 2.3 which displays the relative intensity peak height $I_{\mathrm{coop}}/I_{\mathrm{ind}}$ in dependence on the particle number $N$. For $\epsilon \approx 1$ the strong MPM protection suppresses dephasing, leading to pronounced SR signatures: A strong intensity burst takes place [Fig. 2.2 (III)], whose relative height scales $\propto N$ (for large $N$). In this case, the relative height is reduced only by half compared to the ideal Dicke case [Fig. 2.3 (red solid line)]. For smaller $\epsilon$ it decreases further due to increased dephasing. For $\epsilon \leq 0.3$, where MPM protection is weak and the decay process is significantly slowed down ($c_r \propto \epsilon^2$), even the linear scaling is lost [Fig. 2.3 (purple dashed line)]. From Fig. 2.3 one extrapolates that for a fully polarized initial state a huge intensity overhead of several orders of magnitude ($\sim 10^3$-$10^4$) is predicted. If the initial state is not fully polarized, SR effects are reduced. However, even when, e.g,. starting from a mixture of symmetric Dicke states $|J, J\rangle$ with polarization $P = 60\%$ [178, 183] our simulations predict a strong intensity peak and (for $N \gg 1$) a linear $N$-dependence: $I_{\mathrm{coop}}/I_{\mathrm{ind}} \approx 0.03N$ ($\epsilon = 0.99$), i.e., only a factor 4 weaker than for full polarization.

[5]By applying a time dependent magnetic or spin-dependent AC Stark field such that $\omega_S(t) = g\langle A^z \rangle_t$ we ensure that the measured change in radiation intensity is due to a cooperative emission effect only. Dynamical compensation of the nuclear Overhauser field will be explained in greater detail in Chapter 3.

Note that for the sake of simplicity we consider spin $I = 1/2$ nuclei in our simulations. In terms of particle numbers $N$ this is a pessimistic assumption as typical QD host materials carry a higher spin. We can incorporate this effect by treating higher spins as $2I$ homogeneously coupled spins $1/2$ thus increasing the effective particle number by the factor $2I$. Most QDs consist of a few different species of nuclei with strongly varying magnetic moments, increasing the inhomogeneity of the system. However, in the worst case the different species evolve independently diminishing the effect by a small factor corresponding to the number of species. In our simulations the effect was shown to be much smaller.

We have neglected the dipolar and quadrupolar interaction among the nuclear spins. The former is always negligible on the time scale considered here [98]. The latter is absent for nuclear spin $I = 1/2$ (NV centers, CdSe QDs) or strain-free QDs [178]. In strongly strained QDs it can be important [184], and a term $\sum_i \nu_i (\sigma_i^{z_i})^2$ must be added to Eqn. (2.1), where $z_i$ is defined as the main axis of the local electric-field-gradient tensor, and $\sigma_i^{z_i}$ is the nuclear spin operator along $z_i$.

Having seen that SR can be observed in experimentally accessible nuclear spin ensembles, let us briefly explore a further aspect of this setting: The Master Eqn. (2.3) describes optical pumping of the nuclear spins. Its steady states are the eigenstates of $A^z$ which lie in the kernel of $A^-$, so-called dark states, and include the fully polarized state. Hence the setting described by Eqs. (2.2) and (2.3) can be used to polarize the nuclei [185], i.e., to prepare the initial state required for the observation of SR. By switching the electron spin pumping direction after the nuclei have been polarized in one direction, the superradiant de-excitation proceeds in the opposite direction.

## 2.5 Conclusions and relevance for the upcoming Chapters

We have shown that the nuclear spin environment of individual QDs and NV centers shows superradiant optical emission under suitable optical pumping conditions. While in NV centers a collective intensity enhancement of up to 100% is predicted, the much larger nuclear spin ensembles in QDs could lead to relative peak heights of several orders of magnitude. This would be clear evidence of coherent HF dynamics of nuclear spin ensembles in QDs, arising from a dissipative coupling to an environment. The result that cooperative quantum optical phenomena can take place in solid-state systems, represents an important milestone for the remainder of this Thesis. It is the foundation for the upcoming Chapters:

First, we generalize the idea of SR in the solid state to the case of electrically-defined QDs in a transport setting. Here, photons are replaced by electrons and the cooperative evolution of the system gives rise to an intensity burst in the electron tunnel current rather than the photon emission. This establishes the new paradigm of electronic SR. Second, it is known [77, 186] that, in the thermodynamic limit, an optically driven atomic system with collective superradiant decay – as described by Eqn. (2.3) for homogeneous operators and $m_S = \omega_S = 0$ – can undergo a second-order non-equilibrium phase transition in the steady state. Furthermore, recent experiments in QDs showed the emergence of critical effects like bistability and hysteresis under optical pumping conditions, e.g.[115, 116, 113, 109]. This stimulated a research project, in which we investigated the steady-state phase diagram of a system similar to the one we studied in the present Chapter under additional resonant driving. We find a variety of critical effects in the steady state, and we derive the theoretical tools that enable their complete understanding.

These results are presented in Chapter 4.

# Chapter 3

# Superradiance-like Electron Transport through a Quantum Dot

**After we have seen in the previous Chapter, that the dissipative coupling to optical modes can lead to highly coherent phenomena in solid-state systems, we now demonstrate an analogous effect in electron transport through a electrically-defined quantum dot (EDQD). The focus of this Chapter lies in the rigorous derivation of a master equation based framework for electron transport in the Coulomb-blockade regime which includes hyperfine (HF) interaction with the nuclear spin ensemble in the EDQD. This general tool is then used to study the hyperfine-assisted leakage current through a single EDQD. We find that, for an initially polarized nuclear system, the proposed setup leads to a strong current peak, in close analogy with superradiant emission of photons from atomic ensembles. This effect could be observed with realistic experimental parameters and would as well provide clear evidence of coherent HF dynamics of nuclear spin ensembles in QDs caused by dissipation. This Chapter is based on Publication 1 [SET].**

## 3.1 Introduction

Aside from the aspects discussed above, quantum coherence is also at the very heart of many intriguing phenomena in electronic transport [187]. For example, it is the essential ingredient to the understanding of the famous Aharonov-Bohm-like interference oscillations of the conductance of metallic rings [188] or the well-known conductance steps in quasi-one-dimensional wires [189, 190]. In particular, nonequilibrium electronic transport has emerged as a versatile tool to gain deep insights into the coherent quantum properties of mesoscopic solid-state devices [191, 192]. Here, with the prospect of spintronics and applications in quantum computing, a great deal of research has been directed towards the interplay and feedback mechanisms between electron and nuclear spins in gate-based semiconductor quantum dots [193, 194, 195, 196, 197, 198, 199]. Current fluctuations have been assigned to the random dynamics of the ambient nuclear spins [200] and/or hysteresis effects due to dynamic nuclear polarization [200, 201, 202, 203]. Spin-flip-mediated transport, realized in few-electron quantum dots in the so-called spin blockade regime [204], has been shown to exhibit long time scale oscillations and bistability as a result of a buildup and relaxation of nuclear polarization [200, 201].

The nuclear spins are known to act collectively on the electron spin via hyperfine interaction. In principle, this opens up an exciting testbed for the observation of collective effects which play a remarkable role in a wide range of many-body physics [205, 206, 185].

In this Chapter, we continue along the path paved in the previous Chapter and draw further analogies between mesoscopic solid-state physics and quantum optics: Once more, the nuclear spins surrounding a EDQD are once more identified with an atomic ensemble. However, in contrast to the previous Chapter, the photons of the original setting are associated with electrons tunneling on and off the EDQD in a transport setting. Despite this fundamental difference (electrons are fermions, whereas photons are bosonic particles) this analogy stimulates conjectures about the potential occurrence of related phenomena in these two fields of physics. Led by this line of thought, we address the question of whether superradiant behavior might also be observed in a solid-state environment where the role of photons is played by electrons. To this end, we analyze an EDQD in the Coulomb blockade regime, obtaining two main results, of both experimental and theoretical relevance. First, in analogy to superradiant emission of photons, we show how to observe superradiant emission of electrons in a transport setting through a QD. We demonstrate that the proposed setup, when tuned into the spin blockade regime, carries clear fingerprints of cooperative emission, with no van der Waals dephasing mechanism on relevant time scales. The spin blockade is lifted by the hyperfine (HF) coupling which becomes increasingly more efficient as correlations among the nuclear spins build up. This markedly enhances the spin-flip rate and hence the leakage current running through the QD. Second, we develop a general theoretical master-equation framework that describes the nuclear spin mediated transport through a single QD. Apart from the collective effects due to the HF interaction, the electronic tunneling current is shown to depend on the internal state of the ambient nuclear spins through the effective magnetic field (Overhauser field) produced by the hyperfine interaction. We derive rigorous conditions for the validity of the derived master equation and discuss their implication for the experimental realization.

## 3.2 Executive summary

The Chapter is structured as follows. In Section 3.3, we highlight our key findings and provide an intuitive picture of our basic ideas, allowing the reader to grasp our main results on a qualitative level. By defining the underlying Hamiltonian, Section 3.4 then describes the system in a more rigorous fashion. This enables us to present a detailed derivation of the first main result of this Chapter in Section 3.5: A general master equation for electron transport through a single QD which is coherently enhanced by the HF interaction with the ambient nuclear spins in the QD. It features both collective effects and feedback mechanisms between the electronic and the nuclear subsystem of the QD. We discuss in length the conditions of validity of the approximations in dependence of the temperature and during the coherent evolution of the system. The main result of this Section – including the final master equation and a list of requirements for its validity – are summarized in the Subsection 3.5.3, allowing the reader interested in the phenomenology of electronic SR to skip the mathematical details. Thereafter, in Section 3.6, we investigate the superradiant behavior in the leakage current through a QD. We come to the conclusion that under realistic experimental conditions pronounced superradiant features could be observed, which constitutes the second main result of this Chapter. Section 3.7 backs up our analytical predictions with numerical simulations: When starting from an initially polarized

nuclear spin ensemble, the leakage current through the QD is shown to exhibit a strong peak whose relative height scales linearly with the number of nuclear spins, which we identify as the characteristic feature of superradiant behavior. In Section 3.8 we draw conclusions and give an outlook on future directions of research.

## 3.3 Phenomenological description and the main results of this Chapter

In this section we provide an intuitive exposition of our key ideas and summarize our main findings.

*HF assisted electron transport.–* We study a single EDQD in the Coulomb-blockade regime which is attached to two leads, as schematically depicted in Fig. 3.1. Formally, the Hamiltonian for the total system is given by

$$H = H_Z + H_B + H_T + H_{\mathrm{HF}}. \tag{3.1}$$

Here, $H_Z$ describes the electronic level structure inside the QD in the presence of an external magnetic field. Next, $H_B$ refers to two independent reservoirs of non-interacting electrons, the left and right leads, respectively. The coupling between these and the QD is described in terms of a tunneling Hamiltonian $H_T$ and $H_{\mathrm{HF}}$ models the *collective* hyperfine interaction between an electron confined inside the QD and an ensemble of $N$ proximal nuclear spins surrounding the QD. The specific form of $H$ is given later in Section 3.4.

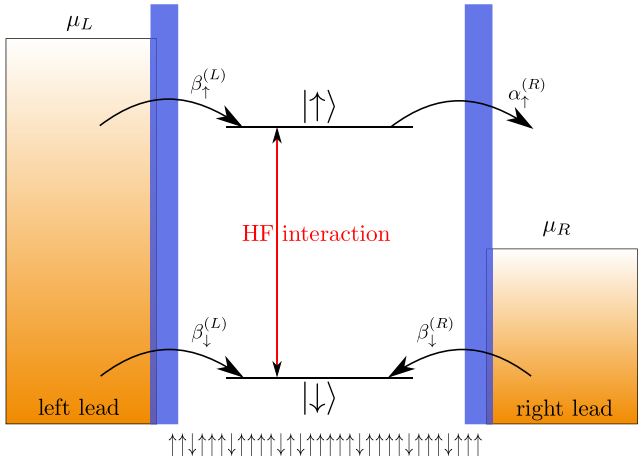


Figure 3.1: Schematic illustration of the transport system: An EDQD is tunnel-coupled to two electron reservoirs, the left and right lead respectively. A bias voltage $eV = \mu_L - \mu_R$ is applied between the two leads in order to induce a current through the QD. An external magnetic field is used to tune the system into the sequential-tunneling regime and the QD effectively acts as an spin-filter. The resulting spin blockade can be lifted by the HF interaction between the QD electron and the nuclear spins in the surrounding host environment.

Our analysis is built on a quantum master-equation approach, a technique originally rooted in the field of quantum optics. By tracing out the unobserved degrees of freedom of the leads we

derive an effective equation of motion for the density matrix of the QD system $\rho_S$ – describing the electron spin inside the QD as well as the nuclear spin ensemble – irreversibly coupled to source and drain electron reservoirs. In addition to the standard assumptions of a weak system-reservoir coupling (Born approximation), a flat reservoir spectral density, and a short reservoir correlation time (Markov approximation), we demand the hyperfine flip-flops to be strongly detuned with respect to the effective magnetic field seen by the electron throughout the dynamics. Under these conditions, the central master equation can be written as

$$\begin{aligned}\dot{\rho}_S(t) &= -i\left[H_Z + H_{\mathrm{HF}}, \rho_S(t)\right] \\ &\quad + \sum_{\sigma=\uparrow,\downarrow} \alpha_\sigma(t)\left[d_\sigma \rho_S(t)\, d_\sigma^\dagger - \frac{1}{2}\left\{d_\sigma^\dagger d_\sigma, \rho_S(t)\right\}\right] \\ &\quad + \sum_{\sigma=\uparrow,\downarrow} \beta_\sigma(t)\left[d_\sigma^\dagger \rho_S(t)\, d_\sigma - \frac{1}{2}\left\{d_\sigma d_\sigma^\dagger, \rho_S(t)\right\}\right],\end{aligned} \tag{3.2}$$

where the tunneling rates $\alpha_\sigma(t)$ and $\beta_\sigma(t)$ describe dissipative processes by which an electron of spin $\sigma$ tunnels from one of the leads into or out of the QD, respectively. Here, the fermionic operator $d_\sigma^\dagger$ creates an electron of spin $\sigma$ inside the QD. While a detailed derivation of Eqn. (3.2) along with the precise form of the tunneling rates is presented in Section 3.5, here we focus on a qualitative discussion of its theoretical and experimental implications. Essentially, our central master equation exhibits two core features:

*Nuclear-state-dependent electronic dissipation.–* First, dissipation only acts on the electronic subsystem with rates $\alpha_\sigma(t)$ and $\beta_\sigma(t)$ that depend dynamically on the state of the nuclear subsystem. This non linear behavior potentially results in hysteretic behavior and feedback mechanisms between the two subsystems as already suggested theoretically [196, 199, 205, 206] and observed in experiments in the context of double QDs in the Pauli-blockade regime (see, e.g., Refs. [197, 198, 203]). On a qualitative level, this finding can be understood as follows: The nuclear spins provide an effective magnetic field for the electron spin, the Overhauser field, whose strength is proportional to the polarization of the nuclear spin ensemble. Thus, a changing nuclear polarization can either dynamically tune or detune the position of the electron levels inside the QD. This, in turn, can have a marked effect on the transport properties of the QD as they crucially depend on the position of these resonances with respect to the chemical potentials of the leads. In our model, this effect is directly captured by the tunneling rates dynamically depending on the state of the nuclei.

*SR in electron transport.–* Second, the collective nature of the HF interaction $H_{\mathrm{HF}}$ allows for the observation of coherent many-body effects. To show this, we refer to the following example: Consider a setting in which the bias voltage and an external magnetic field are tuned such that only one of the two electronic spin components, say the level $|\uparrow\rangle$, lies inside the transport window. In this spin blockade regime the electrons tunneling into the right lead are spin-polarized, i.e., the QD acts as a spin filter [207, 208]. If the HF coupling is sufficiently small compared to the external Zeeman splitting, the electron is predominantly in its $|\downarrow\rangle$ spin state, making it possible to adiabatically eliminate the electronic QD coordinates. In this way we

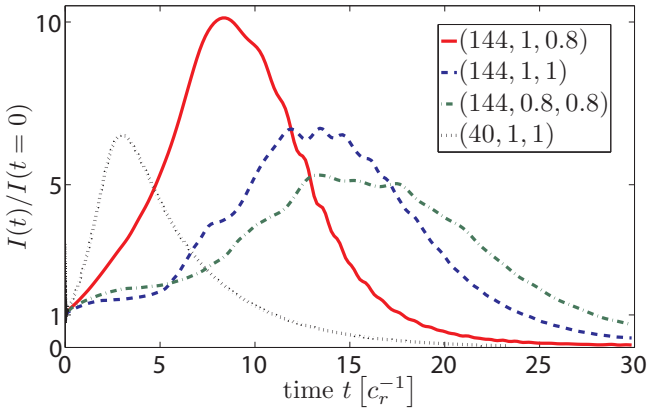


Figure 3.2: Normalized leakage current through a QD in the spin blockade regime for $N$ nuclear spins, initial nuclear polarization $p$ and external Zeeman splitting $\omega_0$ in units of the total HF coupling constant $A_H \approx 100\,\mu$eV, summarized as $(N, p, \omega_0/A_H)$. For homogeneous HF coupling the dynamics can be solved exactly (black dotted line). Compared to this idealized benchmark, the effects are reduced for realistic inhomogeneous HF coupling, but still present: The relative peak height becomes more pronounced for smaller detuning $\omega_0$ or higher polarization $p$ (solid red line compared to the blue dashed and green dash-dotted line, respectively). Even under realistic conditions, the relative peak height is found to scale linearly with $N$, corresponding to a strong enhancement for typically $N \approx 10^5 - 10^6$.

obtain an effective equation of motion for the nuclear density operator $\mu$ only. It reads

$$\begin{aligned}\dot{\mu} &= c_r\left[A^-\mu A^+ - \frac{1}{2}\left\{A^+A^-,\mu\right\}\right] \\ &\quad + ic_i\left[A^+A^-,\mu\right] + i\frac{g}{2}\left[A^z,\mu\right], \end{aligned} \tag{3.3}$$

where $A^\mu = \sum_{i=1}^N g_i\sigma_i^\mu$ with $\mu = +,-,z$ are *collective* nuclear spin operators, composed of *all* $N$ individual nuclear spin operators $\sigma_i^\mu$, with $g_i$ being proportional to the probability of the electron being at the location of the nucleus of site $i$. Again, we highlight the core implications of Eqn. (3.3) and for a full derivation thereof, including the definition of the effective rates $c_r$ and $c_i$, we refer to Section 3.6. Most notably, Eqn. (3.3) has the exact form of Eqn. (2.3) of the previous Chapter 2 which there has been shown to give rise to superradiant effects.

In this Chapter, we find that indeed a corresponding kind of cooperative emission can occur from an ensemble of nuclear spins surrounding an EDQD: The spin blockade can be lifted by the HF interaction as the nuclei pump excitations into the electron. Starting from a highly polarized, weakly correlated nuclear state (which could be prepared by, e.g., dynamic polarization techniques [197, 198, 185]), this process becomes increasingly more efficient, as correlations among the nuclei build up due to the collective nature of the HF interaction. This results in an increased leakage current. Therefore, the current is collectively enhanced by the electron's HF interaction with the ambient nuclear spin ensemble giving rise to a superradiant-like effect in which the leakage current through the QD takes the role of the radiation field: To stress this relation, we also refer to this effect as *superradiant transport of electrons*.

*Comparison to conventional SR.*– As in the optical setting of Chapter 2, the transport system under consideration incorporates two major differences as compared to its conventional atomic counterpart, : First, our setup describes superradiant behavior from a *single* emitter, since in the strong Coulomb-blockade regime the electrons are emitted antibunched. As described above, the superradiant character is due to the nuclear spins acting collectively on the electron spin leading to an increased leakage current on time scales longer than single electron tunneling events. The second crucial difference is the *inhomogeneous* nature ($g_i \neq \text{const.}$) of the collective operators $A^\mu$. Accordingly, the collective spin is not conserved, leading to dephasing between the nuclei which in principle could prevent the observation of superradiant behavior. However, as exemplified in Fig. 3.2, we show that under realistic conditions – taking into account a finite initial polarization of nuclear spins $p$ and dephasing processes due to the inhomogeneous nature of the HF coupling – the leakage current through the QD still exhibits the characteristic peak whose relative height scales linearly with the number of nuclear spins. Even though the effect is reduced compared to the ideal case, for an experimentally realistic number of nuclei $N \approx 10^5 - 10^6$ a strong increase is still predicted. The experimental key signature of this effect, the relative peak height of the leakage current, can be varied by either tuning the external Zeeman splitting or the initial polarization of the nuclear spins.

In the remainder of the Chapter, Eqn. (3.2) and (3.3) are derived from first principles; in particular, the underlying assumptions and approximations are listed. Based on this general theoretical framework, more results along with detailed discussions are presented. For both the idealized case of homogeneous HF coupling – in which an exact solution is feasible even for relatively large $N$ – and the more realistic inhomogeneous case, further numerical simulations prove the existence of a strong superradiant peaking in the leakage current of single QD in the spin blockade regime.

## 3.4 The system

This section gives an in-depth description of the Hamiltonian under study, formally introduced in Eqn. (3.1). The system we consider consists of a single EDQD in a transport setting as schematically depicted in Fig. 3.1. Due to strong confinement only a single orbital level is relevant. Moreover, the QD is assumed to be in the strong Coulomb-blockade regime so that at maximum one electron resides inside the QD. Therefore, the effective Hilbert-space of the QD electron is span $\{|\uparrow\rangle, |\downarrow\rangle, |0\rangle\}$ where the lowest energy states for an additional electron in the QD with spin $\sigma = \uparrow, \downarrow$ are split by an external magnetic field. The Hamiltonian for the total system is given in Eqn. (3.1).

Here, the first term,

$$H_Z = \sum_\sigma \epsilon_\sigma d_\sigma^\dagger d_\sigma, \tag{3.4}$$

describes the electronic levels of the QD. The Zeeman splitting between the two spin components is $\omega_0 = \epsilon_\uparrow - \epsilon_\downarrow$ (we set $\hbar = 1$) and the QD electron operators are $d_\sigma^\dagger = |\sigma\rangle\langle 0|$, describing transitions from the state $|0\rangle$ with no electron inside the QD to a state $|\sigma\rangle$ with one electron of spin $\sigma$ inside the QD.

Electron transport through the QD is induced by attaching the QD to two electron leads (labeled as $L$ and $R$) which are in thermal equilibrium at chemical potentials $\mu_L$ and $\mu_R$,

respectively. The leads themselves constitute reservoirs of non-interacting electrons,

$$H_B = \sum_{\alpha,k,\sigma} \epsilon_{\alpha k} c^\dagger_{\alpha k\sigma} c_{\alpha k\sigma}, \tag{3.5}$$

where $c^\dagger_{\alpha k\sigma}$ ($c_{\alpha k\sigma}$) creates (annihilates) an electron in lead $\alpha = L, R$ with wavevector $k$ and spin $\sigma$. The operators $c^\dagger_{\alpha k\sigma}$ ($c_{\alpha k\sigma}$) fulfill the usual Fermi commutation relations: $\{c^\dagger_{\alpha k\sigma}, c^\dagger_{\alpha' k'\sigma'}\} = \{c_{\alpha k\sigma}, c_{\alpha' k'\sigma'}\} = 0$ and $\{c^\dagger_{\alpha k\sigma}, c_{\alpha' k'\sigma'}\} = \delta_{\alpha,\alpha'}\delta_{k,k'}\delta_{\sigma,\sigma'}$. The effect of the Coulomb interaction in the leads can be taken into account by renormalized effective quasi-particle masses. A positive source-drain voltage $eV = \mu_L - \mu_R$ leads to a dominant tunneling of electrons from left to right. Microscopically, the coupling of the QD system to the electron reservoirs is described in terms of the tunneling Hamiltonian

$$H_T = \sum_{\alpha,k,\sigma} T^{(\alpha)}_{k,\sigma} d^\dagger_\sigma c_{\alpha k\sigma} + \text{h.c.}, \tag{3.6}$$

with the tunnel matrix element $T^{(\alpha)}_{k,\sigma}$ specifying the transfer coupling between the lead $\alpha = L, R$ and the system. There is no direct coupling between the leads and electron transfer is only possible by charging and discharging the QD.

The cooperative effects are based on the collective hyperfine interaction of the electronic spin of the QD with $N$ initially polarized nuclear spins in the host environment of the QD [209]. It is dominated by the isotropic contact term [98] given by

$$H_{\text{HF}} = \frac{g}{2}\left(A^+ S^- + A^- S^+\right) + g A^z S^z. \tag{3.7}$$

Here $S^\mu$ and $A^\mu = \sum_{i=1}^N g_i \sigma_i^\mu$ with $\mu = +, -, z$ denote electron and collective nuclear spin operators, respectively. The coupling coefficients are normalized such that $\sum_i g_i^2 = 1$ and individual nuclear spin operators $\sigma_i^\mu$ are assumed to be spin $1/2$ for simplicity; $g$ is related to the total HF coupling strength $A_H$ via $g = A_H/\sum_i g_i$. We neglect the typically very small nuclear Zeeman and nuclear dipole-dipole terms [98]. For simplicity, we also restrict our analysis to one nuclear species only. These simplifications are addressed in more detail in Section 3.7.

The effect of the HF interaction with the nuclear spin ensemble is twofold: The first part of the above Hamiltonian $H_{\text{ff}} = \frac{g}{2}\left(A^+ S^- + A^- S^+\right)$ is a Jaynes-Cummings-type interaction which exchanges excitations between the QD electron and the nuclei. The second term $H_{\text{OH}} = g A^z S^z$ constitutes a quantum magnetic field, the Overhauser field, for the electron spin generated by the nuclei. If the Overhauser field is not negligible compared to the external Zeeman splitting, it can have a marked effect on the current by (de)tuning the hyperfine flip-flops.

## 3.5 Generalized quantum master equation

Electron transport through a QD can be viewed as a tool to reveal the QD's nonequilibrium properties in terms of the current-voltage $I/V$ characteristics. From a theoretical perspective, a great variety of methods such as the scattering matrix formalism [210] and non-equilibrium Green's functions [211, 192] have been used to explore the $I/V$ characteristics of quantum

systems that are attached to two metal leads. Our analysis is built upon the master equation formalism, a tool widely used in quantum optics for studying the irreversible dynamics of quantum systems coupled to a macroscopic environment.

In what follows, we employ a projection operator based technique to derive an effective master equation for the QD system – comprising the QD electron spin as well as the nuclear spins – which experiences dissipation via the electron's coupling to the leads. This dissipation is shown to dynamically depend on the state of the nuclear system potentially resulting in feedback mechanisms between the two subsystems. We derive conditions which allow for a Markovian treatment of the problem and list the assumptions our master equation based framework is based on.

### 3.5.1 Superoperator formalism - Nakajima-Zwanzig equation

The state of the global system that comprises the QD as well as the environment is represented by the full density matrix $\rho(t)$. However, the actual states of interest are the states of the QD which are described by the reduced density matrix $\rho_S = \mathsf{Tr_B}[\rho]$, where $\mathsf{Tr_B}\ldots$ averages over the unobserved degrees of freedom of the Fermi leads. We derive a master equation that governs the dynamics of the reduced density matrix $\rho_S$ using the superoperator formalism. We start out from the von Neumann equation for the full density matrix

$$\dot{\rho} = -i\left[H(t), \rho\right], \tag{3.8}$$

where $H(t)$ can be decomposed into the following form which turns out to be convenient later on

$$H(t) = H_0(t) + H_1(t) + H_T. \tag{3.9}$$

Here, $H_0(t) = H_Z + H_B + g\langle A^z\rangle_t S^z$ comprises the Zeeman splitting caused by the external magnetic field via $H_Z$ and the Hamiltonian of the non-interacting electrons in the leads $H_B$; moreover, the time-dependent expectation value of the Overhauser field has been absorbed into the definition of $H_0(t)$. The HF interaction between the QD electron and the ensemble of nuclear spins has been split up into the flip-flop term $H_{\mathrm{ff}}$ and the Overhauser field $H_{\mathrm{OH}}$, that is $H_{\mathrm{HF}} = H_{\mathrm{OH}} + H_{\mathrm{ff}}$. The term $H_1(t) = H_{\Delta\mathrm{OH}}(t) + H_{\mathrm{ff}}$ comprises the Jaynes-Cummings-type dynamics $H_{\mathrm{ff}}$ and fluctuations due to deviations of the Overhauser field from its expectation value, i.e., $H_{\Delta\mathrm{OH}}(t) = g\delta A^z S^z$, where $\delta A^z = A^z - \langle A^z\rangle_t$.

The introduction of superoperators – operators acting on the space of linear operators on the Hilbert space – allows for a compact notation. The von Neumann equation is written as $\dot{\rho} = -i\mathcal{L}(t)\rho$, where $\mathcal{L}(t) = \mathcal{L}_0(t) + \mathcal{L}_1(t) + \mathcal{L}_T$ is the Liouville superoperator defined via $\mathcal{L}_\alpha \cdot = [H_\alpha, \cdot]$. Next, we define the superoperator $\mathcal{P}$ as a projector onto the relevant subspace

$$\mathcal{P}\rho(t) = \mathsf{Tr_B}[\rho(t)] \otimes \rho_B^0 = \rho_S(t) \otimes \rho_B^0, \tag{3.10}$$

where $\rho_B^0$ describes separate thermal equilibria of the two leads whose chemical potentials are different due to the bias voltage $eV = \mu_L - \mu_R$. Essentially, $\mathcal{P}$ maps a density operator onto one of product form with the environment in equilibrium but still retains the relevant information on the system state. The complement of $\mathcal{P}$ is $\mathcal{Q} = \mathbb{1} - \mathcal{P}$.

By inserting $\mathcal{P}$ and $\mathcal{Q}$ in front of both sides of the von Neumann equation one can derive a closed equation for the projection $\mathcal{P}\rho(t)$, which for factorized initial condition, where $\mathcal{Q}\rho(0) =$

0, can be rewritten in the form of the generalized Nakajima-Zwanzig master equation,

$$\begin{aligned}\frac{d}{dt}\mathcal{P}\rho &= -i\mathcal{P}\mathcal{L}\mathcal{P}\rho \\ &\quad -\int_0^t dt'\,\mathcal{P}\mathcal{L}\mathcal{Q}\,\hat{T}e^{-i\int_{t'}^t d\tau\mathcal{Q}\mathcal{L}(\tau)}\mathcal{Q}\mathcal{L}\mathcal{P}\rho\left(t'\right),\end{aligned} \tag{3.11}$$

which is non-local in time and contains all orders of the system-leads coupling [212]. Here, $\hat{T}$ denotes the chronological time-ordering operator. Since $\mathcal{P}$ and $\mathcal{Q}$ are projectors onto orthogonal subspaces that are only connected with $\mathcal{L}_T$, this simplifies to

$$\frac{d}{dt}\mathcal{P}\rho = -i\mathcal{P}\mathcal{L}\mathcal{P}\rho - \int_0^t dt'\mathcal{P}\mathcal{L}_T\hat{T}e^{-i\int_{t'}^t d\tau\mathcal{Q}\mathcal{L}(\tau)}\mathcal{L}_T\mathcal{P}\rho\left(t'\right). \tag{3.12}$$

Starting out from this exact integro-differential equation, we introduce some approximations: In the weak coupling limit we neglect all powers of $\mathcal{L}_T$ higher than two (Born approximation). Consequently, we replace $\mathcal{L}(\tau)$ by $\mathcal{L}(\tau)-\mathcal{L}_T$ in the exponential of Eqn. (3.12). Moreover, we make use of the fact that the nuclear spins evolve on a time scale that is very slow compared to all electronic processes: In other words, the Overhauser field is quasi static on the time scale of single electronic tunneling events [185, 146]. That is, we replace $\langle A^z\rangle_\tau$ with $\langle A^z\rangle_t$ in the exponential of Eqn. (3.12), which removes the explicit time dependence in the kernel. By taking the trace over the reservoir and using $\mathsf{Tr}_\mathsf{B}\left[\mathcal{P}\dot{\rho}(t)\right]=\dot{\rho}_S(t)$, we get

$$\begin{aligned}\dot{\rho}_S(t) &= -i\left(\mathcal{L}_Z+\mathcal{L}_{\mathrm{HF}}\right)\rho_S(t) \\ &\quad -\int_0^t d\tau\,\mathsf{Tr}_\mathsf{B}\left(\mathcal{L}_T e^{-i[\mathcal{L}_0(t)+\mathcal{L}_1(t)]\tau}\mathcal{L}_T\mathcal{P}\rho\left(t-\tau\right)\right).\end{aligned} \tag{3.13}$$

Here, we also used the relations $\mathcal{P}\mathcal{L}_T\mathcal{P}=0$ and $\mathcal{L}_B\mathcal{P}=0$ and switched the integration variable to $\tau=t-t'$. Note that, for notational convenience, we suppress the explicit time-dependence of $\mathcal{L}_{0(1)}(t)$ in the following. In the next step, we iterate the Schwinger-Dyson identity

$$\begin{aligned}e^{-i(\mathcal{L}_0+\mathcal{L}_1)\tau} &= e^{-i\mathcal{L}_0\tau} \\ &\quad -i\int_0^\tau d\tau'\,e^{-i\mathcal{L}_0(\tau-\tau')}\mathcal{L}_1 e^{-i(\mathcal{L}_0+\mathcal{L}_1)\tau'}.\end{aligned} \tag{3.14}$$

In what follows, we keep only the first term of this infinite series (note that the next two leading terms are explicitly calculated in Appendix 3.A.1). In quantum optics, this simplification is well known as "approximation of independent rates of variation" [213]. In our setting it is valid, if $\mathcal{L}_1(t)$ is small compared to $\mathcal{L}_0(t)$ and if the bath correlation time $\tau_c$ is short compared to the HF dynamics, $A_H \ll 1/\tau_c$. Pictorially, this means that during the correlation time $\tau_c$ of a tunneling event, there is not sufficient time for the Rabi oscillation with frequency $g \lesssim A_H$ to occur. For typical materials [214], the relaxation time $\tau_c$ is in the range of $\sim 10^{-15}\,\mathrm{s}$ corresponding to a relaxation rate $\Gamma_c=\tau_c^{-1}\approx 10^5\,\mu\mathrm{eV}$. Indeed, this is much faster than all other relevant processes. In this limit, the equation of motion for the reduced density matrix of the system simplifies to

$$\begin{aligned}\dot{\rho}_S(t) &= -i\left(\mathcal{L}_Z+\mathcal{L}_{\mathrm{HF}}\right)\rho_S(t) \\ &\quad -\int_0^t d\tau\,\mathsf{Tr}_\mathsf{B}\left(\mathcal{L}_T e^{-i\mathcal{L}_0(t)\tau}\mathcal{L}_T\rho_S\left(t-\tau\right)\otimes\rho_B^0\right).\end{aligned} \tag{3.15}$$

Note, however, that this master equation is not Markovian as the rate of change of $\rho_S(t)$ still depends on its past. Conditions which allow for a Markovian treatment of the problem are addressed in the following.

### 3.5.2 Markov approximation

Using the general relation $e^{-i\mathcal{L}_0\tau}\mathcal{O} = e^{-iH_0\tau}\mathcal{O}e^{iH_0\tau}$ for any operator $\mathcal{O}$, we rewrite Eqn. (3.15) as

$$\dot{\rho}_S(t) = \tag{3.16}$$
$$-i\left[H_Z + H_{\mathrm{HF}}, \rho_S(t)\right] - \int_0^t d\tau\, \mathsf{Tr}_{\mathsf{B}}\left(\left[H_T, \left[\tilde{H}_T(\tau), e^{-iH_0\tau}\rho_S(t-\tau)\, e^{iH_0\tau} \otimes \rho_B^0\right]\right]\right).$$

In accordance with the previous approximations, we replace $e^{-iH_0\tau}\rho_S(t-\tau)\, e^{iH_0\tau}$ by $\rho_S(t)$ which is approximately the same since any correction to $H_0$ would be of higher order in perturbation theory [215, 216]. In other words, the evolution of $\rho_S(t-\tau)$ is approximated by its unperturbed evolution, which is legitimate provided that the relevant time scale for this evolution $\tau_c$ is very short (Markov approximation). This step is motivated by the typically rapid decay of the lead correlations functions [215]; the precise validity of this approximation is elaborated below. In particular, this simplification disregards dissipative effects induced by $H_T$, which is valid self-consistently provided that the tunneling rates are small compared to the dynamics generated by $H_0$.

Moreover, in Eqn. (3.16) we introduced the tunneling Hamiltonian in the interaction picture as $\tilde{H}_T(\tau) = e^{-iH_0\tau}H_T e^{iH_0\tau}$. For simplicity, we only consider one lead for now and add the terms referring to the second lead later on. Therefore, we can disregard an additional index specifying the left or right reservoir and write explicitly

$$\tilde{H}_T(\tau) = \sum_{k,\sigma} T_{k,\sigma} e^{-i[\epsilon_\sigma(t)-\epsilon_k]\tau} d_\sigma^\dagger c_{k\sigma} + \mathrm{h.c.} \tag{3.17}$$

Here, the resonances $\epsilon_\sigma(t)$ are explicitly time dependent as they dynamically depend on the polarization of the nuclear spins

$$\epsilon_{\uparrow(\downarrow)}(t) = \epsilon_{\uparrow(\downarrow)} \pm \frac{g}{2}\langle A^z\rangle_t\,. \tag{3.18}$$

The quantity

$$\omega = \epsilon_\uparrow(t) - \epsilon_\downarrow(t) = \omega_0 + g\langle A^z\rangle_t \tag{3.19}$$

can be interpreted as an effective Zeeman splitting which incorporates the external magnetic field as well as the mean magnetic field generated by the nuclei.

Since the leads are assumed to be at equilibrium, their correlation functions are given by

$$\mathsf{Tr}_{\mathsf{B}}\left[c_{k\sigma}^\dagger(\tau)\, c_{k'\sigma'}\rho_B^0\right] = \delta_{\sigma,\sigma'}\delta_{k,k'}e^{-i\epsilon_k\tau}f_k, \tag{3.20}$$

$$\mathsf{Tr}_{\mathsf{B}}\left[c_{k\sigma}(\tau)\, c_{k'\sigma'}^\dagger\rho_B^0\right] = \delta_{\sigma,\sigma'}\delta_{k,k'}e^{i\epsilon_k\tau}(1-f_k)\,, \tag{3.21}$$

where the Fermi function $f_k = (1 + \exp[\beta(\epsilon_k - \mu)])^{-1}$ with inverse temperature $\beta = 1/(k_B T)$ gives the thermal occupation number of the respective lead in equilibrium. Note that all terms comprising two lead creation $c^\dagger_{k\sigma}$ or annihilation operators $c_{k\sigma}$ vanish since $\rho^0_B$ contains states with definite electron number only [215]. The correlation functions are diagonal in spin space and the tunneling Hamiltonian preserves the spin projection; therefore only co-rotating terms prevail. If we evaluate all dissipative terms appearing in Eqn. (3.16), due to the conservation of momentum and spin in Eqn. (3.20) and Eqn. (3.21), only a single sum over $k, \sigma$ survives. Here, we single out one term explicitly, but all other terms follow analogously. We obtain

$$\dot{\rho}_S(t) = \ldots + \sum_\sigma \int_0^t d\tau\, \mathcal{C}_\sigma(\tau)\, d^\dagger_\sigma e^{-iH_0\tau} \rho_S(t-\tau)\, e^{iH_0\tau} d_\sigma, \tag{3.22}$$

where the correlation time of the bath $\tau_c$ is determined by the decay of the noise correlations

$$\begin{aligned} \mathcal{C}_\sigma(\tau) &= \sum_k |T_{k,\sigma}|^2 f_k e^{i[\epsilon_\sigma(t) - \epsilon_k]\tau} \\ &= \int_0^\infty d\epsilon\, J_\sigma(\epsilon)\, e^{i[\epsilon_\sigma(t) - \epsilon]\tau}. \end{aligned} \tag{3.23}$$

Here, we made use of the fact that the leads are macroscopic and therefore exhibit a continuous density of states per spin $n(\epsilon)$. On top of that, we have introduced the spectral density of the bath as

$$J_\sigma(\epsilon) = D_\sigma(\epsilon)\, f(\epsilon), \tag{3.24}$$

where $D_\sigma(\epsilon) = n(\epsilon)\,|T_\sigma(\epsilon)|^2$ is the effective density of states. The Markovian treatment manifests itself in a self-consistency argument: We assume that the spectral density of the bath $J_\sigma(\epsilon)$ is flat around the (time-dependent) resonance $\epsilon_\sigma(t)$ over a range set by the characteristic width $\Gamma_\mathrm{d}$. Typically, both the tunneling matrix elements $T_\sigma(\epsilon)$ as well as the density of states $n(\epsilon)$ are slowly varying functions of energy. In the so-called wide-band limit the effective density of states $D_\sigma(\epsilon)$ is assumed to be constant so that the self-consistency argument will exclusively concern the behavior of the Fermi function $f(\epsilon)$ which is intimately related to the temperature of the bath $T$. Under the condition, that $J_\sigma(\epsilon)$ behaves flat on the scale $\Gamma_\mathrm{d}$, it can be replaced with its value at $\epsilon_\sigma(t)$, and the noise correlation simplifies to

$$\mathcal{C}_\sigma(\tau) = J_\sigma(\epsilon_\sigma(t))\, e^{i\epsilon_\sigma(t)\tau} \int_0^\infty d\epsilon\, e^{-i\epsilon\tau}. \tag{3.25}$$

Using the relation

$$\int_0^\infty d\epsilon\, e^{-i\epsilon\tau} = \pi\delta(\tau) - i\mathbb{P}\frac{1}{\tau}, \tag{3.26}$$

with $\mathbb{P}$ denoting Cauchy's principal value, we find that the Markov approximation $\mathrm{Re}[\mathcal{C}_\sigma(\tau)] \propto \delta(\tau)$ is fulfilled provided that the self-consistency argument holds. This corresponds to the white-noise limit where the correlation-time of the bath is $\tau_c = 0$. Pictorially, the reservoir has no memory and instantaneously relaxes to equilibrium. We can then indeed replace $e^{-iH_0\tau}\rho_S(t-\tau)\,e^{iH_0\tau}$ with $\rho_S(t)$ and extend the integration in Eqn. (3.16) to infinity, with negligible contributions due to the rapid decay of the memory kernel. In the following, we derive an explicit condition for the self-consistency argument to be satisfied.

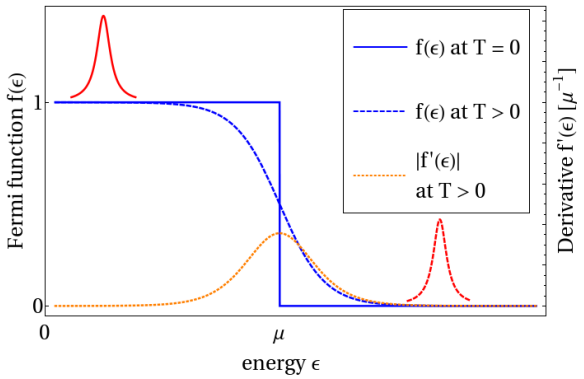


Figure 3.3: Fermi function for finite temperature (dashed blue line) and in the limit $T = 0$ (solid blue line). The absolute value of the derivative of the Fermi function $f'(\epsilon)$ (dotted orange line for finite temperature) is maximized at the chemical potential $\mu$ and tends to a $\delta$ function in the limit $T \to 0$. The Markovian description is valid provided that the Fermi function is approximately constant around the resonances $\epsilon_\sigma(t)$ on a scale of the width of these resonances, schematically shown in red [solid line for $\epsilon_\sigma(t) < \mu$ and dashed line for $\epsilon_\sigma(t) > \mu$].

Let us first consider the limit $T = 0$: As schematically depicted in Fig. 3.3, in this case $f(\epsilon)$ behaves perfectly flat except for $\epsilon = \mu$, where the self-consistency argument is violated. Therefore, the Markovian approximation is valid at $T = 0$ given that the condition $|\epsilon_\sigma(t) - \mu| \gg \Gamma_\mathrm{d}$ is fulfilled. In this limit, all tunneling rates are constant over time and effectively decoupled from the nuclear dynamics. Note that for the observation of superradiant transport it is sufficient to restrict oneself to this case.

For a more general analysis, we now turn to the case of finite temperature $T > 0$. We require the absolute value of the relative change of the Fermi function around the resonance $\epsilon_\sigma(t)$ over a range of the characteristic width $\Gamma_\mathrm{d}$ to be much less than unity, that is

$$\left| \frac{\partial f(\epsilon)}{\partial \epsilon}\bigg|_{\epsilon_\sigma(t)} \right| \Gamma_\mathrm{d} \ll 1. \tag{3.27}$$

An upper bound for the first factor can easily be obtained as this quantity is maximized at the chemical potential $\mu$, for all temperatures. Evaluating the derivative at $\epsilon_\sigma(t) = \mu$ results in the compact condition,

$$\Gamma_\mathrm{d} \ll 4 k_B T. \tag{3.28}$$

Thus, finite temperature $T > 0$ washes out the rapid character of $f(\epsilon)$ at the chemical potential $\mu$ and, provided that Eqn. (3.28) is fulfilled, allows for a Markovian treatment.

Two distinct mechanisms contribute to the width $\Gamma_\mathrm{d}$: dissipation due to coupling to the leads and the effect of $H_1(t)$. Both of them have been neglected self-consistently in the memory kernel when going from Eqn. (3.12) to Eqn. (3.15). Typically, the tunneling rates are of the order of $\sim 5 - 20\mu\mathrm{eV}$, depending on the transparency of the tunnel barrier. Regarding the contribution due to $H_1(t)$, we first consider two limits of particular importance: For a completely mixed state the fluctuation of the nuclear field around its zero expectation value is of

the order of $\sim A_H/\sqrt{N} \approx 0.1\,\mu\mathrm{eV}$. In contrast, for a fully polarized state these fluctuations can be neglected whereas the effective strength of the flip-flop dynamics is $\sim A_H/\sqrt{N}$ as well. Therefore, in both limits considered here, the dominant contribution to $\Gamma_\mathrm{d}$ is due to the coupling to the leads and the self-consistency condition could still be met with cryostatic temperatures $k_B T \gtrsim 10\,\mu\mathrm{eV}$, well below the orbital level spacing. However, we note that in the course of a superradiant evolution, where strong correlations among the nuclei build up, the dominant contribution to $\Gamma_\mathrm{d}$ may come from the flip-flop dynamics, which are $A_H/4 \approx 25\,\mu\mathrm{eV}$ at maximum for homogeneous coupling. For realisitic conditions, though, this effect is significantly reduced, as demonstrated in our simulations in Section 3.7.

### 3.5.3 General master equation for nuclear spin assisted transport

Assuming that the self-consistency argument for a Markovian treatment is satisfied, we now apply the following modifications to Eqn. (3.16): First, we neglect level shifts due to the coupling to the continuum states which can be incorporated by replacing the bare frequencies $\epsilon_\sigma(t)$ with renormalized frequencies. Second, one adds the second electron reservoir that has been omitted in the derivation above. Last, one performs a suitable transformation into a frame rotating at the frequency $\bar{\epsilon} = (\epsilon_\uparrow + \epsilon_\downarrow)/2$ leaving all terms invariant but changing $H_Z$ from $H_Z = \epsilon_\uparrow d_\uparrow^\dagger d_\uparrow + \epsilon_\downarrow d_\downarrow^\dagger d_\downarrow$ to $H_Z = \omega_0 S^z$. After these manipulations one arrives at the central master equation as stated in Eqn. (3.2) where the tunneling rates with $\alpha_\sigma(t) = \sum_{x=L,R} \alpha_\sigma^{(x)}(t)$, $\beta_\sigma(t) = \sum_{x=L,R} \beta_\sigma^{(x)}(t)$, and

$$\begin{aligned} \frac{\alpha_\sigma^{(x)}(t)}{2\pi} &= n_x(\epsilon_\sigma(t)) \left| T_\sigma^{(x)}(\epsilon_\sigma(t)) \right|^2 [1 - f_x(\epsilon_\sigma(t))] \\ \frac{\beta_\sigma^{(x)}(t)}{2\pi} &= n_x(\epsilon_\sigma(t)) \left| T_\sigma^{(x)}(\epsilon_\sigma(t)) \right|^2 f_x(\epsilon_\sigma(t)) \end{aligned} \tag{3.29}$$

govern the dissipative processes in which the QD system exchanges single electrons with the leads. The tunneling rates, as presented here, are widely used in nanostructure quantum transport problems [217, 215, 218]. However, in our setting they are evaluated at the resonances $\epsilon_\sigma(t)$ which dynamically depend on the polarization of the nuclear spins [see Eqn. (3.18)]. Note that Eqn. (3.2) incorporates finite temperature effects via the Fermi functions of the leads. This potentially gives rise to feedback mechanisms between the electronic and the nuclear dynamics, since the purely electronic diffusion markedly depends on the nuclear dynamics.

Since Eqn. (3.2) marks our first main result, at this point we quickly reiterate the assumptions our master equation treatment is based on:

- The system-lead coupling is assumed to be weak and therefore treated perturbatively up to second order (Born approximation).
- In particular, the tunneling rates are small compared to the effective Zeeman splitting $\omega$.
- Level shifts arising from the coupling to the continuum states in the leads are merely incorporated into a redefinition of the QD energy levels $\epsilon_\sigma(t)$.
- There is a separation of time scales between electron-spin dynamics and nuclear-spin dynamics. In particular, the Overhauser field $g\langle A^z\rangle_t$ evolves on a time scale that is slow compared to single electron tunneling events.

- The HF dynamics generated by $H_1(t) = H_{\mathrm{ff}} + H_{\Delta\mathrm{OH}}(t)$ is (i) sufficiently weak compared to $H_0$ and (ii) slow compared to the correlation time of the bath $\tau_c$, that is $A_H \tau_c \ll 1$ (approximation of independent rates of variation). Note that the flip-flop dynamics can become very fast as correlations among the nuclei build up culminating in a maximum coupling strength of $A_H/4$ for homogeneous coupling. This potentially drives the system into the strong coupling regime where condition (i), that is $\omega \gg ||H_1(t)||$, might be violated. However, under realistic conditions of inhomogeneous coupling this effect is significantly reduced.

- The effective density of states $D_\sigma(\epsilon) = n(\epsilon)|T_\sigma(\epsilon)|^2$ is weakly energy-dependent (wide-band limit). In particular, it is flat on a scale of the characteristic widths of the resonances.

- The Markovian description is valid provided that either the resonances are far away from the chemical potentials of the leads on a scale set by the characteristic widths of the resonances or the temperature is sufficiently high to smooth out the rapid character of the Fermi functions of the leads. This condition is quantified in Eqn. (3.28).

In summary, we have derived a quantum master equation describing electronic transport through a single QD which is collectively enhanced due to the interaction with a large ancilla system, namely the nuclear spin ensemble in the host environment. Equation (3.2) incorporates two major intriguing features both of theoretical and experimental relevance: Due to a separation of time scales, only the electronic subsystem experiences dissipation with rates that depend dynamically on the state of the ancilla system. This nonlinearity gives rise to feedback mechanisms between the two subsystems as well as hysteretic behavior. Moreover, the collective nature of the HF interaction offers the possibility to observe intriguing coherent many-body effects. Here, one particular outcome is the occurrence of superradiant electron transport, as shown in the remainder of this Chapter.

Note that in the absence of HF interaction between the QD electron and the proximal nuclear spins, i.e., in the limit $g \to 0$, our results agree with previous theoretical studies [216].

## 3.6 Superradiance-like electron transport

Proceeding from our general theory derived above, this section is devoted to the prediction and analysis of superradiant behavior of nuclear spins, evidenced by the strongly enhanced leakage current through a single QD in the Coulomb-blockade regime; see Fig. 3.1 for the scheme of the setup. A pronounced peak in the leakage current will serve as the main evidence for SR behavior in this setting.

We note that, in principle, an enhancement seen in the leakage current could also simply arise from the Overhauser field dynamically tuning the hyperfine flip-flops. However, we can still ensure that the measured change in the leakage current through the QD is due to cooperative emission only by dynamically compensating the Overhauser field. This can be achieved by applying a time-dependent magnetic or spin-dependent ac Stark field such that $H_{\mathrm{comp}}(t) = -g\langle A^z\rangle_t S^z$, which is done in most of our simulations below to clearly prove the existence of superradiant behavior in this setting. Consequently, in our previous analysis $H_0(t)$ is replaced with $H_0 = H_0(t) - g\langle A^z\rangle_t S^z = H_Z + H_B$ so that the polarization dependence of

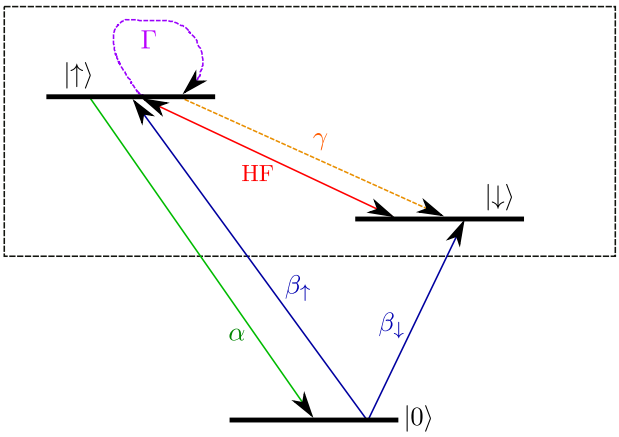


Figure 3.4: The electronic QD system in the local moment regime after the adiabatic elimination of the $|0\rangle$ level including the relevant dissipative processes. Within the effective system (box) we encounter an effective decay term and an effective pure dephasing term, with the rates $\gamma$ and $\Gamma$, respectively. This simplification is possible for fast recharging of the QD, i.e., $\beta \gg \alpha$.

the tunneling rates is removed and we can drop the explicit time-dependence of the resonances $\epsilon_\sigma(t) \to \epsilon_\sigma$. Under this condition, the master equation for the reduced system density operator can be written as

$$\begin{aligned}\dot{\rho}_S(t) &= -i\left[\omega_0 S^z + H_{\mathrm{HF}} + H_{\mathrm{comp}}(t), \rho_S(t)\right] \\ &+ \sum_{\sigma=\uparrow,\downarrow} \alpha_\sigma \left[d_\sigma \rho_S(t) d_\sigma^\dagger - \frac{1}{2}\left\{d_\sigma^\dagger d_\sigma, \rho_S(t)\right\}\right] \\ &+ \sum_{\sigma=\uparrow,\downarrow} \beta_\sigma \left[d_\sigma^\dagger \rho_S(t) d_\sigma - \frac{1}{2}\left\{d_\sigma d_\sigma^\dagger, \rho_S(t)\right\}\right].\end{aligned} \tag{3.30}$$

In accordance with our previous considerations, in this specific setting the Markovian treatment is valid provided that the spectral density of the reservoirs varies smoothly around the (time-independent) resonances $\epsilon_\sigma$ on a scale set by the natural widths of the level and the fluctuations of the dynamically compensated Overhauser field. More specifically, throughout the whole evolution the levels are assumed to be far away from the chemical potentials of the reservoirs [219, 220]; for an illustration see Fig. 3.3. In this wide-band limit, the tunneling rates $\alpha_\sigma$, $\beta_\sigma$ are independent of the state of the nuclear spins. The master equation is of Lindblad form which guarantees the complete positivity of the generated dynamics. Equation (3.30) agrees with previous theoretical results [216], except for the appearance of the collective HF interaction between the QD electron and the ancilla system in the Hamiltonian dynamics of Eqn. (3.30).

To some extent, Eqn. (3.30) bears some similarity with the quantum theory of the laser. While in the latter the atoms interact with bosonic reservoirs, in our transport setting the QD is pumped by the nuclear spin ensemble and emits fermionic particles [211, 218].

If the HF dynamics is the slowest time scale in the problem, Eqn. (3.30) can be recast into a form which makes its superradiant character more apparent. In this case, the system is subject to the slaving principle [211]: The dynamics of the whole system follow that of the subsystem with the slowest time constant, making it possible to adiabatically eliminate the electronic QD coordinates and to obtain an effective equation of motion for the nuclear spins. In this limit, the Overhauser field is much smaller than the Zeeman splitting so that a dynamic compensation of the OH can be disregarded for the moment. For simplicity, we consider a transport setting in which only four tunneling rates are different from zero (see Fig. 3.1). The QD can be recharged from the left and the right lead, but only electrons with spin projection $\sigma =\uparrow$ can tunnel out of the QD into the right lead. We define the total recharging rate $\beta = \beta_\downarrow + \beta_\uparrow = \beta_\downarrow^{(L)} + \beta_\downarrow^{(R)} + \beta_\uparrow^{(L)}$ and for notational convenience unambiguously set $\alpha = \alpha_\uparrow^{(R)}$. First, we project Eqn. (3.30) onto the populations of the electronic levels and the coherences in spin space according to $\rho_{mn} = \langle m| \rho_S |n\rangle$, where $m, n = 0, \uparrow, \downarrow$. This yields

$$\dot{\rho}_{00} = \alpha\rho_{\uparrow\uparrow} - \beta\rho_{00}, \tag{3.31}$$

$$\dot{\rho}_{\uparrow\uparrow} = -i\frac{g}{2}\left[A^z, \rho_{\uparrow\uparrow}\right] - i\frac{g}{2}\left(A^-\rho_{\downarrow\uparrow} - \rho_{\uparrow\downarrow}A^+\right) - \alpha\rho_{\uparrow\uparrow} + \beta_\uparrow\rho_{00}, \tag{3.32}$$

$$\dot{\rho}_{\downarrow\downarrow} = +i\frac{g}{2}\left[A^z, \rho_{\downarrow\downarrow}\right] - i\frac{g}{2}\left(A^+\rho_{\uparrow\downarrow} - \rho_{\downarrow\uparrow}A^-\right) + \beta_\downarrow\rho_{00}, \tag{3.33}$$

$$\dot{\rho}_{\uparrow\downarrow} = -i\omega_0\rho_{\uparrow\downarrow} - i\frac{g}{2}\left(A^z\rho_{\uparrow\downarrow} + \rho_{\uparrow\downarrow}A^z\right) - i\frac{g}{2}\left(A^-\rho_{\downarrow\downarrow} - \rho_{\uparrow\uparrow}A^-\right) - \frac{\alpha}{2}\rho_{\uparrow\downarrow}. \tag{3.34}$$

We can retrieve an effective master equation for the regime in which on relevant time scales the QD is always populated by an electron. This holds for a sufficiently strong recharging rate, that is in the limit $\beta \gg \alpha$, which can be implemented experimentally by making the left tunnel barrier more transparent than the right one. Then, the state $|0\rangle$ is populated negligibly throughout the dynamics and can be eliminated adiabatically according to $\rho_{00} \approx \frac{\alpha}{\beta}\rho_{\uparrow\uparrow}$. In analogy to the Anderson impurity model, in the following this limit is referred to as *local moment regime*. The resulting effective master equation reads

$$\begin{aligned}\dot{\rho}_S = & -i\left[\omega_0 S^z + H_{\mathrm{HF}}, \rho_S\right] \\ & +\gamma\left[S^-\rho_S S^+ - \frac{1}{2}\left\{S^+S^-, \rho_S\right\}\right] \\ & +\Gamma\left[S^z\rho_S S^z - \frac{1}{4}\rho_S\right],\end{aligned} \tag{3.35}$$

where

$$\gamma = \frac{\beta_\downarrow}{\beta}\alpha \tag{3.36}$$

is an effective decay rate and

$$\Gamma = \frac{\beta_\uparrow}{\beta}\alpha \tag{3.37}$$

represents an effective electronic dephasing rate. This situation is schematized in Fig. 3.4. The effective decay (dephasing) describes processes in which the QD is recharged with a spin down (up) electron after a spin up electron has tunneled out of the QD. As demonstrated in Ref. [128], additional electronic dephasing mechanisms only lead to small corrections to the dephasing rate $\Gamma$ and are therefore neglected in Eqn. (3.35).

In the next step we aim for an effective description that contains only the nuclear spins: Starting from a fully polarized state, SR is due to the increase in the operative HF matrix element $\langle A^+A^-\rangle$. The scale of the coupling is set by the total HF coupling constant $A_H = g\sum_i g_i$. For a sufficiently small *relative coupling strength* [209]

$$\epsilon = A_H/\left(2\Delta\right), \tag{3.38}$$

where

$$\Delta = \left|\alpha/2 + i\omega_0\right|, \tag{3.39}$$

the electron is predominantly in its $|\downarrow\rangle$ spin state and we can project Eqn. (3.35) to the respective subspace. As shown in detail in Appendix 3.A.2, in this limit the master equation for the reduced nuclear density operator $\mu = \mathsf{Tr}_{\mathsf{el}}\left[\rho_S\right]$ is given by Eqn. (3.3), where the effective coefficients read

$$c_r = \frac{g^2\alpha}{4\Delta^2}, \tag{3.40}$$

$$c_i = \frac{g^2\omega_0}{4\Delta^2}. \tag{3.41}$$

This master equation is our second main result. Remarkably, the nuclear evolution in the optical setting of Chapter 2 [OSR] is governed by the very same dynamics. There we have theoretically shown that strong SR signatures appear in the optical scattering signal from the system.

In analogy, the superradiant character of Eqn. (3.3) suggests the observation of its prominent intensity peak in the leakage current through the QD in the spin blockade regime. We have employed the method of full-counting-statistics (FCS) [221, 222] in order to obtain an expression for the current and find (setting the electron's charge $e = 1$)

$$I\left(t\right) = \alpha\rho_{\uparrow\uparrow} - \beta_{\downarrow}^{(R)}\rho_{00}. \tag{3.42}$$

This result is in agreement with previous theoretical findings: The current through the device is completely determined by the occupation of the levels adjacent to one of the leads [217, 219, 210]. The first term describes the accumulation of electrons with spin $\sigma =\uparrow$ in the right lead, whereas the second term describes electrons with $\sigma =\downarrow$ tunneling from the right lead into the QD. As done before in Chapter 2, we take the ratio of the maximum current to the initial current (the maximum for independent emitters) $I_{\mathrm{coop}}/I_{\mathrm{ind}}$ as our figure of merit: A relative intensity peak height $I_{\mathrm{coop}}/I_{\mathrm{ind}} > 1$ indicates cooperative effects. One of the characteristic features of SR is that this quantity scales linearly with the number of spins $N$.

In the local-moment regime, described by Eqn. (3.35), the expression for the current simplifies to $I\left(t\right) = (1 - \beta_{\downarrow}^{(R)}/\beta)\alpha\left\langle S^+S^-\right\rangle_t \propto \left\langle S^+S^-\right\rangle_t$, showing that it is directly proportional to the electron inversion. This, in turn, increases as the nuclear system pumps excitations into the electronic system. A compact expression for the relation between the current and the dynamics of the nuclear system can be obtained immediately in the case of homogeneous coupling

$$\frac{d}{dt}\left\langle S^+S^-\right\rangle_t = -\frac{d}{dt}\left\langle I^z\right\rangle_t - \gamma\left\langle S^+S^-\right\rangle_t. \tag{3.43}$$

Since the nuclear dynamics are, in general, much slower than the electron's dynamics, the approximate solution of this equation is $\left\langle S^+S^-\right\rangle_t \approx -\frac{d}{dt}\left\langle I^z\right\rangle_t/\gamma$. As a consequence, the current $I\left(t\right)$ is proportional to the time-derivative of the nuclear polarization,

$$I\left(t\right) \propto -\frac{d}{dt}\left\langle I^z\right\rangle_t. \tag{3.44}$$

Still, no matter how strong the cooperative effects are, on a time scale of single electron tunneling events, the electrons will always be emitted antibunched, since in the strong Coulomb-blockade regime the QD acts as a single-electron emitter [223]. Typically, the rate for single-electron emission events is even below the tunneling rate $\alpha$ due to the spin blockade. On electronic time scales $\sim 1/\alpha$, the SR mechanism manifests in lifting this blockade; as argued above, the efficiency of this process is significantly enhanced by collective effects.

Before we proceed with an in-depth analysis of the current $I(t)$, we note that an intriguing extension of the present work would be the study of fluctuations thereof (see, for example, [224] for studies of the shot noise spectrum in a related system). Insights into the statistics of the current could be obtained by analyzing two-time correlation functions such as $\langle n_\uparrow(t+\tau)n_\uparrow(t)\rangle$, where $n_\uparrow = d_\uparrow^\dagger d_\uparrow$. This can conveniently be done via the Quantum Regression Theorem [225], which yields the formal result $\langle n_\uparrow(t+\tau)n_\uparrow(t)\rangle = \mathsf{Tr}_\mathsf{S}\left[n_\uparrow e^{\mathcal{W}\tau}\left(n_\uparrow \rho_S(t)\right)\right]$. Here, $\mathcal{W}$ denotes the Liouvillian governing the system's dynamics according to $\dot\rho_S = \mathcal{W}\rho_S$ [see Eqn. (3.35)] and $\mathsf{Tr}_\mathsf{S}[\dots]$ refers to the trace over the system's degree of freedoms. This procedure can be generalized to higher-order correlation functions and full evaluation of the current statistics might reveal potential connections between current fluctuations and cooperative nuclear dynamics.

## 3.7 Analysis and numerical results

### 3.7.1 Experimental realization

The proposed setup described here may be realized with state-of-the-art experimental techniques. First, the Markovian regime, valid for sufficiently large bias $eV$, is realized if the Fermi functions of the leads are smooth on a scale set by the natural widths of the levels and residual fluctuations due to the dynamically compensated Overhauser field. Since for typical materials [193] the hyperfine coupling constant is $A_H = 1 - 100\mu\mathrm{eV}$ and tunneling rates are typically [194] of the order of $\sim 10\,\mu\mathrm{eV}$, this does not put a severe restriction on the bias voltage which is routinely [203, 204] in the range of hundreds of $\mu\mathrm{V}$ or $\mathrm{mV}$. Second, in order to tune the system into the spin blockade regime, a sufficiently large external magnetic field has to be applied. More precisely, the corresponding Zeeman splitting $\omega_0$ energetically separates the upper and lower manifolds in such a way that the Fermi function of the right lead drops from one at the lower manifold to zero at the upper manifold. Finite temperature $T$ smears out the Fermi function around the chemical potential by approximately $\sim k_B T$. Accordingly, with cryostatic temperatures of $k_B T \sim 10\,\mu\mathrm{eV}$ being routinely realized in the laboratory [195], this condition can be met by applying an external magnetic field of $\sim 5 - 10\mathrm{T}$ which is equivalent to $\omega_0 \approx 100 - 200\mu\mathrm{eV}$ in GaAs [193, 226]. The charging energy $U$, typically $\sim 1 - 4\mathrm{meV}$ [194, 204], sets the largest energy scale in the problem justifying the Coulomb-blockade regime with negligible double occupancy of the QD provided that the chemical potential of the left lead is well below the doubly occupied level. Lastly, we note that similar setups to the one proposed here have previously been realized experimentally by, e.g., Hanson *et al.* [208, 226].

Proceeding from these considerations, we now show by numerical simulation that an SR peaking of several orders of magnitude can be observed for experimentally relevant parameters in the leakage current through a quantum dot in the spin blockade regime. We first consider the idealized case of homogeneous coupling for which an exact numerical treatment is feasible even for a larger number of coupled nuclei. Then, we continue with the more realistic case of

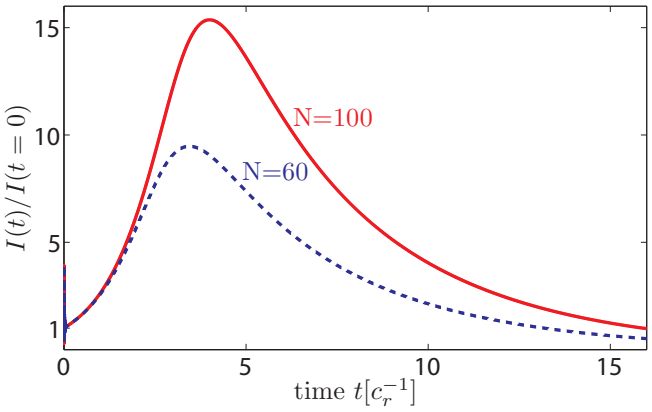


Figure 3.5: Typical time evolution of the normalized current for homogeneous coupling under dynamical compensation of the Overhauser field and a relative coupling strength of $\epsilon = 0.5$, shown here for $N = 60$ and $N = 100$ nuclear spins. The characteristic feature of SR, a pronounced peak in the leakage current proportional to $N$, is clearly observed.

inhomogeneous coupling for which an approximative scheme is applied. Here, we also study scenarios in which the nuclear spins are not fully polarized initially. Moreover, we discuss intrinsic nuclear dephasing effects and undesired cotunneling processes which have been omitted in our simulations. In particular, we show that the inhomogeneous nature of the HF coupling accounts for the strongest dephasing mechanism in our system. We note that this effect is covered in the second set of our simulations. Finally, we self-consistently justify the perturbative treatment of the Overhauser-field fluctuations as well as the HF flip-flop dynamics.

### 3.7.2 Superradiant electron transport

#### Idealized setting

The homogeneous case allows for an exact treatment even for a relatively large number of nuclei as the system evolves within the totally symmetric low-dimensional subspace $\{|J,m\rangle\,, m=-J,\ldots,J\}$. Starting from a fully polarized state, a strong intensity enhancement is observed; typical results obtained from numerical simulations of Eqn. (3.30) are depicted in Fig. 3.5 for $N = 60$ and $N = 100$ nuclear spins. The corresponding relative peak heights display a linear dependence with $N$ (cf. Fig. 3.6), which we identify as the characteristic feature of SR. Here, we have used the numerical parameters $A_H = 1$, $\omega_0 = 1$ and $\alpha = \beta_{\uparrow}^{(L)} = \beta_{\downarrow}^{(L)} = \beta_{\downarrow}^{(R)} = 0.1$ in units of $\sim 100\,\mu$eV, corresponding to a relative coupling strength $\epsilon = 0.5$.

Before we proceed, some further remarks on the dynamic compensation of the Overhauser field seem appropriate: We have merely introduced it in our analysis in order to provide a clear criterion for the presence of purely collective effects, given by $I_{\mathrm{coop}}/I_{\mathrm{ind}} > 1$. In other words, dynamic compensation of the Overhauser field is not a necessary requirement for the observation of collective effects, but it is rather an adequate tool to display them clearly. From an experimental point of view, the dynamic compensation of the Overhauser field might be challenging as it requires accurate knowledge about the evolution of the nuclear spins. Therefore,

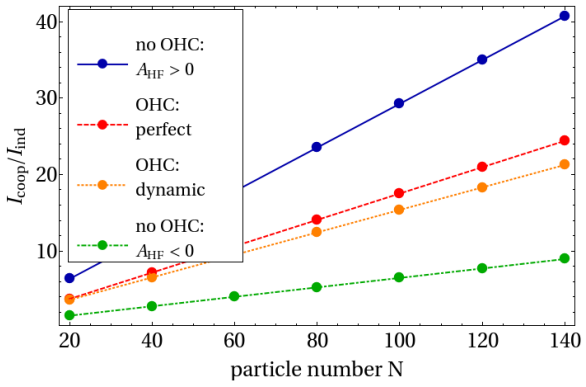


Figure 3.6: Ratio of the maximum current to the initial current $I_{\mathrm{coop}}/I_{\mathrm{ind}}$ as a function of the number of nuclear spins $N$ for homogeneous coupling and a relative coupling strength of $\epsilon = 0.5$: Results for perfect compensation (dashed line) are compared to the case of dynamic compensation (dotted line) of the Overhauser field (OHC). Simulations without compensation of the Overhauser field set bounds for the enhancement of the leakage current, depending on the sign of the HF coupling constant $A_H$; solid and dash-dotted line for $A_H > 0$ and $A_H < 0$, respectively.

we also present results for the case in which the external magnetic field is constant and no compensation is applied. Here, we can distinguish two cases: Depending on the sign of the HF coupling constant $A_H$, the time dependence of the effective Zeeman-splitting $\omega$ can either give rise to an additional enhancement of the leakage current $(A_H > 0)$ or it can counteract the collective effects $(A_H < 0)$. As shown in Fig. 3.6, this sets lower and upper bounds for the observed enhancement of the leakage current.

In Fig. 3.6 we also compare the results obtained for dynamic compensation of the Overhauser field to the idealized case of perfect compensation in which the effect of the Overhauser term is set to zero, i.e., $H_{\mathrm{OH}} = gA^z S^z = 0$. Both approaches display the same features justifying our approximation of neglecting residual (de)tuning effects of the dynamically compensated Overhauser field with respect to the external Zeeman splitting $\omega_0$. This is also discussed in greater detail below.

### Beyond the idealized setting

*Inhomogeneous HF coupling.–* In principle, the inhomogeneous HF coupling could prevent the phasing necessary for SR. However, as shown below, SR is still present in realistically inhomogeneous systems. In contrast to the idealized case of homogeneous coupling, the dynamics cannot be restricted to a low-dimensional subspace so that an exact numerical treatment is not feasible due to the large number of nuclei. We therefore use the approximate approach of Chapter 2 which there has been shown to capture the effect of nuclear spin coherences while allowing for a numerical treatment of hundreds of spins. For simplicity, we restrict ourselves to the local moment regime in which the current can be obtained directly from the electron inversion $I(t) \propto \langle S^+ S^- \rangle_t$. By Eqn. (3.35), this expectation value is related to a hierarchy

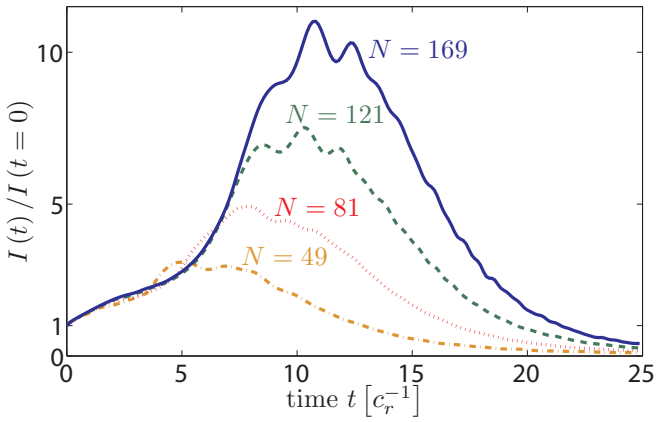


Figure 3.7: Typical time evolution of the normalized current for inhomogeneous coupling, shown here for up to $N = 13^2$ nuclear spins and a relative coupling strength $\epsilon = 0.55$. Compared to the idealized case of homogeneous coupling, the SR effects are reduced, but still clearly present. A Gaussian spatial electron wave function has been assumed and the Overhauser field is compensated dynamically.

of correlation terms involving both the electron and the nuclear spins. Based on a Wick type factorization scheme, higher-order expressions are factorized in terms of the covariance matrix $\gamma_{ij}^{+} = \left\langle \sigma_i^{+} \sigma_j^{-} \right\rangle$ and the "mediated covariance matrix" $\gamma_{ij}^{-} = \left\langle \sigma_i^{+} S^z \sigma_j^{-} \right\rangle$. For further details, see Refs. [185, 209].

The coupling constants $g_j$ have been obtained from the assumption of a two-dimensional Gaussian spatial electron wavefunction of width $\sqrt{N}/2$. Specifically, we present results for two sets of numerical parameters, corresponding to a relative coupling strength of $\epsilon = 0.5$, where $A_H = 1$, $\omega_0 = 1$, $\gamma = 0.1$, and $\Gamma = 0.08$, and $\epsilon = 0.55$ with $A_H = 1$, $\omega_0 = 0.9$, $\gamma = 0.1$, and $\Gamma = 0.067$.

As shown in Figs. 3.7 and 3.8, the results obtained with these methods demonstrate clear SR signatures. In comparison to the ideal case of homogeneous coupling, the relative height is reduced, but for a *fully polarized* initial state we still find a linear enhancement $I_{\mathrm{coop}}/I_{\mathrm{ind}} \approx 0.043N$ $(\epsilon = 0.5)$; therefore, as long as this linear dependence is valid, for typically $N \approx 10^5 - 10^6$ a strong intensity enhancement of several orders of magnitude is predicted $\left(\sim 10^3 - 10^4\right)$.

*Imperfect initial polarization.*– If the initial state is not fully polarized, SR effects are reduced: However, when starting from a mixture of symmetric Dicke states $|J, J\rangle$ with polarization $p = 80(60)\%$, we find that the linear $N$ dependence is still present: $I_{\mathrm{coop}}/I_{\mathrm{ind}} \approx 0.0075(0.0025)N$ for $\epsilon = 0.5$, i.e., the scaling is about a factor of $\sim 5(15)$ weaker than for full polarization[1]. Still, provided the linear scaling holds up to an experimentally realistic number of nuclei $N \approx 10^5 - 10^6$, this amounts to a relative enhancement of the order of $I_{\mathrm{coop}}/I_{\mathrm{ind}} \sim 10^2 - 10^3$. To clearly resolve this peak experimentally, any spurious current should not be larger than the initial HF-mediated leakage current. As we argue below, this con-

[1]For finite polarization the initial covariance matrix has been determined heuristically from the dark state condition $\left\langle A^{-} A^{+} \right\rangle = 0$ in the homogeneous limit.

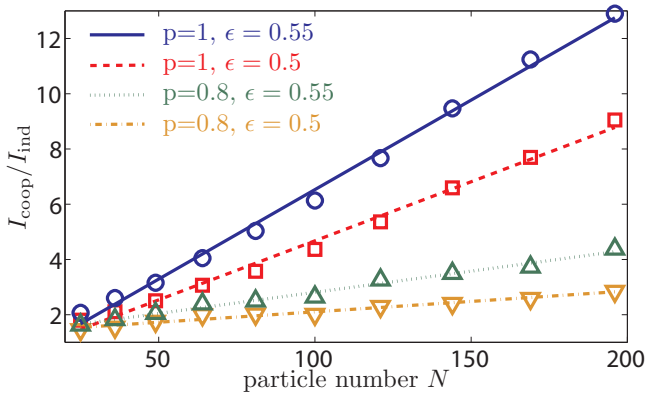


Figure 3.8: Ratio of the maximum current to the initial current $I_{\mathrm{coop}}/I_{\mathrm{ind}}$ as a function of the number of nuclear spins $N$ for relative coupling strengths $\epsilon = 0.5$ and $\epsilon = 0.55$: Results for inhomogeneous coupling. The linear dependence is still present when starting from a nuclear state with finite polarization $p = 0.8$.

dition can be fulfilled in our setup, since the main spurious mechanism, cotunneling, is strongy suppressed.

*Nuclear Zeeman term and species inhomogeneity.*– In our simulations we have disregarded the nuclear Zeeman energies. For a single nuclear species, this term plays no role in the SR dynamics. However, in typical QDs several nuclear species with different $g$ factors are present ("species inhomogeneity"). In principle, these are large enough to cause additional dephasing between the nuclear spins, similar to the inhomogeneous Knight field [185]. However, this dephasing mechanism only applies to nuclei which belong to different species [185]. This leads to few (in GaAs three) mutually decohered subsystems each of which is described by our theory.

*Nuclear interactions.*– Moreover, we have neglected the dipolar and quadrupolar interactions among the nuclear spins. First, the nuclear dipole-dipole interaction can cause diffusion and dephasing processes. Diffusion processes that can change $A^z$ are strongly detuned by the Knight field and therefore are of minor importance, as corroborated by experimentally measured spin diffusion rates [227, 228]. Resonant processes such as $\propto I_i^z I_j^z$ can lead to dephasing similar to the inhomogeneous Knight shift. This competes with the phasing necessary for the observation of SR as expressed by the first term in Eqn. (3.3). The SR process is the weakest at the very beginning of the evolution where we estimate its strength as $c_r^{\mathrm{min}} \approx 10\,\mu\mathrm{eV}/N$. An upper bound for the dipole-dipole interaction in GaAs has been given in Ref. [98] as $\sim 10^{-5}\,\mu\mathrm{eV}$, in agreement with values given in Refs. [146, 128]. Therefore, the nuclear dipole-dipole interaction can safely be neglected for $N \lesssim 10^5$. In particular, its dephasing effect should be further reduced for highly polarized ensembles.

Second, the nuclear quadrupolar interactions can have two origins: strain (largely absent in EDQDs) and electric field gradients originating from the electron. These have been estimated for typical EDQDs in Ref. [128] to lead to an additional nuclear level splitting on the order of $\sim 10^{-5}\,\mu\mathrm{eV}$. Moreover, they are absent for nuclear spin $I = 1/2$ (e.g. CdSe QDs). To summarize, the additional dephasing mechanisms induced by nuclear interactions are much smaller than the terms arising from the inhomogeneous Knight field [146]. As argued above

and confirmed by our simulations, the latter does not prevent the observation of SR behavior due to the presence of the MPM-term (cf. Chapter 2) in Eqn. (3.3).

### Quantitative aspects

Initially, the HF-mediated SR dynamics is rather slow, with its characteristic time scale set by $c_r^{-1}$; for experimentally realistic parameters – in what follows we use the parameter set $\left(\epsilon = 0.5,\ \alpha \approx 10\,\mu\text{eV},\ N \approx 10^5\right)$ for numerical estimates – this corresponds to $c_r^{-1} \approx 10\,\mu\text{s}$. Based on fits as shown in Fig. 3.9, we then estimate for the SR process duration $\langle t_D \rangle \approx 50 c_r^{-1} \approx 500\,\mu\text{s}$ which is still smaller than recently reported [229] nuclear decoherence times of $\sim 1\,\text{ms}$. Therefore, it should be possible to observe the characteristic enhancement of the leakage current before the nuclear spins decohere.

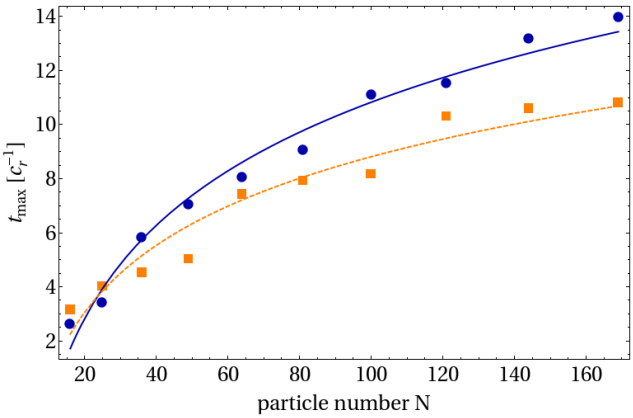


Figure 3.9: Total time till the observation of the characteristic SR peaking $t_{\max}$ for $\epsilon = 0.5$ (blue dots) and $\epsilon = 0.55$ (orange squares). Based on Eqn. (2.6), logarithmic fits are obtained from which we estimate $t_{\max}$ for experimentally realistic number of nuclear spins $N \approx 10^5$.

*Leakage current.–* Accordingly, in the initial phasing stage, the HF-mediated lifting of the spin blockade is rather weak, resulting in a low leakage current, approximatively given by $I\,(t=0)\,/(e\hbar^{-1}) \approx \epsilon^2\alpha/N$. Therefore, the initial current due to HF processes is inversely proportional to the number of nuclear spins $N$. However, as correlations among the nuclei build up, the HF-mediated lifting becomes more efficient culminating in a maximum current of $I_{\max}/(e\hbar^{-1}) \approx \epsilon^2\alpha$, independent of $N$. For realistic experimental values – also taking into account the effects of inhomogeneous HF coupling and finite initial polarization $p \approx 0.6$ – we estimate the initial (maximum) leakage current to be of the order of $I\,(t=0) \approx 6\,\text{fA}$ ($I_{\max} \approx 10\,\text{pA}$). Leakage currents in this range of magnitudes have already been detected in single QD spin-filter experiments [208], as well as double QD Pauli-blockade experiments [200, 201, 203, 204]; here, leakage currents below 10 fA and 150 fA, respectively, have been attributed explicitly to other spurious processes [208, 203]. These are addressed in greater detail in the following.

Our transport setting is tuned into the sequential tunneling regime and therefore we have disregarded cotunneling processes which are fourth order in $H_T$. In principle, cotunneling pro-

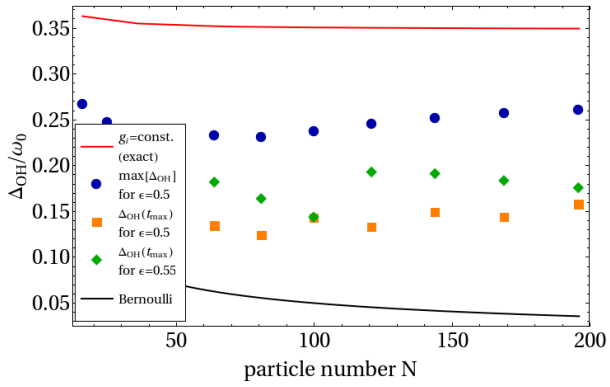


Figure 3.10: Fluctuations of the Overhauser field relative to the external Zeeman splitting $\omega_0$. In the limit of homogeneous HF coupling, strong fluctuations build up towards the middle of the emission process (red line, $\epsilon = 0.5$). For inhomogeneous coupling this build-up of fluctuations is hindered by the dephasing between the nuclear spins, resulting in considerably smaller fluctuations: The value of the Overhauser fluctuations is shown at the time of the SR peak $t_{\max}$ for $\epsilon = 0.5$ (orange squares) and $\epsilon = 0.55$ (green diamonds). The Overhauser fluctuations reach a maximum value later than $t_{\max}$, see blue dots for $\epsilon = 0.5$. For independent homogeneously coupled nuclear spins, one can estimate the fluctuations via the binominal distribution (black line).

cesses could lift the spin blockade and add an extra contribution to the leakage current that is independent of the HF dynamics. However, note that cotunneling current scales as $I_{\rm ct} \propto \alpha^2$, whereas sequential tunneling current $I \propto \alpha$; accordingly, cotunneling current can always be suppressed by making the tunnel barriers less transparent [208]. Moreover, inelastic cotunneling processes exciting the QD spin can be ruled out for $eV, k_B T < \omega_0$ due to energy conservation [207]. The effectiveness of a single quantum dot to act as an electrically tunable spin filter has also been demonstrated experimentally [208]: The spin-filter efficiency was measured to be nearly $100\%$, with $I_{\rm ct}$ being smaller than the noise floor $\sim 10\,\mathrm{fA}$. Its actual value has been calculated as $\sim 10^{-4}\,\mathrm{fA}$, from which we roughly estimate $I_{\rm ct} \sim 10^{-2}\,\mathrm{fA}$ in our setting. This is smaller than the initial HF-mediated current $I\,(t=0)$ and considerably smaller than $I_{\max}$, even for an initially not fully polarized nuclear spin ensemble. Still, if one is to explore the regime where cotunneling cannot be neglected, phenomenological dissipative terms – effectively describing the corresponding spin-flip and pure dephasing mechanisms for inelastic and elastic processes, respectively – should be added to Eqn. (3.30).

### Self-consistency

In our simulations we have self-consistently verified that the fluctuations of the Overhauser field, defined via

$$\Delta_{\rm OH}\,(t) = g\sqrt{\langle A_z^2\rangle_t - \langle A_z\rangle_t^2}, \tag{3.45}$$

are indeed small compared to the external Zeeman splitting $\omega_0$ throughout the entire evolution. This ensures the validity of our perturbative approach and the realization of the spin blockade regime. From atomic SR it is known that in the limit of homogeneous coupling large fluctuations can build up, since in the middle of the emission process the density matrix becomes a broad distribution over the Dicke states [17]. Accordingly, in the idealized, exactly solvable case of homogeneous coupling we numerically find rather large fluctuations of the Overhauser field; as demonstrated in Fig. 3.10, this holds independently of $N$. In particular, for a relative coupling strength $\epsilon = 0.5$ the fluctuations culminate in $\max\left[\Delta_{\mathrm{OH}}\right]/\omega_0 \approx 0.35$. However, in the case of inhomogeneneous HF coupling the Overhauser field fluctuations are found to be smaller as the build-up of these fluctuations is hindered by the Knight term causing dephasing among the nuclear spins. As another limiting case, we also estimate the fluctuations for completely independent homogeneously coupled nuclear spins via the binominal distribution as $\max\left[\Delta_{\mathrm{OH}}\right] \sim 0.5 A_H/\sqrt{N}$[2].

Moreover, we have also ensured self-consistently the validity of the perturbative treatment of the flip-flop dynamics; that is, throughout the entire evolution, even for maximum operative matrix elements $\langle A^+ A^- \rangle_t$, the strength of the flip-flop dynamics $\|H_{\mathrm{ff}}\|$ was still at least five times smaller than $\omega_0$.

## 3.8 Conclusion and outlook

In summary, we have developed a master-equation-based theoretical framework for nuclear-spin-assisted transport through a QD. Due to the collective nature of the HF interaction, it incorporates intriguing many-body effects as well as feedback mechanisms between the electron spin and nuclear spin dynamics. As a prominent application, we have shown that the current through a single EDQD in the spin blockade regime naturally exhibits superradiant behavior. This effect stems from the collective hyperfine interaction between the QD electron and the nuclear spin ensemble in the QD. Its most striking feature is a lifting of the spin blockade and a pronounced peak in the leakage current. The experimental observation of this effect would provide clear evidence of coherent HF dynamics of nuclear spin ensembles in QDs.

Finally, we highlight possible directions of research going beyond our present work: Apart from superradiant electron transport, the setup proposed here is inherently well suited for other experimental applications like dynamic polarization of nuclear spins (DNP): In analogy to optical pumping, Eqn. (3.3) describes *electronic* pumping of the nuclear spins. Its steady states are eigenstates of $A^z$, which lie in the kernel of the collective jump operator $A^-$. In particular, for a completely inhomogeneous system the only steady state is the fully polarized one, the ideal initial state required for the observation of SR effects. When starting from a completely unpolarized nuclear state, the uni directionality of Eqn. (3.3) – electrons with one spin orientation exchange excitations with the nuclear spins, while electrons of opposite spin primarily do not – implies that the rather warm electronic reservoir can still extract entropy out of the nuclear system. More generally, the transport setting studied here possibly opens up the route towards the (feedback-based) electronic preparation of particular nuclear states in single QDs. This is in line with similar ideas previously developed in double QD settings (see, e.g., [197, 200, 203, 205, 229]).

In this work we have specialized on a single QD. However, our theory could be extended to

[2] This limit is realized if strong nuclear dephasing processes prevent the coherence build-up of the SR evolution.

a double QD (DQD) setting which is likely to offer even more possibilities. DQDs are routinely operated in the Pauli-blockade regime where despite the presence of an applied source-drain voltage the current through the device is blocked whenever the electron tunneling into the DQD has the same spin orientation as the one already present. The DQD parameters and the external magnetic field can be tuned such that the role of the states $|\sigma\rangle\,, \sigma =\downarrow, \uparrow$, in our model is played by a pair of singlet and triplet states, while all other states are off-resonant. Then, along the lines of our study, nonlinearities appear due to dependencies between the electronic and nuclear subsystems and collective effects enter via the HF-mediated lifting of the spin blockade.

While we have focused on the Markovian regime and the precise conditions for its validity, Eqn. (3.15) offers a starting point for studies of non-Markovian effects in the proposed transport setting. All terms appearing in the memory kernel of Eqn. (3.15) are quadratic in the fermionic creation and annihilation operators allowing for an efficient numerical simulation, without having to explicitly invoke the flatness of the spectral density of the leads. This should then shed light on possibly abrupt changes in the QD transport properties due to feedback mechanism between the nuclear spin ensemble and the electron spin.

Last and in analogy to the optical setting of Chapter 2, our work also opens the door towards studies of dissipative phase transitions in the transport setting: When combined with driving, the SR dynamics can lead to a variety of strong-correlation effects, non-equilibrium, and dissipative phase transitions [173, 77, 230, 79], which could now be studied in a mesoscopic solid-state system, complementing other approaches to dissipative phase transitions in QDs [231, 232, 233]. In the following Chapter we will study a related driven central spin model with collective dissipation, and we investigate the numerous critical effects in the steady-state phase diagram.

## 3.A Supplementary material 3

### 3.A.1 Microscopic derivation of the master equation

In this Appendix we provide some details regarding the derivation of the master equations as stated in Eqn. (3.2) and Eqn. (3.30). It comprises the effect of the HF dynamics in the memory kernel of Eqn. (3.13) and the subsequent approximation of independent rates of variation.

In the following, we show that it is self-consistent to neglect the effect of the HF dynamics $\mathcal{L}_1(t)$ in the memory kernel of Eqn. (3.13) provided that the bath correlation time $\tau_c$ is short compared to the Rabi flips produced by the HF dynamics. This needs to be addressed as cooperative effects potentially drive the system from a weakly coupled into a strongly coupled regime. First, we reiterate the Schwinger-Dyson identity in Eqn. (3.14) as an infinite sum over time-ordered nested commutators

$$e^{-i(\mathcal{L}_0+\mathcal{L}_1)\tau} = e^{-i\mathcal{L}_0\tau}\sum_{n=0}^{\infty}(-i)^n\int_0^{\tau}d\tau_1\int_0^{\tau_1}d\tau_2\ldots\int_0^{\tau_{n-1}}d\tau_n\,\tilde{\mathcal{L}}_1(\tau_1)\,\tilde{\mathcal{L}}_1(\tau_2)\ldots\tilde{\mathcal{L}}_1(\tau_n)\,, \tag{3.46}$$

where for any operator $X$

$$\tilde{\mathcal{L}}_1(\tau)\,X = e^{i\mathcal{L}_0\tau}\mathcal{L}_1 e^{-i\mathcal{L}_0\tau}X = \left[e^{iH_0\tau}H_1e^{-iH_0\tau},X\right] = \left[\tilde{H}_1(\tau),X\right]. \tag{3.47}$$

More explicitly, up to second order Eqn. (3.46) is equivalent to

$$\begin{aligned} e^{-i(\mathcal{L}_0+\mathcal{L}_1)\tau}X &= e^{-i\mathcal{L}_0\tau}X - ie^{-i\mathcal{L}_0\tau}\int_0^\tau d\tau_1\left[\tilde{H}_1(\tau_1),X\right] \\ &\quad -e^{-i\mathcal{L}_0\tau}\int_0^\tau d\tau_1\int_0^{\tau_1}d\tau_2\left[\tilde{H}_1(\tau_1),\left[\tilde{H}_1(\tau_2),X\right]\right]+\dots \end{aligned} \tag{3.48}$$

Note that the time-dependence of $\tilde{H}_1(\tau)$ is simply given by

$$\tilde{H}_1(\tau) = e^{i\omega\tau}H_+ + e^{-i\omega\tau}H_- + H_{\Delta\mathrm{OH}}, \qquad H_\pm = \frac{g}{2}S^\pm A^\mp, \tag{3.49}$$

where the effective Zeeman splitting $\omega = \omega_0 + g\langle A^z\rangle_t$ is time dependent. Accordingly, we define $\tilde{\mathcal{L}}_1(\tau) = \tilde{\mathcal{L}}_+(\tau) + \tilde{\mathcal{L}}_-(\tau) + \tilde{\mathcal{L}}_{\Delta\mathrm{OH}}(\tau) = e^{i\omega\tau}\mathcal{L}_+ + e^{-i\omega\tau}\mathcal{L}_- + \mathcal{L}_{\Delta\mathrm{OH}}$, where $\mathcal{L}_x\cdot = [H_x,\cdot]$ for $x = \pm, \Delta\mathrm{OH}$. In the next steps, we explicitly evaluate the first two contributions to the memory kernel that go beyond $n = 0$ and then generalize our findings to any order $n$ of the Schwinger-Dyson series.

### First-order correction

The first order contribution $n = 1$ in Eqn. (3.13) is given by

$$\Xi^{(1)} = i\int_0^t d\tau\int_0^\tau d\tau_1 \mathsf{Tr_B}\left(\mathcal{L}_T e^{-i\mathcal{L}_0\tau}\left[\tilde{H}_1(\tau_1),X\right]\right). \tag{3.50}$$

Performing the integration in $\tau_1$ leads to

$$\begin{aligned} \Xi^{(1)} &= \int_0^t d\tau\Big\{\frac{g}{2\omega}\left(1-e^{-i\omega\tau}\right)\mathsf{Tr_B}\left(\mathcal{L}_T\left[S^+A^-,\tilde{X}_\tau\right]\right) \\ &\quad +\frac{g}{2\omega}\left(e^{i\omega\tau}-1\right)\mathsf{Tr_B}\left(\mathcal{L}_T\left[S^-A^+,\tilde{X}_\tau\right]\right) \\ &\quad +ig\tau\mathsf{Tr_B}\left(\mathcal{L}_T\left[\left(A^z-\langle A^z\rangle_t\right)S^z,\tilde{X}_\tau\right]\right)\Big\} \end{aligned} \tag{3.51}$$

where, for notational convenience, we introduced the operators $X = \mathcal{L}_T\rho_S(t-\tau)\rho_B^0$ and $\tilde{X}_\tau = e^{-iH_0\tau}\left[H_T,\rho_S(t-\tau)\rho_B^0\right]e^{iH_0\tau} \approx \left[\tilde{H}_T(\tau),\rho_S(t)\rho_B^0\right]$. In accordance with previous approximations, we have replaced $e^{-iH_0\tau}\rho_S(t-\tau)e^{iH_0\tau}$ with $\rho_S(t)$ since any additional term besides $H_0$ would be of higher order in perturbation theory [215, 216]. In particular, this disregards dissipative effects: In our case, this approximation is valid self-consistently provided that the tunneling rates are small compared to effective Zeeman splitting $\omega$. The integrand decays on the leads-correlation time scale $\tau_c$, which is typically much faster than the time scale set by the effective Zeeman splitting, $\omega\tau_c \ll 1$. This separation of time scales allows for an expansion in the small parameter $\omega\tau$, e.g. $\frac{g}{\omega}\left(e^{i\omega\tau}-1\right) \approx ig\tau$. We see that the first order correction can be neglected if the the bath correlation time $\tau_c$ is sufficiently short compared to the time scale of the HF dynamics, that is $g\tau_c \ll 1$. The latter is bounded by the total hyperfine coupling constant $A_H$ (since $||gA^x|| \leq A_H$) so that the requirement for disregarding the first-order term reads $A_H\tau_c \ll 1$.

### Second-order correction

The contribution of the second term $n = 2$ in the Schwinger-Dyson expansion can be decomposed into

$$\Xi^{(2)} = \Xi^{(2)}_{\mathrm{zz}} + \Xi^{(2)}_{\mathrm{ff}} + \Xi^{(2)}_{\mathrm{fz}}. \tag{3.52}$$

The first term $\Xi^{(2)}_{\mathrm{zz}}$ contains contributions from $H_{\Delta\mathrm{OH}}$ only,

$$\begin{aligned}\Xi^{(2)}_{\mathrm{zz}} &= \int_0^t d\tau \int_0^\tau d\tau_1 \int_0^{\tau_1} d\tau_2 \mathsf{Tr}_\mathsf{B}\left(\mathcal{L}_T e^{-i\mathcal{L}_0\tau}\left[\tilde{H}_{\Delta\mathrm{OH}}(\tau_1), \left[\tilde{H}_{\Delta\mathrm{OH}}(\tau_2), X\right]\right]\right) &(3.53)\\ &= -\int_0^t d\tau\,(g\tau)^2\,\mathsf{Tr}_\mathsf{B}\left[\mathcal{L}_T\left(\delta A^z S^z \tilde{X}_\tau \delta A^z S^z - \frac{1}{2}\left\{\delta A^z S^z \delta A^z S^z, \tilde{X}_\tau\right\}\right)\right] &(3.54)\end{aligned}$$

Similarly, $\Xi^{(2)}_{\mathrm{ff}}$ which comprises contributions from $H_{\mathrm{ff}}$ only is found to be

$$\begin{aligned}\Xi^{(2)}_{\mathrm{ff}} &= \frac{g^2}{4\omega^2}\int_0^t d\tau \Big\{\left(1 + i\omega\tau - e^{i\omega\tau}\right)\mathsf{Tr}_\mathsf{B}\left[\mathcal{L}_T\left(S^+S^-A^-A^+\tilde{X}_\tau + \tilde{X}_\tau S^-S^+A^+A^-\right)\right]\\ &\quad + \left(1 - i\omega\tau - e^{-i\omega\tau}\right)\mathsf{Tr}_\mathsf{B}\left[\mathcal{L}_T\left(S^-S^+A^+A^-\tilde{X}_\tau + \tilde{X}_\tau S^+S^-A^-A^+\right)\right]\Big\}. \end{aligned}\tag{3.55}$$

Here, we have used the following simplification: The time-ordered products which include flip-flop terms only can be simplified to two possible sequences in which $\mathcal{L}_+$ is followed by $\mathcal{L}_-$ and vice versa. This holds since

$$\mathcal{L}_\pm\mathcal{L}_\pm X = [H_\pm, [H_\pm, X]] = H_\pm H_\pm X + X H_\pm H_\pm - 2H_\pm X H_\pm = 0. \tag{3.56}$$

Here, the first two terms drop out immediately since the electronic jump-operators $S^\pm$ fulfill the relation $S^\pm S^\pm = 0$. In the problem at hand, also the last term gives zero because of particle number superselection rules: In Eqn. (3.13) the time-ordered product of superoperators acts on $X = \left[H_T, \rho_S(t-\tau)\rho_B^0\right]$. Thus, for the term $H_\pm X H_\pm$ to be nonzero, coherences in Fock space would be required, which are consistently neglected (compare Ref. [216]). This is equivalent to ignoring coherences between the system and the leads. Note that the same argument holds for any combination $H_\mu X H_\nu$ with $\mu, \nu = \pm$.

Similar results can be obtained for $\Xi^{(2)}_{\mathrm{fz}}$ which comprises $H_\pm$ as well as $H_{\Delta\mathrm{OH}}$ in all possible orderings. Again, using that the integrand decays on a time scale $\tau_c$ and expanding in the small parameter $\omega\tau$ shows that the second-order contribution scales as $\sim (g\tau_c)^2$. Our findings for the first and second order correction suggest that the $n$-th order correction scales as $\sim (g\tau_c)^n$. This is proven in the following by induction.

### n-th-order correction

The scaling of the $n$-th term in the Dyson series is governed by the quantities of the form

$$\xi^{(n)}_{+-\ldots}(\tau) = g^n \int_0^\tau d\tau_1 \int_0^{\tau_1} d\tau_2 \ldots \int_0^{\tau_{n-1}} d\tau_n e^{i\omega\tau_1} e^{-i\omega\tau_2}\ldots, \tag{3.57}$$

where the index suggests the order in which $H_\pm$ (giving an exponential factor) and $H_{\Delta\mathrm{OH}}$ (resulting in a factor of 1) appear. Led by our findings for $n = 1, 2$, we claim that the expansion

of $\xi^{(n)}_{+-\ldots}(\tau)$ for small $\omega\tau$ scales as $\xi^{(n)}_{+-\ldots}(\tau) \sim (g\tau)^n$. Then, the $(n+1)$-th terms scale as

$$\begin{aligned}
&\xi^{(n+1)}_{-(\Delta\mathrm{OH})+-\ldots}(\tau) \\
&\quad = g^{n+1}\int_0^\tau d\tau_1 \int_0^{\tau_1} d\tau_2 \ldots \int_0^{\tau_{n-1}} d\tau_n \int_0^{\tau_n} d\tau_{n+1} \begin{pmatrix} e^{-i\omega\tau_1} \\ 1 \end{pmatrix} e^{+i\omega\tau_2} \ldots && (3.58)\\
&\quad = g\int_0^\tau d\tau_1 \begin{pmatrix} e^{-i\omega\tau_1} \\ 1 \end{pmatrix} \xi^{(n)}_{+-\ldots}(\tau_1) && (3.59)\\
&\quad \sim (g\tau)^{n+1}. && (3.60)
\end{aligned}$$

Since we have already verified this result for $n = 1, 2$, the general result follows by induction. This completes the proof.

### 3.A.2 Adiabatic elimination of the QD electron

For a sufficiently small relative coupling strength $\epsilon$ the nuclear dynamics are slow compared to the electronic QD dynamics. This allows for an adiabatic elimination of the electronic degrees of freedom yielding an effective master equation for the nuclear spins of the QD.

Our analysis starts out from Eqn. (3.35), which we write as

$$\dot{\rho} = \mathcal{W}_0\rho + \mathcal{W}_1\rho, \tag{3.61}$$

where

$$\begin{aligned}
\mathcal{W}_0\rho &= -i\left[\omega_0 S^z, \rho\right] + \gamma\left[S^-\rho S^+ - \frac{1}{2}\left\{S^+S^-, \rho\right\}\right] + \Gamma\left[S^z\rho S^z - \frac{1}{4}\rho\right], && (3.62)\\
\mathcal{W}_1\rho &= -i\left[H_{\mathrm{HF}}, \rho\right]. && (3.63)
\end{aligned}$$

Note that the superoperator $\mathcal{W}_0$ only acts on the electronic degrees of freedom. It describes an electron in an external magnetic field that experiences a decay as well as a pure dephasing mechanism. In zeroth order of the coupling parameter $\epsilon$ the electronic and nuclear dynamics of the QD are decoupled and SR effects cannot be expected. These are contained in the interaction term $\mathcal{W}_1$.

Formally, the adiabatic elimination of the electronic degrees of freedom can be achieved as follows [234]: To zeroth-order in $\epsilon$ the eigenvectors of $\mathcal{W}_0$ with zero eigenvector $\lambda_0 = 0$ are

$$\mathcal{W}_0\mu \otimes \rho_{SS} = 0, \tag{3.64}$$

where $\rho_{SS} = |\downarrow\rangle\langle\downarrow|$ is the stationary solution for the electronic dynamics and $\mu$ describes some arbitrary state of the nuclear system. The zero-order Liouville eigenstates corresponding to $\lambda_0 = 0$ are coupled to the subspaces of "excited" nonzero (complex) eigenvalues $\lambda_k \neq 0$ of $\mathcal{W}_0$ by the action of $\mathcal{W}_1$. Physically, this corresponds to a coupling between electronic and nuclear degrees of freedom. In the limit where the HF dynamics are slow compared to the electronic frequencies, i.e. the Zeeman splitting $\omega_0$, the decay rate $\gamma$, and the dephasing rate $\Gamma$, the coupling between these blocks of eigenvalues and Liouville subspaces of $\mathcal{W}_0$ is weak, justifying a perturbative treatment. This motivates the definition of a projection operator $P$ onto the subspace with zero eigenvalue $\lambda_0 = 0$ of $\mathcal{W}_0$ according to

$$P\rho = \mathsf{Tr}_{\mathsf{el}}\left[\rho\right] \otimes \rho_{SS} = \mu \otimes |\downarrow\rangle\langle\downarrow|, \tag{3.65}$$

where $\mu = \mathsf{Tr}_{\mathsf{el}}[\rho]$ is a density operator for the nuclear spins, $\mathsf{Tr}_{\mathsf{el}} \ldots$ denotes the trace over the electronic subspace, and, by definition, $\mathcal{W}_0 \rho_{SS} = 0$. The complement of $P$ is $Q = 1 - P$. By projecting the master equation on the $P$ subspace and tracing over the electronic degrees of freedom we obtain an effective master equation for the nuclear spins in second-order perturbation theory,

$$\dot{\mu} = \mathsf{Tr}_{\mathsf{el}}\left[P\mathcal{W}_1 P\rho - P\mathcal{W}_1 Q\mathcal{W}_0^{-1} Q\mathcal{W}_1 P\rho\right]. \tag{3.66}$$

Using $\mathsf{Tr}_{\mathsf{el}}[S^z \rho_{SS}] = -1/2$, the first term is readily evaluated and yields the Knight shift seen by the nuclear spins,

$$\mathsf{Tr}_{\mathsf{el}}[P\mathcal{W}_1 P\rho] = +i\frac{g}{2}[A^z, \mu]. \tag{3.67}$$

The derivation of the second term is more involved. It can be rewritten as

$$\begin{aligned} &-\mathsf{Tr}_{\mathsf{el}}\left[P\mathcal{W}_1 Q\mathcal{W}_0^{-1} Q\mathcal{W}_1 P\rho\right] \\ &\quad = -\mathsf{Tr}_{\mathsf{el}}\left[P\mathcal{W}_1 (1-P)\mathcal{W}_0^{-1}(1-P)\mathcal{W}_1 P\rho\right] &(3.68)\\ &\quad = \int_0^\infty d\tau\, \mathsf{Tr}_{\mathsf{el}}\left[P\mathcal{W}_1 e^{\mathcal{W}_0\tau}\mathcal{W}_1 P\rho\right] - \int_0^\infty d\tau\, \mathsf{Tr}_{\mathsf{el}}[P\mathcal{W}_1 P\mathcal{W}_1 P\rho]. &(3.69)\end{aligned}$$

Here, we used the Laplace transform $-\mathcal{W}_0^{-1} = \int_0^\infty d\tau\, e^{\mathcal{W}_0\tau}$ and the property $e^{\mathcal{W}_0\tau}P = Pe^{\mathcal{W}_0\tau} = P$.

Let us first focus on the first term in Eqn. (3.69). It contains terms of the form

$$\begin{aligned} \mathsf{Tr}_{\mathsf{el}}\left[P\left[A^+S^-, e^{\mathcal{W}_0\tau}\left[A^-S^+, \mu\otimes\rho_{SS}\right]\right]\right] =& \mathsf{Tr}_{\mathsf{el}}\left[S^- e^{\mathcal{W}_0\tau}\left(S^+\rho_{SS}\right)\right]A^+A^-\mu &(3.70)\\ &- \mathsf{Tr}_{\mathsf{el}}\left[S^- e^{\mathcal{W}_0\tau}\left(S^+\rho_{SS}\right)\right]A^-\mu A^+ &(3.71)\\ &+ \mathsf{Tr}_{\mathsf{el}}\left[S^- e^{\mathcal{W}_0\tau}\left(\rho_{SS}S^+\right)\right]\mu A^-A^+ &(3.72)\\ &- \mathsf{Tr}_{\mathsf{el}}\left[S^- e^{\mathcal{W}_0\tau}\left(\rho_{SS}S^+\right)\right]A^+\mu A^-. &(3.73)\end{aligned}$$

This can be simplified using the following relations: Since $\rho_{SS} = |\downarrow\rangle\langle\downarrow|$, we have $S^-\rho_{SS} = 0$ and $\rho_{SS}S^+ = 0$. Moreover, $|\uparrow\rangle\langle\downarrow|$ and $|\downarrow\rangle\langle\uparrow|$ are eigenvectors of $\mathcal{W}_0$ with eigenvalues $-(i\omega_0 + \alpha/2)$ and $+(i\omega_0 - \alpha/2)$, where $\alpha = \gamma + \Gamma$, yielding

$$\begin{aligned} e^{\mathcal{W}_0\tau}\left(S^+\rho_{SS}\right) &= e^{-(i\omega_0+\alpha/2)\tau}|\uparrow\rangle\langle\downarrow|, &(3.74)\\ e^{\mathcal{W}_0\tau}\left(\rho_{SS}S^-\right) &= e^{+(i\omega_0-\alpha/2)\tau}|\downarrow\rangle\langle\uparrow|. &(3.75)\end{aligned}$$

This leads to

$$\mathsf{Tr}_{\mathsf{el}}\left[P\left[A^+S^-, e^{\mathcal{W}_0\tau}\left[A^-S^+, \mu\otimes\rho_{SS}\right]\right]\right] = e^{-(i\omega_0+\alpha/2)\tau}\left(A^+A^-\mu - A^-\mu A^+\right). \tag{3.76}$$

Similarly, one finds

$$\mathsf{Tr}_{\mathsf{el}}\left[P\left[A^-S^+, e^{\mathcal{W}_0\tau}\left[A^+S^-, \mu\otimes\rho_{SS}\right]\right]\right] = e^{+(i\omega_0-\alpha/2)\tau}\left(\mu A^+A^- - A^-\mu A^+\right). \tag{3.77}$$

Analogously, one can show that terms containing two flip or two flop terms give zero. The same holds for mixed terms that comprise one flip-flop and one Overhauser term with $\sim A^zS^z$. The term consisting of two Overhauser contributions gives

$$\mathsf{Tr}_{\mathsf{el}}\left[P\left[A^zS^z, e^{\mathcal{W}_0\tau}\left[A^zS^z, \mu\otimes\rho_{SS}\right]\right]\right] = -\frac{1}{4}\left[2A^z\mu A^z - [A^zA^z, \mu]\right]. \tag{3.78}$$

However, this term exactly cancels with the second term from Eqn. (3.69). Thus, we are left with the contributions coming from Eqn. (3.76) and Eqn. (3.77). Restoring the prefactors of $-ig/2$, we obtain

$$\begin{aligned}\mathsf{Tr}_{\mathsf{el}}\left[P\mathcal{W}_1Q\left(-\mathcal{W}_0^{-1}\right)Q\mathcal{W}_1P\rho\right] &= \frac{g^2}{4}\int_0^\infty d\tau\left[e^{-(i\omega_0+\alpha/2)\tau}\left(A^-\mu A^+ - A^+A^-\mu\right)\right.\\ &\left.+e^{+(i\omega_0-\alpha/2)\tau}\left(A^-\mu A^+ - \mu A^+A^-\right)\right]. \end{aligned} \tag{3.79}$$

Performing the integration and separating real from imaginary terms yields

$$\mathsf{Tr}_{\mathsf{el}}\left[P\mathcal{W}_1Q\left(-\mathcal{W}_0^{-1}\right)Q\mathcal{W}_1P\rho\right] = c_r\left[A^-\mu A^+ - \frac{1}{2}\left\{A^+A^-,\mu\right\}\right] + ic_i\left[A^+A^-,\mu\right], \tag{3.80}$$

where $c_r = g^2/\left(4\omega_0^2+\alpha^2\right)\alpha$ and $c_i = g^2/\left(4\omega_0^2+\alpha^2\right)\omega_0$. Combining Eqn. (3.67) with Eqn. (3.80) directly gives the effective master equation for the nuclear spins given in Eqn. (3.3) in the main text.

### 3.A.3 Full counting statistics: The leakage current

The method of Full Counting Statistics (FCS) gives access to the full information about all transport properties of a given device as it allows for the evaluation of the probability distribution function $P_n(t)$ of the number of transferred electrons $n$ in a given time period $t$. The associated cumulant generating function $\mathcal{C}(\chi,t)$ is defined via

$$e^{\mathcal{C}(\chi,t)} = \sum_{n=0}^{\infty} P_n(t)\, e^{in\chi}, \tag{3.81}$$

where $\chi$ is the counting field. The cumulants of the distribution function $P_n(t)$ are straightforwardly related to transport characteristics of the system and can be obtained as $\left\langle\left\langle n^k(t)\right\rangle\right\rangle = \left(-i\partial_\chi\right)^k \mathcal{C}(\chi,t)\,|_{\chi=0}$, where

$$\mathcal{C}(\chi,t) = \ln \mathsf{Tr}\left[\rho_\chi(t)\right] = \ln \mathsf{Tr}\left[e^{\mathcal{L}_\chi t}\rho(0)\right]. \tag{3.82}$$

Following the approach developed by Bagrets and Nazarov [221], the cumulant generating operator $\rho_\chi(t)$ obeys the equation of motion

$$\frac{d}{dt}\rho_\chi(t) = \mathcal{L}_\chi\rho_\chi(t), \tag{3.83}$$

where $\mathcal{L}_\chi$ is an auxiliary $\chi$-dependent linear operator. In our setting, see Fig. 3.1, it reads

$$\begin{aligned}\mathcal{L}_\chi\rho_\chi(t) &= -i\left[\omega_0S^z + H_{HF} + H_{comp}(t), \rho_\chi(t)\right] + \alpha e^{i\chi}d_\uparrow\rho_\chi(t)\,d_\uparrow^\dagger - \frac{\alpha}{2}\left\{\rho_\chi(t), d_\uparrow^\dagger d_\uparrow\right\}\\ &+\left(\beta_\downarrow^{(L)} + \beta_\downarrow^{(R)}e^{-i\chi}\right)d_\downarrow^\dagger\rho_\chi(t)\,d_\downarrow - \frac{\left(\beta_\downarrow^{(L)}+\beta_\downarrow^{(R)}\right)}{2}\left\{\rho_\chi(t), d_\downarrow d_\downarrow^\dagger\right\}\\ &+\beta_\uparrow^{(L)}d_\uparrow^\dagger\rho_\chi(t)\,d_\uparrow - \frac{\beta_\uparrow^{(L)}}{2}\left\{\rho_\chi(t), d_\uparrow d_\uparrow^\dagger\right\}. \end{aligned} \tag{3.84}$$

Here, counting factors $e^{\pm i\chi}$ have been added to the entries of the original Liouvillian of the system that are related to changes of the dot occupation [222]. By definition, an electron tunneling into the right reservoir gives a positive contribution whereas electrons tunneling from the right reservoir into the QD give a negative one. For the moment, we restrict ourselves to the first moment of the distribution function which is directly linked to the current $I(t) = \frac{d}{dt}\langle n(t)\rangle$ (we set the electric charge $e$ to one). We start out from

$$I(t) = (-i\partial_\chi)\frac{d}{dt}\mathcal{C}(\chi,t)\,|_{\chi=0}, \tag{3.85}$$

where the derivative of the cumulant generating function $\mathcal{C}(\chi,t)$ w.r.t. time is

$$\frac{d}{dt}\mathcal{C}(\chi,t) = \frac{\mathsf{Tr}\left[\mathcal{L}_\chi e^{\mathcal{L}_\chi t}\rho_\chi(0)\right]}{\mathsf{Tr}\left[e^{\mathcal{L}_\chi t}\rho_\chi(0)\right]}. \tag{3.86}$$

Using the conservation of probability $\mathsf{Tr}[\rho(t)] = 1$ and the fact that

$$\mathsf{Tr}\left[\mathcal{L}_{\chi=0}\mathcal{O}\right] = 0 \tag{3.87}$$

for an arbitrary operator $\mathcal{O}$, we get for the current

$$\begin{aligned} I(t) &= -i\mathsf{Tr}\left[\mathcal{L}'_{\chi=0}e^{\mathcal{L}_{\chi=0}t}\rho_{\chi=0}(0)\right] = -i\mathsf{Tr}\left[\mathcal{L}'_{\chi=0}\rho(t)\right] &(3.88)\\ &= \alpha\mathsf{Tr}\left[d^\dagger_\uparrow d_\uparrow\rho(t)\right] - \beta^{(R)}_\downarrow\mathsf{Tr}\left[d_\uparrow d^\dagger_\uparrow\rho(t)\right]. &(3.89)\end{aligned}$$

Since the system is in the strong Coulomb-blockade regime, this expression can equivalently be written as

$$I(t) = \alpha\left\langle S^+S^-\right\rangle_t - \beta^{(R)}_\downarrow\rho_{00}. \tag{3.90}$$

### 3.A.4 Cotunneling current

In this Appendix we will investigate cotunneling processes by which electrons tunnel from lead $l$ onto the dot and form a virtual state, followed by tunneling into lead $l'$. The spin state of the dot changes $\sigma \to \sigma'$: This process is referred to as elastic cotunneling if $\sigma = \sigma'$ and inelastic cotunneling otherwise. Assuming $T = 0$ for simplicity, inelastic cotunneling exciting the QD spin cannot occur for $\Delta\mu = eV < \omega_0$ [217] due to energy conservation. However, cotunneling events that relax the QD spin can still be present. In the following we will focus on cotunneling processes that contribute to transport ($l \neq l'$) and disregard particle-hole excitations in the left or right lead. We assume the virtual energy cost of an intermediate triplet state to be much higher than that for a singlet state: thus, we can restrict ourselves to cotunneling events involving the singlet state with energy $\epsilon_S$.

The cotunneling rates can be calculated in a "golden rule" approach up to second order in $H_T$ [217]

$$\Gamma^{l'l}_{\sigma'\sigma} = 2\pi n^2\int d\epsilon f_l(\epsilon)\left(1 - f_{l'}(\epsilon - \Delta_{\sigma'\sigma})\right)\left|\sum_m \frac{T^{(l')}_{\sigma'}T^{(l)*}_{\sigma}}{\Delta_{m\sigma} - \epsilon}\right|^2. \tag{3.91}$$

Here, $n$ is the lead density of states at the Fermi energy, $\Delta_{\sigma'\sigma}$ is the change of Zeeman energy on the dot and $\Delta_{m\sigma} = \epsilon_m - \epsilon_\sigma$ is the energy cost of the virtual intermediate state.

Let us first examine elastic cotunneling processes which contribute to transport and spin decoherence but not to spin relaxation via the intermediate doubly occupied singlet state. For simplicity, we neglect the spin dependence of the tunneling rates. The relevant elastic rates are given by [207, 217]

$$\Gamma_{\sigma\sigma}^{RL} = \frac{\beta^{(L)}\alpha^{(R)}}{2\pi} \frac{\Delta\mu}{(\Delta_{S\sigma} - \mu_L)(\Delta_{S\sigma} - \mu_R)} \approx \frac{\beta^{(L)}\alpha^{(R)}}{2\pi} \frac{\Delta\mu}{(\Delta_{S\sigma} - \mu)^2}, \tag{3.92}$$

where the last approximation holds for $\Delta\mu < \Delta_{S\sigma} - \mu$, with $\mu = (\mu_L + \mu_R)/2$. We see that for sufficiently large charging energy of the QD, this rate is efficiently suppressed.

In the same way, the inelastic cotunneling rate is approximately given by

$$\Gamma_{\downarrow\uparrow}^{RL} \approx \frac{\beta^{(L)}\alpha^{(R)}}{2\pi} \frac{\omega_0 + \Delta\mu}{(\Delta_{S\uparrow} - \mu)(\Delta_{S\uparrow} + \omega_0 - \mu)}, \tag{3.93}$$

which can also be neglected in the strong Coulomb blockade regime. We also see that the cotunneling processes scale as $\propto \beta^{(L)}\alpha^{(R)}$. Since sequential tunneling scales as $\propto \alpha^{(R)}$, cotunneling can always be suppressed compared to sequential tunneling by making the tunnel barriers less transparent.

# Chapter 4

# Dissipative Phase Transition in a Central Spin System

**In the previous Chapters we have established the concept of superradiant collective effects in the de-excitation of the nuclear spin environments of mesoscopic solid-state systems. It is known that atomic ensembles, which show cooperative effects in spontaneous emission, can display critical behavior in the steady state under additional driving by a coherent laser source [77, 186]. Motivated by these results, in the present Chapter we investigate dissipative phase transitions in an open central spin system, similar to the one studied in Chapter 2. In this model the central spin interacts coherently with the surrounding many-particle spin environment and is subject to coherent driving and dissipation. We develop analytical tools based on a self-consistent Holstein-Primakoff approximation that enable us to determine the complete phase diagram associated with the steady states of this system. It includes a series of interesting quantum effects, such as first- and second-order phase transitions, as well as regions of bistability, spin squeezing and altered spin-pumping dynamics. The analytical solution we provide grants deep insights to the nature of criticality in open systems, and allows for the establishment of a classification criterion for dissipative phase transitions. Furthermore, the numerous phenomena demonstrate that coherence in solid-state systems does not only emerge in the transient, but also in the steady state of dissipative dynamics. This Chapter is based on Publication 3 [DPT].**

## 4.1 Introduction

Statistical mechanics classifies phases of a given system in thermal equilibrium according to its physical properties. It also explains how changes in the system parameters allow us to transform one phase into another, sometimes abruptly, which results in the phenomenon of phase transitions. A special kind of phase transitions occurs at zero temperature: such transitions are driven by quantum fluctuations instead of thermal ones and are responsible for the appearance of exotic quantum phases in many areas of physics. These quantum phase transitions have been a subject of intense research in the last thirty years, and are expected not only to explain interesting behavior of systems at low temperature, but also to lead to new states of matter with desired properties (e.g., superconductors, -fluids, and -solids, topological insulators

[66, 235, 236, 76, 237, 238]).

Phase transitions can also occur in systems away from their thermal equilibrium. For example, this is the case when the system interacts with an environment and, at the same time, is driven by some external coherent source. Due to dissipation, the environment drives the system to a steady state, $\rho_0(g)$, which depends on the system and environment parameters, $g$. As $g$ is changed, a sudden change in the system properties may occur, giving rise to a so called *dissipative phase transition* (DPT) [77, 239, 240, 80, 241, 242, 29, 243]. DPTs have been much less studied than traditional or quantum ones. With the advent of new techniques that allow them to be observed experimentally, they are starting to play an important role [78]. Moreover, they offer the intriguing possibility of observing critical effects non-destructively because of the constant intrinsic exchange between system and environment [83]. In equilibrium statistical mechanics a large variety of toy models exist that describe different kinds of transitions. Their study led to a deep understanding of many of them. In contrast, in the case of DPTs only few models have been developed. The textbook example of a DPT occurs in the Dicke model of resonance fluorescence [244, 77]. There, a system of spins interacts with a thermal reservoir and is externally driven. Experimental [245] and theoretical studies [246, 247, 186, 248] revealed interesting features such as optical multistability, first- and second-order phase transitions, and bipartite entanglement.

In this Chapter, we analyze another prototypical open system: The model is closely related to the central spin system (CSS) which has been thoroughly studied in thermal equilibrium [111, 112, 98]. In its simplest form, it consists of a set of spin-1/2 particles (in the following referred to as the *nuclear spins*), uniformly coupled to a single spin-1/2 (referred to as the *electron spin*). In the model we consider, the central spin is externally driven and decays through interaction with a Markovian environment. Recently, the CSS model has found application in the study of solid-state systems such as electron and nuclear spins in a quantum dot [98] or a Nitrogen Vacancy center.

In what follows, we first provide a general framework for analyzing DPTs in open systems. In analogy with the analysis of low-energy excitations for closed systems, it is based on the study of the excitation gap of the system's Liouville operator $\mathcal{L}$. We illustrate these considerations using the central spin model. For a fixed dissipation strength $\gamma$, there are two external parameters one can vary, the Rabi frequency of the external driving field, $\Omega$, and the Zeeman shift, $\omega$. We present a complete phase diagram as a function of those parameters, characterize all the phases, and analyze the phase transitions occurring among them. To this end, we develop a series of analytical tools, based on a self-consistent Holstein-Primakoff approximation, which allows us to understand most of the phase diagram. In addition, we use numerical methods to investigate regions of the diagram where the theory yields incomplete results. Combining these techniques, we can identify two different types of phase transitions and regions of bistability, spin squeezing, and enhanced spin polarization dynamics. We also identify regions where anomalous behavior occurs in the approach to the steady state. Intriguingly, recent experiments with quantum dots, in which the central (electronic) spin is driven by a laser and undergoes spontaneous decay, realize a situation very close to the one we study here and show effects such as bistability, enhanced fluctuations, and abrupt changes in polarization in dependence of the system parameters [116, 249].

## 4.2 Executive summary

This Chapter is organized as follows. Before we start the investigation of the actual system, in Section 4.3 we set the general theoretical background underlying our study of DPTs. We discuss the relation between DPTs and the low-excitation spectrum of the Liouville operator governing the system dynamics. After that, Section 4.4 introduces the model we consider. It is a generalization of the central spin model studied in the context of superradiance (Chapter 2), which introduces an additional resonant laser driving term. After having presented the model under consideration, we explain phenomenologically the key features of the phase diagram and provide a structured summary of the main results. In Section 4.5 we then develop the theoretical techniques which enable a complete analytical understanding of most of the phase diagram. We use those techniques to analyze the various phases and to gain a deep understanding of the nature of criticality in open systems. Finally, we employ the developed techniques to classify the different transitions according to properties of the spectrum of the Liouvillian. In addition, in Section 4.6 numerical techniques are employed to explain the features of the phase diagram which are not captured by the previous theory. The potential of hysteresis effects are discussed against the background of the related phenomenon of optical bistability. In the view of the observation of criticality in several recent polarization experiments in QDs, possible experimental realizations and a generalization of the model to inhomogeneous coupling are discussed in Section 4.7. Finally, we summarize the results and discuss potential applications in Section 4.8.

## 4.3 General theoretical framework

The theory of quantum phase transitions in closed systems is a well-established and extensively studied area in the field of statistical mechanics. The typical scenario is the following: a system is described by a Hamiltonian, $H(g)$, where $g$ denotes a set of systems parameters (like magnetic fields, interactions strengths, etc.). At zero temperature and for a fixed set of parameters, $g$, the system is described by a quantum state, $\psi_0(g)$, fulfilling $[H(g) - E_{\psi_0}(g)]|\psi_0(g)\rangle = 0$, where $E_{\psi_0}(g)$ is the ground-state energy. As long as the Hamiltonian is gapped (i.e., the difference between $E_0(g)$ and the first excitation energy is finite), any small change in $g$ will alter the physical properties related to the state $|\psi_0(g)\rangle$ smoothly and we remain in the same phase. However, if the first excitation gap $\Delta = E_{\psi_1}(g) - E_{\psi_0}(g)$ closes at a given value of the parameters, $g = g_0$, it may happen that the properties change abruptly, in which case a phase transition occurs.

In the following we adapt analogous notions to the case of DPTss and introduce the concepts required for the subsequent study of a particular example of a generic DPT in a central spin model.

We consider a Markovian open system, whose evolution is governed by a time-independent master equation $\dot{\rho} = \mathcal{L}(g)\rho$. The dynamics describing the system are contractive, implying the existence of a steady state. This steady state $\rho_0(g)$ is a zero eigenvector to the Liouville superoperator $\mathcal{L}(g)\rho_0(g) = 0$. This way of thinking parallels that of quantum phase transitions, if one replaces $[H(g) - E_{\psi_0}(g)] \to \mathcal{L}(g)$. Despite the fact that these mathematical objects are very different (the first is a Hermitian operator, and the second a Hermiticity-preserving superoperator), one can draw certain similarities between them. For instance, for an abrupt change of $\rho_0(g)$ (and thus of certain system observables) it is necessary that the gap in the

| | TPT | QPT | DPT |
|---|---|---|---|
| System operator | Hamiltonian $H = H^\dagger$ | Hamiltonian $H = H^\dagger$ | Liouvillian $\mathcal{L}$ – Lindblad |
| Relevant quantity | Free energy $F(\rho) = \langle H\rangle_\rho - T\langle S\rangle_\rho$ | Energy eigenvalues $E_\psi : H\,\lvert\psi\rangle = E_\psi\,\lvert\psi\rangle$ | "Complex energy" eigenvalues $\lambda_\rho : \mathcal{L}\rho = \lambda_\rho\rho$ |
| State | Gibbs state $\rho_T = \underset{\rho\geq 0,\mathrm{Tr}(\rho)=1}{\mathrm{argmin}}\,[F(\rho)]$ $\rho_T \propto \exp[-H/k_BT]$ | Ground state $\lvert\psi_0\rangle = \underset{\lVert\psi\rVert=1}{\mathrm{argmin}}[\langle\psi\rvert H\,\lvert\psi\rangle]$ $[H - E_{\psi_0}]\lvert\psi_0\rangle = 0$ | Steady state $\rho_0 = \underset{\lVert\rho\rVert_{\mathrm{tr}}=1}{\mathrm{argmin}}[\lVert\mathcal{L}\rho\rVert_{\mathrm{tr}}]$ $\mathcal{L}\rho_0 = 0$ |
| Phase transition | Non-analyticity in $F(\rho_T)$ | $\Delta = E_{\psi_1} - E_{\psi_0}$ vanishes | ADR $= \max[\mathrm{Re}(\lambda_\rho)]$ vanishes |

Table 4.1: Non-exhaustive comparison of thermal phase transitions (TPTs), quantum phase transitions (QPTs) and DPTs. The concepts for DPTs parallel in many respects the considerations for QPTs and TPTs. $||\cdot||_{\mathrm{tr}}$ denotes the trace norm and $S$ the entropy. Note that if the steady state is not unique, additional steady states may come with a non-zero imaginary part of the eigenvalue and then appear in pairs: $\mathcal{L}\rho = \pm iy\rho$ ($y \in \mathbb{R}$).

(in general complex) excitation spectrum of the system's Liouville operator $\mathcal{L}(g)$ closes. The relevant gap in this context is determined by the eigenvalue with largest real part different from zero (it can be shown that $\mathrm{Re}(\lambda) \leq 0$ for all eigenvalues of $\mathcal{L}$ [250]). The vanishing of the real part of this eigenvalue – from here on referred to as *asymptotic decay rate* (ADR) [251] – indicates the possibility of a non-analytical change in the steady state and thus is a necessary condition for a phase transition to occur.

In our model system, the Liouvillian low-excitation spectrum, and the ADR in particular, can in large parts of the phase diagram be understood from the complex energies of a stable Gaussian mode of the nuclear field. We find first-order transitions where the eigenvalue of this stable mode crosses the eigenvalue of a metastable mode at zero in the projection onto the real axis. The real part of the Liouvillian spectrum closes *directly* as the stable mode turns metastable and vice versa. A finite difference in the imaginary parts of the eigenvalues across the transition prevents a mixing of the two modes and the emergence of critical phenomena, such as a change in the nature of the steady-state correlations at the critical point. In contrast, we also find a second-order phase transition where the ADR vanishes *asymptotically* as both mode energies become zero (in both real and imaginary part) in the thermodynamic limit. At this critical point a true degeneracy emerges in the Liouvillian spectrum and mixing of the two modes point gives rise to diverging correlations in the nuclear system. This observation parallels the classification of quantum phase transitions in closed systems. There, a direct crossing of the ground- and first-excited-state energy for finite systems (mostly arising from a symmetry in the system) typically gives rise to a first-order phase transition. An asymptotical closing of the first excitation gap of the Hamiltonian in the thermodynamic limit represents the generic case of a second-order transition [65].

Besides the analogies described so far [cf. Table 4.1], there are obvious differences, like the fact that in DTP $\rho_0(g)$ may be pure or mixed, and that some of the characteristic behavior of

a phase may also be reflected in how the steady state is approached. Non-analyticities in the higher excitation spectrum of the Liouvillian are associated to such dynamical phases.

## 4.4 Model and phase diagram

### 4.4.1 The model

We investigate the steady-state properties of a homogeneous central spin model. The central spin – also referred to as electronic spin in the following – is driven resonantly via suitable optical or magnetic fields. Dissipation causes electronic spin transitions from the spin-up to the spin-down state. It can be introduced via standard optical pumping techniques [101, 120]. Furthermore, the central spin is assumed to interact with an ensemble of ancilla spins – also referred to as nuclear spins in view of the mentioned implementations [98] – by an isotropic and homogeneous Heisenberg interaction. In general, this hyperfine interaction is assumed to be detuned. Weak nuclear magnetic dipole-dipole interactions are neglected.

After a suitable transformation which renders the Hamiltonian time-independent, the system under consideration is governed by the master equation

$$\begin{aligned}\dot{\rho} &= \mathcal{L}\rho \\ &= J\gamma(S^-\rho S^+ - \frac{1}{2}\{S^+S^-,\rho\}) - i[H_S + H_I + H_{SI},\rho],\end{aligned} \tag{4.1}$$

where $\{\cdot,\cdot\}$ denotes the anticommutator and

$$H_S = J\Omega(S^+ + S^-), \tag{4.2}$$

$$H_I = \delta\omega I_z, \tag{4.3}$$

$$H_{SI} = a/2(S^+I^- + S^-I^+) + aS^+S^-I_z. \tag{4.4}$$

$S^\alpha$ and $I^\alpha$ ($\alpha = +,-,z$) denote electron and collective nuclear spin operators, respectively. Collective nuclear operators are defined as the sum of $N$ individual nuclear operators $I^\alpha = \sum_{i=1}^{N}\sigma_i^\alpha$. $J\Omega$ is the Rabi frequency of the resonant external driving of the electron (in rotating wave approximation), while $\delta\omega = \omega - a/2$ is the difference of hyperfine detuning $\omega$ and half the individual hyperfine coupling strength $a$. $\delta\omega$, for instance, can be tuned via static magnetic fields in $z$-direction. Note that $H_I + H_{SI} = a\vec{S}\vec{I} + \omega I_z$, describing the isotropic hyperfine interaction and its detuning. The rescaling of the electron driving and dissipation in terms of the total (nuclear) spin quantum number $J$[1] is introduced here for convenience and will be justified later. Potential detunings of the electron driving – corresponding to a term $\Delta S_z$ in the Hamiltonian part of the master equation – can be neglected if $\Delta \ll Ja$.

In the limit of strong dissipation $\gamma \gg a$ the electron degrees of freedom can be eliminated and Eqn. (4.1) reduces to

$$\begin{aligned}\dot{\sigma} := Tr_S(\dot{\rho}) =& \gamma_{\text{eff}}(I^-\sigma I^+ - \frac{1}{2}\{I^+I^-,\sigma\}) \\ & -i\left[\Omega_{\text{eff}}I_y + \delta\omega I_z\right],\end{aligned} \tag{4.5}$$

[1] Note that the total spin quantum number $J$ is conserved under the action of $\mathcal{L}$.

where $\gamma_{\text{eff}} = \frac{a^2}{\gamma}$, $\Omega_{\text{eff}} = \frac{\Omega a}{2\gamma}$, and $\sigma$ is the reduced density matrix of the nuclear system. This is a generalization of the Dicke model of resonance fluorescence as discussed in [77, 248, 80].

In Chapter 2, Master Eqn. (4.1) has been theoretically shown to display cooperative nuclear effects such as superradiance (even for inhomogeneous electron nuclear coupling). Furthermore, it was demonstrated recently that a similar model exhibits nuclear spin squeezing in the transient evolution of polarized initial states [252]. In analogy to the field of cooperative resonance fluorescence, the system's rich steady-state behavior comprises various critical effects such as first- and second-order DPTs and bistabilities. In the following we provide a qualitative summary of the phase diagram and of the techniques developed to study the various phases and transitions.

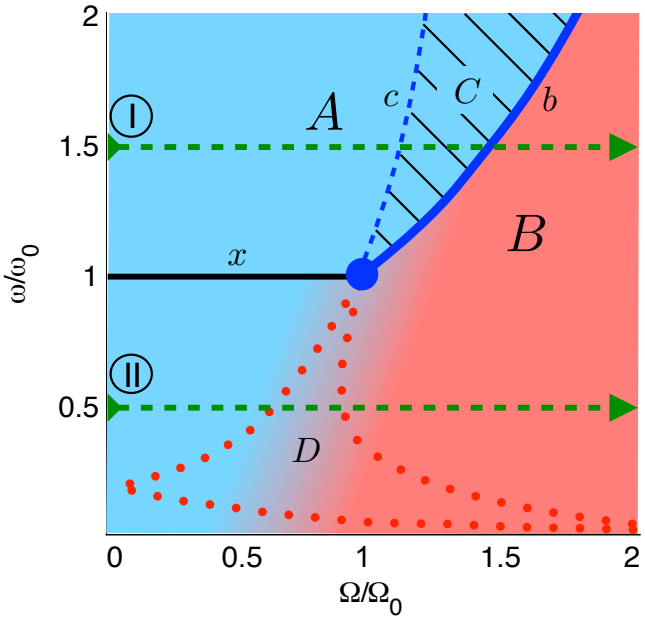


Figure 4.1: Schematic of the different phases and transitions of Master Eqn. (4.1). In the two main phases of the system $A$ (blue) and $B$ (red) – which together cover the whole phase diagram – the system is found in a RSTSS (cf. text). While phase $A$ is characterized by normal spin-pumping behavior (large nuclear polarization in the direction of the dissipation) and a low effective temperature, phase $B$ displays anomalous spin-pumping behavior (large nuclear polarization in opposing direction to the dissipation) and high temperature. They are separated by the first-order phase boundary $b$ which is associated with a region of bistability $C$ (framed by the boundary $c$). Here a second non-Gaussian solution appears, besides the normal spin-pumping mode of $A$. The region of bistability $C$ culminates in a second-order phase transition at $(\omega_0, \Omega_0)$. Below this critical point the system is supercritical and no clear distinction between phases $A$ and $B$ exists. In this region a dynamical phase $D$ emerges, characterized by anomalous behavior in the approach to the steady state. For a detailed description of the different phases and transitions see Section 4.4.2.

### 4.4.2 Phenomenological description of the phase diagram

For a fixed dissipation rate $\gamma = a$ the different phases and transitions of the system are displayed schematically in Fig. 4.1 in dependence on the external driving $\Omega$ and the hyperfine detuning $\omega$. We stress the point that none of the features discussed in the following depends critically on this particular value of the dissipation. In Appendix 4.A.1 we discuss briefly the quantitative changes in the phase diagram for moderately lower (higher) values of $\gamma$. Further, we concentrate our studies on the quadrant $\Omega, \omega > 0$, in which all interesting features can be observed. In the following, we outline the key features of the phase diagram.

First we consider the system along the line segment $x$ ($\omega = \omega_0, \Omega \leq \Omega_0$), where $\Omega_0 = \omega_0 = a/2$ ($a$ is the individual hyperfine coupling constant) define a critical driving strength and critical hyperfine detuning, respectively. Here $H_I$ vanishes and the steady state can be constructed analytically as a zero-entropy factorized state of the electron and nuclear system. The nuclear field builds up to compensate for the external driving – forcing the electron in its dark state $|\downarrow\rangle$ – until the maximal polarization is reached at the critical value $\Omega_0$. Above this point the nuclear system cannot compensate for the driving $\Omega$ anymore and a solution of different nature, featuring finite electron inversion and entropy is found. The point $\Omega_0$ features diverging spin entanglement and is identified below as a second-order phase transition.

For the separable density matrix $\rho_0 = |\psi\rangle\langle\psi|$, $|\psi\rangle = |\downarrow\rangle \otimes |\alpha\rangle$ the only term in Master Eqn. (4.1) which is not trivially zero is the Hamiltonian term $S^+(\frac{a}{2}I^- + J\Omega)$. However, choosing $|\alpha\rangle$ as an approximate eigenstate of the lowering operator $I^-|\alpha\rangle \approx \alpha|\alpha\rangle$ (up to second order in $\epsilon = 1/\sqrt{J}$) with $\alpha = -2J\Omega/a \equiv -J\Omega/\Omega_0$, the corresponding term in Eqn. (4.1) vanishes in the thermodynamic limit. In Appendix 4.A.2 we demonstrate that approximate eigenstates $|\alpha\rangle$ can be constructed as squeezed and displaced vacua in a Holstein-Primakoff [253] picture up to a correction of order 1/J. The squeezing of the nuclear state depends uniquely on the displacement such that these states represent a subclass of *squeezed coherent atomic states* [254]. Remarkably, this solution – where along the whole segment $x$ the system settles in a separable pure state – exists for all values of the dissipation strength $\gamma$.

In the limit of vanishing driving $\Omega = 0$ the steady state trivially is given by the fully polarized state (being the zero eigenstate of the lowering operator), as the model realizes a standard optical spin-pumping setting for dynamical nuclear polarization [51]. With increasing $\Omega$, the collective nuclear spin is rotated around the $y$-axis on the surface of the Bloch sphere such that the effective Overhauser field in $x$-direction compensates exactly for the external driving field on the electron spin. As a consequence along the whole segment $x$ the dissipation forces the electron in its dark state $|\downarrow\rangle$, and all electron observables, but also the entropy and some nuclear observables, are independent of $\Omega$.

Furthermore, the steady state displays increased nuclear spin squeezing in $y$-direction (orthogonal to the mean polarization vector) when approaching the critical point. A common measure of squeezing is defined via the spin fluctuations orthogonal to the mean polarization of the spin system. A state of a spin-$J$ system is called spin squeezed [254] if there exists a direction $\vec{n}$, orthogonal to the mean spin polarization $\langle\vec{I}\rangle$ such that

$$\xi_{\vec{n}}^2 \equiv 2\langle\Delta I_{\vec{n}}^2\rangle / |\langle\vec{I}\rangle| < 1. \tag{4.6}$$

In [255] it was shown that every squeezed state also contains entanglement among the individual constituents. Moreover, if $\xi_{\vec{n}}^2 < \frac{1}{k}$ then the spin squeezed state contains $k$-particle

entanglement [256, 257, 258]. In Appendix 4.A.2 we show that the squeezing parameter in $y$-direction for an approximate $I^-$ eigenstate $|\alpha\rangle$ is given as $\xi^2_{\hat{e}_y} = \sqrt{1-\alpha^2/J^2} + \mathcal{O}(1/J) = \sqrt{1-(\Omega/\Omega_0)^2} + \mathcal{O}(1/J)$. Note, however, that this equation is valid only for $\xi^2_{\hat{e}_y} \geq 1/\sqrt{J}$. For higher squeezing the operator expectation values constituting the term of order $\mathcal{O}(1/J)$ can attain macroscopic values of order $\sqrt{J}$. For $\Omega \lesssim \Omega_0$ we find that the nuclear spins are in a highly squeezed minimum uncertainty state, with $k$-particle entanglement[2]. Close to the critical point $k$ becomes of the order of $\sqrt{J}$ [$\xi^2_{\hat{e}_y} = \mathcal{O}(1/\sqrt{J})$] indicating diverging entanglement in the system.

Since the lowering operator is bounded ($||I^-|| \leq J$), at $\Omega = \Omega_0$ where the nuclear field has reached its maximum value, the zero entropy solution constructed above ceases to exist. For large electron driving, where $\Omega \gg \Omega_0$ sets the dominant energy scale, the dissipation $\gamma$ results in an undirected diffusion in the dressed state picture and in the limit $\Omega \to \infty$ the system's steady state is fully mixed. In order to describe the system for driving strength $\Omega > \Omega_0$, in Section 4.5.1 we develop a perturbative theory designed to efficiently describe a class of steady states where the electron and nuclear spins are largely decoupled and the nuclear system is found in a fully polarized and rotated state with, potentially squeezed, thermal Gaussian fluctuations (also referred to as *rotated squeezed thermal spin states – RSTSS* or the *Gaussian mode*). It is fully characterized by its mean polarization as well as the spin squeezing and effective temperature $T_{\text{eff}}$ of the fluctuations (cf. Appendix 4.A.2). Squeezed coherent atomic states, which constitute the solution along segment $x$, appear as a limiting case of this class for zero temperature $T_{\text{eff}} = 0$.

In order to describe these RSTSS solutions, we conduct a systematic expansion of the system's Liouville operator in orders of the system size $1/\sqrt{J}$, by approximating nuclear operators by their semiclassical values and incorporating bosonic fluctuations up to second order in an Holstein-Primakoff picture. The resulting separation of time scales between electron and nuclear dynamics is exploited in a formalized adiabatic elimination of the electron degrees of freedom. The semiclassical displacements (i.e., the electron and nuclear direction of polarization) are found self-consistently by imposing first-order stability of the nuclear fluctuations and correspond to the nuclear and electron steady-state expectation values derived from the semiclassical Bloch equations (i.e., after a brute force factorization $\langle S_i I_j\rangle \to \langle S_i\rangle\langle I_j\rangle$, for $i,j = x,y,z$) in the equations of motion (cf. Appendix 4.A.3). For a given set of semiclassical solutions we derive a second-order reduced master equation for the nuclear fluctuations which, in the thermodynamic limit, contains all information on the nuclear state's stability, its steady-state quantum fluctuations and entanglement, as well as the low excitation dynamics in the vicinity of the steady state and thus allows for a detailed classification of the different phases and transitions.

Using this formalism, we find that the system enters a new phase at the critical point $\Omega_0$, in which the nuclear field can no longer compensate for the external driving, leading to a finite electron inversion and a nuclear state of rising temperature for increasing driving strength. At the transition between the two phases, the properties of the steady state change non-analytically and in Section 4.5.2 we will find an asymptotic closing of the Liouvillian gap (cf. Section 4.3) at the critical point, as the Liouvillian's spectrum becomes continuous in the thermodynamic limit. We will characterize the critical point $(\omega_0, \Omega_0)$ as a second-order phase transition.

[2] As in Ref. [257] we call a pure state $|\psi\rangle$ of $N$-qubits $k$-particle entangled if $|\psi\rangle$ is a product of states $|\psi_l\rangle$ each acting on at most $k$ qubits and at least one of these does not factorize. A mixed state is at least $k$-particle entangled if it cannot be written as a mixture of $l < k$-particle entangled states.

Allowing for arbitrary hyperfine detunings $\omega$, a phase boundary emerges from the second-order critical point (line $b$ in Fig. 4.1), separating two distinct phases $A$ (blue) and $B$ (red) of the Gaussian mode. The subregion $C$ of $A$ indicates a region of bistability associated with the phase boundary $b$ and is discussed below.

At $\Omega = 0$ the semiclassical equations of motion feature two steady-state solutions. Not only the trivial steady state of the spin-pumping dynamics – the fully polarized state in $-z$ direction – but also an inverted state where the nuclear system is fully polarized in $+z$ direction is a (unstable) solution of the semiclassical system. Quantum fluctuations account for the decay of the latter solution of anomalous spin-pumping behavior. The two semiclassical solutions (the corresponding quantum states are from here on referred to as the *normal* and *anomalous spin-pumping modes*, respectively) persist for finite $\Omega$. As we show employing the formalism described above (Section 4.5.2), quantum fluctuations destabilize the mode of anomalous behavior in region $A$ of the phase diagram. The stable Gaussian solution in phase $A$ displays a behavior characterized by the competition of dissipation $\gamma$ and the onsetting driving field $\Omega$. The nuclear state is highly polarized in the direction set by the decay, and the electron spin starts aligning with the increasing external driving field. Furthermore, the normal spin-pumping mode of phase $A$ is characterized by a low effective spin temperature.

The analysis of the low excitation spectrum of the Liouvillian (Section 4.5.2) shows a direct vanishing of the ADR at the phase boundary $b$ between $A$ and $B$, while the imaginary part of the spectrum is gapped at all times. At this boundary, the normal mode of phase $A$ destabilizes while at the same the metastable anomalous mode turns stable defining the second phase $B$. The two mode energies are non-degenerate across the transition preventing a mixing of the two modes and the emergence of critical phenomena such as diverging entanglement in the system. Phase $B$ – anomalous spin pumping – is characterized by a large nuclear population inversion, as the nuclear field builds up in opposite direction of the dissipation. At the same time the electron spin counter aligns with the external driving field $\Omega$. In contrast to the normal mode of phase $A$, phase $B$ features large fluctuations (i.e., high effective temperature) in the nuclear state, which increase for high $\Omega$, until at some point the perturbative description in terms of RSTSS breaks down and the system approaches the fully mixed state. Note that region $A$ also transforms continuously to $B$ via the lower two quadrants of the phase diagram (Fig. 4.1). In this supercritical region [259] no clear distinction between the two phases exist.

To complete the phase diagram, we employ numerical techniques in order to study steady-state solutions that go beyond a RSTSS description in Section 4.6. The subregion of $A$ labeled $C$ indicates a region of bistability where a second steady-state solution (besides the normal spin-pumping Gaussian solution described above) appears, featuring a non-Gaussian character with large fluctuations of order $J$. Since this mode cannot be described by the perturbative formalism developed in Section 4.5 (which by construction is only suited for low fluctuations $\ll J$) we use numerical methods to study this mode in Section 4.6 for finite systems. We find that the non-Gaussian mode (in contrast to the Gaussian mode of region $A$) is polarized in $+z$ direction and features large fluctuations of the order of $J$. Additionally this solution displays large electron-nuclear connected correlations $\langle S_i I_j\rangle - \langle S_i\rangle\langle I_j\rangle$. It emerges from the anomalous spin-pumping mode coming from region $B$ and the system shows hysteretic behavior in region $C$ closely related to the phenomenon of optical bistability [260].

A fourth region is found in the lower half of the phase diagram ($D$). In contrast to the previous regions, area $D$ has no effects on steady-state properties. Instead, the region is charac-

terized by an anomalous behavior in the low excitation dynamics of the system. The elementary excitations in region $D$ are overdamped. Perturbing the system from its steady state leads to a non-oscillating exponential return. This behavior is discussed at the end of Section 4.5.2, where we study the low excitation spectrum of the Liouvillian in this region within the perturbative approach.

In summary, all the phases and transitions of the system are displayed in Fig. 4.1. Across the whole phase diagram one solution can be described as a RSTSS – a largely factorized electron-nuclear state with rotated nuclear polarization and Gaussian fluctuations. Phase $A$ hereby represents a region of normal spin-pumping behavior. The system is found in a cold Gaussian state, where the nuclear spins are highly polarized in the direction set by the electron dissipation and the electron spin aligns with the external driving for increasing field strength. In contrast, phase $B$ displays anomalous spin-pumping behavior. The nuclear system displays population inversion (i.e., a polarization opposing the electron pumping direction) while the electron aligns in opposite direction of the driving field. Furthermore, the state becomes increasingly noisy, quantified by a large effective temperature, which results in a fully mixed state in the limit of large driving strength $\Omega \to \infty$. Along segment $x$ the state becomes pure and factorizes exactly with a nuclear field that cancels the external driving exactly. The nuclear state can be described using approximate eigenstates of the lowering operator $I^-$ which display diverging squeezing approaching the second-order critical point $\Omega_0$. From this critical point a first-order phase boundary emerges separating phases $A$ and $B$. It is associated with a region of bistability (area $C$), where a second solution appears featuring a highly non-Gaussian character. The system shows hysteretic behavior in this region. Region $D$ is a phase characterized by its dynamical properties. The system shows an overdamping behavior approaching the steady state, which can be inferred from the excitation spectrum of the Liouvillian.

Let us now describe the phases and transitions involving the Gaussian mode in detail.

## 4.5 Perturbative treatment of the gaussian mode

As seen in the previous Section along the segment $x$ the system settles in a factorized electronic-nuclear state, where the nuclear system can be described as a lowering operator eigenstate up to second order in $\epsilon = J^{-1/2}$. Motivated by this result, we develop in Section 4.5.1 a perturbative theory based on a self-consistent Holstein-Primakoff transformation that enables the description of a class of steady states, which generalizes the squeezed coherent atomic state solution along $x$ to finite thermal fluctuations (RSTSS, Appendix 4.A.2). A solution of this nature can be found across the entire phase diagram and we show that this treatment becomes exact in the thermodynamic limit.

In Section 4.5.2 we discuss this Gaussian mode across the whole phase diagram. Steady-state properties of the nuclear fluctuations derived from a reduced second-order master equation provide deep insights in the nature of the various phases and transitions. Observed effects include criticality in both the steady state and the low-excitation spectrum, spin squeezing and entanglement as well as altered spin-pumping dynamics. Whenever feasible we compare the perturbative results with exact diagonalization techniques for finite systems and find excellent agreement even for systems of a few hundred spins only. First, in Section 4.5.2 we apply the developed theory exemplarily along the segment $x$, to obtain further insights in the associated transition at $\Omega_0$. In Section 4.5.2 we then give a detailed description of the different phases that

emerge in the phase diagram due to the Gaussian mode. Thereafter, in Section 4.5.2 we conduct a classification of the different transitions found in the phase diagram.

### 4.5.1 The theory

In this section we develop the perturbative theory to derive an effective second-order master equation for the nuclear system in the vicinity of the Gaussian steady state.

For realistic parameters, the Liouville operator $\mathcal{L}$ of Eqn. (4.1) does not feature an obvious hierarchy, that would allow for a perturbative treatment. In order to treat the electron-nuclear interaction as a perturbation, we first have to separate the macroscopic semiclassical part of the nuclear fields. To this end we conduct a self-consistent Holstein-Primakoff approximation describing nuclear fluctuations around the semiclassical state up to second order.

The (exact) Holstein-Primakoff transformation expresses the truncation of the collective nuclear spin operators to a total spin $J$ subspace in terms of a bosonic mode ($b$ denotes the respective annihilation operator):

$$\begin{aligned} I^- &= \sqrt{2J - b^\dagger b}\, b \\ I_z &= b^\dagger b - J. \end{aligned} \tag{4.7}$$

In the following we introduce a macroscopic displacement $\sqrt{J}\beta \in \mathbb{C}$ ($|\beta| \leq 2$) on this bosonic mode to account for a rotation of the mean polarization of the state, expand the operators of Eqn. (4.7) and accordingly the Liouville operator of equation Eqn. (4.1) in orders of $\epsilon = 1/\sqrt{J}$. The resulting hierarchy in the Liouvillian allows for an perturbative treatment of the leading orders and adiabatic elimination of the electron degrees of freedom whose evolution is governed by the fastest timescale in the system. The displacement $\beta$ is self-consistently found by demanding first-order stability of the solution. The second order of the new effective Liouvillian then provides complete information on second-order stability, criticality, and steady-state properties in the thermodynamic limit.

The macroscopic displacement of the nuclear mode,

$$b \to b + \sqrt{J}\beta, \tag{4.8}$$

allows for an expansion of the nuclear operators [Eqn. (4.7)] in orders of $\epsilon$

$$\begin{aligned} I^-/J =& \sqrt{k}\sqrt{1 - \epsilon\frac{\beta b^\dagger + \beta^* b}{k} - \epsilon^2\frac{b^\dagger b}{k}}\,(\beta + \epsilon b) \\ =& \sum_i \epsilon^i \mathcal{J}_i^-, \end{aligned} \tag{4.9}$$

where

$$\mathcal{J}_0^- = \sqrt{k}\beta, \tag{4.10}$$

$$\mathcal{J}_1^- = \frac{1}{2\sqrt{k}}\left[(2k-|\beta|^2)b - \beta^2 b^\dagger\right], \tag{4.11}$$

$$\begin{aligned}\mathcal{J}_2^- = -\Bigg[&\frac{\beta^* b + \beta b^\dagger}{2\sqrt{k}} b \\ &+ \frac{\sqrt{k}\beta}{8}\left([\frac{\beta b^\dagger + \beta^* b}{k}]^2 + 4\frac{b^\dagger b}{k}\right)\Bigg],\end{aligned} \tag{4.12}$$

$$\vdots$$

and $k = 2 - |\beta|^2$. Analogously, one finds

$$I_z/J = \sum_{i=0}^{2} \epsilon^i \mathcal{J}_i^z, \tag{4.13}$$

$$\mathcal{J}_0^z = |\beta|^2 - 1, \tag{4.14}$$

$$\mathcal{J}_1^z = \beta b^\dagger + \beta^* b, \tag{4.15}$$

$$\mathcal{J}_2^z = b^\dagger b. \tag{4.16}$$

This expansion is meaningful only if the fluctuations in the bosonic mode $b$ are smaller than $\mathcal{O}(\sqrt{J})$. Under this condition, any nuclear state is thus fully determined by the state of the bosonic mode $b$ and its displacement $\beta$.

According to the above expansions Master Eqn. (4.1) can be written as

$$\dot{\rho}/J = \left[\mathcal{L}_0 + \epsilon\mathcal{L}_1 + \epsilon^2\mathcal{L}_2 + \mathcal{O}(\epsilon^3)\right]\rho, \tag{4.17}$$

where

$$\begin{aligned}\mathcal{L}_0\rho = \gamma(S^-\rho S^+ - \frac{1}{2}\{S^+S^-,\rho\}_+) \\ -i[S^+(\Omega + a/2\mathcal{J}_0^-) + S^-(\Omega + a/2\mathcal{J}_0^+) \\ + aS^+S^-\mathcal{J}_0^z, \rho],\end{aligned} \tag{4.18}$$

$$\begin{aligned}\mathcal{L}_{1,2}\rho = -i[a/2(S^+\mathcal{J}_{1,2}^- + S^-\mathcal{J}_{1,2}^+) \\ + (aS^+S^- + \delta\omega)\mathcal{J}_{1,2}^z, \rho].\end{aligned} \tag{4.19}$$

The zeroth order superoperator $\mathcal{L}_0$ acts only on the electron degrees of freedom. This separation of time scales between electron and nuclear degrees of freedom implies that for a given semiclassical nuclear field (defined by the displacement $\beta$) the electron settles to a quasi-steady state on a timescale shorter than the nuclear dynamics and can be eliminated adiabatically on a coarse grained timescale. In the following we determine the effective nuclear evolution in the submanifold of the electronic quasi steady states of $\mathcal{L}_0$.

Let $P$ be the projector on the subspace of zero eigenvalues of $\mathcal{L}_0$, i.e., the zeroth order steady states, and $Q = \mathbb{1} - P$. Since $\mathcal{L}_0$ features a unique steady state, we find $P\rho = \mathrm{Tr}_S(\rho) \otimes \rho_{ss}$, where $\mathrm{Tr}_S$ denotes the trace over the electronic subspace and $\mathcal{L}_0\rho_{ss} = 0$. By definition it is

$P\mathcal{L}_0 = \mathcal{L}_0 P = 0$. After a generalized Schrieffer-Wolff transformation (this method will be explained in detail in the following Chapter 5), we derive an effective Liouvillian within the zeroth-order-steady-state subspace in orders of the perturbation

$$\begin{aligned}\mathcal{L}_{\text{eff}} =&\epsilon P\mathcal{L}_1 P \\ &+\epsilon^2(P\mathcal{L}_2 P - P\mathcal{L}_1 Q\mathcal{L}_0^{-1}Q\mathcal{L}_1 P) + \mathcal{O}(\epsilon^3).\end{aligned} \tag{4.20}$$

After tracing out the electron degrees of freedom the dynamics of the nuclear fluctuations $b$ are consequently governed by the reduced master equation

$$\dot{\sigma} := \text{Tr}_S(P\dot{\rho}) = \text{Tr}_S(\mathcal{L}_{\text{eff}} P\rho). \tag{4.21}$$

The first-order term in $\epsilon$ of Eqn. (4.20) can be readily calculated,

$$Tr_s(P\mathcal{L}_1 P\rho) = -i\left[\langle A\rangle_{ss} b + \langle A^\dagger\rangle_{ss} b^\dagger, \sigma\right], \tag{4.22}$$

where $A$ is an electronic operator,

$$\begin{aligned}A =&\beta^*(aS^+S^- + \delta\omega) \\ &+\frac{a}{4\sqrt{k}}\left[(2k - |\beta|^2)S^+ - (\beta^*)^2 S^-\right].\end{aligned} \tag{4.23}$$

$\langle A\rangle_{ss}$ denotes the steady-state expectation value according to $\mathcal{L}_0$, which depends on the system parameters $\gamma$ and $\Omega$ and on the semiclassical displacement $\beta$ via optical Bloch equations derived from $\mathcal{L}_0$ as described below. Eqn. (4.22) represents a driving of the nuclear fluctuations to leading order in the effective dynamics. Thus, for the steady state to be stable to first order, we demand

$$\langle A\rangle_{ss} = 0. \tag{4.24}$$

This equation defines self-consistently the semiclassical nuclear displacement $\beta$ in the steady state in dependence on the system parameters $\gamma, \Omega$ and $\delta\omega$.

The calculation of the second-order term of Eqn. (4.20) is more involved and presented in Appendix 4.A.4. We find the effective nuclear master equation to second order,[3]

$$\begin{aligned}\dot{\sigma} =&2R_a\left(b\sigma b^\dagger - \frac{1}{2}\{b^\dagger b, \sigma\}\right) \\ &+2R_b\left(b^\dagger\sigma b - \frac{1}{2}\{bb^\dagger, \sigma\}\right) \\ &+c\left(b\sigma b - \frac{1}{2}\{bb, \sigma\}\right) \\ &+c^*\left(b^\dagger\sigma b^\dagger - \frac{1}{2}\{b^\dagger b^\dagger, \sigma\}\right) \\ &-i\left[(I_a + I_b + F)b^\dagger b + (\alpha + B^*)b^2 + (\alpha^* + B)(b^\dagger)^2, \sigma\right],\end{aligned} \tag{4.25}$$

[3] In Chapter 5 we will show that this type of master equation is always of Lindblad form, generating physical evolutions.

with

$$B = -\frac{a\beta}{16\sqrt{k^3}}\left[(4k+|\beta|^2)\langle S^-\rangle_{ss} + \beta^2\langle S^+\rangle_{ss}\right], \tag{4.26}$$

$$F = -\frac{a}{8\sqrt{k^3}}(4k+|\beta|^2)\left(\beta\langle S^+\rangle_{ss} + \beta^*\langle S^-\rangle_{ss}\right) + a(\langle S^+S^-\rangle_{ss} + \delta\omega/a), \tag{4.27}$$

and

$$\begin{aligned} R_a &= \int_0^\infty dt\ \mathrm{Re}\left(\langle A^\dagger(t)A(0)\rangle_{ss}\right), \\ I_a &= \int_0^\infty dt\ \mathrm{Im}\left(\langle A^\dagger(t)A(0)\rangle_{ss}\right), \\ R_b &= \int_0^\infty dt\ \mathrm{Re}\left(\langle A(t)A^\dagger(0)\rangle_{ss}\right), \\ I_b &= \int_0^\infty dt\ \mathrm{Im}\left(\langle A(t)A^\dagger(0)\rangle_{ss}\right), \\ c &= \int_0^\infty dt\ \langle\{A(t),A(0)\}\rangle_{ss}, \\ \alpha &= \frac{1}{2i}\int_0^\infty dt\ \langle[A(t),A(0)]\rangle_{ss}. \end{aligned} \tag{4.28}$$

For a given set of system parameters the coefficients defining the nuclear dynamics [Eqns. (4.26), (4.27) and (4.28)] depend only on the nuclear displacement $\beta$. After choosing $\beta$ self-consistently to fulfill Eqn. (4.24) in order to guarantee first-order stability, Eqn. (4.25) contains all information of the nuclear system within the Gaussian picture, such as second-order stability as well as purity and squeezing of the nuclear steady state. Also it approximates the Liouville operator's low excitation spectrum to leading order and thus contains information on criticality in the system. Eqn. (4.25) therefore forms the basis for the subsequent discussion of the RSTSS mode and the corresponding phases and transitions in Section 4.5.

In order to calculate the coefficients of Eqn. (4.28), we have to determine integrated electronic autocorrelation functions of the type $\int_0^\infty dt\ \langle S^i(t)S^j(0)\rangle_{ss}$ and $\int_0^\infty dt\ \langle S^i(0)S^j(t)\rangle_{ss}$, where $i,j = +,-,z$. The dynamics of single electron operator expectation values are governed by the optical Bloch equations derived from $\mathcal{L}_0$,

$$\frac{d}{dt}\langle\Delta\vec{S}\rangle = \mathcal{M}\langle\Delta\vec{S}\rangle, \tag{4.29}$$

where $\Delta\vec{S} := \vec{S} - \langle\vec{S}\rangle_{ss}$ and $\vec{S} = (S^+, S^-, S_z)^T$ and

$$\mathcal{M} = \begin{pmatrix} -(\frac{\gamma}{2} - ia\mathcal{L}_0^z) & 0 & -2i\tilde{\Omega}^* \\ 0 & -(\frac{\gamma}{2} + ia\mathcal{L}_0^z) & 2i\tilde{\Omega} \\ -i\tilde{\Omega} & i\tilde{\Omega}^* & -\gamma \end{pmatrix}, \tag{4.30}$$

where we defined $\tilde{\Omega} = \Omega + \frac{a}{2}\sqrt{k}\beta$ and $\mathcal{L}_0^z$ is given in Eqn. (4.14). The steady-state solutions

can readily be evaluated:

$$\langle S^+\rangle_{ss} = 2i\frac{\tilde{\Omega}^*(\gamma + 2ia\mathcal{L}_0^z)}{\gamma^2 + 4a\mathcal{L}_0^{z2} + 8|\tilde{\Omega}|^2}, \tag{4.31}$$

$$\langle S_z\rangle_{ss} = -\frac{1}{2}\frac{\gamma^2 + 4a\mathcal{L}_0^{z2}}{\gamma^2 + 4a\mathcal{L}_0^{z2} + 8|\tilde{\Omega}|^2}. \tag{4.32}$$

Defining the correlation matrix $\mathbf{S} = \langle \Delta\vec{S}\Delta\vec{S}^\dagger\rangle_{ss}$ and $\mathbf{S}_t = \langle \Delta\vec{S}_t\Delta\vec{S}^\dagger\rangle_{ss}$, the Quantum Regression Theorem [262] yields the simple result

$$\mathbf{S}_t = e^{\mathcal{M}t}\mathbf{S}, \tag{4.33}$$

$$\mathbf{S}_t^\dagger = \langle \Delta\vec{S}\Delta\vec{S}_t^\dagger\rangle_{ss} = \mathbf{S}e^{\mathcal{M}^\dagger t}. \tag{4.34}$$

Finally, the time-integrated autocorrelation functions reduce to the simple expression

$$\mathcal{F}_1 = \int_0^\infty dt\mathbf{S}_t = \int_0^\infty dt e^{\mathcal{M}t}\mathbf{S} = -\mathcal{M}^{-1}\mathbf{S}, \tag{4.35}$$

$$\mathcal{F}_2 = \int_0^\infty dt\mathbf{S}_t^\dagger = \mathcal{F}_1^\dagger = -\mathbf{S}\left(\mathcal{M}^{-1}\right)^\dagger. \tag{4.36}$$

These matrices straightforwardly define the coefficients of the effective master equation of the nuclear fluctuations [Eqn. (4.25)]. In Appendix 4.A.4 we provide explicit formulas to calculate the relevant coefficients.

### 4.5.2 Phase diagram of the gaussian mode

In this Section we use the theory developed above to study the RSTSS mode across the phase diagram. As outlined in the previous Section we first determine self-consistently possible semiclassical displacements $\beta$, which guarantee first-order stability [Eqn. (4.24)]. For each of these solutions we determine the effective master equation for the nuclear fluctuations [Eqn. (4.25)], which in the thermodynamic limit contains all information on the steady-state and the low-excitation dynamics and we discuss properties like second-order stability, criticality, as well as purity and squeezing of the nuclear steady state. Using this information we provide a complete picture of the various phases and transitions involving the RSTSS solution.

#### Methods and general features

In order to determine the semiclassical displacements $\beta$ which guarantee first-order stability, we show in Appendix 4.A.3 that Eqn. (4.24) is equivalent to the steady-state conditions derived from the semiclassical Bloch equations of the system. Due to a symmetry in the equation, the steady-state displacements appear in pairs $\beta_-$, $\beta_+$. Any semiclassical displacement $\beta$ can be straightforwardly converted to the mean spin polarizations up to leading order in $\epsilon$ according to Eqn. (4.10), Eqn. (4.14), Eqn. (4.31), and Eqn. (4.32). In the thermodynamic limit the two sets of steady-state expectation values extracted from $\beta_-$ and $\beta_+$ share the symmetry $(\pm\langle S_x\rangle, \langle S_y\rangle, \langle S_z\rangle, \langle I_x\rangle, \pm\langle I_y\rangle, \pm\langle I_z\rangle)$. In large parts of the phase diagram the solution $\beta_-$ ($\beta_+$) displays high nuclear polarization in the same (opposite) direction as the the electron

spin pumping. We define the corresponding quantum states as the normal (anomalous) spin-pumping mode.

The two solutions $\beta_\pm$ define two corresponding master equations of the nuclear fluctuations around the respective semiclassical expectation values according to Eqn. (4.25). These master equations are subsequently used to determine second-order stability of the nuclear fluctuations and, if the dynamics turn out to be stable, the steady-state properties of the nuclear system. We emphasize that the effective Master Eqn. (4.25) not only can be used to determine steady-state properties, but also reproduces accurately the low excitation spectrum of the exact Liouvillian. It thus also describes the system dynamics in the vicinity of the steady state (increasingly accurate for large $J$).

From Eqn. (4.25) one readily derives a dynamic equation for the first-order bosonic moments

$$\begin{pmatrix} \dot{\langle b \rangle} \\ \langle b^\dagger \rangle \end{pmatrix} = \Sigma \begin{pmatrix} \langle b \rangle \\ \langle b^\dagger \rangle \end{pmatrix}, \tag{4.37}$$

with

$$\Sigma = \begin{pmatrix} -(R_a - R_b) - i\chi & -2i\xi \\ 2i\xi^* & -(R_a - R_b) + i\chi \end{pmatrix}, \tag{4.38}$$

$$\chi = I_a + I_b + F, \tag{4.39}$$

$$\xi = \alpha^* + B, \tag{4.40}$$

where all parameters are functions of the semiclassical displacements $\beta_\pm$. This equation of motion – and thus the corresponding master equation itself – features a fixed point if the eigenvalues of the matrix $\Sigma$ have negative real part ($\mathrm{Re}[\lambda_{1,2}] < 0$). Due to the symmetry between $\beta_+$ and $\beta_-$ one finds that the eigenvalues of the two $\Sigma$ matrices corresponding to $\beta_\pm$ fulfill $\mathrm{Re}[\lambda_{1,2}(\beta_+)] = -\mathrm{Re}[\lambda_{1,2}(\beta_-)]$ such that across the whole phase diagram only one solution is stable at a time and defines the corresponding phase in the phase diagram. Note however, that the unstable solution decays at a rate that is second order in $\epsilon$. Preparing the system in this state consequently leads to slow dynamics, such that this solution exhibits metastability.

In the following we implicitly choose the stable $\beta$ for which the real parts of the eigenvalues of $\Sigma$ are negative and discard the unstable solution. Fig. 4.2 displays a selection of steady-state expectation values in the thermodynamic limit across the phase diagram for the stable solution. Different expectation values illustrate the different nature of phases $A$ and $B$ and show distinct signatures of first- and second-order phase transitions which will be discussed in greater detail in Section 4.5.2 and 4.5.2. The approximate steady-state polarizations found in this way coincide with the exact values found via diagonalization techniques to an extraordinary degree ($\sim 10^{-3}$ relative deviation for J=150). Corrections to the perturbative solutions are of the order $1/J$ since the first-order expectation values of the bosonic mode vanish by construction, since $\langle b \rangle = 0$ [Compare Eqn. (4.9) and Eqn. (4.13)]. In the thermodynamic limit the perturbative solution becomes exact.

The two eigenvalues of $\Sigma$ are typically of the form $\lambda_{1,2} = a \pm ib$ (except in region $D$, which is discussed below) and define the complex energy of the mode. In this case the matrix $\Sigma$ contains all information on the low excitation spectrum of the Liouvillian which is approximated by multiples of the mode energies within the perturbative treatment [4]. The low excitation spec-

[4]The inset of Fig. 4.9 clearly shows these bosonic characteristics of the exact spectrum for J=150. Outside the region of bistability the real part of the spectrum is approximately equidistant.

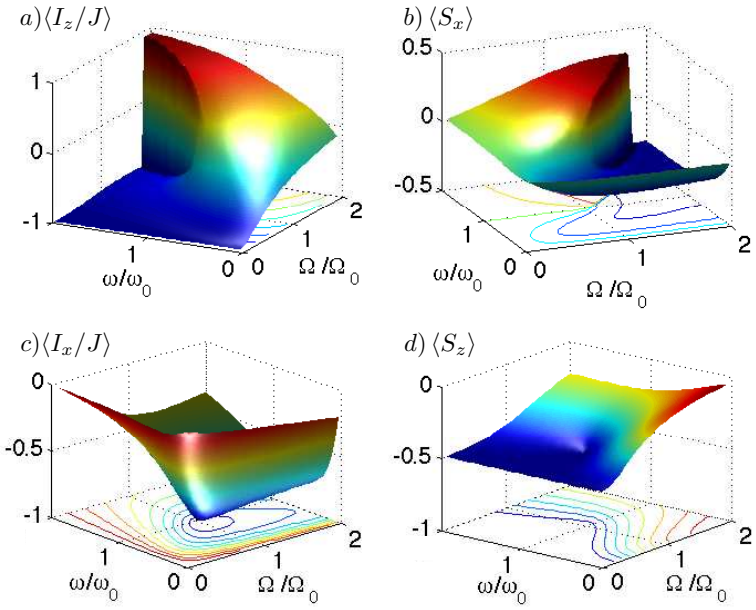


Figure 4.2: The system observables of the RSTSS solution in the thermodynamic limit show clear signatures of first and second-order transitions ($\gamma = a$). (a) The nuclear polarization in $z$-direction $\langle I_z/J\rangle_{ss}$ switches abruptly from minus to plus at the phase boundary $b$. (b) The electron polarization in $x$-direction $\langle S_x\rangle_{ss}$ shows a similar discontinuous behavior along $b$. (c) The nuclear polarization in $x$-direction changes smoothly across the phase boundary $b$. Along the segment $x$ ($\omega = \omega_0, \Omega < \Omega_0$) the nuclear field in $x$-direction builds up linearly to cancel the external driving. (d) The electron polarization in $z$-direction also does not show signatures of the first-order transition $b$. Along segment $x$ the electron is fully polarized in $-z$-direction up to the second-order critical point $(\omega_0, \Omega_0)$, where it changes non-analytically (see also Fig. 4.6).

trum contains information about criticality of the system and the dynamics in the vicinity of the steady state and is used to discuss and classify the different transitions in the phase diagram. In particular, the eigenvalue of $\Sigma$ with largest real part approximates the ADR in the thermodynamic limit in those regions of the phase diagram where the Gaussian mode is responsible for the lowest excitations in the Liouvillian spectrum (only in the region of bistability $C$ this is not the case).

The ADR according to the perturbative descriptions based on Gaussian modes is displayed in Fig. 4.3. It is used to study the transitions involving the Gaussian mode in the thermodynamic limit. The ADR vanishes along a line $b$ indicating a phase boundary separating the normal and anomalous spin-pumping phase, which is described in Section 4.5.2. Furthermore a non-analyticity of the ADR at a finite value defines region $D$, which characterizes a dynamical phase and is explained in Section 4.5.2.

The dynamical matrix of the first-order moments $\Sigma$ provides information on the stability of the semiclassical solutions, the criticality of the Liouvillian, and the non-analyticities of region $D$. In order to understand the character of the solutions in the different regions of the phase diagram we consider next the steady-state covariance matrix (CM) of the bosonic system. For a

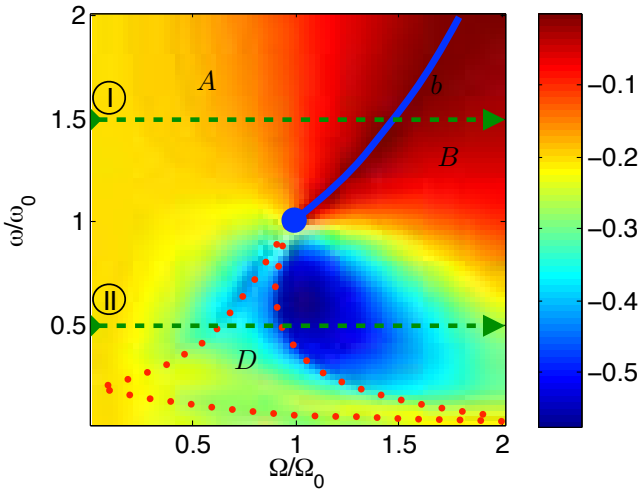


Figure 4.3: Asymptotic decay rate (ADR, cf. text) for $\gamma = a$ within the perturbative framework. Along $b$ the ADR vanishes non-analytically, indicating the stabilizing and destabilizing of the modes of regions $A$ and $B$, respectively. $b$ is a first-order phase boundary culminating in a second-order critical point at $(\omega_0, \Omega_0)$. From here region $D$ opens, which is characterized by a non-analyticity in the ADR at a finite value. This indicates a change in the dynamic properties of the system which can not be detected in steady-state observables. Within $D$ the system shows an over damped behavior in the vicinity of the steady state.

quadratic evolution like the one of Eqn. (4.25) the steady-state CM contains all information on the state. We deduce the effective temperature and the squeezing of the nuclear spin system, which connects to criticality in the system.

For a one-mode system with vanishing displacements $\langle x\rangle$ and $\langle p\rangle$ [in the steady state of Eqn. (4.25) this is always the case] the CM is defined as

$$\Gamma = \begin{pmatrix} 2\langle x^2\rangle & 2\langle xp\rangle - i \\ 2\langle px\rangle + i & 2\langle p^2\rangle \end{pmatrix}, \tag{4.41}$$

with the usual definitions $x = \frac{1}{\sqrt{2}}(b + b^\dagger)$ and $p = \frac{1}{\sqrt{2}i}(b - b^\dagger)$. Using Eqn. (4.25) we straightforwardly calculate the steady-state CM $\Gamma_{\text{ss}}$ across the phase diagram. As $\Gamma = \Gamma^T > 0$, $\Gamma$ is symplectically diagonalizable, with

$$\Gamma = DO \begin{pmatrix} M^2 & 0 \\ 0 & M^{-2} \end{pmatrix} O^{-1}, \tag{4.42}$$

where $O$ is orthogonal with $\det(O) = 1$. For a single mode, $D \geq 1$ and $M \geq 1$ are real numbers. While $D$ is a measure of the purity of the state [$Tr(\rho^2) = 1/\sqrt{|\Gamma|} = 1/D$], the smallest eigenvalue of $\Gamma$, $\lambda_{\text{min}} \equiv DM^{-2}$ determines the amount of squeezing in the system [263]. $\lambda_{\text{min}} < 1$ indicates squeezing in the bosonic mode. For $M = 1$, the CM Eqn. (4.42) describes a thermal state of the bosonic mode and $D$ can be straightforwardly associated to a

dimensionless effective temperature

$$T_{\text{eff}} = \ln\left[\frac{2}{\sqrt{D}-1}+1\right]^{-1}. \tag{4.43}$$

This definition is also meaningful for $M > 1$, since the squeezing operation is entropy-conserving. $T_{\text{eff}}$ is also a measure for the entropy of the spin system, as to leading order it is connected to the bosonic mode via an unitary (i.e., entropy-conserving) transformation. The effective temperature of the different phases will be discussed below in Sections 4.5.2 & 4.5.2 [cf. Fig. 4.7].

We stress the point that all properties of the CM derived within the second order of the perturbative approach are independent of the system size $J$. In particular, the amount of fluctuations (i.e., the purity) in the state does not depend on the particle number. In order to self-consistently justify the perturbative approach, $D$ has to be small with regard to $J$. This implies that in the thermodynamic limit $J \to \infty$ the perturbative results to second (i.e., leading) order become exact. The inverse purity $D$ is displayed in Fig. 4.4 a). Except for for a small region

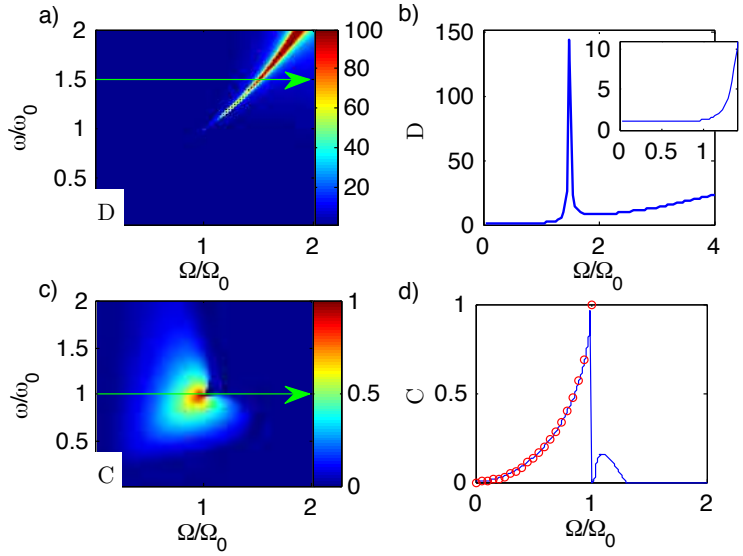


Figure 4.4: Properties of the steady-state CM $\Gamma_{ss}$ [Eqn. (4.42)]. a) The fluctuations $D$ are low in most parts of the phase diagram except for a small wedge around the Gaussian phase boundary. b) Fluctuations $D$ along the line ① [green line of a)]. The phase boundaries separate a mode with low fluctuations (enlarged in the inset), from a mode with large fluctuations. For large $\Omega$ fluctuations increase, and the system eventually approaches a fully mixed state. c) The squeezing measure $C$ (c.f. text) in the thermodynamic limit. $C$ approaches 1 at $(\omega_0, \Omega_0)$ indicating diverging entanglement in the system. d) $C$ along the line $\omega = \omega_0$ (solid line). The red circles indicate the the squeezing parameter $1 - \xi^2_{\hat{e}_y} = 1 - \sqrt{1-(\Omega/\Omega_0)^2}$ (cf. text).

around the Gaussian phase boundary $b$ the fluctuations are much smaller than $J = 150$, which justifies the validity of the perturbative approach and explains the excellent agreement with the exact diagonalization for this system size.

The squeezing $\lambda_{\text{min}}$ in the auxiliary bosonic mode does not necessarily correspond to spin squeezing in the nuclear system. In order to deduce the spin squeezing in the nuclear system

from the squeezing of the bosonic mode a transformation according to Eqn. (4.11) and Eqn. (4.15) is necessary. In Appendix 4.A.2 we show that for $|\beta| < 1$ Eqn. (4.11) can be reformulated to connect the spin fluctuations to a squeezed and rescaled bosonic mode

$$\mathcal{J}_1^- = \sqrt{2(1-|\beta|^2)}S^\dagger(r)bS(r), \tag{4.44}$$

where $S(r) = e^{(r^*b^2 - rb^{\dagger 2})/2}$ is the squeezing operator and $\cosh(r) = \mu = (2k - |\beta|^2)/[2\sqrt{2k(1-|\beta|^2)}]$ and $\sinh(r) = -\nu = \beta^2/[2\sqrt{2k(1-|\beta|^2)}]$.

Thus, squeezing $\lambda_{\text{min}}$ of the mode $b$ does, in general, not imply reduced spin fluctuations in a direction orthogonal to the mean spin polarization since the transformation between spin fluctuations and $b$ involves a squeezing operation itself and a scaling by a factor $0 < \sqrt{2(1-|\beta|^2)} \leq \sqrt{2}$.

In general, we thus have to apply a more involved squeezing criterion. In [255] it was shown that for systems of $N$ spin-1/2 particles and for all directions $\vec{n}$ the quantity

$$C_{\vec{n}} \equiv 1 - \frac{2}{J}\langle \Delta I_{\vec{n}}^2 \rangle - \frac{1}{J^2}\langle I_{\vec{n}} \rangle^2 < 1, \tag{4.45}$$

signals entanglement if $C_{\vec{n}} > 0$ for some direction $\vec{n}$. Moreover, $\langle \Delta I_{\vec{n}}^2 \rangle < J/2$ indicates a generalized spin-squeezing of the state[5].

In the following we use the quantity $C = \max\{0, C_{\vec{n}} \,|\vec{n} \in \mathbb{R}^3\}$ to investigate squeezing and bipartite entanglement in the nuclear system. In order to calculate $C_{\vec{n}}$ we reconstruct the approximate nuclear operators according to Eqn. (4.9) and Eqn. (4.14) from the semiclassical displacement $\beta$ and evaluate the expectation values according to the steady-state CM Eqn. (4.41). Finally, we maximize $C_{\vec{n}}$ with regard to all possible directions $\vec{n}$ to obtain $C$. The results are discussed in Section 4.5.2. As discussed in more detail in the next Section, the fact that $C \to 1$ as $\Omega \to \Omega_0$ on the line segment $x$ indicates a diverging entanglement length in the sense that $O(1/(1-C)) = O(\sqrt{J})$-particle entanglement is present [257].

### A second-order phase transition: The segment $x$

The segment $x$ at $\omega = \omega_0$ (Fig. 4.1) represents a very peculiar region in the phase diagram, where the solution below the critical point can be constructed analytically as demonstrated in Section 4.4.2. The electron and nuclear system decouple, resulting in a zero entropy product steady state. A nuclear polarization builds up to cancel the external driving up to the point of maximal Overhauser field ($\Omega_0$). At this point squeezing and entanglement in the system diverge, indicating a second-order phase transition. In the following we exemplarily employ the formalism developed above along this line to obtain further insight about the criticality at $(\omega_0, \Omega_0)$. We calculate the analytical steady-state solution as well as the effective master equation governing the nuclear fluctuation dynamics in its vicinity. We find that here the spectrum of the Liouvillian becomes continuous (implying a closing gap) and real. At the same time the creation operators of the elementary excitations from the steady state turn Hermitian, giving rise to diverging spin entanglement.

[5] In distinction to the criterion Eqn. (4.6) the squeezed component $J_{\vec{n}}$ is not necessarily orthogonal to the mean spin.

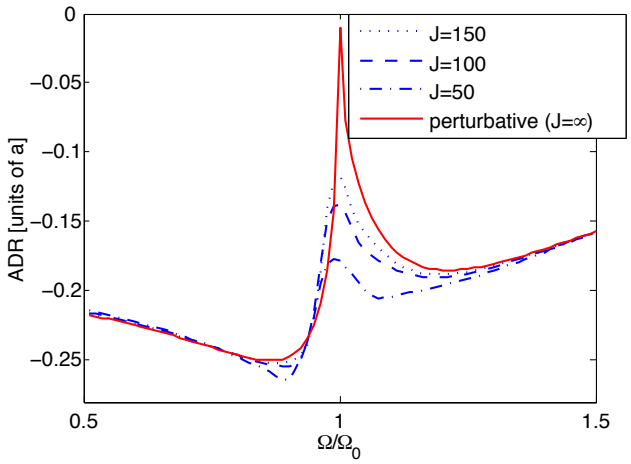


Figure 4.5: The ADR ($\gamma = a$) for $J = 50$, 100, 150 (broken lines) in comparison with the perturbatively calculated (solid line, cf. Section 4.5.2) along $\omega = \omega_0$. For finite systems one finds an avoided crossing at $\Omega_0$. The size of the gap reduces with the system size until it closes in the thermodynamic limit (solid line). Below $\Omega_0$ the ADR in the thermodynamic limit is given by Eqn. (4.52).

The first-order stability condition Eqn. (4.24) is fulfilled, if $\tilde{\Omega} = 0$ [compare Eqn. (4.31) and Eqn. (4.32)], which yields the possible semiclassical steady-state displacements

$$\begin{aligned} \sqrt{k}\beta &= -\Omega/\Omega_0 \\ \Leftrightarrow \beta_\pm &= -\sqrt{1 \pm \sqrt{1-(\Omega/\Omega_0)^2}}, \end{aligned} \tag{4.46}$$

corresponding to a normal ('$-$') and anomalous ('$+$') spin-pumping mode, respectively.

Next, we explicitly calculate the second-order corrective dynamics of the nuclear degrees of freedom for the normal mode. The vanishing of the effective driving $\tilde{\Omega} = 0$ forces the electron in its dark state – implying $\langle S^+\rangle_{ss} = \langle S^-\rangle_{ss} = \langle S^+S^-\rangle_{ss} = 0$ – and directly yields $B = F = 0$ [Eqn. (4.26) and Eqn. (4.27)]. The remaining constants can be calculated as described above and introducing new bosonic operators (for the normal mode $\beta = \beta_- \leq 1$)

$$d = \mu b + \nu b^\dagger, \tag{4.47}$$

with

$$\mu = \frac{2k - |\beta|^2}{2\sqrt{2k(1-|\beta|^2)}}, \tag{4.48a}$$

$$\nu = -\frac{\beta^2}{2\sqrt{2k(1-|\beta|^2)}}, \tag{4.48b}$$

one finds the effective evolution of the nuclear fluctuations given as

$$\begin{aligned} \dot{\sigma} =& \Gamma_{\text{eff}} \left( d\sigma d^\dagger - \frac{1}{2}\{d^\dagger d, \sigma\} \right) \\ & - i \left[ \Theta_{\text{eff}} d^\dagger d, \sigma \right], \end{aligned} \tag{4.49}$$

with

$$\Gamma_{\text{eff}} = 2a^2 \text{Re}\left(\frac{1}{\gamma + i2a(|\beta|^2 - 1)}\right)(1 - |\beta|^2), \tag{4.50}$$

$$\Theta_{\text{eff}} = a^2 \text{Im}\left(\frac{1}{\gamma + i2a(|\beta|^2 - 1)}\right)(1 - |\beta|^2). \tag{4.51}$$

$d$ and $d^\dagger$ fulfill boson commutation relations, since Eqn. (4.47) defines a symplectic transformation ($|\mu|^2 - |\nu|^2 = 1$). The eigenvalues of the dynamical matrix $\Sigma$ associated to Eqn. (4.49) are straightforwardly given as $\lambda_{1,2} = -\Gamma_{\text{eff}}/2 \pm i\Theta_{\text{eff}}$. The real part – representing the ADR of the system in thermodynamic limit (compare Fig. 4.5) – is always negative, indicating the stability of the normal spin-pumping mode ($\beta_-$). In an analogous calculation one shows that the semiclassical solution $\beta_+ > 1$ is not stable to second order since the eigenvalues of $\Sigma$ have a positive real part, i.e., the fluctuations diverge, violating the initial assumptions that the mode $b$ has to be lowly occupied.

Selected steady-state expectation values derived from the stable displacement $\beta_-$ to leading order in $J$ (i.e., in the thermodynamic limit) are displayed in Fig. 4.6. Already for $J = 150$ we

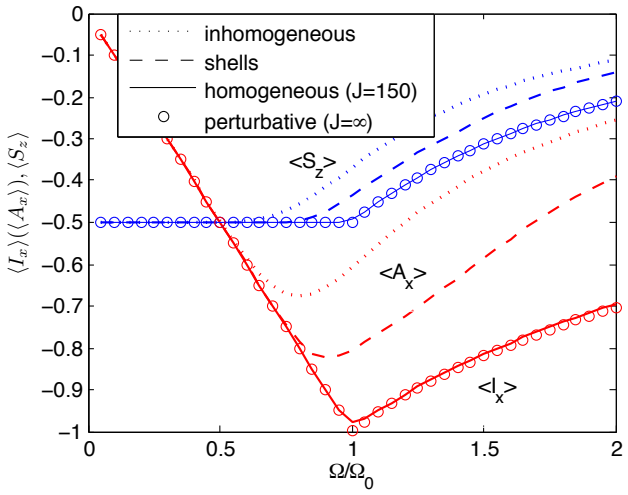


Figure 4.6: Electron inversion $\langle S_z \rangle$ and the nuclear field in $x$ direction $\langle I_x \rangle$ along $\omega = \omega_0$, in the thermodynamic limit according to the perturbative theory (circles) in comparison with the numeric values from exact diagonalization for a finite system of $J = 150$ (solid lines). The perturbative theory shows excellent agreement with the numerical solutions. Further, the numerically determined electron inversion and the expectation value of the inhomogeneous nuclear operator $\langle A_x \rangle$ are displayed for a model of two inhomogeneously coupled nuclear shells ($g_1 = 2g_2$) of size $J_{1,2} = 8$ (dashed lines) and for five inhomogeneously coupled nuclear spins (dotted lines) are displayed (discussion see Section 4.7).

find excellent agreement between the perturbative and exact mean polarizations. The nuclear field builds up to exactly cancel the external magnetic field $\Omega$ forcing the electron in its dark state $|\downarrow\rangle$ along $x$ and thus realizing the model of cooperative resonance fluorescence [77] even for weak dissipation $\gamma \leq a$ [compare Eqn. (4.5)]. This solution is available only if $\Omega \leq \Omega_0$

(defining segment $x$), i.e., up to the point where the nuclear field reaches its maximum. At this point the system enters a new phase of anomalous spin pumping (described below) and the steady-state properties change abruptly.

Inserting solution $\beta_-$ in the coefficients of Master Eqn. (4.49) yields

$$\Gamma_{\text{eff}} = 2a^2 \text{Re}\left(\frac{1}{\gamma - i2a\sqrt{1-(\Omega/\Omega_0)^2}}\right)\sqrt{1-(\Omega/\Omega_0)^2}, \tag{4.52}$$

$$\Theta_{\text{eff}} = a^2 \text{Im}\left(\frac{1}{\gamma - i2a\sqrt{1-(\Omega/\Omega_0)^2}}\right)\sqrt{1-(\Omega/\Omega_0)^2}. \tag{4.53}$$

In the close vicinity below the critical point $\Omega_0$ the real part of the gap in the Liouvillian's spectrum closes as

$$\Gamma_{\text{eff}} \approx 2\frac{a^2}{\gamma}\sqrt{1-(\Omega/\Omega_0)^2}, \tag{4.54}$$

and the imaginary part as

$$|\Theta_{\text{eff}}| \approx 2\frac{a^3}{\gamma^2}[1-(\Omega/\Omega_0)^2], \tag{4.55}$$

indicating criticality. Fig. 4.5 displays the ADR along $\omega = \omega_0$ in the thermodynamic limit [which is given on the segment $x$ by Eqn. (4.52)] and for finite systems. It displays an avoided crossing at $\Omega_0$ with a gap that vanishes in the thermodynamic limit. This closing of the gap coincides with diverging time scales in the system, which renders the model more susceptible to potential perturbing effects, a phenomenon well known in the context of criticality [260].

In contrast to the general form Eqn. (4.25), Eqn. (4.49) contains only one Lindblad term and the dynamics drive the system into the vacuum $|0_d\rangle$ of the squeezed mode $d$. As the system approaches the critical value $\Omega = \Omega_0$ (i.e., $\beta_- = -1$) the mode $d$ adopts more and more a $\hat{p} = \frac{1}{\sqrt{2}i}(b - b^\dagger)$-like character and thus the squeezing of this mode's vacuum increases. The (in general complicated) transformation between the squeezing of the bosonic mode $b$ and the spin operators (cf. Section 4.5.2) can readily be established along $x$, since the operator $d$ is trivially related to the spin operators [cf. Eqn. (4.11)]

$$\begin{aligned}\mathcal{J}_1^- &= \frac{1}{2\sqrt{k}}[(2k-|\beta|^2)b - \beta^2 b^\dagger] \\ &= \sqrt{2(1-|\beta|^2)}(\mu b + \nu b^\dagger) \\ &= \sqrt{2(1-|\beta|^2)}d.\end{aligned} \tag{4.56}$$

The fluctuations in $y$-direction, for example, are consequently given as

$$\mathcal{J}_1^y = \sqrt{(1-|\beta|^2)}\hat{p}_d, \tag{4.57}$$

where $\hat{p}_d = \frac{1}{\sqrt{2}i}(d - d^\dagger)$. One readily shows that

$$\langle \Delta I_y^2 \rangle = J\langle \mathcal{J}_1^{y2} \rangle = J(1-|\beta|^2)\langle \hat{p}_d^2 \rangle, \tag{4.58}$$

up to order $O(1)$ and we used $\langle d\rangle = 0$ in the steady state. In the $\hat{p}$ vacuum $|0_p\rangle$ it is $\langle \hat{p}_d^2\rangle = 1/2$, such that we evaluate

$$\begin{aligned}\xi^2_{\hat{e}_y} &= 2\langle \Delta I_y^2\rangle / |\langle \vec{I}\rangle| \\ &= 2(1-|\beta|^2)\langle \hat{p}_d^2\rangle = \sqrt{1-\left(\frac{\Omega}{\Omega_0}\right)^2},\end{aligned} \tag{4.59}$$

where we used $|\langle \vec{I}\rangle| = J$ and inserted the semiclassical displacement $\beta_-$.

This is the same result we derived in Section 4.4.2 and Appendix 4.A.2 by constructing approximate eigenstates of the lowering operator $I^-$ and along $x$ we find that $C \approx 1 - \xi^2_{\hat{e}_y}$, as shown in Fig. 4.4 d). Note that here $\hat{e}_y$ is orthogonal to the direction of the mean spin $\langle \vec{I}\rangle$. This allows us to deduce that $O(\sqrt{J})$ nuclear spins must be entangled close to the critical point, which establishes a "diverging entanglement length" in this system. To see this, we employ a variant of the criterion Eqn. (4.6), as discussed in [256]. There, it was shown that $\xi^2_{\hat{e}_y} < 1/k$ sets a lower bound of $N\xi^{-2}_{\hat{e}_y}$ on the quantum Fisher information $F_Q$ of the state. In [257] it was shown that for states containing at most $k$-particle entanglement, $F_Q$ is upper bounded by $Nk$. Consequently, the values of $\xi^2_{\hat{e}_y}$ obtained close to the critical point [cf. Eqn. (4.59) and Appendix 4.A.2] imply that at least $O(\sqrt{J})$-particle entanglement must be present. Note that the bosonic description does not make it possible to describe the range $\xi^2_{\hat{e}_y} = O(1/J)$, i.e., $k = O(J)$, where the fluctuations become larger than the expansion parameter.

The nuclear squeezing and entanglement in the system diverges approaching the critical point, as the Lindblad operator $d$ (defining the steady state $|0_d\rangle$) becomes more and more $\hat{p}$-like. The fluctuations in $y$-direction tend to zero, while at the same time – due to the Heisenberg uncertainty relation – the steady state is in a superposition of an increasing number of $I_z$ eigenstates. Since in a system with infinite range interactions (as the one we are considering) there is no obvious definition of a coherence length, the range of the involved $I_z$ eigenstates can be considered as an analogous concept.

At the critical value $\Omega = \Omega_0$ the symplectic transformation Eq. (4.47) becomes ill defined ($d$ becomes a $\hat{p}$-like operator) while both the dissipation rate and the mode energy tend to zero. While the coefficients in Eqs. (4.48) diverge, the total master equation is well defined [due to the factors $(1-|\beta|^2)$ in $\Gamma_{\text{eff}}$] and straightforwardly can be written as

$$\dot{\sigma} = \frac{a^2}{2\gamma}\left(\hat{p}\sigma\hat{p} - \frac{1}{2}\{\hat{p}^2,\sigma\}\right). \tag{4.60}$$

The Liouville operator's spectrum is real and continuous with Hermitian creation operators of the elementary excitations.

We stress the point that along segment $x$ in the phase diagram highly dissipative dynamics drive the system in a pure and separable steady state with zero effective temperature $T_{\text{eff}} = 0$ [cf. Fig. 4.7 b)]. At the critical point $\Omega_0$ the steady state changes its nature abruptly as the system enters a high-temperature phase.

Furthermore, we remark that this steady state has no relation to the system's ground state. This is in contrast to the extensively studied Dicke phase transition [78, 264, 84] where the steady state is in close relation to the Hamiltonian's ground state (in fact, in the normal phase it is identical). In the present model dissipation drives the system to a highly excited state of

the Hamiltonian and the observed critical phenomena are disconnected from the Hamiltonian's low excitation spectrum.

We have seen that at the critical point $(\omega_0, \Omega_0)$ the gap of the Liouville operator's spectrum (in both real and imaginary part) closes in the thermodynamic limit [Eqn. (4.54) and Eqn. (4.55)]. Approaching the critical point the steady-state fluctuations become more and more squeezed due to the increasing $\hat{p}$-like character of the mode $d$. The spin squeezing close to the critical point [Eqn. (4.59)] can be interpreted as a diverging coherence length in a system with infinite range interactions (the electron mediates interactions between remote spins). These are clear indications for a second-order phase transition, which is formalized in Section 4.5.2.

### Phases

In the present Section we study the different phases of the system, which involve the RSTSS solution ($A$, $B$ and $D$) using the analytic tools developed above. By construction, the RSTSS solution describes steady states where the electron and nuclear states factorize to leading order in the system size and the nuclear system is found in a fully polarized and rotated state with Gaussian fluctuations, which are fully characterized by their effective temperature and squeezing. Figure 4.2 displays different steady-state observables of the Gaussian solution determined via the formalism described above in the thermodynamic limit.

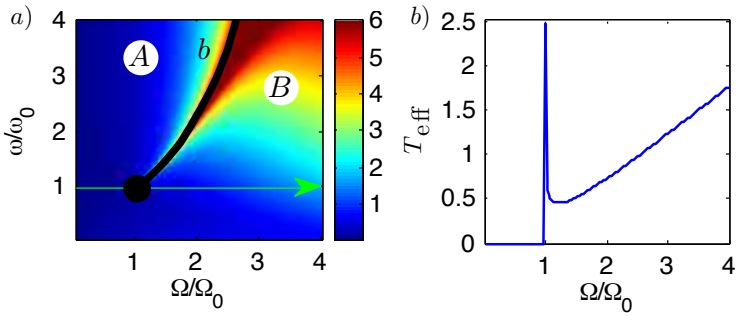


Figure 4.7: Effective temperature $T_{\text{eff}}$ of the Gaussian mode. Temperatures $T_{\text{eff}} > 6$ are cut off, as the temperature diverges along the phase boundary $b$. a) The first-order phase boundary $b$ separates the low-temperature phase $A$ from the high-temperature phase $B$. b) $T_{\text{eff}}$ along $\omega = \omega_0$: On segment $x$ the system is in a zero entropy state ($T_{\text{eff}}$=0). Above the second-order critical point $\Omega > \Omega_0$ the system enters a high-temperature phase. Here the temperature rises with increasing driving strength.

In phase $A$ the system is characterized by normal spin-pumping behavior. Only the semi-classical displacement $\beta_-$ (normal mode) leads to a dynamical matrix $\Sigma$ that has negative real parts of its eigenvalues, while for $\beta_+$ the eigenvalues have positive real parts, indicating the instability of that mode in second order. The nuclear system in the normal mode settles in a state highly polarized in $-z$-direction following the direction of the electron spin pumping [Fig. 4.2 a)]. Meanwhile, increasing the external driving $\Omega$ and approaching the phase boundary $b$, a nuclear field in $x$ direction builds up, but only along $x$ it can fully cancel the external driving [Fig. 4.2 c)]. Therefore, in general, the electron spin aligns more and more with the external field [Fig. 4.2 (b,d)]. Furthermore, the effective temperature (and thus the entropy) of the phase

is low, as displayed in Fig. 4.7 a).

In region $B$, in contrast, $\beta_+$ is the only stable solution, defining the phase of anomalous spin-pumping behavior. The nuclear system now shows strong population inversion: i.e., the nuclear polarization is found in direction opposite to the external pumping ($z$). In the same way the electron now aligns in opposite direction to the external driving field ($x$). Also, in contrast to phase $A$, the RSTSS now is in a high-temperature state. For larger electron driving the temperature increases until eventually the Gaussian description breaks down (as $D \propto J$) and for $\Omega \to \infty$ the system is found in a completely mixed state [compare Fig. 4.4 b)].

In the upper half of the phase diagram ($\omega > \omega_0$) phase $A$ changes abruptly into phase $B$ at the boundary $b$ and certain steady-state spin observables [$\langle I_z \rangle$, $\langle S_x \rangle$ [Fig. 4.2 a) & b)] and $\langle I_y \rangle$ (not displayed)] show distinct features of a first-order phase transition, changing sign as the normal (anomalous) mode destabilizes (stabilizes). This transition is discussed in greater detail in the following Section 4.5.2. Following this boundary toward the critical point ($\omega_0, \Omega_0$) the two phases become progressively more similar. Below the critical point ($\omega < \omega_0$) there is no clear distinction between the normal and anomalous spin-pumping mode anymore, a phenomenon known from thermodynamics as *supercriticality*. Phase $A$ transforms continuously to phase $B$ in this region. Close to the critical point, supercritical media typically respond very sensitively to the external control parameters of the phase diagram (e.g., temperature or pressure) [259]. In our system we observe that small changes in the parameter $\omega$ leads to large changes in electron spin observables.

Next, we consider the third region associated with the RSTSS solution, region $D$. We will find that this region differs from the previous ones by the fact that it cannot be detected in the system's steady state but rather in dynamical observables.

The eigenvalues of the dynamic matrix $\Sigma$ can be calculated as $\lambda_{1,2} = -(R_a - R_b) \pm 2\sqrt{4|\xi|^2 - \chi^2}$ and provide information on the approximate low excitation spectrum of the Liouvillian. We can distinguish two cases for the low excitation spectrum, which differ only in the Hamiltonian properties of Eqn. (4.25) (fully determined by $\chi$ and $\xi$ [Eqn. (4.39) & Eqn. (4.40)]). In the first case the quadratic bosonic Hamiltonian can be symplectically transformed to be diagonal in a Fock basis (i.e., to be of the form $\propto \tilde{b}^\dagger \tilde{b}$). This is the case if $\chi^2 > 4|\xi|^2$. As a consequence the two eigenvalues of $\Sigma$ have an identical real part and imaginary parts $\pm 2\sqrt{\chi^2 - 4|\xi|^2}$. In the second case the Hamiltonian transforms symplectically into a squeezing Hamiltonian $\propto (\tilde{b}^{\dagger 2} + \tilde{b}^2)$. Here one finds $\chi^2 < 4|\xi|^2$, such that the eigenvalues become real and symmetrically distributed around $-(R_a - R_b)$. In region $D$ in Fig. 4.1 we find the effective Hamiltonian for the nuclear fluctuations to be symplectically equivalent to a squeezing Hamiltonian.

Fig. 4.8 shows the ADR exemplarily along the line $\omega = 0.5\,\omega_0$ (Ⓘ in Fig. 4.1) calculated according to the perturbative theory and via exact diagonalization, respectively. The perturbative theory approximates accurately the low excitation spectrum of the Liouvillian. We find that in region $D$ the ADR splits up when the coherent part of Eqn. (4.25) changes to a squeezing Hamiltonian. As mentioned above, this non-analyticity occurs at a non zero value of the ADR and thus does not leave signatures in the steady-state behavior. The steady state transforms smoothly along Ⓘ. However, the nature of dynamical observables change within region $D$ as the system displays anomalous behavior approaching the steady state. The splitting of the ADR coincides with the vanishing of the imaginary part of the lowest non-zero Liouvillian eigenvalues. Thus, the system is overdamped in $D$. Perturbing the system from its steady state will

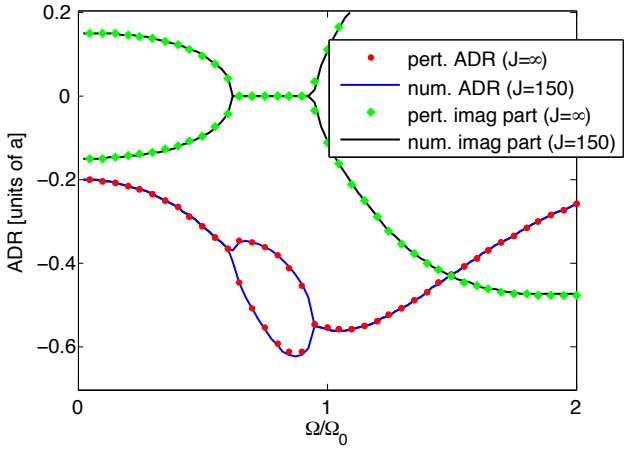


Figure 4.8: The ADR and the imaginary part of the respective eigenvalue ($\gamma = a$) for $J = 150$ (solid lines) in comparison with the perturbatively calculated value (dots) along (II). In the region where the coherent part of Eqn. (4.25) is a squeezing Hamiltonian, the ADR (i.e. real part of the lowest Liouvillian eigenvalue pair) splits. At the same time the imaginary part of the lowest eigenvalue pair vanishes (black lines), indicating that the system is overdamped.

not lead to a damped oscillatory behavior, but to an exponential, oscillation-free return to the steady state.

The blue area in the vicinity of region $D$ in Fig. 4.3 does not represents a new phase but is another interesting feature of the system. Here, the ADR exceeds the value at $\Omega = 0$ by a factor of $\sim 3$. For $\Omega = 0$ the model describes the standard spin-pumping setting. Large gaps in the low excitation spectrum indicate the possibility to improve the effective spin-pumping rate (remember that also in this region the steady state is fully polarized, however, not in $-z$-direction, as is the case for the normal spin-pumping configuration $\Omega = 0$). Indeed, simulations show that starting from a fully mixed state, the system reaches the steady state faster than in the standard setting ($\Omega = 0$). This feature becomes more distinct in systems, where the electron pumping rate $\gamma$ is limited. For $\gamma = 0.1a$ the time to reach the fully polarized steady state from a fully mixed state is shortened by a factor of $\sim 6$.

### Transitions

In this Section we consider the transitions involving the RSTSS solution in greater detail providing a classification in analogy to quantum phase transitions in closed systems (compare Section 4.3).

As seen in the previous Section, certain steady-state observables show clear signatures of a first-order phase transition at $b$ (Fig. 4.2). In order to understand this sharp transition we consider the ADR exemplarily along path (I) in Fig. 4.9. The broken lines represent numeric results of exact diagonalization of the Liouvillian for $J = 50$, 100, and 150, while the solid line indicates the result of the perturbative approach. As described in Section 4.5.2, we implicitly choose the semiclassical displacement $\beta_-$ (for $\Omega < 1.5\Omega_0$) or $\beta_+$ (for $\Omega > 1.5\Omega_0$) for which the ADR is negative, indicating a stable solution. For increasing system size the ADR is increasingly

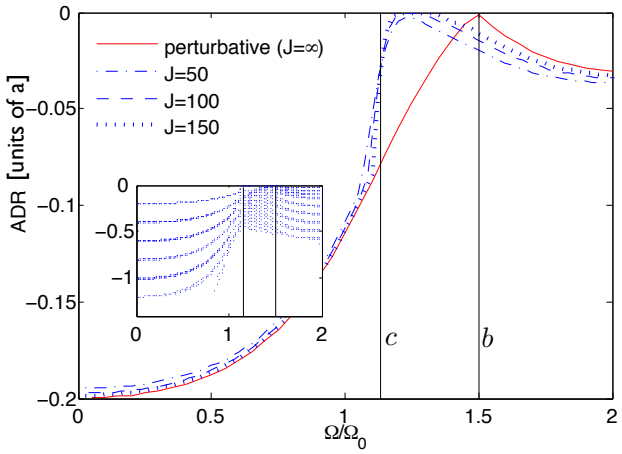


Figure 4.9: The ADR ($\gamma = a$) for $J = 50$, 100, 150 (broken lines) in comparison with the perturbatively calculated (solid line) along ①. The vertical black lines indicate the asymptotic boundaries of the region of bistability. In the whole region the ADR tends to zero in the thermodynamic limit due to the appearance of a non-gaussian stable mode. *Inset:* The next higher excitations in the spectrum for $J = 150$ display equidistant splittings in regions far from the region of bistability. This is an indication for the bosonic character of the steady state, which is exploited in the perturbative approach.

well approximated by the perturbative solution.

We stress the point that the red line represents the first Gaussian excitation energy only. However, within the region of bistability (indicated by two vertical bars and discussed below in Section 4.6), a non-Gaussian mode is responsible for additional excitations in the exact spectrum. The Gaussian mode eigenvalue (red line) in this region is reproduced approximately by higher excitations of the exact spectrum (not displayed) . The perturbative theory is still correct within the region of bistability but, as expected, it misses all non-Gaussian eigenstates of the exact Liouvillian.

At the boundary $b$ ($\Omega \approx 1.5\ \Omega_0$) the gap in the real part of the spectrum of the Liouvillian closes non-analytically, indicating critical behavior. This observation is supported by the effective temperature (and thus the fluctuations in the system), which is increased in the vicinity of the boundary $b$, and diverges at the boundary [Fig. 4.7 a) & Fig. 4.4 a)]. The vanishing of the ADR at $b$ (i.e., the vanishing due to the RSTSS solution) can be observed at finite $J$ (dashed lines in Fig. 4.9) and is not a feature appearing in the thermodynamic limit only. The position of this closing of the gap – which in the thermodynamic limit (solid line) is found at $\Omega \approx 1.5\ \Omega_0$ – is shifted for finite system sizes to lower drivings $\Omega$.

The origin of this closing of the Liouvillian gap becomes more transparent if we take the mode energy of the respective metastable solution into account.

In Fig. 4.10 a) the complex energy of both the stable and the unstable mode are displayed (i.e., the first eigenvalue of the matrix $\Sigma$ [Eqn. (4.37)]). The normal spin-pumping mode ($\beta_-$; blue lines) is stable ($\mathrm{Re}[\lambda(\beta_-)] < 0$) up to the critical point where it destabilizes and the anomalous mode appears ($\beta_+$; red lines). At the critical point the two solutions are macroscopically

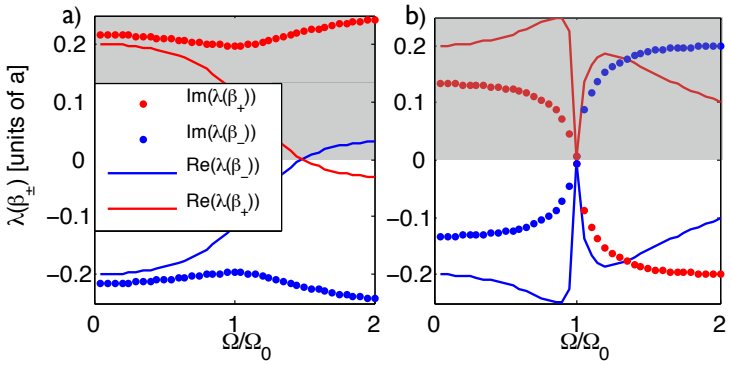


Figure 4.10: Complex energy of the two modes corresponding to the semiclassical solutions $\beta_\pm$ for $\gamma = a$. The solid line in the non-shaded area represents the ADR of Fig. 4.9 and Fig. 4.5, respectively. a) Along ① ($\omega = 1.5\ \omega_0$). The eigenvalues miss each other in the complex plane. The real parts cross directly. b) $\omega = \omega_0$. The eigenvalues degenerate asymptotically (in both real and imaginary parts) at the critical point. This closing of the gap originates from an avoided crossing in finite systems with the relevant gap vanishing in the thermodynamic limit (see also Fig. 4.5).

different $\beta_- \neq \beta_+$ and their energy (i.e., $\mathrm{Im}[\lambda(\beta_\pm)]$) is distinct across the transition [dotted lines in Fig. 4.10 a)]. Although the projection of the eigenvalues on the real axis vanishes at the critical point for both modes (indicating the stabilizing / destabilizing of the modes) the eigenvalues pass each other in the complex plane at large distance. There is no degeneracy in the spectrum of the Liouvillian at the critical point and consequently there can be no mixing of the two modes; the real parts of the eigenvalues cross *directly* without influencing each other. Except for the change in stability the modes do not change their character approaching the phase boundary and no diverging correlations (indicated by the squeezing parameter $C$) can be observed. Together with the discontinuous change in system observables such as mean polarizations we classify this Gaussian transition as of first order.

Second, we consider the transition along $\omega = \omega_0$ (including the line segment $x$). In contrast to the situation before we find that the semiclassical displacements $\beta_+$ and $\beta_-$ merge approaching the critical point such that the two modes become asymptotically identical at $\Omega_0$ [Eqn. (4.46)]. Approaching the critical point, the eigenvalues of the two modes tend to zero (both the real and the imaginary parts), causing the gap of the Liouvillian's spectrum to close [Fig. 4.10 b), Eqn. (4.54), Eqn. (4.55)]. As we have seen in Section 4.5.2 at $(\omega_0, \Omega_0)$ the spectrum becomes real and continuous, signaling criticality. The perturbative treatment intrinsically is a description in the thermodynamic limit. If we consider the exact spectrum we indeed find an avoided crossing due to the mode mixing at the critical point with a gap that is closing for $J \to \infty$ (cf. Fig. 4.5). As we discussed in Section 4.5.2 the elementary excitations become $\hat{p}$-like, causing a diverging coherence length in the system [indicated by the diverging squeezing parameter $C$ in Fig. 4.4(c,d)]. Together with the continuous but non-analytical change of the mean polarizations these properties classify the point $(\Omega_0, \omega_0)$ as a second-order transition.

## 4.6 Region of bistability: Non-Gaussian solution

As noted in Section 4.4.2 along the Gaussian boundary $b$ extends a region of bistability [$C$ in (Fig. 4.1)] – culminating in the critical point $(\Omega_0, \omega_0)$ – in which a second stable solution appears. Within the perturbative framework from Section 4.5 this highly non-Gaussian solution could not be detected because it features large fluctuations of the order of the system size $J$. In the following we use numerical techniques to construct and study this mode for finite systems. In the thermodynamic limit the ADR tends to zero within $C$, such that there exists a two-dimensional subspace of steady states. Here we find two independent, physical solutions within the kernel of the Liouvillian, one of which will turn out to be the Gaussian normal spin-pumping mode described in Section 4.5. We analyze the nature and properties of the other, non-Gaussian solution, exemplarily along the line $\omega = 1.5\,\omega_0$ (Ⓘ in Fig. 4.1).

Figure 4.9 displays the ADR for different particle numbers. Within the indicated region of bistability (the black vertical lines represent the boundaries $c$ and $b$, respectively) the ADR tends to zero with increasing particle number. Already for $J = 150$ one finds a small region, where the ADR is small enough (of the order of $10^{-6}a$) that one can construct two linearly independent (quasi) steady-state solutions. Although we find the eigenmatrix $\rho_1$ associated with the ADR to be non-positive and traceless (the latter being a consequence of $\mathcal{L}$ being the generator of a trace-preserving map) we can linearly combine it with the true steady state $\rho_0$ to obtain two linear independent, positive solutions with trace one, $\rho_{\text{lo}}$ (corresponding to the normal spin-pumping mode) and $\rho_{\text{up}}$. These solutions span the two-dimensional space of steady states in that region.

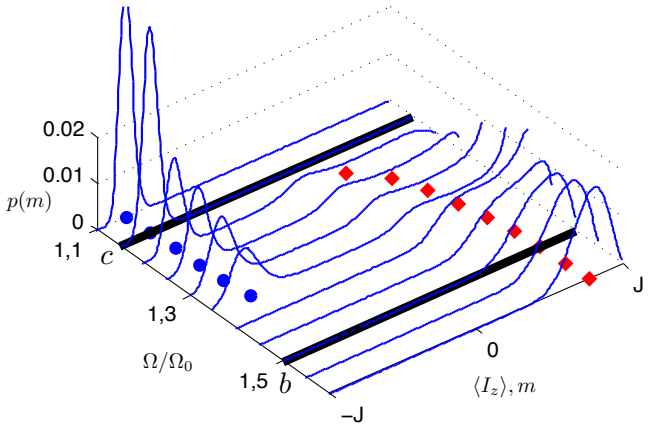


Figure 4.11: Diagonal elements $p(m) = \langle m|\,\rho\,|m\rangle$ of the nuclear density matrix in $z$-basis ($I_z\,|m\rangle = m\,|m\rangle$) across the region of bistability for $\omega = 1.5\omega_0$ ($J = 150$, $\gamma = a$). In the bistable region two stable modes – the Gaussian normal spin-pumping mode (lower branch; $\rho_{\text{lo}}$) and a non-Gaussian (upper branch; $\rho_{\text{up}}$) – coexist. At the boundary $b$ the latter transforms into the anomalous spin-pumping mode, which is the sole stable solution above $b$. The blue dots (red diamonds) in the plane indicate the average polarization in $z$-direction $\langle I_z\rangle$ for the lower (upper) solution.

Fig. 4.11 illustrates the solutions $\rho_{\text{lo}}$ and $\rho_{\text{up}}$ around the bistable region in an equally weighted

mixture. The density matrices are represented by their diagonal elements in the $I_z$ basis. In the plane the blue dots (red diamonds) represent the polarization in $z$-direction $\langle I_z \rangle$ of the lower (upper) solution $\rho_{\text{lo}}$ ($\rho_{\text{up}}$). Coming from below the critical region ($\Omega < 1.15\ \Omega_0$) the nuclear system is found in the Gaussian normal spin-pumping mode, fully polarized, slightly rotated away from the $-z$-direction and with fluctuations of the order of $\sqrt{J}$. This Gaussian solution persists within the critical region where it becomes noisier until eventually – approaching the right boundary $b$ at $\Omega = 1.5\ \Omega_0$ – it destabilizes. In the thermodynamic limit the lower solution is stable up to the right boundary, where a first-order transition occurs and the anomalous spin-pumping mode appears. Approaching boundary $b$ from above ($\Omega > 1.5\ \Omega_0$) this mode transforms into a non-Gaussian solution, which – in contrast to the coexisting normal mode – features fluctuations of the order of $J$ and is not fully polarized. It shows large electron-nuclear and nuclear-nuclear connected correlations $\langle S_i I_j \rangle - \langle S_i \rangle \langle I_j \rangle$, and can consequently not be approximated by the semiclassical solutions, which rely on negligibility of these correlations (cf. Appendix 4.A.3). Approaching the left boundary $c$ at $\Omega = 1.15\ \Omega_0$ this mode destabilizes eventually as the ADR becomes finite again and the normal mode is the only stable solution in the system.

The bistable behavior of the system in region $C$ bears close resemblance to the phenomenon of optical bistability for saturable absorbers [265], where connections to phase transitions have been established [260]. In this region the system displays strong hysteretic behavior. Recent experiments in quantum dots, realizing a setting close to our model system display distinct signatures of hysteresis upon application of an external driving field on the electronic spin [116, 249]. Our results suggest the observed optical bistability in central spin systems as a possible pathway to understand these experimental results, which will be a subject of further studies.

## 4.7 Implementations and extensions of the model

In the present Section we discuss potential physical realizations of the Master Eqn. (4.1) and address certain aspects of an extension of the model for inhomogeneous hyperfine couplings.

As mentioned above, the model we study is a generic central spin model with various potential physical implementations. The most prominent ones represent singly charged semiconductor quantum dots, where the electron spin couples to the nuclear spins of the host material [98, 51], and diamond nitrogen vacancy (NV) centers coupled to either nuclear ($^{13}C$ spins of the host material) or electron (e.g., nearby nitrogen impurities) spin ensembles [119, 137]. Recently, diamond nano-crystals containing single NV centers coated with organic molecule spin labels, which are dipole coupled to the NV center spin have been manufactured [138].

NV centers represent a natural realization of the Master Eqn. (4.1). Their ground state consists of three spin sublevels (of spin projection quantum number $m = 0, \pm 1$) featuring a zero field splitting due to anisotropic crystal fields of $2.88\,\text{GHz}$ [119]. In a static magnetic field this zero field splitting can be compensated for and one of the transitions (e.g., $m = 0 \leftrightarrow 1$) is brought into near hyperfine resonance with the ancilla spin system, defining an effective two-level system. Since the $m = 0$ level does not carry a magnetic moment, the hyperfine interaction of the effective two-level system and the ancilla system takes the anisotropic form of Eqn. (4.4). Potential counterrotating terms of the dipole-dipole interaction are neglected in the static magnetic field in a rotating wave approximation. Optical pumping of the electron

spin in the $m = 0$ spin state and resonant driving (either by optical Raman transitions or radio frequency fields) realizes Master Eqn. (4.1) [120].

In general, the hyperfine interaction in such a setting will not be homogeneous and the truncation to a symmetric subspace of total spin $J$ is not justified. In the following we consider an extension of the model taking into account the inhomogeneous nature of the hyperfine coupling in a shell model. Along $x$ we show that up to the critical point steady states can be constructed analytically as electron-nuclear product states involving nuclear eigenstates of the (inhomogeneous) lowering operator. In analogy to the homogeneous case, such solutions cease to exist after the critical point at which we find diverging nuclear squeezing. These results are supported by numerical simulations that confirm the analytical considerations and provide further indications that other features of the phase diagram aside from the second-order transition can be found in the inhomogeneous model.

In order to take into account inhomogeneities in the hyperfine coupling, we replace the homogeneous spin operators of Eqn. (4.4) with inhomogeneous operators $I_\alpha \to A_\alpha$ ($\alpha = x, y, z$). We approximate the actual distribution of coupling strengths by $n$ shells of spins with identical coupling

$$A_\alpha = \sum_{i=1}^{n} g_i A_\alpha^{(i)}, \tag{4.61}$$

where $A_\alpha^{(i)}$ represent homogeneous spin operators within the $i$th shell. Each homogeneous shell is assumed to be in a symmetric subspace $J_i$.

In analogy to the homogeneous case we can construct approximate eigenstates of the lowering operator $A^- |\alpha\rangle = \alpha |\alpha\rangle$. To this end we perform a Holstein-Primakoff transformation on the homogeneous spin operators within each shell and displace the respective bosonic mode $b_i$ by $\beta_i$ and expand the resulting operators in orders of $1/\sqrt{J_i}$. As we demonstrate in Appendix 4.A.2 the choice of a particular displacement $\beta_i$ uniquely defines the squeezing of the respective mode $b_i$ if we demand that the corresponding state is an $A^-$ eigenstate to second order in the expansion parameters, i.e., of order $\mathcal{O}(\sum_i 1/J_i)$. The corresponding eigenvalue is then given as $\alpha = \sum_{i=1}^{n} g_i \sqrt{k_i} \beta_i$ ($k_i = 2 - |\beta_i|^2$). As discussed in Section 4.4.2, $|\psi\rangle = |\downarrow\rangle \otimes |\alpha\rangle$ is a steady state of the evolution to second order, if $\alpha = \sum_i g_i \sqrt{k_i} \beta_i = -J\Omega/\Omega_0$. In contrast to the homogeneous case ($n = 1$) the latter condition does not determine the steady state uniquely. Several sets of displacements within the different shells can fulfill the steady-state condition. However, all these microscopic realizations lead to the same macroscopic behavior of the system such as the locking of the electron inversion $\langle S_z \rangle = 0$. Furthermore, at the critical point, the solution is unique again ($\beta_i = 1$ for all shells) and the considerations on entanglement of Appendix 4.A.2 can be straightforwardly generalized to the inhomogeneous case with the result that also here at the critical point the entanglement in the system diverges, indicating a second-order phase transition. Obviously, above the critical point no such solution can be constructed and the system observables change non-analytically.

Figure 4.6 shows numerical results which confirm the above considerations. We find numerically the exact steady-state solution for a model of two inhomogeneously coupled shells ($g_1 = 2g_2$) of size $J_{1,2} = 8$ (broken lines), as well as for a system of five nuclear spins with coupling strengths ($\{g_i\}_{i=1\ldots5} = \{0.67, 0.79, 0.94, 1.15, 1.4\}$, dotted lines). For low driving strengths $\Omega$ we find the Overhauser field building up linearly, as expected. The emergence of the thermodynamic phase transitions can be anticipated already for these low particle numbers.

These analytical and numerical arguments for the emergence of a second order phase transition in the inhomogeneous case, suggest the possibility to find other features of the homogeneous phase diagram also in inhomogeneous systems, such as NV centers in diamond.

Another attractive realization of a central spin system is provided by singly charged semiconductor quantum dots: Up to several $10^4$ nuclear spins are coupled to a central spin-1/2 electron, driving and spin pumping of the electronic state have been demonstrated experimentally with high efficiency [266, 101]. In this setting, however, the inhomogeneity of the hyperfine coupling and the absence of an $m = 0$ central spin state lead to a situation in which the effective nuclear Zeeman term $H_I$ in Eq. (4.1) becomes inhomogeneous [it is composed of the Knight field, the nuclear Zeeman energy, and the (homogeneous) detuning] and does not vanish for any choice of parameters. Therefore, the above argument for a persistence of the second-order phase transition does not apply. However, critical phenomena similar to the ones described above were observed in optically driven quantum dots [116]. The adaptation of our model to this and other more general settings is subject to future studies.

## 4.8 Conclusions

In analogy to closed systems where critical phenomena arise from non-analyticities of the Hamiltonian low-energy spectrum, in open systems critical phenomena are intimately related to the low excitation spectrum of the Liouville operator. We investigated a generic driven and damped central spin model and its rich steady-state behavior, including critical effects such as bistabilities, first- and second-order phase transitions, and altered spin-pumping dynamics. We developed a two-step perturbative theory involving the expansion of nuclear fluctuations up to second order in a self-consistent Holstein-Primakoff transformation and the subsequent adiabatic elimination of the electron degrees of freedom in the vicinity of the steady state, which enabled us to provide a complete picture of the system's phase diagram. Linking common ideas from closed-system phase transitions to the dissipative scenario, we were able to introduce a classification of the different transitions in the phase diagram.

The relevance of the considered model involves two aspects. On the one hand, Eqn. (4.1) describes a simple yet rich model, which displays a large variety of critical phenomena. The limitation to symmetric states allows for an efficient (and in the thermodynamic limit exact) perturbative treatment that gives deep insights into the nature of dissipative critical phenomena from a fundamental point of view. On the other hand, the central spin model is general enough to have realizations in a large variety of physical systems (e.g., QDs, NV centers). Our understanding of the critical phenomena in this model could provide insight into recent observation of critical behavior in related systems [116, 249]. Furthermore the main features of the phase diagram discussed above can also be found if the central (two-level) spin is replaced by a different physical system, e.g., a larger spin or a bosonic mode. The theory developed in Section 4.5 can straightforwardly be adapted to different scenarios and opens the possibility to study dissipative critical effects in a variety of different physical systems [78].

Finally, we showed that in a more realistic adaptation of the model incorporating an inhomogeneous hyperfine coupling, the second-order phase transition persists, indicating the possibility that the phase diagram remains qualitatively correct in this experimentally more realistic case. A more thorough analysis of the effects of inhomogeneities is subject to future work.

## 4.A Supplementary material 4

### 4.A.1 Phase diagram for alternative dissipation strengths $\gamma$

In the main text of this article we discussed the steady-state phase diagram of the Master Eqn. (4.1) exemplarily in the case $\gamma = a$. However, we stress the point that the features we describe do not depend critically on this particular value, but rather prevail qualitatively for all dissipation strengths of this order of magnitude. Most importantly, we noted before the interesting phenomena that all considerations concerning the segment $x$, including the second-order phase transition at $(\omega_0, \Omega_0)$ are entirely independent of the value of $\gamma$. In the following we briefly discuss the remaining regions of the phase diagram by means of two examples of a lower ($\gamma = 0.2a$) and higher ($\gamma = 5a$) dissipation strength.

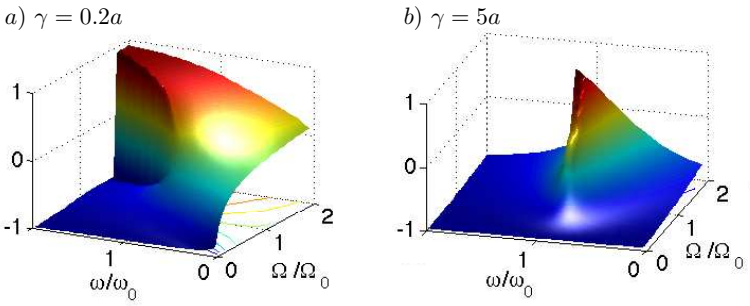


Figure 4.12: (a) The nuclear polarization in $z$-direction $\langle I_z/J\rangle_{ss}$ of the RSTSS solution in the thermodynamic limit for a) $\gamma = 0.2a$ and b) $\gamma = 5a$. In the first case [a)] the phase diagram bears strong resemblance with the case $\gamma = a$ (compare Fig. 4.29. In the case of large dissipation [b)] the first-order boundary is rotated clockwise toward the line $(\omega_0, \Omega > \Omega_0)$ and the distinction of the phases according to their nuclear polarization in $z$-direction becomes less prominent. Instead, other criteria like the polarization in $y$-direction (not displayed) emerge.

The case of low dissipation ($\gamma = 0.2a$) bears strong resemblance to the case we discussed in the main text ($\gamma = a$), which is shown exemplarily in Fig. 4.12 a) for the nuclear steady-state polarization in $z$-direction $\langle I_z/J\rangle_{ss}$ [compare Fig. 4.2 a)]. The first-order boundary is only slightly shifted toward lower driving strength $\Omega$, and all the other features prevail qualitatively. One finds a region of bistability, as well as a high and low-temperature phase (not displayed). However, one finds that with decreasing dissipation strength the steady state becomes increasingly noisy.

The situation for higher dissipation is slightly different. First, we note that as the dissipation is increased the first-order boundary is rotated clockwise until in the limit $\gamma \gg a$ [where the electron can be trivially adiabatically eliminated; compare Eqn. (4.5)] it coincides with the line $(\omega_0, \Omega > \Omega_0)$. This behavior can already be seen for $\gamma = 5a$ in Fig. 4.12 b), which displays the nuclear steady-state polarization in $z$-direction. Interestingly, with increasing dissipation, the system's steady state becomes more pure and the region of bistability shrinks in size. At the same time, the distinction in a high and low-temperature phase becomes less clear. However, a second criterion characterizing the phases emerges in the form of the nuclear polarization in $y$-direction. In phase $A$ ($B$) the system is highly polarized in $-y$-direction ($y$-direction). A more detailed analysis of this regime with the tools we have developed is an interesting subject

for future studies.

### 4.A.2 Approximate eigenstates of the lowering operator

#### Homogeneous case

In Section 4.4.2 we have seen that we can construct the exact steady state along segment $x$ if we assume the nuclear system to be in an eigenstate of the spin lowering operator $I^- |\alpha\rangle = \alpha |\alpha\rangle$. Although it readily can be shown that this operator exactly features only the eigenvalue $\alpha = 0$, we can construct approximate eigenvalues in an expansion in $1/J$.

We stress the point that in the bosonic analoge eigenstates of the annihilation operator are coherent minimum uncertainty states that display no squeezing. As we will see, the eigenvectors of the atomic lowering operator in contrast are squeezed coherent atomic states (on the southern hemisphere of the Bloch sphere), where the squeezing parameter depends uniquely on the rotation angle of the Bloch vector.

As noted in Section 4.5 the Holstein-Primakoff transformation [Eqn. (4.7)] provides an exact mapping between spin operators and a bosonic operator in the subspace of total spin quantum number $J$. In the following we show that approximate eigenstates of the lowering operator $I^-$ can be expressed as a squeezed and displaced vacuum of the bosonic mode $b$

$$D(\beta)S(-r(\beta))\,|0\rangle =: |\beta\rangle\,, \tag{4.62}$$

where $D(\beta) = e^{\sqrt{J}\beta b^\dagger - \sqrt{J}\beta^* b}$ and $S(r) = e^{(r^* b^2 - r b^{\dagger 2})/2}$ are the displacement and squeezing operators, respectively and $|0\rangle \equiv |J - J\rangle$ the fully polarized nuclear state. We find the squeezing parameter uniquely defined by the displacement $r = r(\beta)$.

Without loss of generality we assume $\beta \in \mathbb{R}$ (and thus $r \in \mathbb{R}$), i.e., the Bloch vector lies in the $x - z$ plane. General states $\beta \in \mathbb{C}$ with arbitrary Bloch vectors on the southern hemisphere, can straightforwardly be derived by a rotation around the $z$-axis. Note that the corresponding states on the northern hemisphere can be constructed accordingly as eigenstates of the ascending operator $I^+$.

In order to show that Eqn. (4.62) defines an approximate eigenstate of $I^-$ we first consider the transformation of the nuclear operator under the displacement and squeezing operator. Recall that according to Eqn. (4.9) the displaced nuclear operators can be expanded in orders of $\epsilon = 1/\sqrt{J}$

$$\begin{aligned} &D^\dagger(\beta) I^- D(\beta) \\ &\quad = \sqrt{2J - (b^\dagger + \sqrt{J}\beta^*)(b + \sqrt{J}\beta)}\,\Big(b + \sqrt{J}\beta\Big) \\ &\quad = J\mathcal{J}_0^- + \sqrt{J}\mathcal{J}_1^- + \mathcal{O}(1), \end{aligned} \tag{4.63}$$

where

$$\mathcal{J}_0^- = \sqrt{k}\beta, \tag{4.64}$$

$$\begin{aligned} \mathcal{J}_1^- &= \sqrt{2(1-\beta^2)}(\mu b + \nu b^\dagger) \\ &= \sqrt{2(1-\beta^2)} S^\dagger(r) b S(r), \end{aligned} \tag{4.65}$$

and $\cosh(r) = \mu = \frac{2k-\beta^2}{2\sqrt{2k(1-\beta^2)}}$ and $\sinh(r) = -\nu = \frac{\beta^2}{2\sqrt{2k(1-\beta^2)}}$, which defines $r = r(\beta)$ (the generalization to complex $\beta$ is straightforward and leads to Eqn. (4.44)). Thus it follows

$$\begin{aligned} S^\dagger(-r)D^\dagger(\beta)I^- D(\beta)S(-r)\,|0\rangle \\ = J\mathcal{J}_0^-\,|0\rangle + \mathcal{O}(1), \end{aligned} \tag{4.66}$$

since $b\,|0\rangle = 0$.

Multiplying both sides by $D(\beta)S(-r)$ yields the desired approximate eigenvalue equation

$$I^-\,|\beta\rangle = J\sqrt{k}\beta\,|\beta\rangle + \mathcal{O}(1). \tag{4.67}$$

In the thermodynamic limit the term $\mathcal{O}(1)$ is negligible and the eigenvalue equation is exact[6].

Using the above representation we study the spin properties of the states $|\alpha\rangle$. In the following all expectation values are understood to be evaluated in the squeezed coherent state $|\beta\rangle$: $\langle O\rangle \equiv \langle\beta|\,O\,|\beta\rangle$.

Straightforwardly, one derives the nuclear mean polarizations

$$\langle I_x\rangle = \frac{1}{2}\langle\beta|\,(I^+ + I^-)\,|\beta\rangle = J\sqrt{k}\beta + \mathcal{O}(1), \tag{4.68}$$

$$\langle I_y\rangle = \frac{1}{2i}\langle\beta|\,(I^+ - I^-)\,|\beta\rangle = 0 + \mathcal{O}(1), \tag{4.69}$$

$$\langle I_z\rangle = J(\beta^2 - 1) + \mathcal{O}(1), \tag{4.70}$$

where in the last equation we used the expansion Eqn. (4.14). Note that the Bloch vector is orthogonal (up to order $\mathcal{O}(1)$) to the $y$-direction for all (real) $\alpha$ and of length $|\langle\vec{I}\rangle| = \sqrt{\langle I_x\rangle^2 + \langle I_y\rangle^2 + \langle I_z\rangle^2} = J + \mathcal{O}(1)$.

Using Eqn. (4.67) and the angular momentum commutation relations one readily calculates

$$\begin{aligned} \langle\Delta I_y^2\rangle &= -\frac{1}{2}\langle I_z\rangle + \mathcal{O}(1), \\ &= \frac{1}{2}J(1-\beta^2) + \mathcal{O}(1), \\ &= \frac{1}{2}J\sqrt{1-(\sqrt{k}\beta)^2} + \mathcal{O}(1) \end{aligned} \tag{4.71}$$

where as usual $\langle\Delta O^2\rangle := \langle O^2\rangle - \langle O\rangle^2$ and we used the identity $1-(\sqrt{k}\beta)^2 = (1-\beta^2)^2$.

Thus, we find for the squeezing parameter in $y$-direction,

$$\xi_y^2 = 2\langle\Delta I_y^2\rangle/|\langle\vec{I}\rangle| = \sqrt{1-(\sqrt{k}\beta)^2} + \mathcal{O}(1/J). \tag{4.72}$$

The squeezing diverges for the state that realizes the maximal eigenvalue of the lowering operator ($\sqrt{k}\beta = 1$). This corresponds to a state fully polarized in $x$ direction.

[6] This is true even for $\beta \to 0$ since all terms in the expansion Eqn. (4.63) that do not vanish upon application on $|0\rangle$ contain at least one factor $\beta$ as well.

### Inhomogeneous case

We approximate a system of inhomogeneous hyperfine coupling by grouping the nuclear spins into $n$ shells. Within a shell $i$ the nuclear spins have identical coupling $g_i$ and the respective (homogeneous) spin operators $A_\alpha^{(i)}$ ($\alpha = x, y, z$) are truncated to a symmetric subspace $J_i$. The total spin operators can then be written as

$$A_\alpha = \sum_{i=1}^{n} g_i A_\alpha^{(i)}. \tag{4.73}$$

We define collective displacement and squeezing operators

$$\mathcal{D} = \Pi_{i=1}^{n} e^{\sqrt{J}_i \beta_i b_i^\dagger - \sqrt{J}_i \beta_i^* b_i}, \tag{4.74}$$

$$\mathcal{S} = \Pi_{i=1}^{n} e^{(r_i^* b_i^2 - r_i b_i^{\dagger 2})/2}, \tag{4.75}$$

where the $b_i$ is the respective bosonic operator for shell $i$. Also here the squeezing parameter $r_i$ depends uniquely (with the same functional dependence as before; cf. Eqn. (4.65)) on the displacement $\beta_i$ within the shell, if we demand the first order in the eigenvalue equation to vanish,

$$A^- \mathcal{D}\mathcal{S} \left|0\right\rangle = (\sum_i J_i \sqrt{k_i} \beta_i) \mathcal{D}\mathcal{S} \left|0\right\rangle + \mathcal{O}(1), \tag{4.76}$$

where $k_i = \sqrt{2 - \beta_i^2}$ and $\left|0\right\rangle \equiv \left|0\right\rangle^{\otimes n}$ is the vacuum of the shell modes.

We emphasize that, in general, the eigenvalues are highly degenerate. For a given eigenvalue $\alpha$ there are infinitely many microscopic realizations (i.e. sets of $\beta_i$) that fulfill $\alpha = \sum_i J_i \sqrt{k_i} \beta_i$. Only the maximal eigenvalue $\alpha = J$ features a unique steady state that displays diverging squeezing as one readily shows analogous to the homogeneous case.

### Rotated squeezed thermal spin states

A key concept are RSTSSs, a generalization of squeezed coherent spin states to mixed states, parametrized via an effective temperature. They describe nuclear states which are fully polarized and rotated and feature fluctuations which can be described by a bosonic mode in a thermal (potentially squeezed) Gaussian state. In Section 4.5.1 we show that the truncation of every nuclear operator to a subspace of total spin $J$ can be expressed in terms of a bosonic mode $b$ and its displacement $\beta \in \mathbb{C}$, using a Holstein-Primakoff transformation [compare Eqn. (4.9), Eqn. (4.13)]

$$I^\alpha / J = \sum_n \epsilon^n \mathcal{J}_n^\alpha, \tag{4.77}$$

where $\epsilon = 1/\sqrt{J}$, and the bosonic operators $\mathcal{J}_n^\alpha$ contain combinations of products of $n$ bosonic operators $b, b^\dagger$. $\mathcal{J}_0^\alpha \in \mathbb{C}$, describes the semiclassical expectation value which is fully determined by the displacement $\beta$. $\beta$ quantifies a rotation of the fully polarized nuclear state on the Bloch sphere. The higher order operators $\mathcal{J}_n^\alpha$ ($n > 0$) describe quantum fluctuations around this semiclassical nuclear state. RSTSSs are those states where the mode $b$ is in an undisplaced

($\langle b\rangle = 0$), squeezed thermal state, which is fully determined by its CM $\Gamma$ [Eqn. (4.41)]. These bosonic states constitute the natural steady states of the quadratic Master Eqn. (4.25), and we find in Section 4.5.2 that across the whole phase diagram one steady state of the system can always be described as a RSTSS.

Note that in the limit where the effective temperature of the Gaussian state is zero, we recover the class of squeezed coherent spin states [254], which constitute the solution along segment $x$.

### 4.A.3 Solving Eqn. (4.24)

In order to find the solutions to Eqn. (4.24) (which are numerically difficult to find) we first note that

$$\langle A\rangle_{ss} = 0 \Leftrightarrow \langle \dot{b}\rangle = \langle \dot{b^\dagger}\rangle = 0 \Leftrightarrow \langle \dot{\mathcal{J}_1^-}\rangle = \langle \dot{\mathcal{J}_1^+}\rangle = 0, \tag{4.78}$$

where the time derivative is understood with respect to the first-order Liouvillian

$$\mathcal{L}_1\rho = -i[a(S_x\mathcal{J}_1^x + S_y\mathcal{J}_1^y) + (aS^+S^- + \delta\omega)\mathcal{J}_1^z, \rho], \tag{4.79}$$

and in the usual way we define

$$\mathcal{J}_1^x = \frac{1}{2}(\mathcal{J}_1^+ + \mathcal{J}_1^-), \tag{4.80}$$

$$\mathcal{J}_1^y = \frac{1}{2i}(\mathcal{J}_1^+ - \mathcal{J}_1^-). \tag{4.81}$$

Using the relation $\left[J_1^i, J_1^j\right] = i\epsilon_{ijk}J_0^k$ one finds the equations

$$0 = \langle \dot{\mathcal{J}_1^x}\rangle = a\left(\langle S_y\rangle_{ss}\mathcal{J}_0^z - \langle S_z\rangle_{ss}\mathcal{J}_0^y\right) - \omega\mathcal{J}_0^y, \tag{4.82}$$

$$0 = \langle \dot{\mathcal{J}_1^y}\rangle = -a\left(\langle S_x\rangle_{ss}\mathcal{J}_0^z - \langle S_z\rangle_{ss}\mathcal{J}_0^x\right) + \omega\mathcal{J}_0^x, \tag{4.83}$$

$$0 = \langle \dot{\mathcal{J}_1^z}\rangle = a\left(\langle S_y\rangle_{ss}\mathcal{J}_0^x - \langle S_x\rangle_{ss}\mathcal{J}_0^y\right). \tag{4.84}$$

Furthermore, from the definitions of the $\mathcal{J}_0^i$'s one finds

$$1 = (\mathcal{J}_0^x)^2 + (\mathcal{J}_0^y)^2 + (\mathcal{J}_0^z)^2. \tag{4.85}$$

The steady-state expectation values $\langle S_i\rangle_{ss}$ are found directly via [cf. Eqn. (4.18)]

$$\begin{aligned}\mathcal{L}_0\rho =& \gamma(S^-\rho S^+ - \frac{1}{2}\{S^+S^-, \rho\}_+) \\ &- i[S_x(2\Omega + a\mathcal{J}_0^x) + aS_y\mathcal{J}_0^y + aS^+S^-\mathcal{J}_0^z, \rho],\end{aligned} \tag{4.86}$$

by solving the resulting optical Bloch equations,

$$0 = -\frac{\gamma}{2}\langle S_x\rangle + a\mathcal{J}_0^y\langle S_z\rangle - a\mathcal{J}_0^z\langle S_y\rangle, \tag{4.87}$$

$$0 = -\frac{\gamma}{2}\langle S_y\rangle - (2\Omega + a\mathcal{J}_0^x)\langle S_z\rangle + a\mathcal{J}_0^z\langle S_x\rangle, \tag{4.88}$$

$$0 = -\gamma(\langle S_z\rangle + 1/2) + (2\Omega + a\mathcal{J}_0^x)\langle S_y\rangle - a\mathcal{J}_0^y\langle S_x\rangle. \tag{4.89}$$

This set of coupled equations for the six variables $\{\langle S_i\rangle, \mathcal{J}_0^j\}$ can be solved analytically and corresponds to the semiclassical Bloch equations (derived from a brute force factorization: $\langle S_i I_j\rangle \to \langle S_i\rangle\langle I_j\rangle$, for $i,j = x,y,z$ in the equations of motion). The solutions which feature second-order stability (see Section 4.5.2) are displayed in Fig. 4.2. Via Eqn. (4.10) and Eqn. (4.14) $\beta$ can be deduced unambiguously from a given set $\{\langle S_i\rangle, \mathcal{J}_0^j\}$.

### 4.A.4 Deriving the second-order term of Eqn. (4.20)

The first term of the second order of Eqn. (4.20) is of the same form as the first order and can readily be calculated:

$$\begin{aligned} Tr_S(P\mathcal{L}_2 P\rho) &= -i[a/2(\langle S^+\rangle_{ss}\mathcal{J}_2^- + \langle S^-\rangle_{ss}\mathcal{J}_2^+) \\ &\quad + (a\langle S^+S^-\rangle_{ss} + \delta\omega)\mathcal{J}_2^z, \sigma], \\ &= -i[B^* b^2 + B(b^\dagger)^2 + F b^\dagger b, \sigma], \end{aligned} \tag{4.90}$$

with the $\beta$-dependent coefficients (remember that also the electron steady-state expectation values are functions of $\beta$)

$$B = -\frac{a\beta}{16\sqrt{k^3}}\left[(4k+|\beta|^2)\langle S^-\rangle_{ss} + \beta^2\langle S^+\rangle_{ss}\right], \tag{4.91}$$

$$\begin{aligned} F = &-\frac{a}{8\sqrt{k^3}}(4k+|\beta|^2)\left(\beta\langle S^+\rangle_{ss} + \beta^*\langle S^-\rangle_{ss}\right) \\ &+ a(\langle S^+S^-\rangle_{ss} + \delta\omega/a). \end{aligned} \tag{4.92}$$

Next, we consider the second term of the second-order perturbative master equation

$$\begin{aligned} &-Tr_s(P\mathcal{L}_1 Q\mathcal{L}_0^{-1} Q\mathcal{L}_1 P\rho) \\ &\quad = -Tr_s(P\mathcal{L}_1(\mathbb{1}-P)\mathcal{L}_0^{-1}(\mathbb{1}-P)\mathcal{L}_1 P\rho) \\ &\quad = \int_0^\infty d\tau Tr_s(P\mathcal{L}_1 e^{\mathcal{L}_0\tau}\mathcal{L}_1 P\rho) \\ &\qquad - \int_0^\infty d\tau Tr_s(P\mathcal{L}_1 P\mathcal{L}_1 P\rho), \end{aligned} \tag{4.93}$$

where we used the Laplace transform $-\mathcal{L}_0^{-1} = \int_0^\infty d\tau e^{\mathcal{L}_0\tau}$ and the property $e^{\mathcal{L}_0\tau}P = Pe^{\mathcal{L}_0\tau} = P$.

Noting that

$$Tr_s(P\mathcal{L}_1 X) = -iTr_s(\Big[bA + b^\dagger A^\dagger, X\Big]), \tag{4.94}$$

and using Eqn. (4.22) we find

$$\begin{aligned} &-\int_0^\infty d\tau Tr_s(P\mathcal{L}_1 P\mathcal{L}_1 P\rho) \\ &\qquad = \int_0^\infty d\tau\langle A^\alpha\rangle_{ss}\langle A^\beta\rangle_{ss}\left[b^\alpha, \left[b^\beta, \sigma\right]\right], \end{aligned} \tag{4.95}$$

where $\alpha,\beta = \dagger, '\text{void}'$, and the Einstein sum convention is used.

In the same fashion we find

$$\begin{aligned}&\int_0^\infty d\tau Tr_s(P\mathcal{L}_1 e^{\mathcal{L}_0\tau}\mathcal{L}_1 P\rho) \\ &= -\int_0^\infty d\tau\langle A^\alpha(\tau)A^\beta(0)\rangle_{ss}\left[b^\alpha,\left[b^\beta,\sigma\right]\right] \\ &\quad -\int_0^\infty d\tau\langle\left[A^\alpha(\tau),A^\beta(0)\right]\rangle_{ss}\left[b^\alpha,\sigma b^\beta\right].\end{aligned} \tag{4.96}$$

Here we defined the autocorrelation functions $\langle A^\alpha(\tau)A^\beta(0)\rangle_{ss} = Tr_s(A^\alpha e^{\mathcal{L}_0\tau}A^\beta\rho_{ss})$ and $\langle\left[A^\alpha(\tau),A^\beta(0)\right]\rangle_{ss} = Tr_s(A^\alpha e^{\mathcal{L}_0\tau}\left[A^\beta,\rho_{ss}\right])$ (cf. e.g., [225], pp. 22).

Putting together the results Eqn. (4.93) reduces to

$$\begin{aligned}&-Tr_s(P\mathcal{L}_1\mathcal{Q}\mathcal{L}_0^{-1}\mathcal{Q}\mathcal{L}_1 P\rho) \\ &= -\int_0^\infty d\tau\langle\Delta A^\alpha(\tau)\Delta A^\beta(0)\rangle_{ss}\left[b^\alpha,\left[b^\beta,\sigma\right]\right] \\ &\quad -\int_0^\infty d\tau\langle\left[\Delta A^\alpha(\tau),\Delta A^\beta(0)\right]\rangle_{ss}\left[b^\alpha,\sigma b^\beta\right],\end{aligned} \tag{4.97}$$

$\Delta O := O - \langle O\rangle_{ss}$. Since we choose the displacement $\beta$ such that $\langle A^\alpha\rangle_{ss} = 0$ [Eqn. (4.24)] it is $\Delta A^\alpha = A^\alpha$. Merging Eqn. (4.90) and Eqn. (4.97), and regrouping the terms, one readily derives equation Eqn. (4.25).

### Calculation of the coefficients

In order to determine the coefficients Eqn. (4.28) we have to calculate terms of the kind $\int_0^\infty d\tau\langle\Delta A^\alpha(\tau)\Delta A^\beta(0)\rangle_{ss}$ and $\int_0^\infty d\tau\langle\Delta A^\alpha(0)\Delta A^\beta(\tau)\rangle_{ss}$. Exemplarily, we calculate the two terms for $\alpha = \beta = \prime\text{void}\prime$.

First, defining $\vec{v} = (\frac{a}{4\sqrt{k}}(2k-|\beta|^2), -\frac{a}{4\sqrt{k}}\beta^2, \beta a)^T$ we can write $\Delta A = \vec{v}^* \cdot \Delta\vec{S}$ (and with $\vec{w} = (-\frac{a}{4\sqrt{k}}(\beta^*)^2, \frac{a}{4\sqrt{k}}(2k-|\beta|^2), \beta^* a)^T$ we find $\Delta A^\dagger = \vec{w}^* \cdot \Delta\vec{S}$ ). Likewise it is $\Delta A^\dagger = \Delta\vec{S}^\dagger \cdot \vec{v}$ ($\Delta A = \Delta\vec{S}^\dagger \cdot \vec{w}$).

Consequently we compute

$$\begin{aligned}&\int_0^\infty d\tau\langle\Delta A_\tau \Delta A\rangle_{ss} \\ &= \vec{v}^*\left(\int_0^\infty d\tau\langle\Delta\vec{S}_\tau\Delta\vec{S}^\dagger\rangle_{ss}\right)\vec{w} \\ &= \vec{v}^*\left(\int_0^\infty d\tau e^{\mathcal{M}\tau}\langle\Delta\vec{S}\Delta\vec{S}^\dagger\rangle_{ss}\right)\vec{w} \\ &= \vec{v}^*\left(-\mathcal{M}^{-1}\langle\Delta\vec{S}\Delta\vec{S}^\dagger\rangle_{ss}\right)\vec{w} = \vec{v}^*\mathcal{F}_1\vec{w},\end{aligned} \tag{4.98}$$

where we applied the Quantum Regression Theorem in the second step and used the definitions of Section (4.5.1).

Noting that

$$\begin{aligned}\int_0^\infty d\tau \langle \Delta\vec{S}\Delta\vec{S}_\tau^\dagger\rangle_{ss} &= \left(\int_0^\infty d\tau \langle \Delta\vec{S}_\tau\Delta\vec{S}^\dagger\rangle_{ss}\right)^\dagger \\ &= \left(-\mathcal{M}^{-1}\langle \Delta\vec{S}\Delta\vec{S}^\dagger\rangle_{ss}\right)^\dagger \\ &= -\langle \Delta\vec{S}\Delta\vec{S}^\dagger\rangle_{ss}\mathcal{M}^{-\dagger} = \mathcal{F}_2 = \mathcal{F}_1^\dagger,\end{aligned} \tag{4.99}$$

we write

$$\int_0^\infty d\tau \langle \Delta A\Delta A_\tau\rangle_{ss} = \vec{v}^*\mathcal{F}_2\vec{w}. \tag{4.100}$$

Analogously, we find the relations

$$\begin{aligned}\int_0^\infty d\tau \langle \Delta A_\tau^\dagger\Delta A\rangle_{ss} &= \vec{w}^*\mathcal{F}_1\vec{w}, \\ \int_0^\infty d\tau \langle \Delta A^\dagger\Delta A_\tau\rangle_{ss} &= \vec{w}^*\mathcal{F}_2\vec{w}, \\ \int_0^\infty d\tau \langle \Delta A_\tau\Delta A^\dagger\rangle_{ss} &= \vec{v}^*\mathcal{F}_1\vec{v}, \\ \int_0^\infty d\tau \langle \Delta A\Delta A_\tau^\dagger\rangle_{ss} &= \vec{v}^*\mathcal{F}_2\vec{v}, \\ &\vdots\end{aligned} \tag{4.101}$$

such that all coefficients of the effective Master Eqn. (4.20) can be calculated by simple matrix multiplication.

# Chapter 5

# Generalized Schrieffer-Wolff Formalism for Dissipative Systems

**The adiabatic elimination of fast-evolving degrees of freedom is a technique of vital importance and routinely applied in quantum optics. However, in contrast to the the situation for Hamiltonian systems, for open systems formalized approaches a not far developed, and the success of such a perturbative treatment relies to a great deal on physical intuition [267]. In this Chapter we aim to fill this theoretical gap: We present a formalized perturbation theory for Markovian master equations in the language of a generalized Schrieffer-Wolff (SW) transformation. A non-unitary rotation decouples the unperturbed steady states from all fast degrees of freedom, in order to obtain an effective Liouvillian, that reproduces the exact low excitation spectrum of the system. The transformation is derived in a constructive way, yielding a perturbative expansion of the effective Liouville operator. The presented formalism realizes an adiabatic elimination of fast degrees of freedom to arbitrary order. We exemplarily employ the SW formalism to two generic open systems and discuss general properties of the different orders of the perturbation. Furthermore, this theoretical tool enabled the derivation of several analytical results in Chapters 3 and 4. This Chapter is based on Publication 2 [GSW].**

## 5.1 Introduction

After more than a century of intensive research, many-body physics is an increasingly thriving field describing most of the phenomena appearing in nature. Its goal is to understand the macroscopic properties of large collections of interacting particles (typically of the order of $10^{23}$) from their microscopic laws of motion. In typical situations the dynamics of the ensemble is governed by a Hamiltonian $H$ whose complexity and vast dimension impedes a direct solution. However, many complex quantum phenomena can be understood solely from the low-energy spectrum of $H$, such as quantum phase transitions, topological insulation, and superconductivity, just to name a few. Therefore a common strategy of many-body physics is the derivation of a perturbative effective Hamiltonian $H_{\text{eff}}$, which approximates the low-energy spectrum of $H$ and reduces the complexity of the problem by integrating out the high-energy degrees of freedom. One of the most prominent examples of the success of this approach is the

connection between the Kondo model and the low-excitation spectrum of the Anderson model, which was established in 1966 [140]. It was achieved by a formalized version of (quasi-) degenerate perturbation theory [165, 164, 268], which is nowadays known as *Schrieffer-Wolff* (SW) *transformation* and which paved the way for a deep understanding of these two distinguished models of condensed-matter theory [269]. The many analytical and numerical applications of this perturbative tool in contemporary physics are far too numerous to list here exhaustively (e.g., [270, 271, 272, 273, 274]).

Due to the inevitable coupling of a quantum system to its environment, a paradigm shift could be observed in quantum physics in recent years, as the description of open systems moved into the focus of the field. Many seminal works in the context of, e.g., metrology in the presence of noise [275, 276], dissipative quantum phase transitions [78, 277], as well as dissipation-assisted quantum state preparation and quantum computation [23, 32, 54], appeared over the past years. The situation for open systems in many respects parallels the considerations above. For Markovian environments in the Born-Markov regime, the system dynamics are described by a non-Hermitian Liouville operator $\mathcal{L}$. In many cases one is interested only in the low-excitation spectrum of $\mathcal{L}$, which describes the steady-state behavior of the system and comprises in many situations the relevant dynamics, since higher excitations are typically negligibly occupied during the system's evolution. One prominent example constitutes the emerging field of dissipative phase transitions, which is intimately related to the low-excitation spectrum of the Liouvillian, as we have seen n the previous Chapter 4 [79, 80, 77]. Also the widespread method of adiabatic elimination of fast-evolving degrees of freedom – routinely employed in the field of quantum optics – corresponds to the derivation of a perturbative effective Liouvillian describing the low excitation dynamics of a system. In [278] various methods for the elimination of fast degrees of freedom from linear and non-linear differential equations are reviewed and classified from a mathematical point of view. In particular, adiabatic elimination in linear differential equations is considered with regard to dissipative systems and the (typically tedious) approaches to derive higher order corrections are discussed. More formalized perturbative tools that accomplish the goal of deriving effective dynamics for open systems to second order have been developed for specific scenarios using projection operator techniques [234, 279] and in terms of an effective operator formalism [280]. However, the available tools for open quantum systems are far less advanced than their Hamiltonian analogs.

In this paper, we present a perturbation theory for Markovian quantum master equations[1], in the language of a generalized SW transformation. It formalizes the usual procedure of adiabatic elimination of the fast evolving (due to coherent and/or non-coherent dynamics) degrees of freedom in open systems. We consider the most general case of a time-independent Liouvillian operator that features an internal hierarchy, i.e., it can be divided into a unperturbed part and a perturbation $\mathcal{L} = \mathcal{L}_0 + \epsilon\mathcal{V}$. A non-unitary similarity transformation on $\mathcal{L}$ dresses the zero eigenstates of $\mathcal{L}_0$ (i.e., the unperturbed steady states) with higher excitation eigenstates according to the perturbation $\epsilon\mathcal{V}$ and by construction decouples exactly the corresponding *slow* and *fast space*, respectively. The projection of the transformed Liouvillian onto this slow space

[1]Following [279], a quantum master equation is called Markovian iff it can be written in Lindblad form. The generated map $\mathcal{D}(t)$ then trivially fulfills the semigroup property $\mathcal{D}(t+t') = \mathcal{D}(t)\mathcal{D}(t')$. The term Markovian will be used in this spirit throughout the paper. It denotes a system property rather than a bath property. Although in many physical situations, Markovianity of the bath (i.e. the negligibility of the bath correlation time) implies a Markovian evolution of the system, there is no general equivalence between the two concepts.

(spanned by the dressed steady states of $\mathcal{L}_0$) reproduces the exact low-excitation spectrum and describes the system evolution in the vicinity of the steady state. In analogy to the unitary SW transformation, this effective Liouvillian $L_{\text{eff}}$ can naturally be expanded in orders of the perturbation parameter $\epsilon$, yielding a systematic perturbative series of the low-excitation spectrum and, in particular, the steady-state properties. We stress the point that in contrast to some previous perturbative approaches, our formalism works with only a few assumptions on the specific nature of $\mathcal{L}_0$ and produces perturbative results to arbitrary order. In practice, the derivation of higher-order corrections is much easier than with previous approaches [278].

The phenomenon that the effective low-energy Hamiltonian derived from integrating out high-energy degrees of freedom, often features a higher complexity than the original one, led in closed systems to the concept of perturbation gadgets [281, 282, 283]. Along these lines, the idea of *dissipative gadgets*, i.e., the engineering of dissipation for quantum state preparation and protection has recently been proposed [32, 23, 33]. The presented SW formalism provides a natural tool for designing dissipation according to desired steady state properties.

## 5.2 Executive summary

This Chapter is structured as follows. In Section 5.3 we derive the generalized SW transformation for open systems. We show, that in the new basis a subspace of slow dynamics decouples exactly from all fast degrees of freedom and we derive an effective Liouvillian within this subspace in a perturbative series. This central result is expressed in Eqn. (5.27). The reader who is not interested in the details of the derivations can skip Section 5.3 and directly use this result.

In Section 5.4 we employ the derived formalism in two generic examples, where we present two alternative strategies to evaluate the formal expressions for the effective Liouvillians and discuss general properties of the different orders of the perturbation. In the first example (Section 5.4.1) we prove that the effective second-order Liouville operator in a generic ancilla setting is always of Lindblad form, irrespective of the nature of the ancilla system and its dynamics. In the second part (Section 5.4.2) we provide an example where higher order corrections have significant impact on the accuracy of the approximate evolution of a superradiant system. For illustrative purposes, in the two examples we employ two different strategies to calculate the relevant coefficients of the effective master equation. In practice one has to decide depending on the specific situation on which approach to choose, since both methods feature different advantages. Finally, in Section 5.5 we summarize the results and provide a brief outlook.

## 5.3 Formalism

We consider an open system whose evolution is governed by a Markovian master equation. The corresponding time-independent Liouville operator can be partitioned in a zeroth-order term $\mathcal{L}_0$ and a perturbation $\mathcal{V}$,

$$\dot{\chi} = \mathcal{L}\chi = (\mathcal{L}_0 + \epsilon\mathcal{V})\chi, \tag{5.1}$$

where $\epsilon$ denotes the dimensionless perturbation parameter. $\mathcal{L}_0$ is a linear operator on the vector space of $\mathbb{C}^{d\times d}$ matrices ($d$ is the dimension of the system's Hilbert space). We introduce the set

of left and right eigenvectors for the non-Hermitian operator $\mathcal{L}_0$,

$$\mathcal{L}_0 |r_i\rangle = \lambda_i |r_i\rangle , \tag{5.2}$$

$$\langle l_i| \mathcal{L}_0 = \lambda_i \langle l_i| , \tag{5.3}$$

which are chosen to be biorthonormal $\langle l_i|r_j\rangle = \delta_{i,j}$ and generically satisfy the completeness relation $\sum |r_i\rangle \langle l_i| = \mathbb{1}^2$. The eigenvalues $\lambda_i$ are in general complex.

Since $\mathcal{L}_0$ is the generator of a universal dynamical map (i.e., a contractive semigroup), its eigenvalues fulfill $\mathrm{Re}(\lambda_i) \leq 0$ [250]. The generated maps are trace preserving, which guarantees that the kernel of $\mathcal{L}_0$ is at least one dimensional. We partition its spectrum in two subsets $\mathcal{P} = \{\lambda_\alpha | \lambda_\alpha = 0\} \neq \{\}$ and $\mathcal{Q} = \{\lambda_i | \lambda_i \neq 0\}$ (throughout the paper we will refer to eigenvalues from the two sets and the corresponding eigenvectors with greek and arabic indices, respectively). The spectral gap of the unperturbed Liouville operator is denoted as $\Delta = \min_{\lambda_i \in \mathcal{Q}} (|\lambda_i|)$. The in general non-orthogonal projectors [3]

$$P = \sum_{\alpha:\lambda_\alpha \in \mathcal{P}} |r_\alpha\rangle \langle l_\alpha| , \tag{5.4}$$

$$Q = \mathbb{1} - P = \sum_{i:\lambda_i \in \mathcal{Q}} |r_i\rangle \langle l_i| . \tag{5.5}$$

define the subspaces corresponding to the spectral sets $\mathcal{P}$ and $\mathcal{Q}$. These subspaces are referred to in the following as the slow (defined by $P$) and fast (defined by $Q$) space, respectively, according to their evolution under the action of $\mathcal{L}_0$.

We use this partition of the left and right eigenbases to introduce a block structure for arbitrary superoperators $A : \mathbb{L}(\mathcal{H}) \to \mathbb{L}(\mathcal{H})$, where $\mathbb{L}(\mathcal{H})$ denotes the space of linear operators acting on the system's Hilbert space $\mathcal{H}$ (an example for such a superoperator constitutes the Liouville operator $\mathcal{L}$ itself),

$$A = \begin{pmatrix} A^P & A^- \\ A^+ & A^Q \end{pmatrix} = \begin{pmatrix} PAP & PAQ \\ QAP & QAQ \end{pmatrix} . \tag{5.6}$$

Further we introduce block diagonal and block off-diagonal operators

$$A^D = \begin{pmatrix} A^P & 0 \\ 0 & A^Q \end{pmatrix} , \tag{5.7}$$

$$A^O = \begin{pmatrix} 0 & A^- \\ A^+ & 0 \end{pmatrix} . \tag{5.8}$$

By construction the unperturbed Liouville operator is block diagonal in this basis ($\mathcal{L}_0 = \mathcal{L}_0^D = \mathcal{L}_0^Q$), while the perturbation in general contains both block diagonal and off-diagonal terms ($\mathcal{V} = \mathcal{V}^D + \mathcal{V}^O$). In analogy to the Hamiltonian SW transformation our goal is to find a similarity transformation

$$\mathcal{L} \to L = U^{-1} \mathcal{L} U, \tag{5.9}$$

[2] For generic dynamics this is always possible. However, in principle one can construct examples where the Liouvillian is similar to a Jordan form and not diagonalizable. We will not consider this case here.

[3] A projector is called orthogonal if its range and null space are orthogonal subspaces.

such that the two subspaces decouple

$$L^O = 0. \tag{5.10}$$

Being similar [Eqn. (5.9)], the transformed ($L$) and original ($\mathcal{L}$) Liouvillian share the same spectrum. For bounded operators $\mathcal{V}$, the perturbation shifts any eigenvalue by at most $\|\epsilon\mathcal{V}\|$ in the complex plane. Therefore, in the perturbative limit $\Delta > 2\epsilon\|\mathcal{V}\|$ [268], the eigenvalues $\mathcal{P}$ remain on the disk $D = \{z \in \mathbb{C}, |z| \leq \Delta/2\}$ after we turn on the perturbation, while the eigenvalues $\mathcal{Q}$ stay in the complement of $D$. Thus the eigenvalues of the superoperator $L_{\text{eff}} = PLP$ (referred to as *effective Liouville operator*) reproduce the exact low excitation spectrum of $\mathcal{L}$ (which is defined as the subset of eigenvalues of $\mathcal{L}$ which lie on $D$). The master equation

$$\dot{\mu} = L_{\text{eff}}\mu \tag{5.11}$$

describes accurately the steady state properties and low excitation dynamics, i.e., the system evolution in the vicinity of the steady state. In addition, the SW transformation offers by construction a natural expansion of the effective Liouvillian $L_{\text{eff}}$ in the perturbation parameter $\epsilon$, as will be shown below.

In the case of unbounded perturbations $\mathcal{V}$ (for instance, if the perturbation contains bosonic operators) there is no such concise condition, because in principle the perturbation can lead to arbitrarily large shifts and eigenvalues from $\mathcal{Q}$ may be pushed onto $D$, such that $PLP$ does not necessarily reproduce the low excitation spectrum. This is the case if eigenvalues of $QLQ$ are closer to zero than some eigenvalues of $PLP$. In analogy to other perturbative approaches, the SW transformation can still be meaningful in this case, if the part of the low excitation spectrum that is not captured, corresponds to states that are irrelevant during the system evolution (e.g., Fock states of large particle number). However, like in the case of the Hamiltonian SW transformation, this case has to be treated with care, and the validity of the approximation has to be checked self-consistently[4]. To avoid the mathematical subtleties that come along with infinite Hilbert spaces, we restrict ourselves to the finite case (or the case where unbounded operators can be truncated for physical reasons) in the following.

We further note that, if the initial state of the system has large components in the fast space, a transient evolution takes place, which is governed to leading order by $\mathcal{L}_0$, and rapidly brings the system close to the unperturbed steady states. This fast initial slip is in principle described by the effective Liouville operator in the fast space $QLQ$, but will not be discussed further.

In the following we generalize the generic procedure to construct the transformation matrix $U$ for Hermitian matrices (for a review see, e.g., [164, 268]) to the non-Hermitian case. It can be shown that Eqn. (5.10) does not uniquely define the decoupling operator $U$. We will here only consider the so-called "canonical" choice $U = e^S$, where the generator $S$ is imposed to be block off-diagonal $S^D = 0$. Other choices of $S^D$ are possible, which then lead to different perturbation theory formalisms, as outlined in [164] for the Hermitian case. Depending on the specific problem, alternative gauge choices for $S^D$ may prove to be advantageous. The discussion of the properties of the various formalisms represents an interesting subject for future studies.

[4] An example where the generalized SW transformation is successfully applied to unbounded operators is the perturbative treatment of the hyperfine coupling in Chapter 4.

To simplify the formalism we introduce a compact notation where the commutation with an operator $A$ is expressed via the superoperator $\hat{A}$ defined via:

$$\hat{A}B = [B, A]. \tag{5.12}$$

Here, $B$ denotes an arbitrary operator. This notation allows for a compact representation of the similarity transformation Eqn. (5.9)

$$\begin{aligned} L = U^{-1}\mathcal{L}U &= e^{-S}\mathcal{L}e^{S} \\ &= \mathcal{L} + [\mathcal{L}, S] + \frac{1}{2!}[[\mathcal{L}, S], S] + \dots \\ &= \sum_{i=0}^{\infty} \frac{1}{i!}\hat{S}^i\mathcal{L} = e^{\hat{S}}\mathcal{L}. \end{aligned} \tag{5.13}$$

We partition the latter superoperator into its odd and even powers

$$e^{\hat{S}} = \cosh(\hat{S}) + \sinh(\hat{S}). \tag{5.14}$$

The convenience of the canonical choice $S^D = 0$ now becomes evident. While the odd operator $\sinh(\hat{S})$ changes block diagonal to off-diagonal operators and vice versa, the even powers $\cosh(\hat{S})$ respect that structure. Therefore, we can rewrite condition Eqn. (5.10)

$$\begin{aligned} L^O = 0 &\Leftrightarrow (e^{\hat{S}}\mathcal{L})^O = 0 \\ &\Leftrightarrow \sinh(\hat{S})\mathcal{L}^D + \cosh(\hat{S})\mathcal{L}^O = 0 \qquad (5.15) \\ &\Leftrightarrow \frac{\sinh(\hat{S})}{\hat{S}}\hat{S}\mathcal{L}^D + \cosh(\hat{S})\mathcal{L}^O = 0 \\ &\Leftrightarrow \hat{S}\mathcal{L}^D = -\hat{S}\coth(\hat{S})\mathcal{L}^O \\ &\Leftrightarrow \hat{S}\mathcal{L}_0 = -\hat{S}\epsilon\mathcal{V}^D - \epsilon\hat{S}\coth(\hat{S})\mathcal{V}^O, \qquad (5.16) \end{aligned}$$

where in the last step we used $\mathcal{L}^D = \mathcal{L}_0 + \epsilon\mathcal{V}^D$ and $\mathcal{L}^O = \epsilon\mathcal{V}^O$. Equation (5.16) can be solved formally using resolvent operator techniques. Since by construction the slow space (defined by the set $\mathcal{P}$) contains only unperturbed eigenvalues $\lambda_\alpha = 0$, it is $\mathcal{L}_0 P = P\mathcal{L}_0 = 0$ and the resolvent operator takes the simple form

$$\mathcal{R}_0(A) = Q\mathcal{L}_0^{-1}AP - PA\mathcal{L}_0^{-1}Q. \tag{5.17}$$

By construction the projection of the zero order Liouvillian into the fast space $Q\mathcal{L}_0 = \mathcal{L}_0 Q = Q\mathcal{L}_0 Q$ has full rank and its inverse is well defined. For simplicity we denote $(Q\mathcal{L}_0 Q)^{-1} \equiv \mathcal{L}_0^{-1}$. For block off-diagonal operators $X = X^O$ the resolvent operator fulfills

$$\mathcal{R}_0(\hat{X}\mathcal{L}_0) = X, \tag{5.18}$$

as can be checked straightforwardly. Applying this superoperator to Eqn. (5.16) gives the conditional equation for the generating matrix $S$,

$$S = -\epsilon\mathcal{R}_0\hat{S}\mathcal{V}^D - \epsilon\mathcal{R}_0\hat{S}\coth(\hat{S})\mathcal{V}^O. \tag{5.19}$$

Having derived a formal implicit expression for the transformation matrix $S$ which renders the Liouville operator block diagonal $L^O = 0$, we now derive a compact expression for the diagonal blocks $L^D$ in terms of $S$, $\mathcal{V}$, and $\mathcal{L}_0$. As before, the block off-diagonal structure of $S$ allows us to write $L^D$ as a combination of even and odd powers of the superoperator $\hat{S}$

$$\begin{aligned} L = L^D &= \left(e^{\hat{S}}\mathcal{L}\right)^D \\ &= \cosh(\hat{S})\mathcal{L}^D + \sinh(\hat{S})\mathcal{L}^O \\ &= \mathcal{L}^D - \frac{\cosh(\hat{S})-1}{\tanh(\hat{S})}\mathcal{L}^O + \sinh(\hat{S})\mathcal{L}^O, \end{aligned} \tag{5.20}$$

where in the second line we used Eqn. (5.15). Using the basic trigonometric relation $\sinh(x) - [\cosh(x)-1]/\tanh(x) = \tanh(x/2)$ we find

$$\begin{aligned} L &= \mathcal{L}^D + \tanh(\hat{S}/2)\mathcal{L}^O \\ &= \mathcal{L}_0 + \epsilon\left(\mathcal{V}^D + \tanh(\hat{S}/2)\mathcal{V}^O\right). \end{aligned} \tag{5.21}$$

As discussed in [268] all the above hyperbolic transformations are well defined for infinitesimal transformation matrices $S$, which is guaranteed for appropriate perturbation parameters $\epsilon$. We denote the perturbative correction to $\mathcal{L}_0$ as

$$\mathcal{W} = \epsilon\left[\mathcal{V}^D + \tanh(\hat{S}/2)\mathcal{V}^O\right]. \tag{5.22}$$

Since by construction $\mathcal{L}_0 P = P\mathcal{L}_0 = 0$ the effective Liouville operator in the slow space is then given as

$$L_{\text{eff}} = PLP = P\mathcal{W}P. \tag{5.23}$$

As we have seen, the SW transformation accounts for an exact decoupling of the slow and fast space ($L^O = 0$). In general however, the exact transformation is hard to find. The success of the SW methods roots in the fact that it allows for a natural expansion in orders of the perturbation, which we discuss in the following.

Expanding $S$ in orders of the perturbation parameter $\epsilon$ in a Taylor series

$$S = \sum_{n=0}^{\infty} \epsilon^n S_n, \tag{5.24}$$

and using Eqn. (5.19) one can deduce a recursive equation for the operators $S_n$. With these results we can directly construct the perturbative correction $\mathcal{W}$ via Eqn. (5.22) order by order.

The first few Taylor matrices read

$$\begin{aligned} &S_0 = 0, \\ &S_1 = -\mathcal{R}_0\mathcal{V}^O = \mathcal{V}^-\mathcal{L}_0^{-1} - \mathcal{L}_0^{-1}\mathcal{V}^+, \\ &S_2 = \mathcal{R}_0\hat{\mathcal{V}}^D S_1 = -\mathcal{R}_0\hat{\mathcal{V}}^D\mathcal{R}_0\mathcal{V}^O, \\ &\vdots \end{aligned} \tag{5.25}$$

The corresponding expansion for the perturbative correction matrix $\mathcal{W} = \sum_{n=0}^{\infty} \epsilon^n \mathcal{W}_n$ can be found via Eqn. (5.22)

$$\begin{aligned} \mathcal{W}_0 &= 0, \\ \mathcal{W}_1 &= \mathcal{V}^D, \\ \mathcal{W}_2 &= -\frac{1}{2}\hat{\mathcal{V}}^O S_1 = \frac{1}{2}\hat{\mathcal{V}}^O R_0 \mathcal{V}^O, \\ \mathcal{W}_3 &= -\frac{1}{2}\hat{\mathcal{V}}^O S_2 = \frac{1}{2}\hat{\mathcal{V}}^O \mathcal{R}_0 \hat{\mathcal{V}}^D \mathcal{R}_0 \mathcal{V}^O, \\ &\vdots \end{aligned} \tag{5.26}$$

In [268] a formal expression for the $n$th order as well as a diagrammatic technique has been derived, which can be directly applied to the case of non-hermitian matrices. Straightforward evaluation of Eqs. (5.26) and subsequent projection onto $\mathcal{P}$ yields the first orders of the effective Liouville operator in the slow space [cf. Eqn. (5.23)]

$$\begin{aligned} L_1^{\text{eff}} &= P\mathcal{V}^D P = \mathcal{V}^P, \\ L_2^{\text{eff}} &= -P\mathcal{V}Q\mathcal{L}_0^{-1}Q\mathcal{V}P = -\mathcal{V}^-\mathcal{L}_0^{-1}\mathcal{V}^+ \\ L_3^{\text{eff}} &= \mathcal{V}^-\mathcal{L}_0^{-1}\mathcal{V}^Q\mathcal{L}_0^{-1}\mathcal{V}^+ - \frac{1}{2}\{\mathcal{V}^P, \mathcal{V}^-\mathcal{L}_0^{-2}\mathcal{V}^+\}_+, \\ &\vdots \end{aligned} \tag{5.27}$$

where we employed the notation introduced in Eqn. (5.6) and $\{A, B\}_+ = AB + BA$ denotes the anticommutator. Note that $\mathcal{L}_2^{\text{eff}}$ reproduces the well-known second-order result of adiabatic elimination in dissipative systems [234].

## 5.4 Examples

In this section we will exemplarily employ the formalism developed above in two generic situations and present two alternative strategies to evaluate the expressions for the effective Liouvillians of Eqs. (5.27).

First, in Section 5.4.1 we consider the general setting of an ancilla system, which undergoes fast (in general dissipative) dynamics and is weakly coupled to a second system. We adiabatically eliminate the ancilla to second order, employing the SW formalism. The coefficients of the effective Liouvillian are expressed in terms of ancilla time correlation functions, which can readily be evaluated using the quantum regression theorem [225]. We show that the effective Liouville operator to second order is always of Lindblad form [284], implying a Markovian evolution of the system.

If the zeroth-order Liuovillian $\mathcal{L}_0$ is simple, it is advisable to explicitly calculate matrix representations of $\mathcal{V}$ and $\mathcal{L}_0^{-1}$. Given these matrices, arbitrary orders of the perturbation can readily be evaluated by simple matrix multiplication according to Eqn. (5.27). In Section 5.4.2 we reconsider the model of Chapter 2 [OSR] which features simple zeroth-order dynamics. We derive an explicit matrix representation of $\mathcal{V}$ in the biorthonormal eigenbasis of $\mathcal{L}_0$. This enables

us to directly determine the effective Liouvillian up to third order and we show numerically that the typically neglected third order has a significant impact on the evolution of the nuclear system[5].

### 5.4.1 General ancilla setting

In the following we consider an example of how to apply the formalism in a generic ancilla setting. A system is weakly coupled to an (unspecified) ancilla system, which undergoes fast (dissipative and/or coherent) dynamics. The Hilbert space of the total system is the product of the ancilla and system spaces $\mathcal{H} = \mathcal{H}_A \otimes \mathcal{H}_S$. We assume that the evolution of the ancilla is governed by fast dynamics given by $\mathcal{L}_0$. $\mathcal{L}_0$ contains an arbitrary combination of Lindblad and Hamiltonian terms

$$\mathcal{L}_0\chi = \sum_k \gamma_k (L_k \chi L_k^\dagger - \frac{1}{2}\{L_k^\dagger L_k, \chi\}_+) - i[H_0, \chi], \tag{5.28}$$

where both the $L_k$'s and $H_0$ act only on the ancilla space. Let us for simplicity assume that $\mathcal{L}_0$ features a unique steady state $\mathcal{L}_0\sigma_{ss} = 0$ such that the projector on the space of zeroth-order steady states can be written in the simple form $P\chi = \sigma_{ss} \otimes \mathrm{Tr}_A(\chi) \equiv \sigma_{ss} \otimes \mu$ [285]. In the last step we introduced the reduced density matrix $\mu \equiv \mathrm{Tr}_A(\chi)$. The perturbation comprises the most general Hamiltonian interaction between the system and ancilla and a system Hamiltonian

$$\epsilon\mathcal{V}\chi = -i\epsilon[\sum_{\alpha=1}^{k} \tilde{A}_\alpha \otimes S_\alpha, \chi] - i\epsilon[\sum_{\alpha=1}^{k} a_\alpha \mathbb{1} \otimes S_\alpha, \chi], \tag{5.29}$$

where $\tilde{A}_\alpha$ and $S_\alpha$ are arbitrary Hermitian ancilla and system operators (including the null operator), respectively, and $a_\alpha \in \mathbb{R}$, $k \in \mathbb{N}$. Introducing the ancilla operators $A_\alpha = \tilde{A}_\alpha + a_\alpha \mathbb{1}$, Eqn. (5.29) simplifies to

$$\epsilon\mathcal{V}\chi = -i\epsilon[\sum_{\alpha=1}^{k} A_\alpha \otimes S_\alpha, \chi]. \tag{5.30}$$

For notational convenience we will suppress the $\otimes$-symbol in the following: $A \otimes S \equiv AS$. The full master equation thus reads

$$\dot{\chi} = \mathcal{L}\chi = \mathcal{L}_0\chi + \epsilon\mathcal{V}\chi. \tag{5.31}$$

Note that the example we consider here corresponds to the often encountered situation of a bipartite system with separation of time scales. The ancilla evolution occurs on a timescale much faster than the system evolution. Thus we can consider the system's evolution under the condition that the ancilla has settled to its steady state. The method presented above represents a formal approach to adiabatically eliminate the fast ancilla dynamics.

[5]Note however, that the conclusions of Chapter 2 remain unchanged since in the numerical simulations we considered the full master equation before the adiabatic elimination.

### First order

The first order in the expansion Eqn. (5.27) can readily be evaluated:

$$\begin{aligned} L_1^{\text{eff}}\chi = P\mathcal{V}P\chi &= -i\sum_\alpha P[A_\alpha S_\alpha, \sigma_{ss}\mu] \\ &= -i\sum_\alpha P\left(A_\alpha\sigma_{ss}[S_\alpha,\mu] + [A_\alpha,\sigma_{ss}]S_\alpha\mu\right). \end{aligned} \tag{5.32}$$

The second term vanishes, since the trace over a commutator is zero: $P[A_\alpha,\sigma_{ss}]S_\alpha\mu = \sigma_{ss}\text{Tr}_A([A_\alpha,\sigma_{ss}])S_\alpha\mu = 0$. Thus we find the first order of the effective evolution

$$L_1^{\text{eff}}\chi = \sigma_{ss}L_1^{\text{eff}}\mu = -i\sigma_{ss}\sum_\alpha[\langle A_\alpha\rangle S_\alpha,\mu]. \tag{5.33}$$

Since we are only interested in the evolution of the reduced density matrix $\mu = \text{Tr}_A(\chi)$ we can trace out the ancilla degrees of freedom and find the first-order correction of the system's evolution,

$$\begin{aligned} L_1^{\text{eff}}\mu &= -i\sum_\alpha[\langle A_\alpha\rangle S_\alpha,\mu] \\ &= -i\sum_\alpha[\langle\tilde{A}_\alpha\rangle S_\alpha,\mu] - i\sum_\alpha[a_\alpha S_\alpha,\mu]. \end{aligned} \tag{5.34}$$

Expectedly, to first order, the system experiences merely the effect of the mean values of the ancilla operators and the original action of the system Hamiltonian.

### Second order

The second order of the effective Liouville operator gives rise to more involved dynamics. We calculate the exact expressions and prove its Lindblad form for arbitrary ancilla dynamics $\mathcal{L}_0$.

For the effective system evolution to second order we have to calculate the expression

$$\text{Tr}_A(L_2^{\text{eff}}\chi) = -\text{Tr}_A(P\mathcal{V}Q\mathcal{L}_0^{-1}Q\mathcal{V}P\chi). \tag{5.35}$$

In order to avoid the direct computation of $\mathcal{L}_0$ which may be impractical for large ancilla systems and for analytical purposes, we express the inverse via the Laplace transform $\mathcal{L}_0^{-1} = -\int_0^\infty d\tau e^{\mathcal{L}_0\tau}$, and we find

$$\begin{aligned} \text{Tr}_A(L_2^{\text{eff}}\chi) &= \int_0^\infty d\tau\text{Tr}_A(P\mathcal{V}Qe^{\mathcal{L}_0\tau}Q\mathcal{V}P\chi) \\ &= \int_0^\infty d\tau\text{Tr}_A\left[P\mathcal{V}(1-P)e^{\mathcal{L}_0\tau}(1-P)\mathcal{V}P\chi\right] \\ &= \int_0^\infty d\tau\text{Tr}_A(P\mathcal{V}e^{\mathcal{L}_0\tau}\mathcal{V}P\chi) \qquad \}\textcircled{1} \\ &\quad -\int_0^\infty d\tau\text{Tr}_A(P\mathcal{V}P\mathcal{V}P\chi), \qquad \}\textcircled{2} \end{aligned} \tag{5.36}$$

where we exploited the property $Pe^{\mathcal{L}_0\tau} = e^{\mathcal{L}_0\tau}P = P$.

We first evaluate expression (1):

$$
\begin{aligned}
(1) &= \int d\tau \mathrm{Tr}_A P\mathcal{V} e^{\mathcal{L}_0\tau} \left( -i \left[ \sum_j A_j S_j, \sigma_{ss}\mu \right] \right) \\
&= -i \int d\tau \sum_j \mathrm{Tr}_A P\mathcal{V} \left( e^{\mathcal{L}_0\tau} A_j \sigma_{ss} \left[ S_j, \mu \right] \right. \\
&\qquad \left. + e^{\mathcal{L}_0\tau} \left[ A_j, \sigma_{ss} \right] \mu S_j \right) \\
&= (-i)^2 \sum_{i,j} \left\{ \int d\tau \mathrm{Tr}_A \left( A_i e^{\mathcal{L}_0\tau} A_j \sigma_{ss} \right) \left[ S_i, \left[ S_j, \mu \right] \right] \right. \\
&\qquad \left. + \int d\tau \mathrm{Tr}_A \left( A_i e^{\mathcal{L}_0\tau} [A_j, \sigma_{ss}] \right) \left[ S_i, \mu S_j \right] \right\} \\
&= -\sum_{i,j} \left\{ \left( \int d\tau \langle A_i A_j(\tau) \rangle_{ss} \right) \left[ S_i, \left[ S_j, \mu \right] \right] \right. \\
&\qquad \left. + \left( \int d\tau \langle [A_i, A_j(\tau)] \rangle_{ss} \right) \left[ S_i, \mu S_j \right] \right\}.
\end{aligned}
\tag{5.37}
$$

In the last step, we defined the time correlation functions in the usual way $\langle A_i A_j(\tau) \rangle_{ss} \equiv \mathrm{Tr}_A \left( A_i e^{\mathcal{L}_0\tau} A_j \sigma_{ss} \right)$ and $\langle [A_i, A_j(\tau)] \rangle_{ss} \equiv \mathrm{Tr}_A \left( A_i e^{\mathcal{L}_0\tau} [A_j, \sigma_{ss}] \right)$.

In the same fashion, (2) can be readily evaluated to the formal expression

$$
(2) = \sum_{i,j} \left( \int_0^\infty d\tau \right) \langle A_i \rangle_{ss} \langle A_j \rangle_{ss} \left[ S_i, \left[ S_j, \mu \right] \right]. \tag{5.38}
$$

In general both formal expressions (1) and (2) are diverging. However their sum

$$
\begin{aligned}
\mathrm{Tr}_A(L_2^{\mathrm{eff}} \chi) &= (1) + (2) \\
&= -\sum_{i,j} \left\{ \left( \int d\tau \langle \Delta A_i \Delta A_{j\tau} \rangle_{ss} \right) \left[ S_i, \left[ S_j, \mu \right] \right] \right. \\
&\qquad \left. + \left( \int d\tau \langle [\Delta A_i, \Delta A_{j\tau}] \rangle_{ss} \right) \left[ S_i, \mu S_j \right] \right\},
\end{aligned}
\tag{5.39}
$$

represents a converging and meaningful expression. We defined $\Delta O_t \equiv O(t) - \langle O \rangle_{ss}$, for arbitrary ancilla operators $O$. (2) cancels the diverging parts in (1) and renders the integral over correlation functions finite. Note that the system Hamiltonian $\epsilon \sum_\alpha a_\alpha S_\alpha$ has no effect to second order, since $\langle \Delta A_i \Delta A_{j\tau} \rangle_{ss} = \langle \Delta \tilde{A}_i \Delta \tilde{A}_{j\tau} \rangle_{ss}$.

Next, we show that the second order derived above [Eqn. (5.39)] is always of Lindblad form, meaning that it generates a completely positive, trace preserving map. According to Eqn. (5.39) the system evolution to second order is entirely determined by the matrix

$$
\mathcal{A} \equiv \left( \int d\tau \langle \Delta A_i \Delta A_{j\tau} \rangle_{ss} \right)_{i,j} = \int d\tau \langle \Delta \vec{A} \Delta \vec{A}^*_\tau \rangle_{ss}, \tag{5.40}
$$

which can be written as a dyadic product of the vector $\Delta\vec{A} = (\Delta A_1, \ldots, \Delta A_n)^T$. In fact, Eqn. (5.39) can be rewritten in the more familiar form

$$\begin{aligned} &\mathrm{Tr}_A(L_2^{\mathrm{eff}}\chi) \\ &= \sum_{i,j} \frac{1}{2}(\mathcal{A}+\mathcal{A}^\dagger)_{i,j}\,(2S_j\mu S_i - \{S_iS_j,\mu\}_+) \\ &\qquad - i\left[\frac{1}{2i}\sum_{i,j}(\mathcal{A}-\mathcal{A}^\dagger)_{i,j}S_iS_j,\mu\right]. \end{aligned} \tag{5.41}$$

The Hermitian part of $\mathcal{A}$ is responsible for the dissipative part of the evolution, while the anti-Hermitian part defines the coherent evolution. One readily checks that $\frac{1}{2i}\sum_{i,j}(\mathcal{A}-\mathcal{A}^\dagger)_{i,j}S_iS_j$ defines a Hermitian operator. On the other hand, in the Appendix 5.A.1 we show the positivity of the coefficient matrix $\mathcal{A}+\mathcal{A}^\dagger \geq 0$, which guarantees Lindblad form of the dissipative term of Eqn. (5.41). Thus, the evolution of the system after adiabatic elimination of the ancilla is physical and up to second order Markovian.

Aside from this general result, we now show that the coefficient matrix $\mathcal{A}$ can readily be calculated without evaluating the respective integrals explicitly, by using the quantum regression theorem [262]. Let us assume the equations of motion for the mean deviations of the ancilla operator set $\{A_\alpha\}$ close under $\mathcal{L}_0$,

$$\frac{d}{dt}\langle\Delta\vec{A}_t\rangle = \mathcal{M}\langle\Delta\vec{A}_t\rangle. \tag{5.42}$$

In a finite-dimensional system this can always be achieved by extending the set $\{A_\alpha|\alpha = 1,\ldots,k\}$ to a larger set $\{A_\alpha|\alpha = 1,\ldots,n\}$ $(n \geq k)$ which forms an operator basis of the ancilla Hilbert space.

Under these conditions the quantum regression theorem allows for a simple evaluation of the relevant time correlation functions

$$\begin{aligned} &\frac{d}{dt}\langle\Delta\vec{A}_t\Delta\vec{A}^*\rangle_{ss} = \mathcal{M}\langle\Delta\vec{A}_t\Delta\vec{A}^*\rangle_{ss}, \\ &\Rightarrow\langle\Delta\vec{A}_t\Delta\vec{A}^*\rangle_{ss} = e^{\mathcal{M}t}\langle\Delta\vec{A}\Delta\vec{A}^*\rangle_{ss}. \end{aligned} \tag{5.43}$$

All eigenvalues of the Bloch matrix $\mathcal{M}$ have a strictly negative real part (and thus $\mathcal{M}$ is invertible), since $\mathcal{L}_0$ generates a contractive semigroup with (by assumption) unique steady state. Therefore the latter equation can be readily integrated yielding a simple expression for the coefficient matrix

$$\mathcal{A}^\dagger = \int_0^\infty d\tau\langle\Delta\vec{A}_\tau\Delta\vec{A}^*\rangle_{ss} = -\mathcal{M}^{-1}\langle\Delta\vec{A}\Delta\vec{A}^*\rangle_{ss}. \tag{5.44}$$

The latter expression can be readily evaluated for a given system and uniquely defines the effective second-order dynamics of the system according to Master Eqn. (5.41). As shown in Appendix 5.A.1, independent of the nature and dynamics of the ancilla system, the effective Master Eqn. (5.41) is of Lindblad form and gives rise to a Markovian time evolution of the system.

We emphasize that in many situations the size of the minimal set of operators that close under $\mathcal{L}_0$ (defining the dimension of $\mathcal{M}$) will be much smaller than the dimension of the Hilbert space. For illustration, consider the case where the ancilla system is constituted by a driven and damped spin $J$ and $\{A_\alpha|\alpha = x, y, z\}$ are the usual spin operators. In this case Eqn. (5.42) represents optical Bloch equations and the matrix $\mathcal{M}$ is of dimension three. Therefore, although the dimension of $\mathcal{L}_0$ maybe large (for large $J$), the calculation of all coefficients of the effective second-order dynamics reduce to a trivial three-dimensional matrix multiplication.

### 5.4.2 Mediated superradiance: Third order

In this Section we examine a specific example of an ancilla setting as discussed above. It is motivated by the study of superradiance from nuclear environments of single photon emitters in Chapters 2 and 3. A radiatively decaying spin (e.g., a spin pumped electron spin in a quantum dot or nitrogen-vacancy (NV) center [120, 101]) is weakly hyperfine coupled to a large spin environment (e.g., nuclear spins of the host material). After each photon emission the electron spin can escape from the dark state of the dissipation via exchange of an excitation with the nuclear spin environment. Superradiant features in the photon emission originate from a collective enhancement of the hyperfine flip-flop interaction for highly symmetric nuclear states.

In the following, we derive the effective evolution of the nuclear system after adiabatic elimination of the electron spin up to third order. In contrast to the previous example, where we expressed the effective Liouvillian in terms of integrated time correlation functions (which were evaluated using the quantum regression theorem), we now calculate an explicit matrix representation of the perturbation operator $\mathcal{V}$, in the biorthonormal eigenbasis of $\mathcal{L}_0$. Given this representation, all orders can readily be derived by simple matrix multiplication. We will find that the third order in the perturbation significantly improves the accuracy of the perturbative evolution.

The model we consider is governed by the master equation

$$\dot{\chi} = (\mathcal{L}_0 + \mathcal{V})\chi, \tag{5.45}$$

where

$$\begin{aligned}\mathcal{L}_0\chi =& \gamma\left(\sigma^-\chi\sigma^+ - \frac{1}{2}\left\{\sigma^+\sigma^-,\chi\right\}_+\right) \\ &- i\omega\left[\sigma^+\sigma^-,\chi\right],\end{aligned} \tag{5.46}$$

$$\mathcal{V}\rho = -ig\left[\frac{1}{2}\left(\sigma^+ I^- + \sigma^- I^+\right) + \sigma^+\sigma^- I^z, \chi\right], \tag{5.47}$$

where $I^\alpha = \sum_{i=1}^N g_i\sigma_i^\alpha$ are collective nuclear spin operators, while $\sigma_i^\alpha$ and $\sigma^\alpha$ are individual nuclear and electronic spin-$1/2$ operators, respectively ($\alpha = \pm, z$). The individual hyperfine coupling constants $g_i$ are normalized to $\sum g_i^2 = 1$. $\gamma$ and $\omega$ denote the photon emission rate of the electron spin and the hyperfine detuning, respectively. The nuclear and electronic systems are weakly hyperfine coupled with $g\sqrt{N} \ll \gamma, \omega$. This model describes the superradiant evolution of an NV center coupled to a nuclear spin environment, as discussed in Chapter 2 [OSR].

| | $\lambda_i$ | $\|r_i\rangle$ | $\|l_i\rangle$ |
|---|---|---|---|
| #1 | $\lambda_1 = 0$ | $\|r_1\rangle = \|\downarrow\downarrow\rangle$ | $\|l_1\rangle = \|\downarrow\downarrow\rangle + \|\uparrow\uparrow\rangle$ |
| #2 | $\lambda_2 = -\gamma/2 + i\omega$ | $\|r_2\rangle = \|\downarrow\uparrow\rangle$ | $\|l_2\rangle = \|\downarrow\uparrow\rangle$ |
| #3 | $\lambda_3 = -\gamma/2 - i\omega$ | $\|r_3\rangle = \|\uparrow\downarrow\rangle$ | $\|l_3\rangle = \|\uparrow\downarrow\rangle$ |
| #4 | $\lambda_4 = -\gamma$ | $\|r_4\rangle = \|\uparrow\uparrow\rangle - \|\downarrow\downarrow\rangle$ | $\|l_4\rangle = \|\uparrow\uparrow\rangle$ |

Table 5.1: Eigenvalues and left and right eigenvectors of $\mathcal{L}_0$. We used the simplified notation $|ij\rangle \equiv |i\rangle \otimes |j\rangle$ ($i, j = \uparrow, \downarrow$), which are the vector representations of the basis matrices $|i\rangle\langle j|$ of the electronic space (cf. text).

After the assignment $\chi = \sum_{i,j} \chi_{i,j} |i\rangle\langle j| \to \vec{\chi} = \sum_{i,j} \chi_{i,j} |i\rangle \otimes |j\rangle$ (where $\{|i\rangle\langle j|\}$ is an arbitrary basis of the matrix vector space), the linear superoperators of Eqn. (5.45) can be written in matrix representation as

$$\begin{aligned}\mathcal{L}_0 =& \gamma \left[\sigma^- \otimes (\sigma^+)^T - \frac{1}{2}\left(\sigma^+\sigma^- \otimes \mathbb{1} + \mathbb{1} \otimes (\sigma^+\sigma^-)^T\right)\right] \\ & - i\omega \left(\sigma^+\sigma^- \otimes \mathbb{1} - \mathbb{1} \otimes (\sigma^+\sigma^-)^T\right),\end{aligned} \tag{5.48}$$

and

$$\begin{aligned}\mathcal{V} = -ig \Bigg[ & \left(\frac{1}{2}\left(\sigma^+ I^- + \sigma^- I^+\right) + \sigma^+\sigma^- I^z\right) \otimes \mathbb{1} \\ & - \mathbb{1} \otimes \left(\frac{1}{2}\left(\sigma^+ I^- + \sigma^- I^+\right) + \sigma^+\sigma^- I^z\right)^T \Bigg],\end{aligned} \tag{5.49}$$

where the superscript $T$ denotes the matrix transpose. Since $\mathcal{L}_0$ acts only on the electronic space, it can be straightforwardly diagonalized in the basis of left and right eigenvectors,

$$\mathcal{L}_0 = \sum_{i=1}^{4} \lambda_i |r_i\rangle\langle l_i| . \tag{5.50}$$

The eigenvalues and the biorthonormal ($\langle l_i | r_j\rangle = \delta_{i,j}$) left and right eigenvectors are given in Table 5.1.

The representation of the perturbation in this basis

$$\mathcal{V} = \sum_{i,j=1}^{4} \mathcal{V}_{i,j} |r_i\rangle\langle l_j| , \tag{5.51}$$

$$\mathcal{V}_{i,j} = \langle l_i | \mathcal{V} | r_j\rangle , \tag{5.52}$$

can readily be derived and is given as

$$\mathcal{V} = \left(\begin{array}{c|c} \mathcal{V}^P & \mathcal{V}^- \\ \hline \mathcal{V}^+ & \mathcal{V}^Q \end{array}\right), \tag{5.53}$$

with the definitions

$$\mathcal{V}^P = 0, \tag{5.54}$$

$$\mathcal{V}^+ = \begin{pmatrix} ig/2\ \mathbb{1} \otimes (I^+)^T \\ -ig/2\ I^- \otimes \mathbb{1} \\ 0 \end{pmatrix}, \tag{5.55}$$

$$\mathcal{V}^- = \begin{pmatrix} -ig/2\left(I^- \otimes \mathbb{1} - \mathbb{1} \otimes (I^-)^T\right) \\ -ig/2\left(I^+ \otimes \mathbb{1} - \mathbb{1} \otimes (I^+)^T\right) \\ -ig\left(I^z \otimes \mathbb{1} - \mathbb{1} \otimes (I^z)^T\right) \end{pmatrix}^T. \tag{5.56}$$

$$\mathcal{V}^Q = \begin{pmatrix} ig\ \mathbb{1} \otimes (I^z)^T & 0 & -ig/2\left(I^+ \otimes \mathbb{1} + \mathbb{1} \otimes (I^+)^T\right) \\ 0 & -ig\ I^z \otimes \mathbb{1} & ig/2\left(I^- \otimes \mathbb{1} + \mathbb{1} \otimes (I^-)^T\right) \\ -ig/2\ I^- \otimes \mathbb{1} & ig/2\ \mathbb{1} \otimes (I^+)^T & -ig\left(I^z \otimes \mathbb{1} - \mathbb{1} \otimes (I^z)^T\right) \end{pmatrix}, \tag{5.57}$$

Note that for simplicity we denote operators [e.g., Eqn. (5.51)] and their representation in the $\mathcal{L}_0$ eigenbasis [e.g., Eqn. (5.53)] with the same symbols. The inverse of $\mathcal{L}_0$ in the fast space is simply given as

$$\mathcal{L}_0^{-1} \equiv (Q\mathcal{L}_0 Q)^{-1} = \begin{pmatrix} 1/\lambda_2 & 0 & 0 \\ 0 & 1/\lambda_3 & 0 \\ 0 & 0 & 1/\lambda_4 \end{pmatrix}. \tag{5.58}$$

All orders of the perturbation can now readily be derived from products of the above matrices (5.53) and (5.58), according to Eqn. (5.27). In the following we calculate explicitly the first three orders of the effective nuclear Liouville operator $L^{\text{eff}}$. The first order $L_1^{\text{eff}}$ vanishes, since the perturbation vanishes in the slow space, $\mathcal{V}^P = 0$. The second order yields

$$\begin{aligned} L_2^{\text{eff}} &= -\mathcal{V}^- \mathcal{L}_0^{-1} \mathcal{V}^+ \\ &= \gamma_{\text{eff}} \left[ I^- \otimes (I^+)^T - \frac{1}{2}\left(\mathbb{1} \otimes (I^+ I^-)^T + I^+ I^- \otimes \mathbb{1}\right) \right] \\ &\quad - i\omega_{\text{eff}} \left[ I^+ I^- \otimes \mathbb{1} - \mathbb{1} \otimes (I^+ I^-)^T \right], \end{aligned} \tag{5.59}$$

where $\gamma_{\text{eff}} = -2\text{Re}(g^2/\lambda_2) = g^2\gamma/[(\gamma/2)^2 + \omega^2]$ and $\omega_{\text{eff}} = \text{Im}(g^2/\lambda_2) = -g^2\omega/[(\gamma/2)^2 + \omega^2]$.

In the standard representation this corresponds to the second-order master equation

$$\begin{aligned} \dot{\mu} = L_2^{\text{eff}}\mu = &\gamma_{\text{eff}} \left[ I^- \mu I^+ - \frac{1}{2}\left\{ I^+ I^-, \mu \right\}_+ \right] \\ &- i\omega_{\text{eff}} \left[ I^+ I^-, \mu \right], \end{aligned} \tag{5.60}$$

which describes the collective decay of the nuclear spins at rate $\gamma_{\text{eff}}$, responsible for a superradiant evolution as discussed in Chapter 2 and 3. It is of Lindblad form and agrees with the result derived using standard adiabatic elimination techniques.

After having derived the matrix representation of $\mathcal{V}$ [Eqn. (5.53)] the SW formalism allows us to readily evaluate higher-order corrections according to Eqn. (5.27). This contrasts the

situation for the standard techniques of adiabatic elimination, where the derivation of higher-order terms is tedious [278]. The third order of Eqn. (5.27) yields the more involved expression (note that $\mathcal{V}^P = 0$)

$$\begin{aligned} L_3^{\text{eff}} =& \mathcal{V}^- \mathcal{L}_0^{-1} \mathcal{V}^Q \mathcal{L}_0^{-1} \mathcal{V}^+ \\ =& i\frac{g^3}{4\lambda_2^2}\left[I^- \otimes (I^+ I^z)^T - \mathbb{1} \otimes (I^+ I^z I^-)^T\right] \\ & - i\frac{g^3}{4\lambda_2\lambda_4}\left[I^z I^- \otimes (I^+)^T - I^- \otimes (I^+ I^z)^T\right] \\ & + i\frac{g^3}{4\lambda_3^2}\left[I^+ I^z I^- \otimes \mathbb{1} - I^z I^- \otimes (I^+)^T\right] \\ & - i\frac{g^3}{4\lambda_3\lambda_4}\left[I^z I^- \otimes (I^+)^T - I^- \otimes (I^+ I^z)^T\right], \end{aligned} \tag{5.61}$$

All terms involve contributions of the term $\propto \sigma^+\sigma^- I_z$ in Eqn. (5.47). It enters via $\mathcal{V}^Q$ in the intermediate process of Eqn. (5.61). In contrast, the second order was entirely independent of this term.

In Fig. 5.1 we compare simulations of the emitted photon intensity according to the exact evolution [cf. Eqn. (5.45), solid line] with the perturbative solution up to second (dotted line) and third (dashed line) order, respectively, for a system of $N = 100$ homogeneously coupled nuclear spins. The spins are initially fully polarized in the $z$ direction. We find that the third order effective Liouvillian has a significant impact on the accuracy of the approximation.

It can be shown that the Liouvillian of Eqn. (5.61) is hermiticity and trace preserving. Furthermore, the density matrix of the system remains positive throughout the evolution, although the third-order Liouvillian is not obviously of Lindblad form. In the following we show that in the limit $\omega = 0$ one can recover Lindblad form by adding terms of higher order in the perturbation. In this case, all non-Lindblad effects are of an order that is deliberately neglected.

For $\omega = 0$, Eqn. (5.61) reduces to the simple expression (in standard representation)

$$L_3^{\text{eff}}\mu = i\frac{g}{2\gamma}\gamma_{\text{eff}}[I^-\mu I^+, I_z] + i\frac{g}{4\gamma}\gamma_{\text{eff}}[I^+ I^z I^-, \mu]. \tag{5.62}$$

The first term of $L_2^{\text{eff}}$ can be combined with the first term of $L_3^{\text{eff}}$,

$$\begin{aligned} & \gamma_{\text{eff}}\left(I^-\mu I^+ + i\frac{g}{2\gamma}[I^-\mu I^+, I_z]\right) \\ =& \gamma_{\text{eff}}\left(e^{-i\frac{g}{2\gamma}I^z} I^-\mu I^+ e^{i\frac{g}{2\gamma}I^z} + O\left[(g/\gamma)^2\right]\right), \end{aligned} \tag{5.63}$$

where we used relation Eqn. (5.13). The term $O\left[(g/\gamma)^2\right]$ is of fourth order in the perturbation and can consistently be neglected. The resulting master equation up to third order then has Lindblad form

$$\begin{aligned} & \left(L_2^{\text{eff}} + L_3^{\text{eff}}\right)\mu \\ =& \gamma_{\text{eff}}\left[e^{-i\frac{g}{2\gamma}I^z} I^-\mu I^+ e^{i\frac{g}{2\gamma}I^z} - \frac{1}{2}\left\{I^+ I^-, \mu\right\}_+\right] \\ & + i\frac{g}{4\gamma}\gamma_{\text{eff}}[I^+ I^z I^-, \mu]. \end{aligned} \tag{5.64}$$

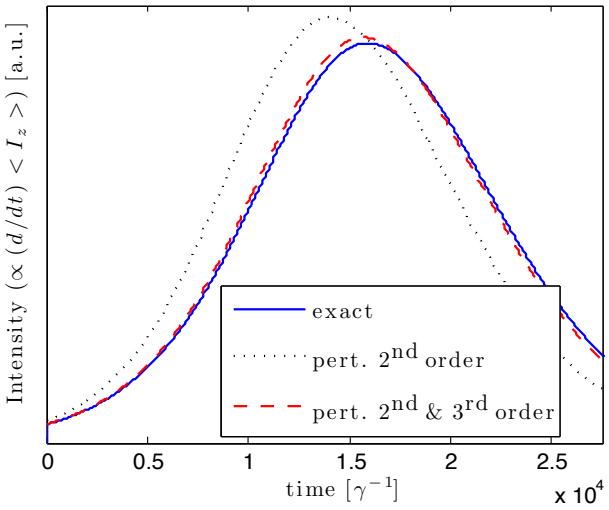


Figure 5.1: Comparison of the exact evolution according to Eqn. (5.45) (dashed) with the approximate solution up to second (dotted) and third (solid) order [Eqn. (5.59) & Eqn. (5.61)]. The figure shows the radiation intensity emitted from the electron spin ($\propto d/dt\langle I_z\rangle$) for a system of $N = 100$ nuclear spins, initially fully polarized in $z$ direction. The emission intensity shows clearly the characteristic superradiant burst (compare Figs. 2.2 and 3.2). Parameters are $\omega = \gamma/5$ and $\sqrt{N}g = 0.2\gamma$. The second-order effective evolution ($L_2^{\text{eff}}$) shows significant deviation from the exact dynamics. Addition of the third order $L_3^{\text{eff}}$, improves the approximation substantially.

The excellent agreement of the perturbative and exact solutions displayed in Fig. 5.1 supports the expectation that similar arguments hold in the general case $\omega \neq 0$ [Eqn. (5.61)] and effects due to the non-Lindblad form of the effective Liouvillian are of higher order in the perturbation. This question as well as the possibility to use the gauge invariance under the choice of $S^D$, in order to enforce exact Lindblad form in every order of the perturbation, is subject to future work.

## 5.5 Conclusions

We presented a generalized SW formalism, which adapts the successful perturbative tool of Hamiltonian quantum mechanics to the case of open quantum systems, whose evolution is governed by a Liouville operator. In analogy to the coherent case, we derive a transformation that decouples subspaces of slow dynamics from fast evolving degrees of freedom in a perturbative series. In comparison with alternative schemes for adiabatic elimination [278, 280, 279, 234], the advantages of the presented method are twofold. First, only marginal assumptions on the specific type of the zero-order dynamics $\mathcal{L}_0$ have to be made. The subspace to be eliminated can be high dimensional and undergoing involved dynamics. Second, our approach in principle is an exact decoupling scheme, and can be applied to all orders in the perturbation. This property is of particular relevance for instance in numerical studies of low excitation spectra

of the Liouville operator, e.g., in the context of dissipative phase transitions [79, 80, 77], and for error estimation in the context of quantum information processing [33]. The SW formalism provides a natural framework for the engineering of dissipative gadgets, e.g., in the context of state preparation and protection [32, 23, 33].

We employed the SW formalism exemplarily to two model systems and presented different schemes to evaluate the expressions for the effective Liouvillians. In a generic ancilla setting, we proved that the effective evolution of the weakly coupled system is up to second order Markovian, irrespective of the specific realization of the ancilla. In a second example we demonstrated that - in contrast to the standard schemes of adiabatic elimination - higher order corrections can readily be derived within the SW framework. In this model, the third order correction plays a significant role in the perturbative dynamics.

Further, we point out that the freedom of a gauge choice in the derivation of the transformation matrix could lead to a set of alternative perturbative approaches, which, in analogy to the standard SW transformation and depending on the specific problem, could prove to be advantageous under certain conditions. Potentially, this gauge freedom could also be used to ensure Lindblad form of the higher order effective Liouvillians. Lastly, we mention the numerous theoretical results [268] (e.g., linked cluster theorem, additivity of effective Hamiltonian), which have been derived in the context of coherent SW transformations as well as different variations of the SW method (e.g., continuous SW [286]), which may have open system analogs. These questions will be subject to future studies.

## 5.A Supplementary material 5

### 5.A.1 Lindblad form of Eqn. (5.41)

In the following, we prove that the dissipative part of the second-order effective Liouvillian Eqn. (5.41) is of Lindblad form. For this we have to show positivity of the respective coefficient matrix

$$\begin{aligned} &\mathcal{A} + \mathcal{A}^\dagger \geq 0, \\ \Leftrightarrow\ &\vec{v}^*(\mathcal{A} + \mathcal{A}^\dagger)\vec{v} \geq 0, \qquad \forall \vec{v} \in \mathbb{C}^n \end{aligned} \tag{5.65}$$

Expressing $\mathcal{A}$ as the integrated dyadic product [Eqn. (5.40)] we write

$$\begin{aligned} &\vec{v}^*(\mathcal{A} + \mathcal{A}^\dagger)\vec{v} \\ &= \int_0^\infty d\tau \left( \langle \vec{v}^* \Delta\vec{A} \Delta\vec{A}^*_\tau \vec{v} \rangle_{ss} + \langle \vec{v}^* \Delta\vec{A}_\tau \Delta\vec{A}^* \vec{v} \rangle_{ss} \right) \\ &= \int_0^\infty d\tau \left( \langle \sigma\sigma^\dagger_\tau \rangle_{ss} + \langle \sigma_\tau \sigma^\dagger \rangle_{ss} \right), \end{aligned} \tag{5.66}$$

where we introduced the ancilla operator $\sigma \equiv \vec{v}^* \Delta\vec{A}$.

Since the expectation values are evaluated in the ancilla's steady state, the two-time correlation functions are invariant under a total time translation $t$:

$$\langle \sigma\sigma^\dagger_\tau \rangle_{ss} = \langle \sigma_t \sigma^\dagger_{t+\tau} \rangle_{ss}, \tag{5.67}$$

$$\langle \sigma_\tau \sigma^\dagger \rangle_{ss} = \langle \sigma_{t+\tau} \sigma^\dagger_t \rangle_{ss}. \tag{5.68}$$

We exploit that property in symmetrizing Eqn. (5.66) in the time arguments. First we "average" Eqn. (5.66) over a total time translation

$$\begin{aligned}&\vec{v}^*(\mathcal{A}+\mathcal{A}^\dagger)\vec{v} \\ &= \frac{1}{t_0}\int_0^{t_0} dt \int_0^\infty d\tau \left(\langle\sigma_t\sigma_{t+\tau}^\dagger\rangle_{ss} + \langle\sigma_{t+\tau}\sigma_t^\dagger\rangle_{ss}\right) \\ &= \frac{1}{t_0}\int_0^{t_0} dt \int_t^\infty dt' \left(\langle\sigma_t\sigma_{t'}^\dagger\rangle_{ss} + \langle\sigma_{t'}\sigma_t^\dagger\rangle_{ss}\right),\end{aligned} \tag{5.69}$$

where the new variable $t' = t + \tau$ has been introduced. Basic integral transformations lead to the expression

$$\begin{aligned}&\vec{v}^*(\mathcal{A}+\mathcal{A}^\dagger)\vec{v} \\ &= \frac{1}{t_0}\int_0^{t_0} dt \int_0^{t_0} dt' \langle\sigma_t\sigma_{t'}^\dagger\rangle_{ss} \qquad \Big\} \text{(a)} \\ &\quad + \frac{1}{t_0}\int_0^{t_0} dt \int_{t_0}^\infty dt' \langle\sigma_t\sigma_{t'}^\dagger\rangle_{ss} \qquad \Big\} \text{(b)} \\ &\quad + \frac{1}{t_0}\int_0^{t_0} dt' \int_{t_0}^\infty dt \langle\sigma_t\sigma_{t'}^\dagger\rangle_{ss}. \qquad \Big\} \text{(c)}\end{aligned} \tag{5.70}$$

The first term of the latter equation ((a)) is positive since

$$\text{(1)} = \langle RR^\dagger\rangle_{ss} \geq 0, \tag{5.71}$$

with $R = \left(1/\sqrt{t_0}\right)\int_0^{t_0} dt\, \sigma_t$.

We show that the remaining terms vanish in the limit $t_0 \to \infty$, proving the Lindblad form of Eqn. (5.39). We estimate

$$\begin{aligned}\left|\text{(b)}\right| &= \left|\frac{1}{t_0}\int_0^{t_0} dt \int_{t_0-t}^\infty d\tau \langle\sigma\sigma_\tau^\dagger\rangle_{ss}\right| \\ &\leq \frac{1}{t_0}\int_0^{t_0} dt \int_{t_0-t}^\infty d\tau \left|\langle\sigma\sigma_\tau^\dagger\rangle_{ss}\right|,\end{aligned} \tag{5.72}$$

where we reintroduced the time difference integration variable $\tau = t' - t$ and used the time translation symmetry, Eqn. (5.67). Next the integration over $dt$ is divided into two parts defined by the parameter $x$: $\int_0^{t_0} dt = \int_0^{t_0-x} dt + \int_{t_0-x}^{t_0} dt$. The first term can be upper bounded as

$$\begin{aligned}&\frac{1}{t_0}\int_0^{t_0-x} dt \int_{t_0-t}^\infty d\tau \left|\langle\sigma\sigma_\tau^\dagger\rangle_{ss}\right| \\ &\qquad \leq \frac{1}{t_0}\int_0^{t_0-x} dt \int_x^\infty d\tau \left|\langle\sigma\sigma_\tau^\dagger\rangle_{ss}\right| \\ &\qquad \leq \int_x^\infty d\tau \left|\langle\sigma\sigma_\tau^\dagger\rangle_{ss}\right|.\end{aligned} \tag{5.73}$$

The second term can be estimated as

$$\begin{aligned}\frac{1}{t_0}\int_{t_0-x}^{t_0} dt \int_{t_0-t}^{\infty} d\tau \left|\langle\sigma\sigma_\tau^\dagger\rangle_{ss}\right| \\ \leq & \frac{1}{t_0}\int_{t_0-x}^{t_0} dt \int_{0}^{\infty} d\tau \left|\langle\sigma\sigma_\tau^\dagger\rangle_{ss}\right| \\ = & \frac{x}{t_0}\int_{0}^{\infty} d\tau \left|\langle\sigma\sigma_\tau^\dagger\rangle_{ss}\right| .\end{aligned} \tag{5.74}$$

Using the quantum regression theorem one shows that the time correlation function $\langle\sigma\sigma_\tau^\dagger\rangle_{ss}$ decays exponentially. Choosing the parameter $x = \sqrt{t_0}$ both the right-hand sides of Eqn. (5.73) and Eqn. (5.74) vanish in the limit $t_0 \to \infty$. In an analogous estimation one shows the vanishing of the remaining term (c) which proves the positivity, Eqn. (5.65), and thus the Lindblad form of Eqn. (5.41).

# Bibliography


[1] J. P. Dowling and G. J. Milburn. *Quantum technology: the second quantum revolution.* Philosophical Transactions of the Royal Society A: Mathematical, Physical and Engineering Sciences **361**(1809), 1655 (2003).

[2] T. H. Maiman. *Stimulated Optical Radiation in Ruby.* Nature Physics **187**(4736), 493 (1960).

[3] A. Javan, W. R. Bennett, and D. R. Herriott. *Population Inversion and Continuous Optical Maser Oscillation in a Gas Discharge Containing a He-Ne Mixture.* Phys. Rev. Lett. **6**(3), 106 (1961).

[4] L. M. Duan, M. D. Lukin, J. I. Cirac, and P. Zoller. *Long-distance quantum communication with atomic ensembles and linear optics.* Nature Physics **414**(6862), 413 (2001).

[5] R. Ursin, *et al.*. *Entanglement-based quantum communication over 144 km.* Nature Physics **3**(7), 481 (2007).

[6] C. H. Bennett. *Quantum Cryptography : Public Key Distribution and Coin Tossing.* Proc of IEEE Int Conf on Computers, Systems and Signal Processing (1984).

[7] A. K. Ekert. *Quantum cryptography based on Bell's theorem.* Phys. Rev. Lett. **67**(6), 661 (1991).

[8] N. Gisin, G. Ribordy, W. Tittel, and H. Zbinden. *Quantum cryptography.* Reviews of Modern Physics **74**(1), 145 (2002).

[9] P. W. Shor. *Polynomial-Time Algorithms for Prime Factorization and Discrete Logarithms on a Quantum Computer.* SIAM Review **41**(2), 303 (1999).

[10] M. W. Johnson, *et al.*. *Quantum annealing with manufactured spins.* Nature Physics **473**(7346), 194 (2011).

[11] T. Udem, R. Holzwarth, and T. W. Hänsch. *Optical frequency metrology.* Nature Physics **416**(6877), 233 (2002).

[12] C. F. Roos, M. Chwalla, K. Kim, M. Riebe, and R. Blatt. *'Designer atoms' for quantum metrology.* Nature Physics **443**(7109), 316 (2006).

[13] V. Giovannetti, S. Lloyd, and L. Maccone. *Advances in quantum metrology.* Nature Photonics **5**(4), 222 (2011).

[14] C. Cohen-Tannoudji, J. Dupont-Roc, and G. Grynberg. *Photons and Atoms: Introduction to Quantum Electrodynamics.* Wiley VCH, Weinheim (1997).

[15] A. Einstein. *Zur Quantentheorie der Strahlung.* Physikalische Zeitschrift **18**, 121 (1917).

[16] R. H. Dicke. *Coherence in Spontaneous Radiation Processes.* Physical Review **93**(1), 99 (1954).

[17] M. Gross and S. Haroche. *Superradiance: An essay on the theory of collective spontaneous emission.* Physics Reports **93**, 301 (1982).

[18] D. F. Walls and G. J. Milburn. *Effect of dissipation on quantum coherence.* Physical Review A **31**(4), 2403 (1985).

[19] A. J. Bray and M. A. Moore. *Influence of Dissipation on Quantum Coherence.* Phys. Rev. Lett. **49**(21), 1545 (1982).

[20] D. P. DiVincenzo. *Topics in Quantum Computers.* arXiv:9612126 (1996).

[21] J. F. Poyatos, J. I. Cirac, and P. Zoller. *Quantum Reservoir Engineering with Laser Cooled Trapped Ions.* Physical Review Letters **77**(23), 4728 (1996).

[22] S. Diehl, A. Micheli, A. Kantian, B. Kraus, H. P. Büchler, and P. Zoller. *Quantum states and phases in driven open quantum systems with cold atoms.* Nature Physics **4**(11), 878 (2008).

[23] B. Kraus, H. Büchler, S. Diehl, A. Kantian, A. Micheli, and P. Zoller. *Preparation of entangled states by quantum Markov processes.* Physical Review A **78**(4), 042307 (2008).

[24] J. Cho, S. Bose, and M. S. Kim. *Optical Pumping into Many-Body Entanglement.* Physical Review Letters **106**(2), 020504 (2011).

[25] A. Tomadin, S. Diehl, and P. Zoller. *Nonequilibrium phase diagram of a driven and dissipative many-body system.* Physical Review A **83**(1) (2011).

[26] J. T. Barreiro, P. Schindler, O. Gühne, T. Monz, M. Chwalla, C. F. Roos, M. Hennrich, and R. Blatt. *Experimental multiparticle entanglement dynamics induced by decoherence.* Nature Physics **6**(12), 943 (2010).

[27] F. Benatti, R. Floreanini, and U. Marzolino. *Entangling two unequal atoms through a common bath.* Physical Review A **81**(1), 012105 (2010).

[28] M. B. Plenio and S. F. huelga. *Entangled Light from White Noise.* Physical Review Letters **88**(19), 197901 (2002).

[29] S. Diehl, A. Tomadin, A. Micheli, R. Fazio, and P. Zoller. *Dynamical Phase Transitions and Instabilities in Open Atomic Many-Body Systems.* Physical Review Letters **105**(1), 015702 (2010).

[30] M. J. Kastoryano, F. Reiter, and A. S. Sørensen. *Dissipative Preparation of Entanglement in Optical Cavities.* Physical Review Letters **106**(9), 090502 (2011).

[31] B. Kraus and J. I. Cirac. *Discrete Entanglement Distribution with Squeezed Light.* Physical Review Letters **92**(1), 013602 (2004).

[32] F. Verstraete, M. M. Wolf, and J. I. Cirac. *Quantum computation and quantum-state engineering driven by dissipation.* Nature Physics **5**(9), 633 (2009).

[33] F. Pastawski, L. Clemente, and J. I. Cirac. *Quantum memories based on engineered dissipation.* Physical Review A **83**(1), 012304 (2011).

[34] J. Kerckhoff, H. I. Nurdin, D. S. Pavlichin, and H. Mabuchi. *Designing Quantum Memories with Embedded Control: Photonic Circuits for Autonomous Quantum Error Correction.* Physical Review Letters **105**(4), 040502 (2010).

[35] J. T. Barreiro, M. Müller, P. Schindler, D. Nigg, T. Monz, M. Chwalla, M. Hennrich, C. F. Roos, P. Zoller, and R. Blatt. *An open-system quantum simulator with trapped ions.* Nature Physics **470**(7335), 486 (2011).

[36] H. Weimer, M. Müller, I. Lesanovsky, P. Zoller, and H. P. Büchler. *A Rydberg quantum simulator.* Nature Physics **6**(5), 382 (2010).

[37] D. Deutsch. *The Fabric of Reality* . Penguin Books (1998).

[38] R. Feynman and P. W. Shor. *Simulating Physics with Computers* . SIAM Journal on Computing **26**, 1484 (1982).

[39] D. Deutsch. *Quantum Theory, the Church-Turing Principle and the Universal Quantum Computer.* Proceedings of the Royal Society A: Mathematical, Physical and Engineering Sciences **400**(1818), 97 (1985).

[40] J. I. Cirac and P. Zoller. *Quantum Computations with Cold Trapped Ions.* Physical Review Letters **74**(20), 4091 (1995).

[41] C. Monroe, D. M. Meekhof, B. E. King, W. M. Itano, and D. J. Wineland. *Demonstration of a Fundamental Quantum Logic Gate.* Physical Review Letters **75**(25), 4714 (1995).

[42] T. D. Ladd, F. Jelezko, R. Laflamme, Y. Nakamura, C. Monroe, and J. L. O'Brien. *Quantum computers.* Nature Physics **464**(7285), 45 (2010).

[43] R. Raussendorf and H. J. Briegel. *A One-Way Quantum Computer.* Physical Review Letters **86**(22), 5188 (2001).

[44] E. Farhi, J. Goldstone, S. Gutmann, and M. Sipser. *Quantum Computation by Adiabatic Evolution.* arXiv:0001106 (2000).

[45] A. Y. Kitaev. *Fault-tolerant quantum computation by anyons.* Annals of Physics **303**(1), 2 (2003).

[46] A. Das and B. K. Chakrabarti. *Colloquium: Quantum annealing and analog quantum computation.* Reviews of Modern Physics **80**(3), 1061 (2008).

[47] J. I. Cirac and P. Zoller. *Goals and opportunities in quantum simulation.* Nature Physics **8**(4), 264 (2012).

[48] B. E. Kane. *A silicon-based nuclear spin quantum computer.* Nature **393**(6681), 133 (1998).

[49] J. Clarke and F. K. Wilhelm. *Superconducting quantum bits.* Nature Physics **453**(7198), 1031 (2008).

[50] D. Loss and D. P. DiVincenzo. *Quantum computation with quantum dots.* Physical Review A **57**(1), 120 (1998).

[51] B. Urbaszek, X. Marie, T. Amand, O. Krebs, P. Voisin, P. Maletinsky, A. Hogele, and A. Imamoglu. *Nuclear spin physics in quantum dots: an optical investigation.* arXiv:1202.4637 (2012).

[52] N. Y. Yao, L. Jiang, A. V. Gorshkov, P. C. Maurer, G. Giedke, J. I. Cirac, and M. D. Lukin. *Scalable architecture for a room temperature solid-state quantum information processor.* Nature Physics **3**, 800 (2012).

[53] A. M. Steane. *Quantum Computing and Error Correction.* arXiv:0304016 (2003).

[54] P. W. Shor. *Fault-tolerantquantum computation.* In *37th Annual Symposium on Foundations of Computer Science*, pp. 56–65. IEEE Comput. Soc. Press (1996).

[55] P. W. Shor. *Scheme for reducing decoherence in quantum computer memory.* Physical Review A **52**(4), R2493 (1995).

[56] R. Raussendorf, J. Harrington, and K. Goyal. *Topological fault-tolerance in cluster state quantum computation.* New Journal of Physics **9**(6), 199 (2007).

[57] D. S. Wang, A. G. Fowler, and L. C. L. Hollenberg. *Surface code quantum computing with error rates over 1$%$.* Physical Review A **83**(2), 020302 (2011).

[58] A. G. Fowler, A. M. Stephens, and P. Groszkowski. *High-threshold universal quantum computation on the surface code.* Physical Review A **80**(5), 052312 (2009).

[59] R. Raussendorf and J. Harrington. *Fault-Tolerant Quantum Computation with High Threshold in Two Dimensions.* Physical Review Letters **98**(19), 190504 (2007).

[60] N. Greenspan and A. Ehlers. *Max Born: Baumeister der Quantenmechanik. Eine Biographie.* Spektrum Akademischer Verlag, Berlin (2008).

[61] S. Wolfram. *A new kind of science.* Wolfram Media, Boston (2002).

[62] P. M. Chaikin and T. C. Lubensky. *Principles of Condensed Matter Physics.* Cambridge University Press, Cambridge (2000).

[63] H. E. Stanley. *Mean field theory of magnetic phase transitions.* Oxford University Press (1971).

[64] J. Bardeen, L. N. Cooper, and J. R. Schrieffer. *Microscopic Theory of Superconductivity.* Physical Review **106**(1), 162 (1957).

[65] S. Sachdev. *Quantum Phase Transitions.* Cambridge University Press, Cambridge (1999).

[66] M. Vojta. *Quantum phase transitions.* Reports on Progress in Physics **66**(12), 2069 (2003).

[67] H. Stanley. *Scaling, universality, and renormalization: Three pillars of modern critical phenomena.* Reviews of Modern Physics **71**(2), S358 (1999).

[68] D. Jaksch, C. Bruder, J. I. Cirac, C. W. Gardiner, and P. Zoller. *Cold Bosonic Atoms in Optical Lattices.* Physical Review Letters **81**(15), 3108 (1998).

[69] F. Dalfovo, S. Giorgini, L. P. Pitaevskii, and S. Stringari. *Theory of Bose-Einstein condensation in trapped gases.* Reviews of Modern Physics **71**(3), 463 (1999).

[70] M. H. Anderson, J. R. Ensher, M. R. Matthews, C. E. Wieman, and E. A. Cornell. *Observation of Bose-Einstein Condensation in a Dilute Atomic Vapor.* Science (New York, N.Y.) **269**(5221), 198 (1995).

[71] K. B. Davis, M. O. Mewes, M. R. Andrews, N. J. van Druten, D. S. Durfee, D. M. Kurn, and W. Ketterle. *Bose-Einstein Condensation in a Gas of Sodium Atoms.* Physical Review Letters **75**(22), 3969 (1995).

[72] X. G. Wen. *Quantum Field Theory of Many-Body Systems.* Oxford University Press, New York (2004).

[73] H. T. Diep. *Frustrated Spin Systems.* World Scientific, Singapore (2005).

[74] A. B. Migdal. *Superfluidity and the moments of inertia of nuclei.* Annals of Physics **13**(5), 655 (1959).

[75] S. Giorgini, L. P. Pitaevskii, and S. Stringari. *Theory of ultracold atomic Fermi gases.* Reviews of Modern Physics **80**(4), 1215 (2008).

[76] E. Kim and M. H. W. Chan. *Probable observation of a supersolid helium phase.* Nature **427**(6971), 225 (2004).

[77] H. J. Carmichael. *Analytical and numerical results for the steady state in cooperative resonance fluorescence.* Journal of Physics B: Atomic and Molecular Physics **13**(18), 3551 (1980).

[78] K. Baumann, C. Guerlin, F. Brennecke, and T. Esslinger. *Dicke quantum phase transition with a superfluid gas in an optical cavity.* Nature **464**(7293), 1301 (2010).

[79] E. M. Kessler, G. Giedke, A. Imamoglu, S. F. Yelin, M. D. Lukin, and J. I. Cirac. *Dissipative phase transition in a central spin system.* Physical Review A **86**(1), 012116 (2012).

[80] S. Morrison and A. S. Parkins. *Dissipation-driven quantum phase transitions in collective spin systems.* Journal of Physics B: Atomic, Molecular and Optical Physics **41**(19), 195502 (2008).

[81] J. Kasprzak, *et al.*. *Bose–Einstein condensation of exciton polaritons.* Nature Physics **443**(7110), 409 (2006).

[82] P. Colli, N. Kenmochi, and J. Sprekels. *Dissipative Phase Transitions.* World Scientific, Singapore (2006).

[83] B. Öztop, M. Bordyuh, Ö. E. Müstecaplıoğlu, and H. E. Türeci. *Excitations of optically driven atomic condensate in a cavity: theory of photodetection measurements.* arXiv:1107.3108v1 **quant-ph** (2011).

[84] N. Lambert, C. Emary, and T. Brandes. *Entanglement and the Phase Transition in Single-Mode Superradiance.* Phys. Rev. Lett. **92**, 73602 (2004).

[85] R. P. Feynman. *There's plenty of room at the bottom.* Engineering and Science **23**(5), 22 (1960).

[86] F. Rossi (ed.). *Semiconductor Macroatoms: Basics Physics and Quantum-Device Applications* . World-Scientific, Singapore (2005).

[87] P. Michler (ed.). *Single Semiconductor Quantum Dots.* Springer (2009).

[88] A. Y. Cho and J. R. Arthur. *Molecular beam epitaxy.* Progress in Solid State Chemistry **10**, 157 (1975).

[89] P. Y. Yu and M. Cardona. *Fundamentals of Semiconductors.* Springer (2010).

[90] C. Kloeffel and D. Loss. *Prospects for Spin-Based Quantum Computing.* arXiv:1204.5917v1 **cond-mat.mes-hall** (2012).

[91] J. M. Elzerman, R. Hanson, L. H. Willems van Beveren, B. Witkamp, L. M. K. Vandersypen, and L. P. Kouwenhoven. *Single-shot read-out of an individual electron spin in a quantum dot.* Nature Physics **430**(6998), 431 (2004).

[92] F. H. L. Koppens, C. Buizert, K. J. Tielrooij, I. T. Vink, K. C. Nowack, T. Meunier, L. P. Kouwenhoven, and L. M. K. Vandersypen. *Driven coherent oscillations of a single electron spin in a quantum dot.* Nature Physics **442**(7104), 766 (2006).

[93] J. R. Petta, A. C. Johnson, J. M. Taylor, L. E. A, A. Yacoby, M. D. Lukin, C. M. Marcus, M. P. Hanson, and A. C. Gossard. *Coherent Manipulation of Coupled Electron Spins in Semiconductor Quantum Dots.* Science (New York, N.Y.) **309**(5744), 2180 (2005).

[94] A. Imamog lu, D. D. Awschalom, G. Burkard, D. P. DiVincenzo, D. Loss, M. Sherwin, and A. Small. *Quantum Information Processing Using Quantum Dot Spins and Cavity QED.* Physical Review Letters **83**(20), 4204 (1999).

[95] A. Badolato, K. Hennessy, M. Atatüre, J. Dreiser, E. Hu, P. M. Petroff, and A. Imamoglu. *Deterministic Coupling of Single Quantum Dots to Single Nanocavity Modes.* Science (New York, N.Y.) **308**(5725), 1158 (2005).

[96] A. Kress, F. Hofbauer, N. Reinelt, M. Kaniber, H. J. Krenner, R. Meyer, G. Böhm, and J. J. Finley. *Manipulation of the spontaneous emission dynamics of quantum dots in two-dimensional photonic crystals.* Physical Review B **71**(24), 241304 (2005).

[97] O. Gywat, H. J. Krenner, and J. Berezovski. *Spins in Optically Active Quantum Dots*. Wiley VCH, Weinheim (2010).

[98] J. Schliemann, A. Khaetskii, and D. Loss. *Electron spin dynamics in quantum dots and related nanostructures due to hyperfine interaction with nuclei*. J. Phys: Cond. Mat. **15**, R1809 (2003).

[99] J. Berezovsky, M. H. Mikkelsen, N. G. Stoltz, L. A. Coldren, and D. D. Awschalom. *Picosecond Coherent Optical Manipulation of a Single Electron Spin in a Quantum Dot*. Science (New York, N.Y.) **320**(5874), 349 (2008).

[100] D. Press, T. D. Ladd, B. Zhang, and Y. Yamamoto. *Complete quantum control of a single quantum dot spin using ultrafast optical pulses*. Nature Physics **456**(7219), 218 (2008).

[101] M. Atatüre, J. Dreiser, A. Badolato, A. Hogele, K. Karrai, and A. Imamoglu. *Quantum-Dot Spin-State Preparation with Near-Unity Fidelity*. Science (New York, N.Y.) **312**(5773), 551 (2006).

[102] T. M. Godden, S. J. Boyle, A. J. Ramsay, A. M. Fox, and M. S. Skolnick. *Fast high fidelity hole spin initialization in a single InGaAs quantum dot*. Applied Physics Letters **97**(6), 061113 (2010).

[103] A. Laucht, J. Villas-Bôas, S. Stobbe, N. Hauke, F. Hofbauer, G. Böhm, P. Lodahl, M. C. Amann, M. Kaniber, and J. Finley. *Mutual coupling of two semiconductor quantum dots via an optical nanocavity*. Physical Review B **82**(7), 075305 (2010).

[104] E. A. Chekhovich, M. N. Makhonin, K. V. Kavokin, A. B. Krysa, M. S. Skolnick, and A. I. Tartakovskii. *Pumping of Nuclear Spins by Optical Excitation of Spin-Forbidden Transitions in a Quantum Dot*. Physical Review Letters **104**(6), 066804 (2010).

[105] F. Klotz, V. Jovanov, J. Kierig, E. Clark, M. Bichler, G. Abstreiter, M. S. Brandt, J. J. Finley, H. Schwager, and G. Giedke. *Asymmetric optical nuclear spin pumping in a single uncharged quantum dot*. Physical Review B **82**(12), 121307 (2010).

[106] D. Stepanenko, G. Burkard, G. Giedke, and A. Imamoglu. *Enhancement of Electron Spin Coherence by Optical Preparation of Nuclear Spins*. Physical Review Letters **96**(13), 136401 (2006).

[107] D. Klauser, W. A. Coish, and D. Loss. *Nuclear spin state narrowing via gate-controlled Rabi oscillations in a double quantum dot*. Physical Review B **73**(20), 205302 (2006).

[108] G. Giedke, J. M. Taylor, D. D'Alessandro, M. D. Lukin, and A. Imamoglu. *Quantum measurement of a mesoscopic spin ensemble*. Physical Review A **74**(3), 032316 (2006).

[109] C. Latta, *et al.*. *Confluence of resonant laser excitation and bidirectional quantum-dot nuclear-spin polarization*. Nature Physics **5**(10), 758 (2009).

[110] I. T. Vink, K. C. Nowack, F. H. L. Koppens, J. Danon, Y. V. Nazarov, and L. M. K. Vandersypen. *Locking electron spins into magnetic resonance by electron–nuclear feedback*. Nature Physics **5**(10), 764 (2009).

[111] M. Gaudin. *Diagonalisation d'une classe d'hamiltoniens de spin.* J. Phys. France **37**(10), 1087 (1976).

[112] M. Bortz and J. Stolze. *Spin and entanglement dynamics in the central-spin model with homogeneous couplings.* J. Stat. Mech. **2007**(06), P06018 (2007).

[113] P. F. Braun, B. Urbaszek, T. Amand, X. Marie, O. Krebs, B. Eble, A. Lemaître, and P. Voisin. *Bistability of the nuclear polarization created through optical pumping in $In_{1-x}Ga_xAs$ quantum dots.* Physical Review B **74**(24), 245306 (2006).

[114] P. Maletinsky, C. W. Lai, A. Badolato, and A. Imamoglu. *Nonlinear dynamics of quantum dot nuclear spins.* Physical Review B **75**(3), 035409 (2007).

[115] A. I. Tartakovskii, *et al.*. *Nuclear Spin Switch in Semiconductor Quantum Dots.* Physical Review Letters **98**(2), 026806 (2007).

[116] O. Krebs, P. Maletinsky, T. Amand, B. Urbaszek, A. Lemaître, P. Voisin, X. Marie, and A. Imamoglu. *Anomalous Hanle Effect due to Optically Created Transverse Overhauser Field in Single InAs/GaAs Quantum Dots.* Physical Review Letters **104**(5), 056603 (2010).

[117] G. Davies and M. F. Hamer. *Optical Studies of the 1.945 eV Vibronic Band in Diamond.* Proceedings of the Royal Society A: Mathematical, Physical and Engineering Sciences **348**(1653), 285 (1976).

[118] A. Gruber, A. Dräbenstedt, C. Tietz, L. Fleury, J. Wrachtrup, and C. v. Borczyskowski. *Scanning Confocal Optical Microscopy and Magnetic Resonance on Single Defect Centers.* Science **276**(5321), 2012 (1997).

[119] F. Jelezko and J. Wrachtrup. *Single defect centres in diamond: A review.* physica status solidi (a) **203**(13), 3207 (2006).

[120] P. Tamarat, *et al.*. *Spin-flip and spin-conserving optical transitions of the nitrogen-vacancy centre in diamond.* New Journal of Physics **10**(4), 045004 (2008).

[121] J. Maze. *Quantum manipulation of nitrogen-vacancy centers in diamond : from basic properties to applications.* Ph.D. thesis, Harvard University (2010).

[122] F. Jelezko, T. Gaebel, I. Popa, A. Gruber, and J. Wrachtrup. *Observation of Coherent Oscillations in a Single Electron Spin.* Physical Review Letters **92**(7), 076401 (2004).

[123] R. Hanson, O. Gywat, and D. D. Awschalom. *Room-temperature manipulation and decoherence of a single spin in diamond.* Physical Review B **74**(16), 161203 (2006).

[124] J. H. N. Loubser and J. A. v. Wyk. *Electron spin resonance in the study of diamond.* Journal of Physics C Solid State Physics **41**(8), 1201 (2001).

[125] L. Robledo, L. Childress, H. Bernien, B. Hensen, P. F. A. Alkemade, and R. Hanson. *High-fidelity projective read-out of a solid-state spin quantum register.* Nature **477**(7366), 574 (2011).

[126] P. Tamarat, *et al.*. *Stark Shift Control of Single Optical Centers in Diamond.* Physical Review Letters **97**(8), 083002 (2006).

[127] P. L. Stanwix, L. M. Pham, J. R. Maze, D. Le Sage, T. K. Yeung, P. Cappellaro, P. R. Hemmer, A. Yacoby, M. D. Lukin, and R. L. Walsworth. *Coherence of nitrogen-vacancy electronic spin ensembles in diamond.* Physical Review B **82**(20), 201201 (2010).

[128] H. Bluhm, S. Foletti, I. Neder, M. Rudner, D. Mahalu, V. Umansky, and A. Yacoby. *Dephasing Time of Gaas Electron-Spin Qubits Coupled to a Nuclear Bath Exceeding 200 microseconds.* Nature Physics **7**(2), 109 (2010).

[129] M. V. G. Dutt, L. Childress, L. Jiang, E. Togan, J. Maze, F. Jelezko, A. S. Zibrov, P. R. Hemmer, and M. D. Lukin. *Quantum Register Based on Individual Electronic and Nuclear Spin Qubits in Diamond.* Science (New York, N.Y.) **316**(5829), 1312 (2007).

[130] K. Stannigel, P. Rabl, A. S. Sørensen, P. Zoller, and M. D. Lukin. *Optomechanical Transducers for Long-Distance Quantum Communication.* Physical Review Letters **105**(22) (2010).

[131] G. Balasubramanian, *et al.*. *Nanoscale imaging magnetometry with diamond spins under ambient conditions.* Nature **455**(7213), 648 (2008).

[132] R. Said, D. Berry, and J. Twamley. *Nanoscale magnetometry using a single-spin system in diamond.* Physical Review B **83**(12) (2011).

[133] J. M. Taylor, P. Cappellaro, L. Childress, L. Jiang, D. Budker, P. R. Hemmer, A. Yacoby, R. Walsworth, and M. D. Lukin. *High-sensitivity diamond magnetometer with nanoscale resolution.* Nature Physics **4**(10), 810 (2008).

[134] A. Gali, M. Fyta, and E. Kaxiras. *Ab initio supercell calculations on nitrogen-vacancy center in diamond: Electronic structure and hyperfine tensors.* Physical Review B **77**(15), 155206 (2008).

[135] L. Childress, M. V. Gurudev Dutt, J. M. Taylor, A. S. Zibrov, F. Jelezko, J. Wrachtrup, P. R. Hemmer, and M. D. Lukin. *Coherent Dynamics of Coupled Electron and Nuclear Spin Qubits in Diamond.* Science (New York, N.Y.) **314**(5797), 281 (2006).

[136] P. C. Maurer, *et al.*. *Room-Temperature Quantum Bit Memory Exceeding One Second.* Science (New York, N.Y.) **336**(6086), 1283 (2012).

[137] E. Togan, Y. Chu, A. Imamoglu, and M. D. Lukin. *Laser cooling and real-time measurement of the nuclear spin environment of a solid-state qubit.* Nature **478**(7370), 497 (2011).

[138] N. Chisholm, P. Maurer, G. Kucsko, P. Lo, N. Yao, B. Shields, H. Park, and M. Lukin. *Towards room temperature magnetic sensing of a single electron spin in biological systems.* APS Division of Atomic, Molecular and Optical Physics Meeting Abstracts (2011).

[139] A. Aspect, E. Arimondo, R. Kaiser, N. Vansteenkiste, and C. Cohen-Tannoudji. *Laser Cooling below the One-Photon Recoil Energy by Velocity-Selective Coherent Population Trapping.* Phys. Rev. Lett. **61**(7), 826 (1988).

[140] J. Schrieffer and P. Wolff. *Relation between the Anderson and Kondo Hamiltonians.* Physical Review **149**(2), 491 (1966).

[141] G. Alzetta, A. Gozzini, L. Moi, and G. Orriols. *An experimental method for the observation of r.f. transitions and laser beat resonances in oriented Na vapour.* Il Nuovo Cimento B **36**(1), 5 (1976).

[142] L. V. Hau, S. E. Harris, Z. Dutton, and C. H. Behroozi. *Light speed reduction to 17 metres per second in an ultracold atomic gas : Article : Nature.* Nature **397**(6720), 594 (1999).

[143] M. Fleischhauer and M. D. Lukin. *Dark-State Polaritons in Electromagnetically Induced Transparency.* Physical Review Letters **84**(22), 5094 (2000).

[144] M. Fleischhauer, A. Imamoglu, and J. P. Marangos. *Electromagnetically induced transparency: Optics in coherent media.* Reviews of Modern Physics **77**(2), 633 (2005).

[145] A. V. Khaetskii, D. Loss, and L. Glazman. *Electron Spin Decoherence in Quantum Dots due to Interaction with Nuclei.* Physical Review Letters **88**(18), 186802 (2002).

[146] J. M. Taylor, J. R. Petta, A. C. Johnson, A. Yacoby, C. M. Marcus, and M. D. Lukin. *Relaxation, dephasing, and quantum control of electron spins in double quantum dots.* Physical Review B **76**(3), 035315 (2007).

[147] M. Claassen, H. E. Türeci, and A. Imamoglu. *Solid-State Spin-Photon Quantum Interface without Spin-Orbit Coupling.* Physical Review Letters **104**(17), 177403 (2010).

[148] D. J. Reilly, J. M. Taylor, J. R. Petta, C. M. Marcus, M. P. Hanson, and A. C. Gossard. *Suppressing Spin Qubit Dephasing by Nuclear State Preparation.* Science **321**, 817 (2008).

[149] S. W. Brown, T. A. Kennedy, D. Gammon, and E. S. Snow. *Spectrally resolved Overhauser shifts in single GaAs/Al$_x$Ga$_1-x$As quantum dots.* Physical Review B **54**, 17339 (1996).

[150] B. Eble, O. Krebs, A. Lemaître, K. Kowalik, A. Kudelski, P. Voisin, B. Urbaszek, X. Marie, and T. Amand. *Dynamic nuclear polarization of a single charge-tunable InAs/GaAs quantum dot.* Physical Review B **74**(8), 081306 (2006).

[151] P. Maletinsky, A. Badolato, and A. Imamoglu. *Dynamics of Quantum Dot Nuclear Spin Polarization Controlled by a Single Electron.* Physical Review Letters **99**(5), 056804 (2007).

[152] E. A. Chekhovich, M. N. Makhonin, K. V. Kavokin, A. B. Krysa, M. S. Skolnick, and A. I. Tartakovskii. *Pumping of Nuclear Spins by Optical Excitation of Spin-Forbidden Transitions in a Quantum Dot.* Physical Review Letters **104**(6), 066804 (2010).

[153] D. Stepanenko, G. Burkard, G. Giedke, and A. Imamoglu. *Enhancement of Electron Spin Coherence by Optical Preparation of Nuclear Spins.* Physical Review Letters **96**(13), 136401 (2006).

[154] X. Xu, W. Yao, B. Sun, D. G. Steel, A. S. Bracker, D. Gammon, and L. J. Sham. *Optically controlled locking of the nuclear field via coherent dark-state spectroscopy.* Nature **459**, 1105 (2009).

[155] D. Brunner, B. D. Gerardot, P. A. Dalgarno, G. Wüst, K. Karrai, N. G. Stoltz, P. M. Petroff, and R. J. Warburton. *A Coherent Single-Hole Spin in a Semiconductor*. Science **325**, 70 (2009).

[156] F. Bardou, J. P. Bouchaud, O. Emile, A. Aspect, and C. Cohen-Tannoudji. *Subrecoil laser cooling and Lévy flights*. Physical Review Letters **72**, 203 (1994).

[157] A. V. Chechkin, R. Metzler, J. Klafter, and V. Y. Gonchar. *Introduction to the Theory of Levy Flights*. In R. Klages, G. Radons, and I. M. Sokolov (eds.), *Anomalous Transport: Foundations and Applications*, pp. 129–162. Wiley VCH (2008).

[158] D. Brockmann, L. Hufnagel, and T. Geisel. *The scaling laws of human travel*. Nature Physics **439**(7075), 462 (2006).

[159] P. Barthelemy, J. Bertolotti, and D. S. Wiersma. *A Lévy flight for light*. Nature Physics **453**(7194), 495 (2008).

[160] N. Mercadier, W. Guerin, M. Chevrollier, and R. Kaiser. *Lévy flights of photons in hot atomic vapours*. Nature Physics **5**(8), 602 (2009).

[161] F. Bardou, J. P. Bouchaud, A. Aspect, and C. Cohen-Tannoudji. *Levy Statistics and Laser Cooling*. Cambridge University Press, Cambridge (2002).

[162] A. Greilich, A. Shabaev, D. R. Yakovlev, A. L. Efros, I. A. Yugova, D. Reuter, A. D. Wieck, and M. Bayer. *Nuclei-Induced Frequency Focusing of Electron Spin Coherence*. Science **317**, 1896 (2007).

[163] W. R. Kelly, Z. Dutton, J. Schlafer, B. Mookerji, and T. A. Ohki. *Direct Observation of Coherent Population Trapping in a Superconducting Artificial Atom*. Physical Review Letters **104**(16), 163601 (2010).

[164] I. Shavitt and L. T. Redmon. *Quasidegenerate perturbation theories. A canonical van Vleck formalism and its relationship to other approaches*. The Journal of Chemical Physics **73**(11), 5711 (1980).

[165] D. J. Klein. *Degenerate perturbation theory*. The Journal of Chemical Physics **61**(3), 786 (1974).

[166] W. K. Hastings. *Monte Carlo sampling methods using Markov chains and their applications*. Biometrika **57**(1), 97 (1970).

[167] V. V. Temnov and U. Woggon. *Superradiance and Subradiance in an Inhomogeneously Broadened Ensemble of Two-Level Systems Coupled to a Low-Q Cavity*. Physical Review Letters **95**(24), 243602 (2005).

[168] C. Leonardi and A. Vaglica. *Superradiance and inhomogeneous broadening. II: Spontaneous emission by many slightly detuned sources*. Nuovo Cimento B Serie **67**, 256 (1982).

[169] N. E. Rehler and J. H. Eberly. *Superradiance*. Physical Review A **3**(5), 1735 (1971).

[170] R. Bonifacio, P. Schwendimann, and F. Haake. *Quantum Statistical Theory of Superradiance. I.* Physical Review A **4**(1), 302 (1971).

[171] C. Lee. *Exact solution of the superradiance master equation. II. Arbitrary initial excitation.* Physical Review A **16**(1), 301 (1977).

[172] M. O. Scully and A. A. Svidzinsky. *The Super of Superradiance.* Science (New York, N.Y.) **325**(5947), 1510 (2009).

[173] T. Brandes. *Coherent and collective quantum optical effects in mesoscopic systems.* Phys. Rep. **408**(5-6), 315 (2005).

[174] G. S. Agarwal. *Master-Equation Approach to Spontaneous Emission. III. Many-Body Aspects of Emission from Two-Level Atoms and the Effect of Inhomogeneous Broadening.* Physical Review A **4**, 1791 (1971).

[175] A. T. Collins, G. Davies, H. Kanda, and G. S. Woods. *Spectroscopic studies of carbon-13 synthetic diamond.* Journal of Physics C Solid State Physics **21**, 1363 (1988).

[176] A. Lenef, S. W. Brown, D. A. Redman, S. C. Rand, J. Shigley, and E. Fritsch. *Electronic structure of the N-V center in diamond: Experiments.* Physical Review B **53**, 13427 (1996).

[177] A. T. Collins, M. F. Thomaz, and M. I. B. Jorge. *Luminescence decay time of the 1.945 eV centre in type Ib diamond.* Journal of Physics C Solid State Physics **16**, 2177 (1983).

[178] A. S. Bracker, *et al.*. *Optical Pumping of the Electronic and Nuclear Spin of Single Charge-Tunable Quantum Dots.* Physical Review Letters **94**(4), 047402 (2005).

[179] G. Finkelstein, V. Umansky, I. Bar-Joseph, V. Ciulin, S. Haacke, J. D. Ganière, and B. Deveaud. *Charged exciton dynamics in GaAs quantum wells.* Physical Review B **58**, 12637 (1998).

[180] F. Henneberger and O. Benson (eds.). *Semiconductor Quantum Bits.* Pan Stanford Publishing, Singapore (2009).

[181] A. M. Rey, L. Jiang, M. Fleischhauer, E. Demler, and M. D. Lukin. *Many-body protected entanglement generation in interacting spin systems.* Physical Review A **77**(5), 052305 (2008).

[182] A. V. Andreev, V. I. Emel'Yanov, and Il'Inskii. *Cooperative Effects in Optics.* IOP Publishing (1993).

[183] P. Maletinsky. *Polarization and manipulation of a mesoscopic nuclear spin ensemble using a single confined electron spin* . Ph.D. thesis, ETH Zürich (2008).

[184] P. Maletinsky, M. Kroner, and A. Imamoglu. *Breakdown of the nuclear-spin-temperature approach in quantum-dot demagnetization experiments.* Nature Physics **5**, 407 (2009).

[185] H. Christ, J. I. Cirac, and G. Giedke. *Quantum description of nuclear spin cooling in a quantum dot.* Physical Review B **75**(15), 155324 (2007).

[186] R. Bonifacio and L. Lugiato. *Optical bistability and cooperative effects in resonance fluorescence.* Physical Review A **18**(3), 1129 (1978).

[187] D. D. Awschalom, N. Samarath, and D. Loss. *Semiconductor Spintronics and Quantum Computation.* Springer, Berlin (2002).

[188] D. Y. Sharvin and Y. V. Sharvin. *Magnetic-flux quantization in a cylindrical film of a normal metal.* JETP letters **34**, 272 (1981).

[189] B. J. van Wees, H. van Houten, C. W. J. Beenakker, J. G. Williamson, L. P. Kouwenhoven, D. van der Marel, and C. T. Foxon. *Quantized conductance of point contacts in a two-dimensional electron gas.* Phys. Rev. Lett. **60**(9), 848 (1988).

[190] D. A. Wharam, T. J. Thornton, R. Newbury, M. Pepper, H. Ahmed, J. E. F. Frost, D. G. Hasko, D. C. Peacock, D. A. Ritchie, and G. A. C. Jones. *One-dimensional transport and the quantisation of the ballistic resistance.* Journal of Physics C Solid State Physics **21**(8), L209 (2000).

[191] Y. V. Nazarov and Y. M. Blanter. *Quantum Transport.* Cambridge University Press, Cambrigde (2009).

[192] S. Datta. *Electronic Transport in Mesoscopic Systems.* Cambridge University Press, Cambridge (1997).

[193] R. Hanson, L. P. Kouwenhoven, J. R. Petta, S. Tarucha, and L. M. K. Vandersypen. *Spins in few-electron quantum dots.* Reviews of Modern Physics **79**(4), 1217 (2007).

[194] W. G. van der Wiel, S. De Franceschi, J. M. Elzerman, T. Fujisawa, S. Tarucha, and L. P. Kouwenhoven. *Electron transport through double quantum dots.* Reviews of Modern Physics **75**(1), 1 (2002).

[195] A. C. Johnson, J. R. Petta, J. M. Taylor, A. Yacoby, M. D. Lukin, C. M. Marcus, M. P. Hanson, and A. C. Gossard. *Triplet–singlet spin relaxation via nuclei in a double quantum dot.* Nature Physics **435**(7044), 925 (2005).

[196] O. N. Jouravlev and Y. V. Nazarov. *Electron Transport in a Double Quantum Dot Governed by a Nuclear Magnetic Field.* Physical Review Letters **96**(17), 176804 (2006).

[197] J. Baugh, Y. Kitamura, K. Ono, and S. Tarucha. *Large Nuclear Overhauser Fields Detected in Vertically Coupled Double Quantum Dots.* Physical Review Letters **99**(9), 096804 (2007).

[198] J. R. Petta, J. M. Taylor, A. C. Johnson, A. Yacoby, M. D. Lukin, C. M. Marcus, M. P. Hanson, and A. C. Gossard. *Dynamic Nuclear Polarization with Single Electron Spins.* Physical Review Letters **100**(6), 067601 (2008).

[199] J. Iñarrea, G. Platero, and A. H. MacDonald. *Electronic transport through a double quantum dot in the spin-blockade regime: Theoretical models.* Physical Review B **76**(8), 085329 (2007).

[200] F. H. L. Koppens, J. A. Folk, J. M. Elzerman, R. Hanson, L. H. W. van Beveren, L. P. Kouwenhoven, and L. M. K. Vandersypen. *Control and Detection of Singlet-Triplet Mixing in a Random Nuclear Field.* Science (New York, N.Y.) **309**(5739), 1346 (2005).

[201] K. Ono and S. Tarucha. *Nuclear-Spin-Induced Oscillatory Current in Spin-Blockaded Quantum Dots.* Physical Review Letters **92**(25), 256803 (2004).

[202] A. Pfund, I. Shorubalko, K. Ensslin, and R. Leturcq. *Suppression of Spin Relaxation in an InAs Nanowire Double Quantum Dot.* Physical Review Letters **99**(3), 036801 (2007).

[203] T. Kobayashi, K. Hitachi, S. Sasaki, and K. Muraki. *Observation of Hysteretic Transport due to Dynamic Nuclear Spin Polarization in a GaAs Lateral Double Quantum Dot.* Physical Review Letters **107**(21), 216802 (2011).

[204] K. Ono, D. G. Austing, Y. Tokura, and S. Tarucha. *Current Rectification by Pauli Exclusion in a Weakly Coupled Double Quantum Dot System.* Science **297**(5585), 1313 (2002).

[205] M. S. Rudner and L. S. Levitov. *Self-Polarization and Dynamical Cooling of Nuclear Spins in Double Quantum Dots.* Physical Review Letters **99**(3), 036602 (2007).

[206] M. Eto, T. Ashiwa, and M. Murata. *Current-Induced Entanglement of Nuclear Spins in Quantum Dots.* Journal of the Physics Society Japan **73**(2), 307 (2004).

[207] P. Recher, E. V. Sukhorukov, and D. Loss. *Quantum Dot as Spin Filter and Spin Memory.* Physical Review Letters **85**(9), 1962 (2000).

[208] R. Hanson, L. M. K. Vandersypen, L. H. W. van Beveren, J. M. Elzerman, I. T. Vink, and L. P. Kouwenhoven. *Semiconductor few-electron quantum dot operated as a bipolar spin filter.* Physical Review B **70**(24), 241304 (2004).

[209] E. M. Kessler, S. Yelin, M. D. Lukin, J. I. Cirac, and G. Giedke. *Optical Superradiance from Nuclear Spin Environment of Single-Photon Emitters.* Physical Review Letters **104**(14), 143601 (2010).

[210] H. Bruus and K. Flensberg. *Many-Body Quantum Theory in Condensed Matter Physics.* Oxford University Press, New York (2006).

[211] Y. Yamamoto and A. Imamoglu. *Mesoscopic Quantum Optics.* Wiley, New York (1999).

[212] S. Welack, M. Esposito, U. Harbola, and S. Mukamel. *Interference effects in the counting statistics of electron transfers through a double quantum dot.* Physical Review B **77**(19), 195315 (2008).

[213] C. Cohen-Tannoudji, J. Dupont-Roc, and G. Grynberg. *Atom-Photon Interactions: Basic Processes and Applica- tions* . Wiley, New York (1992).

[214] C. Timm. *private communication.*

[215] C. Timm. *Tunneling through molecules and quantum dots: Master-equation approaches.* Physical Review B **77**(19), 195416 (2008).

[216] U. Harbola, M. Esposito, and S. Mukamel. *Quantum master equation for electron transport through quantum dots and single molecules.* Physical Review B **74**(23), 235309 (2006).

[217] H.-A. Engel and D. Loss. *Single-spin dynamics and decoherence in a quantum dot via charge transport.* Physical Review B **65**(19), 195321 (2002).

[218] N. Zhao, J.-L. Zhu, R.-B. Liu, and C. Sun. *Quantum noise theory for quantum transport through nanostructures.* New Journal of Physics **13**(1), 013005 (2011).

[219] S. A. Gurvitz and Y. S. Prager. *Microscopic derivation of rate equations for quantum transport.* Physical Review B **53**(23), 15932 (1996).

[220] S. A. Gurvitz. *Rate equations for quantum transport in multidot systems.* Physical Review B **57**(11), 6602 (1998).

[221] D. A. Bagrets and Y. V. Nazarov. *Full counting statistics of charge transfer in Coulomb blockade systems.* Physical Review B **67**(8), 085316 (2003).

[222] M. Esposito, U. Harbola, and S. Mukamel. *Nonequilibrium fluctuations, fluctuation theorems, and counting statistics in quantum systems.* Reviews of Modern Physics **81**(4), 1665 (2009).

[223] C. Emary, C. Pöltl, A. Carmele, J. Kabuss, A. Knorr, and T. Brandes. *Bunching and antibunching in electronic transport.* Physical Review B **85**(16), 165417 (2012).

[224] L. D. Contreras-Pulido and R. Aguado. *Shot noise spectrum of artificial single-molecule magnets: Measuring spin relaxation times via the Dicke effect.* Physical Review B **81**(16), 161309(R) (2010).

[225] H. J. Carmichael. *Statistical Methods in Quantum Optics 1.* Springer Berlin Heidelberg, Berlin (1999).

[226] R. Hanson, B. Witkamp, L. M. K. Vandersypen, L. H. W. van Beveren, J. M. Elzerman, and L. P. Kouwenhoven. *Zeeman Energy and Spin Relaxation in a One-Electron Quantum Dot.* Physical Review Letters **91**(19), 196802 (2003).

[227] D. Paget. *Optical detection of NMR in high-purity GaAs: Direct study of the relaxation of nuclei close to shallow donors.* Physical Review B **25**(7), 4444 (1982).

[228] T. Ota, G. Yusa, N. Kumada, S. Miyashita, T. Fujisawa, and Y. Hirayama. *Decoherence of nuclear spins due to dipole-dipole interactions probed by resistively detected nuclear magnetic resonance.* Applied Physics Letters **91**(19), 193101 (2007).

[229] R. Takahashi, K. Kono, S. Tarucha, and K. Ono. *Voltage-Selective Bidirectional Polarization and Coherent Rotation of Nuclear Spins in Quantum Dots.* Physical Review Letters **107**(2), 026602 (2011).

[230] S. Morrison and A. S. Parkins. *Collective spin systems in dispersive optical cavity QED: Quantum phase transitions and entanglement.* Physical Review A **77**(4), 043810 (2008).

[231] C.-H. Chung, K. Le Hur, M. Vojta, and P. Wölfle. *Nonequilibrium Transport at a Dissipative Quantum Phase Transition.* Physical Review Letters **102**(21), 216803 (2009).

[232] A. Leggett, S. Chakravarty, A. Dorsey, M. Fisher, A. Garg, and W. Zwerger. *Dynamics of the dissipative two-state system.* Reviews of Modern Physics **59**(1), 1 (1987).

[233] M. S. Rudner and L. S. Levitov. *Phase Transitions in Dissipative Quantum Transport and Mesoscopic Nuclear Spin Pumping.* Physical Review B **82**, 155418 (2010).

[234] J. I. Cirac, R. Blatt, P. Zoller, and W. D. Phillips. *Laser cooling of trapped ions in a standing wave.* Physical Review A **46**(5), 2668 (1992).

[235] S. Sachdev. *Colloquium: Order and quantum phase transitions in the cuprate superconductors.* Reviews of Modern Physics **75**(3), 913 (2003).

[236] V. L. Ginzburg. *Superconductivity and superfluidity (what was done and what was not).* Physics-Uspekhi **40**(4), 407 (2007).

[237] D. Belitz and T. Kirkpatrick. *The Anderson-Mott transition.* Reviews of Modern Physics **66**(2), 261 (1994).

[238] M. Hasan and C. Kane. *Colloquium: Topological insulators.* Reviews of Modern Physics **82**(4), 3045 (2010).

[239] P. Werner, K. Volker, M. Troyer, and S. Chakravarty. *Phase Diagram and Critical Exponents of a Dissipative Ising Spin Chain in a Transverse Magnetic Field.* Physical Review Letters **94**(4), 047201 (2005).

[240] L. Capriotti, A. Cuccoli, A. Fubini, V. Tognetti, and R. Vaia. *Dissipation-Driven Phase Transition in Two-Dimensional Josephson Arrays.* Physical Review Letters **94**(15), 157001 (2005).

[241] J. Eisert and T. Prosen. *Noise-driven quantum criticality.* arXiv.org **quant-ph** (2010).

[242] M. J. Bhaseen, J. Mayoh, B. D. Simons, and J. Keeling. *Dynamics of nonequilibrium Dicke models.* Phys. Rev. A **85**, 13817 (2012).

[243] M. Žnidarič. *Solvable quantum nonequilibrium model exhibiting a phase transition and a matrix product representation.* Physical Review E **83**(1), 011108 (2011).

[244] K. Hepp and E. H. Lieb. *On the superradiant phase transition for molecules in a quantized radiation field: the dicke maser model.* Annals of Physics **76**(2), 360 (1973).

[245] H. Gibbs, S. McCall, and T. Venkatesan. *Differential Gain and Bistability Using a Sodium-Filled Fabry-Perot Interferometer.* Physical Review Letters **36**(19), 1135 (1976).

[246] S. V. Lawande, R. R. Puri, and S. S. Hassan. *Non-resonant effects in the fluorescent Dicke model. I. Exact steady state analysis.* Journal of Physics B: Atomic and Molecular Physics **14**(21), 4171 (1981).

[247] R. R. Puri, S. V. Lawande, and S. S. Hassan. *Dispersion in the driven Dicke-model.* Optics Communications **35**(2), 179 (1980).

[248] S. Schneider and G. Milburn. *Entanglement in the steady state of a collective-angular-momentum (Dicke) model.* Physical Review A **65**(4), 042107 (2002).

[249] A. Russell, V. I. Fal'ko, A. I. Tartakovskii, and M. S. Skolnick. *Bistability of optically-induced nuclear spin orientation in quantum dots.* Physical Review B **76**, 195310 (2007).

[250] A. Rivas and S. F. huelga. *Open Quantum Systems. An Introduction.* SpringerBriefs in Physics2191-5423. Springer Berlin Heidelberg, Berlin, Heidelberg (2012).

[251] B. Horstmann. *Quantum Simulations of Out-of-Equilibrium Phenomena* . Ph.D. thesis, Technical University Munich (2011).

[252] M. S. Rudner, L. M. K. Vandersypen, V. Vuletić, and L. S. Levitov. *Generating Entanglement and Squeezed States of Nuclear Spins in Quantum Dots.* Physical Review Letters **107**(20), 206806 (2011).

[253] T. Holstein and H. Primakoff. *Field Dependence of the Intrinsic Domain Magnetization of a Ferromagnet.* Physical Review **58**(12), 1098 (1940).

[254] M. Kitagawa and M. Ueda. *Squeezed spin states.* Physical Review A **47**(6), 5138 (1993).

[255] J. K. Korbicz, J. I. Cirac, and M. Lewenstein. *Spin Squeezing Inequalities and Entanglement of N Qubit States.* Physical Review Letters **95**(12), 120502 (2005).

[256] L. Pezzé and A. Smerzi. *Entanglement, Nonlinear Dynamics, and the Heisenberg Limit.* Physical Review Letters **102**(10), 100401 (2009).

[257] P. Hyllus, W. Laskowski, R. Krischek, C. Schwemmer, W. Wieczorek, H. Weinfurter, L. Pezzé, and A. Smerzi. *Fisher information and multiparticle entanglement.* Physical Review A **85**(2), 022321 (2012).

[258] G. Tóth. *Multipartite entanglement and high-precision metrology.* Physical Review A **85**(2), 022322 (2012).

[259] A. Clifford and T. Clifford. *Fundamentals of Supercritical Fluids.* Oxford University Press (1999).

[260] C. Bowden and C. Sung. *First- and second-order phase transitions in the Dicke model: Relation to optical bistability.* Physical Review A **19**(6), 2392 (1979).

[261] E. M. Kessler. *Generalized Schrieffer-Wolff formalism for dissipative systems.* Physical Review A **86**(1), 012126 (2012).

[262] M. Lax. *Formal Theory of Quantum Fluctuations from a Driven State.* Physical Review **129**(5), 2342 (1963).

[263] M. Kim, J. Lee, and W. Munro. *Experimentally realizable characterizations of continuous-variable Gaussian states.* Physical Review A **66**(3), 030301(R) (2002).

[264] D. Nagy, G. Konya, G. Szirmai, and P. Domokos. *Dicke-Model Phase Transition in the Quantum Motion of a Bose-Einstein Condensate in an Optical Cavity.* Physical Review Letters **104**(13), 130401 (2010).

[265] P. D. Drummond and D. F. Walls. *Quantum theory of optical bistability. I. Nonlinear polarisability model.* Journal of Physics A: Mathematical and General **13**(2), 725 (1980).

[266] M. Kroner, *et al.*. *Optical Detection of Single-Electron Spin Resonance in a Quantum Dot.* Physical Review Letters **100**(15) (2008).

[267] E. Brion, L. H. Pedersen, and K. Mølmer. *Adiabatic elimination in a lambda system.* Journal of Physics A: Mathematical and Theoretical **40**(5), 1033 (2007).

[268] S. Bravyi, D. P. DiVincenzo, and D. Loss. *Schrieffer-Wolff transformation for quantum many-body systems.* Annals of Physics **326**(10), 2793 (2011).

[269] A. C. Hewson. *The Kondo Problem to Heavy Fermions.* Cambridge University Press (1993).

[270] A. H. MacDonald, S. M. Girvin, and D. Yoshioka. *t/U expansion for the Hubbard model.* Physical Review B **37**(16), 9753 (1988).

[271] J. Paaske and K. Flensberg. *Vibrational Sidebands and the Kondo Effect in Molecular Transistors.* Physical Review Letters **94**(17), 176801 (2005).

[272] M. Issler, E. Kessler, G. Giedke, S. Yelin, J. I. Cirac, M. Lukin, and A. Imamoglu. *Nuclear Spin Cooling Using Overhauser-Field Selective Coherent Population Trapping.* Physical Review Letters **105**(26), 267202 (2010).

[273] B. Uchoa, T. G. Rappoport, and A. H. Castro Neto. *Kondo Quantum Criticality of Magnetic Adatoms in Graphene.* Physical Review Letters **106**(1), 016801 (2011).

[274] H. v. Löhneysen and P. Wölfle. *Fermi-liquid instabilities at magnetic quantum phase transitions.* Reviews of Modern Physics **79**(3), 1015 (2007).

[275] B. M. Escher, R. L. de Matos Filho, and L. Davidovich. *General framework for estimating the ultimate precision limit in noisy quantum-enhanced metrology.* Nature Physics **7**(5), 406 (2011).

[276] S. F. huelga, C. Macchiavello, T. Pellizzari, A. Ekert, M. B. Plenio, and J. I. Cirac. *Improvement of Frequency Standards with Quantum Entanglement.* Physical Review Letters **79**(20), 3865 (1997).

[277] F. Dimer, B. Estienne, A. Parkins, and H. J. Carmichael. *Proposed realization of the Dicke-model quantum phase transition in an optical cavity QED system.* Physical Review A **75**(1), 013804 (2007).

[278] N. Van Kampen. *Elimination of fast variables.* Physics Reports **124**(2), 69 (1985).

[279] H. P. Breuer and F. Pertruccione. *The Theory of Open Quantum Systems.* Oxford University Press, Oxford (2002).

[280] F. Reiter and A. S. Sørensen. *An effective operator formalism for open quantum systems.* arXiv.org p. 11 (2011).

[281] S. Bravyi, D. P. DiVincenzo, D. Loss, and B. Terhal. *Quantum Simulation of Many-Body Hamiltonians Using Perturbation Theory with Bounded-Strength Interactions.* Physical Review Letters **101**(7), 070503 (2008).

[282] S. Jordan and E. Farhi. *Perturbative gadgets at arbitrary orders.* Physical Review A **77**(6), 062329 (2008).

[283] J. Kempe, A. Kitaev, and O. Regev. *The Complexity of the Local Hamiltonian Problem.* SIAM Journal on Computing **35**(5), 1070 (2006).

[284] G. Lindblad. *On the generators of quantum dynamical semigroups.* Communications in Mathematical Physics **48**(2), 119 (1976).

[285] P. Zoller and C. W. Gardiner. *Quantum Noise.* Springer, Berlin (2004).

[286] S. K. Kehrein and A. Mielke. *Theory of the Anderson Impurity Model: The Schrieffer-Wolff Transformation Reexamined.* Annals of Physics **252**(1), 1 (1996).

# Acknowledgements

I am deeply thankful to my supervisor, Ignacio Cirac, who supported me greatly in every respect during my Ph.D. studies. His own fascination for physics, and his extraordinary scientific intuition and knowledge were a great inspiration for me throughout the years. I am especially grateful that he kept encouraging me to develop my own scientific independence, and provided the necessary freedom, environment, and guidance to do so.

Also, I want to thank my advisor and coworker Géza Giedke who gave me invaluable mentoring and support throughout my projects. Without his patience in the countless discussions about physics and his great knowledge in the most diverse fields of physics and science, my work would not have been possible.

Further, I am indebted to Misha Lukin, Atac Imamoglu, and Susanne Yelin for their generous guidance, help and hospitality in the course of several fruitful collaborations. I was able to learn a lot from their outstanding expertise, and the numerous research visits in Boston and Zürich were a great experience for me.

It was a great pleasure and a lot of fun to work with Martin Schütz over the past year in our quantum transport, soccer and tennis projects. For the latter two, I also acknowledge Oriol Romero-Isart, especially for not giving up trying to beat me on the tennis court after so many unsuccessful attempts. Besides that, I really enjoyed the many interesting and motivating discussions about physics with him. Of course, I also acknowledge Fernando Pastawski, Heike Schwager, Matteo Rizzi, Anika Pflanzer, Michael Lubasch, Lucas Clemente, Maarten van den Nest, Gemma De las Cuevas, Tassilo Keilmann, and all my other coworkers and friends at the MPQ for the always generous help in physical questions, and the many fun hours together.

Further, I thank Romain Quidant, Mathieu Juan, and Michael Geiselmann for their hospitality in Barcelona and for introducing me to the field of nano-plasmonics, and Mena Issler for

our joint work.

Especially, I want to thank my parents, my sister, and my brother for their always unconditional support. I am deeply grateful for that.

Finally, I thank Amy Celleri for her love and great support during the past year, and, in particular, during the time of writing this Thesis.

I acknowledge financial support by the GIF and the Max-Planck-Society.